University of South Florida
Digital Commons @ University of South Florida

DIGITAL COMMONS
@ UNIVERSITY OF SOUTH FLORIDA

USF Tampa Graduate Theses and Dissertations
USF Graduate Theses and Dissertations

May 2022

Determinations of Chemical Equilibria in Natural Waters Using Spectrophotometric Techniques

Katelyn M. Schockman
University of South Florida

Follow this and additional works at: https://digitalcommons.usf.edu/etd

 Part of the Other Oceanography and Atmospheric Sciences and Meteorology Commons

Scholar Commons Citation

Schockman, Katelyn M., "Determinations of Chemical Equilibria in Natural Waters Using Spectrophotometric Techniques" (2022). *USF Tampa Graduate Theses and Dissertations.*
https://digitalcommons.usf.edu/etd/10405

This Dissertation is brought to you for free and open access by the USF Graduate Theses and Dissertations at Digital Commons @ University of South Florida. It has been accepted for inclusion in USF Tampa Graduate Theses and Dissertations by an authorized administrator of Digital Commons @ University of South Florida. For more information, please contact digitalcommons@usf.edu.

Determinations of Chemical Equilibria in Natural Waters Using Spectrophotometric Techniques

by

Katelyn M. Schockman

A dissertation submitted in partial fulfillment
of the requirements for the degree of
Doctor of Philosophy
College of Marine Science
University of South Florida

Major Professor: Robert H. Byrne, Ph.D.
Kristen Buck, Ph.D.
Richard Feely, Ph.D.
Gary Mitchum, Ph.D.
Rik Wanninkhof, Ph.D.
Kimberly Yates, Ph.D.

Date of Approval:
September 23, 2022

Keywords: Ocean carbon system, bicarbonate dissociation constant, pH, internal consistency, ionic strength, conductometry

Copyright © 2022, Katelyn M. Schockman

ACKNOWLEDGMENTS

I am so immensely grateful and appreciative for those who have helped me along my Ph.D. journey. The biggest influence on my scientific career is my advisor, Dr. Robert Byrne. He has been an extremely supportive mentor both with respect to my academic and personal growth. I always look forward to phone calls from Bob to chat about anything from science, to hijinks, or any range of peculiar topics that come to his mind. As a scientist, he has taught me to be a meticulous analytical chemist, to critically think and question everything, and to describe complex topics in a simple manner. As a person, he has taught me that living life full of joy and being kind to others is far more important than simply being smart. If everyone approached aspects of science, mentoring, and life like Bob, the world would certainly be a better place.

A special shout out is in need for all members, past and present, of the Byrne lab. First is Dr. Sherwood Liu, who has been instrumental in helping me become the chemist I am today. He has been there at all hours to teach me new techniques, help me fix broken instruments, find the missing equipment piece needed (or build a jerry-rigged version), and, most importantly, to bring laughter into the lab when we have all had a long day. I would also like to especially thank Dr. Jon Sharp who guided me along in the lab, has proofread countless pieces of my writing, and has also been a great friend. Thanks to Erin Cuyler for teaching me lab techniques when I first started, and to Macarena Martín-Mayor and Kalla Fleger for being great lab and sailing companions. Also, a special thank you to Dr. Tonya Clayton for providing insightful feedback on my manuscripts and greatly helping to improve the quality of my work.

I would like to thank my committee members – Dr. Kristen Buck, Dr. Richard Feely, Dr. Gary Mitchum, Dr. Rik Wanninkhof, and Dr. Kim Yates – for their continued support throughout this process. I appreciate their role in my success and the thoughtful guidance they have provided. I would also like to thank all the scientists I have sailed with, including Chief Scientists Dr. Leticia Barbero, Dr. Denis Pierrot, Dr. Richard Feely, and Dr. Brendan Carter.

My family is most important to me in this world and deserves the ultimate thank you. Mom and Dad, you have both been my biggest cheerleaders not only over the past six years, but throughout my entire life. You have always encouraged my academic aspirations and set me up for success, for which I will forever be thankful. I am so proud to be your daughter. To Kyle, Brad, and Austin, thank you for being the best brothers I could ask for. I am so grateful for our family and the closeness we all share. And to Christian, my rock and partner in this life, I cannot thank you enough for your love and constant support. Your belief in me has never wavered, and you continually encourage me even in my times of doubt. I certainly could not have done this without you.

Last, but certainly not least, are my incredible friends. To Maegan, who is my oldest and best friend, and has always rooted for me. To Luke and Jay, who make sure life is never dull. To Devin, who can discuss all things chemistry and keeps me sane. To Carey, Cara, Dana, Greta, and Luis, who are all incredible friends and supports to lean on. And to everyone in the CMS community, for making the past six years in St. Pete so memorable and fun.

TABLE OF CONTENTS

LIST OF TABLES

LIST OF FIGURES

ABSTRACT

Accurate characterizations of chemical equilibria and thermodynamic processes in natural waters are key components for assessing the current state of our global climate and predicting future changes, especially for observations of small rates of change over long time scales. One of the most important chemical systems in natural waters is the system of inorganic carbon species comprised of carbon dioxide (CO_2), bicarbonate, and carbonate. The bicarbonate dissociation constant, K_2, describes the relationship between pH and the relative concentrations of bicarbonate and carbonate ions at thermodynamic equilibrium. The carbonate/bicarbonate equilibrium quotient is required in nearly all CO_2 system calculations relevant to freshwater and seawater (i.e., relationships between pH, total dissolved inorganic carbon (C_T), total alkalinity (A_T), and CO_2 fugacity (fCO_2)). There have been many previous characterizations of K_2 in seawater, but most of them are not in statistical agreement with one another. This incongruity has resulted in ongoing speculation as to which K_2 parameterization to use at different salinity and temperature conditions.

One focus of my dissertation was development of techniques to improve the accuracy and precision of K_2 measurements in seawater. Chapter Two describes the development of a novel spectrophotometric method, based on the potentiometric method used by Mehrbach et al. (1973), to experimentally determine K_2 for a range of temperatures ($15 \leq t \leq 35$ °C) and salinities ($20 \leq S \leq 40$). The K_2 values determined in this work, each based on hundreds of spectrophotometric pH measurements, were used to produce a new K_2 parameterization. The residuals (observations minus predictions) of my K_2 parameterization in terms of salinity and temperature are much

smaller than the residuals obtained in previous works, indicating that my characterization is based on more precise measurements than other available K_2 characterizations.

In Chapter Three, this novel spectrophotometric method was adapted to determine K_2 under conditions more applicable to polar surface waters and the deep ocean (i.e., $3 \leq t \leq 15$ °C). Typical spectrophotometric measurements of pH at temperatures below ~15 °C are challenging because condensation on optical surfaces can impede measurement accuracy. To address this challenge, the spectrophotometric method was modified to specifically work at low temperatures. This work involved the use of an environmentally controlled cold room (reducing ambient humidity) and directing moisture-free nitrogen gas on optical surfaces to preclude condensation. The combination of observations described in Chapters Two and Three resulted in a new K_2 parameterization relevant to the open ocean at atmospheric pressure with an associated random uncertainty component that is greatly reduced compared to previous works. This parameterization can be used by oceanographers who make CO_2 system calculations for biogeochemical process studies, carbon budgets, and assessments of both current and future climate.

Another emphasis of this dissertation was assessment of the accuracy of CO_2 system models via examinations of internal consistency (i.e., comparison of measured and calculated CO_2 system parameters). In Chapter Two, several large oceanographic data sets were used to assess the level of internal consistency of CO_2 system calculations obtained with alternative sets of CO_2 system dissociation constant parameterizations. These analyses demonstrated that improved CO_2 system internal consistency was obtained using the set of constants which includes the K_2 parameterization produced with the spectrophotometric procedures described in this work. Importantly, though, these internal consistency assessments (and essentially all assessments found in the literature) are limited to 20 or 25 °C as these are the traditional measurement temperatures

of fCO_2 and pH, respectively. In Chapter Three, results from NOAA's 2021 West Coast Ocean Acidification cruise are presented, where paired pH measurements were made at both the traditional measurement temperature of 25 °C and at an alternative, lower, temperature of 12 °C. These paired measurements, combined with measurements of A_T and C_T, allowed assessment of internal consistency for conditions more representative of the subsurface open ocean. These comparisons of calculations and direct measurements indicated that pH should be directly measured rather than calculated from the A_T and C_T pair. The assessments also demonstrated that pH measurements at either 25 °C or 12 °C can be used to obtain reliable calculations of CO_2 system parameters at in situ conditions (i.e., pH, fCO_2, and calcium carbonate saturation state (Ω)).

Under conditions appropriate to the open ocean, equilibrium constants such as K_2 are generally weakly dependent on salinity or, equivalently, ionic strength (I). In contrast, equilibrium constants vary strongly with ionic strength in dilute solutions such as rivers and lakes. As fresh waters typically have an ionic strength between $0 \leq I \leq 0.01$ mol kg^{-1}, the ability to detect small differences in ionic strength can be critical to understanding freshwater chemistry and associated implications for freshwater organisms. A third focus of this dissertation was development of an improved method to measure the ionic strength of natural freshwaters. The novel method described in Chapter Four is based on a combination of conductometric and spectrophotometric measurements. The spectrophotometric method is based on innovative procedures involving observations of the dissociation characteristics of phosphate buffers. The hybrid (conductometric/spectrophotometric) procedure described in Chapter Four is shown to be both more precise and more accurate than the conductometric procedures that have previously been used to determine I.

This dissertation research exemplifies how analytical techniques, in particular spectrophotometric methods, can be used in a wide variety of studies to better understand the chemical processes and equilibria of natural waters from rivers to the sea.

CHAPTER ONE:

INTRODUCTION

1.1 Background motivation

Humans have been influencing the earth's climate system through emissions of fossil fuels and land-use changes, particularly since the beginning of the industrial era (Keeling et al., 1976; Feely et al., 2009; Johnson et al., 2021; Friedlingstein et al., 2022). Anthropogenic emissions have led to an increase in the concentration of carbon dioxide (CO_2) gas in the atmosphere from pre-industrial levels of 280 ppm to an average of 412 ppm in 2020 (Fig. 1.1) (Dlugokencky and Tans, 2021; Friedlingstein et al., 2022). Current atmospheric concentrations are higher than historic estimates of the past two million years (IPCC, 2021), and have caused increases in both atmospheric and oceanic temperatures.

As shown in Fig. 1.2, anthropogenic CO_2 emissions are absorbed by the ocean, land, and atmosphere. The oceanic uptake, equivalent to approximately 30% of the total anthropogenic CO_2 emissions since pre-industrial times, plays a vital role in global carbon cycling (Le Quéré et al., 2018; Gruber et al., 2019; Friedlingstein et al., 2022). Continual uptake of CO_2 by the ocean changes the chemical composition of seawater, decreasing pH and lowering the concentration of carbonate ions ($[CO_3^{2-}]$) (Bates et al., 2014; Byrne, 2014; Jiang et al., 2019). Surface ocean pH has decreased by approximately 0.1 since the industrial revolution (Caldeira and Wickett, 2003; Orr et al., 2005; Wu et al., 2018). The Intergovernmental Panel on Climate Change (IPCC) model SSP3-7.0, which projects climate scenarios under conditions of maintained high greenhouse gas emissions, estimates atmospheric CO_2 concentrations will approximately double by 2100 (IPCC,

2021). This increase will decrease ocean pH by approximately 0.3 pH units relative to preindustrial values (Orr et al., 2005; Penman et al., 2014), with concomitant decreases in [CO_3^{2-}] and the calcium carbonate ($CaCO_3$) saturation states of seawater (Ω).

Anthropogenically-induced changes in pH, O_2 concentrations, nutrients, temperature, mineral saturation states, etc. are observed in both the open ocean and coastal waters (Feely et al., 2008; Feely et al., 2012), and these changes commonly exert negative impacts on the earth's biosphere (Gruber et al., 2019; Schlunegger et al., 2019). In order to better predict how changes in anthropogenic emissions will influence the earth's biota, it is increasingly important to accurately document environmental conditions, including not only chemical concentrations but also chemical equilibria.

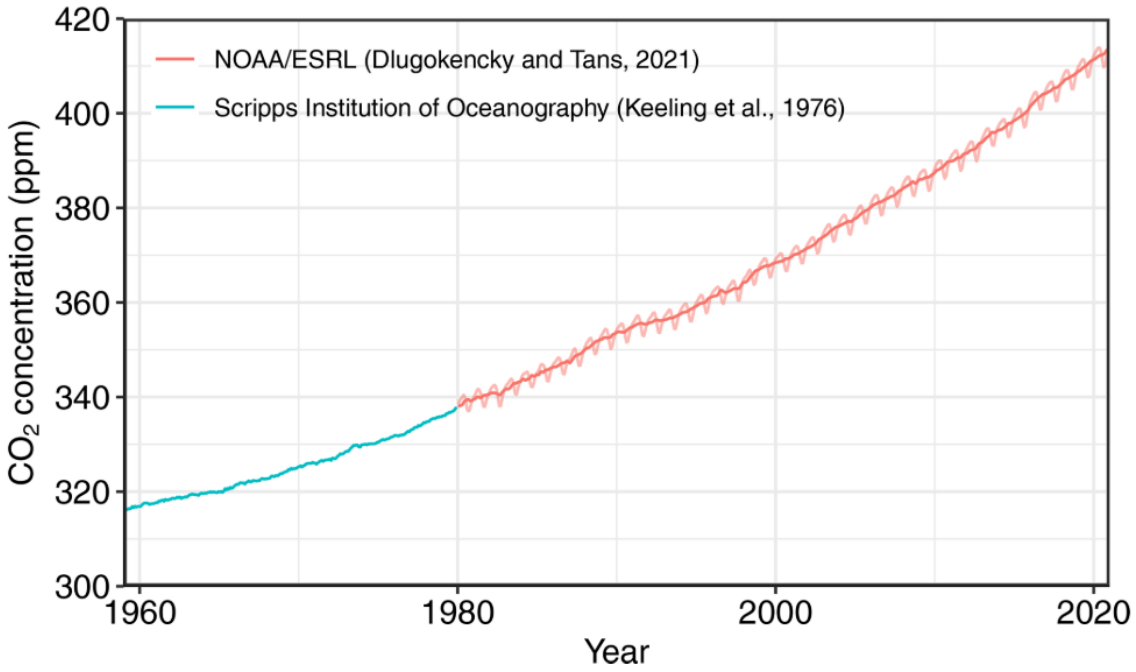

Fig. 1.1. Average surface atmospheric CO_2 concentration (ppm) from around 1960 to present. Data from NOAA/ESRL are an average of multiple stations' direct atmospheric CO_2 measurements. The Scripps Institution of Oceanography data are an average of direct atmospheric CO_2 measurements from Mauna Loa and South Pole stations. (Figure is reproduced from Friedlingstein et al. (2022). Creative Commons Attribution 4.0 License. Reproduced with permission.)

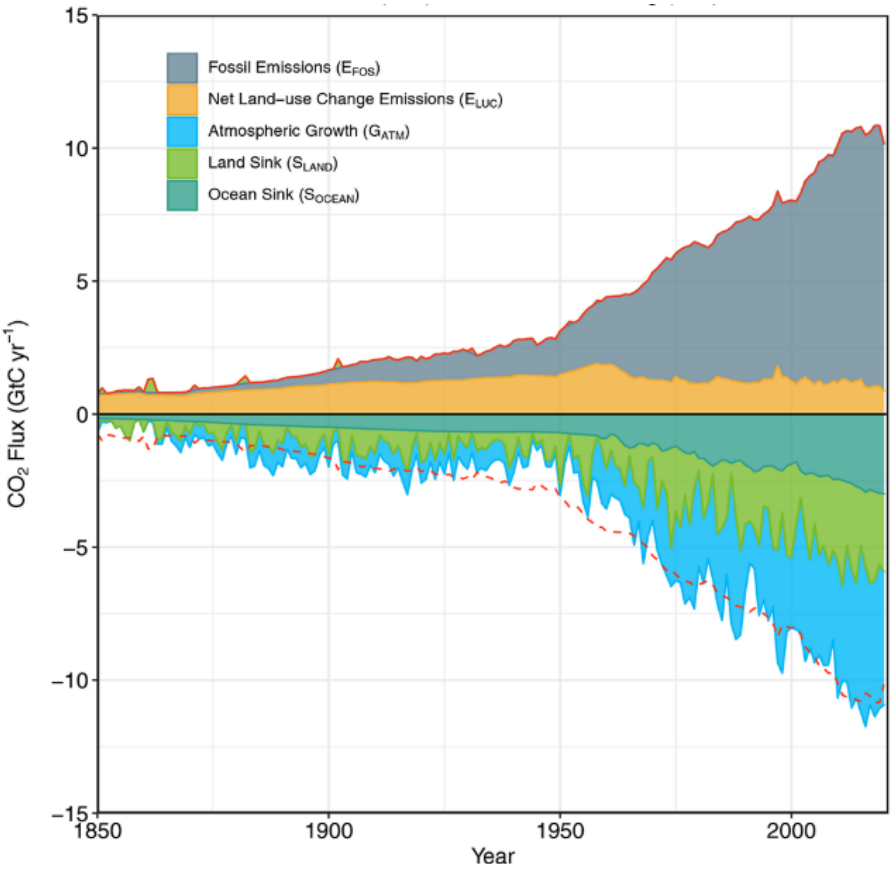

Fig. 1.2. Major sources of anthropogenic emissions from around 1850 to present in terms of CO_2 fluxes (top half of figure) and the associated sinks in which these emissions are partitioned (bottom half of figure), both expressed as gigatons of carbon per year (GtC yr^{-1}). The solid red line follows the total emissions, and the dashed red line is a mirror of that line. The sum of the CO_2 fluxes into the atmosphere, land, and ocean do not exactly match up with the dashed red line, indicating a budget imbalance. (Figure is reproduced from Friedlingstein et al. (2022). Creative Commons Attribution 4.0 License. Reproduced with permission.)

1.2 CO_2 equilibria in seawater

1.2.1 Overview

One of the most important chemical systems in seawater, the inorganic CO_2 system, is comprised of three main species: dissolved carbon dioxide ($CO_2^* = CO_2 + H_2CO_3$), bicarbonate (HCO_3^-), and carbonate (CO_3^{2-}). Gaseous CO_2 is in equilibrium with aqueous CO_2 via the following reaction:

$$CO_{2\,(g)} \leftrightarrow CO_2^* \tag{1.1}$$

The dissociation constant that describes eq. (1.1) is:

$$K_0 = \frac{[CO_2^*]}{fCO_2} \tag{1.2}$$

where [ ] represents concentration in mol kg^{-1} and fCO_2 is CO_2 fugacity.

Aqueous CO_2^* can then react with water to form bicarbonate, releasing an H^+ ion in the process:

$$CO_2^* + H_2O \leftrightarrow HCO_3^- + H^+ \tag{1.3}$$

The dissociation constant that describes eq. (1.3) is:

$$K_1 = \frac{[HCO_3^-]_T[H^+]_T}{[CO_2^*]} \tag{1.4}$$

where $[\ ]_T$ is used to represent a total concentration (i.e., free plus ion paired in mol kg^{-1}) throughout this chapter.

Bicarbonate can further dissociate into carbonate, releasing an additional H^+ ion:

$$HCO_3^- \leftrightarrow CO_3^{2-} + H^+ \tag{1.5}$$

The dissociation constant that describes eq. (1.5) is:

$$K_2 = \frac{[CO_3^{2-}]_T[H^+]_T}{[HCO_3^-]_T} \tag{1.6}$$

These equilibria (i.e., eq. (1.1), (1.3), and (1.5)) constitute the main mechanism for pH buffering in seawater. The equilibrium constants K_0, K_1, and K_2 are functionally dependent on temperature (t in °C or T in K), salinity (S_P, practical salinity scale), and pressure (P).

1.2.2 CO_2 system dissociation constants

The CO_2 system dissociation constants, K_1 and K_2, are required in almost all CO_2 system calculations. Accordingly, extensive effort has been made in numerous studies throughout the past

several decades to experimentally measure these constants. A list of experimental characterizations of the dissociation constants and associated refits of works is provided in Table 1.1. Notably, the parameterizations of pK_2 (where pK_2 = −log K_2) listed in the table are not in statistical agreement (i.e., the differences between pK_2 parameterizations are much larger than the uncertainty in pK_2). Differences in CO_2 system parameters calculated using various pK_2 parameterizations are larger than measurement precisions (Orr et al., 2018), signifying that the uncertainty in pK_2 statistically influences CO_2 system calculations. Furthermore, the parameterizations span different T and S ranges and are commonly provided on different pH scales (i.e., NBS (pH_{NBS}), free (pH_F), seawater (pH_{SWS}), and total (pH_T)).

Table 1.1.
Published CO_2 system dissociation constant parameterizations along with their utilized experimental methods, pH scale, applicable temperature and salinity ranges, and reported pK_2 uncertainty.

Source	Experimental Methods	pH Scale	t (°C)	S	Uncertainty in pK_2 (as reported by investigators)
Hansson (1973)	Potentiometric titration (synthetic seawater)	Total	5–30	20–40 (‰)	0.009
Mehrbach et al. (1973)	Potentiometric titration, Gran titration	NBS	2–35	26–43 (‰)	0.010
Dickson and Millero (1987)	Refit of Mehrbach et al. (1973) to pH_{SWS}	SWS	0–35	20–43 (‰)	0.013
Goyet and Poisson (1989)	Potentiometric titration, Gran titration (synthetic seawater)	SWS	–1–40	10–50 (S_P)	0.011
Roy et al. (1993)	Potentiometric titration (synthetic seawater)	Total	0–45	5–45 (‰)	0.006

Table 1.1. (Continued).

Cai and Wang (1998)	Refit using combination of Harned and Davis (1943), Edmond and Gieskes (1970), Mehrbach et al. (1973), and Mook and Koene (1975)	NBS	0.2–35	0–40 (‰)	0.030
Lueker et al. (2000)	Refit of Mehrbach et al. (1973) to pH_T	Total	2–35	26–43 (‰)	0.010
Millero et al. (2002)	Fit oceanographic measurements of carbonate system parameters	SWS	–1–38	33–37 (no scale specified)	0.010
Mojica Prieto and Millero (2002)	Potentiometric titration, Spectrophotometric method	SWS	0–45	5–42 (S_P)	0.010
Millero et al. (2006)	Potentiometric titration	SWS	0–50	1–50 (S_P)	0.011
Millero (2010)	Refit using combination of Mehrbach et al. (1973), Mojica Prieto and Millero (2002), and Millero et al. (2006)	SWS	1–50	0–50 (S_P)	0.010
Waters et al. (2013, 2014)	Refit of Millero (2010) to pH_F, pH_{SWS}, and pH_T	Free, SWS, Total	0–45	0–45 (no scale specified)	not specified
Papadimitriou et al. (2018)	Fit laboratory measurements of carbonate system parameters	Total	–6–25	33–100 (S_P)	0.020

Table 1.1. (Continued).

Sulpis et al. (2020)	Refit of Lueker et al. (2000) using oceanographic measurements of carbonate system parameters	Total	−2−32	30−38 (S_P)	0.011
Schockman and Byrne (2021) (Ch. 2)	Spectrophotometric determination of K_1K_2	Total	15−35	20−40 (S_P)	0.010

Among the several available parameterizations of K_1 and K_2, many studies have concluded that the constants to use in best-practice calculations are those of Mehrbach et al. (1973) as refit by Dickson and Millero (1987) on the pH_{SWS} scale and refit by Lueker et al. (2000) on the pH_T scale (Wanninkhof et al., 1999; Lee et al., 2000; Dickson et al., 2007; Woosley, 2021). These recommendations are largely based on internal consistency assessments of the CO_2 system (i.e., comparisons between measured and calculated values of the CO_2 system parameters (for more details see Section 1.3.1)). Specifically, the recommendations are determined by assessing which set of K_1 and K_2 parameterizations utilized in CO_2 system calculations produces calculated values of CO_2 system parameters that most closely equal measured values. While this type of analysis can be useful, these assessments have been performed under limited ranges of temperature and salinity. For example, the recommendation of Wanninkhof et al. (1999) is based on comparisons of constants and internal consistency assessments at 20 °C. Recommendations from Lee et al. (2000) and Woosley (2021) are based on comparisons from a wider range of temperature but for a narrow range of salinity ($31 \leq S_P \leq 36$). These limited comparisons to determine an optimal set of constants have led several studies to suggest that the dissociation constants be re-evaluated with

improved (i.e., spectrophotometric) techniques not available when previous determinations were made (Fong and Dickson, 2019; Sulpis et al., 2020; Woosley, 2021).

1.3 CO_2 system model

1.3.1 Overview

The CO_2 system in seawater can be described using four quantitative parameters: total alkalinity, A_T; total dissolved inorganic carbon, C_T; total scale pH, pH_T; and partial pressure of CO_2, pCO_2 (similarly CO_2 fugacity, fCO_2). Measurement of any two CO_2 system parameters allows for calculations of the other two parameters via thermodynamic relationships. This is important as rarely are all four CO_2 system parameters measured simultaneously. Calculations are necessary for determining (1) CO_2 system parameters not directly measured and (2) descriptions of temperature-dependent parameters under in situ conditions (i.e., pH, fCO_2, and Ω). Calculations are conveniently made using the program CO2SYS which is available in Excel, Matlab, and other programming languages (Pierrot et al., 2006; Van Heuven et al., 2011; Orr et al., 2015).

CO_2 system calculations are a useful tool for assessing carbon fluxes, biological productivity, ocean acidification, calcification rates, etc. – all critical components to understanding climate change. However, comparisons between measured and calculated values of the same parameter have highlighted systematic inconsistencies, whereby measured and calculated values are not in statistical agreement with one another (McElligott et al., 1998; Patsavas et al., 2015; Woosley et al., 2017; Fong and Dickson, 2019). For example, a commonly observed inconsistency is the pH-dependent pH offset seen between measured pH and pH calculated with A_T and C_T (Fig. 1.3) (McElligott et al., 1998; Williams et al., 2017; Carter et al., 2018). Another consequence of CO_2 system calculation inconsistencies is that estimates of Ω are dependent on the choice of input

parameters. As shown in Fig. 1.4, the differences between in situ calculations of Ω limit our ability to predict where calcium carbonate will precipitate/dissolve (i.e., where Ω = 1) (Patsavas et al., 2015).

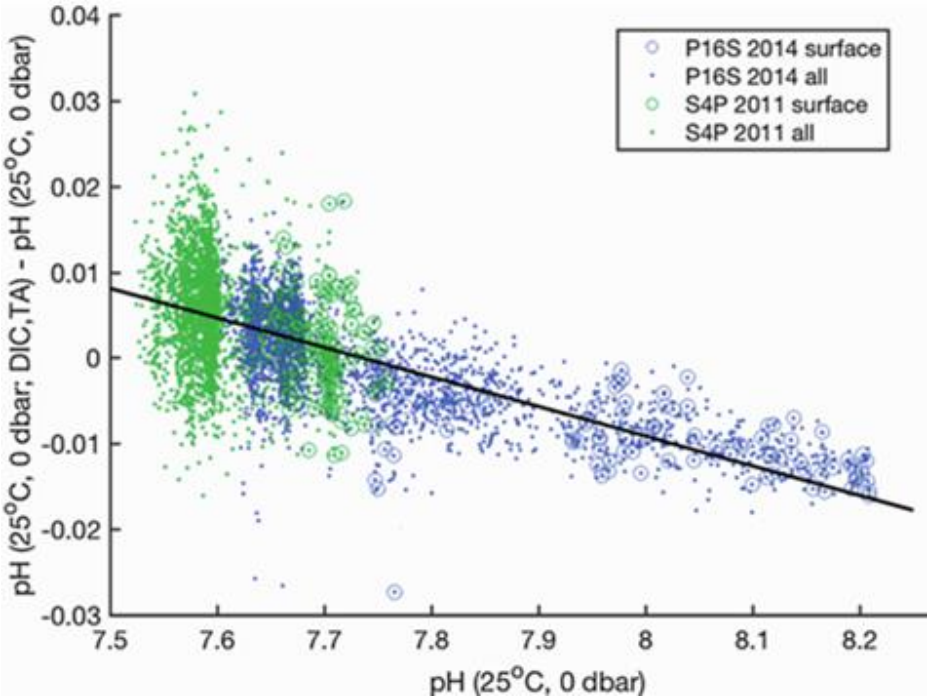

Fig. 1.3. The differences between calculated pH using A_T and C_T (also denoted as TA and DIC) and spectrophotometrically measured pH as a function of measured pH. Data are from the GO-SHIP/SOCCOM cruises P16S 2014 (denoted in blue) and S4P 2011 (denoted in green). (Figure is adapted from Williams et al. (2017). Reproduced with permission.)

These inconsistencies have been attributed to a variety of potential systematic errors in the characterizations of the CO_2 system dissociation constants (K_1, K_2), the boric acid dissociation constant (K_B), the total boron to salinity ratio (B_T/S), CO_2 system measurements themselves, and unaccounted organic acid contributions to A_T (Fong and Dickson, 2019). Furthermore, there may be additional uncertainties that are presently unrecognized. Because all systematic uncertainties create ambiguity when calculating CO_2 system parameters, reducing error in each term is of high priority for the oceanographic community. Over time, the measurement accuracy and precision of

CO_2 system parameters has greatly improved, making uncertainties in the thermodynamic equilibria (K_1, K_2, K_B, B_T/S) more significant contributors to overall calculation uncertainties (Orr et al., 2018). The uncertainty in K_2 is of substantial importance relative to other factors and is therefore a focus of this dissertation (Ch. 2 and 3).

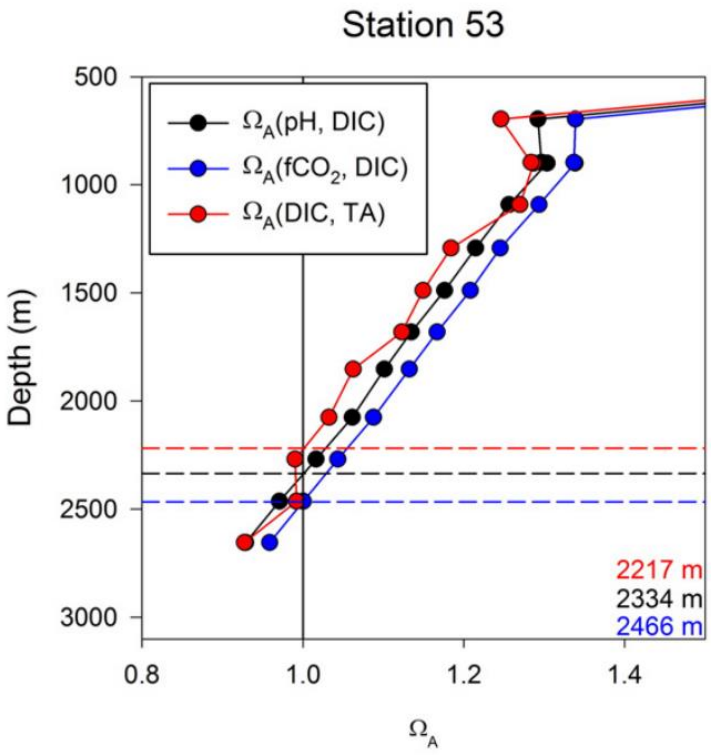

Fig. 1.4. Depth profiles of aragonite saturation state (Ω_A) calculated using various input parameters (denoted in the box in the upper left corner) for a station of NOAA's 2012 Gulf of Mexico and East Coast Carbon (GOMECC-2) Cruise. The dashed horizontal lines represent the saturation horizon (where $\Omega_A = 1$) with the corresponding depth provided in the lower right corner. (Figure is reproduced from Patsavas et al. (2015). Copyright Elsevier. Reproduced with permission.)

1.3.2 Uncertainty in K_2

The reported uncertainties in pK_1 and pK_2 are 0.0075 and 0.015, respectively (Orr et al., 2018). Specifically focusing on pK_2, estimates of uncertainty vary between sources (Table 1.1). K_2 is required in most CO_2 system calculations, so uncertainty in K_2 is propagated into estimates of essentially all CO_2 system parameters. Table 1.2 demonstrates how an 0.011 uncertainty in pK_2

can influence calculated CO_2 system parameters (Millero et al., 2006). Importantly, the uncertainties in calculated CO_2 system parameters vary substantially between low and high fCO_2 conditions (i.e., the uncertainties are not constant). In all instances, the uncertainties of calculated parameters are larger than conjugate measurement precisions. For example, pH calculated from the (A_T,C_T) pair has an uncertainty of ±0.008, roughly 20 times larger than the precision of state-of-the-art spectrophotometric pH measurements (±0.0004 (Clayton and Byrne, 1993)). Overall, uncertainties in the CO_2 system dissociation characterizations produce nonlinear (i.e., unpredictable) outcomes in CO_2 system calculations (Patsavas et al., 2015).

Table 1.2.
Difference (Δ) in calculated CO_2 system parameters based on an uncertainty of 0.011 in pK_2 at two fCO_2 conditions*. The input pair of CO_2 system parameters utilized in each set of calculations is also shown. (Table is adapted from Millero et al. (2006). Copyright Elsevier. Reproduced with permission.)

fCO_2 (µatm)	ΔC_T (µmol kg^{-1}) (A_T,pH)	ΔA_T (µmol kg^{-1}) (C_T,pH)	ΔpH (A_T,C_T)	ΔfCO_2 (µatm) (A_T,C_T)
350	4.9	−5.5	0.008	−5.8
1400	2.2	−2.2	0.006	−17.9

*Calculation inputs: A_T = 2400 µmol kg^{-1}, pH_{SWS} = 8.094, C_T = 2052.3 and 2308.9 µmol kg^{-1} for fCO_2 = 350 and 1400 µatm respectively, at 25 °C and S = 35.

The importance of minimizing the contributions of K_2 uncertainties to parameter calculations is also highlighted in the recent study by Orr et al. (2018). Sensitivity analyses were performed to demonstrate how uncertainties in thermodynamic equilibria contribute to the standard uncertainty of calculated CO_2 system parameters. Calculations of pH and fCO_2 are especially influenced by the uncertainty in K_2 when using the (A_T,C_T) input pair (Fig. 1.5a and 1.5b). Fig. 1.5c shows that the uncertainty in K_2 dominates the uncertainty in calculated [CO_3^{2-}]

regardless of choice of input pair (Orr et al., 2018). These uncertainties in [CO_3^{2-}] are then propagated in calculations of Ω (Fig. 1.5d), which are critical to understanding impacts of ocean acidification on calcifying organisms (Dickson et al., 2007; Cuyler and Byrne, 2018). Importantly, uncertainties in estimates of Ω can significantly change predictions of where calcium carbonate production/dissolution will occur (i.e., where Ω = 1, as discussed in Section 1.3.1).

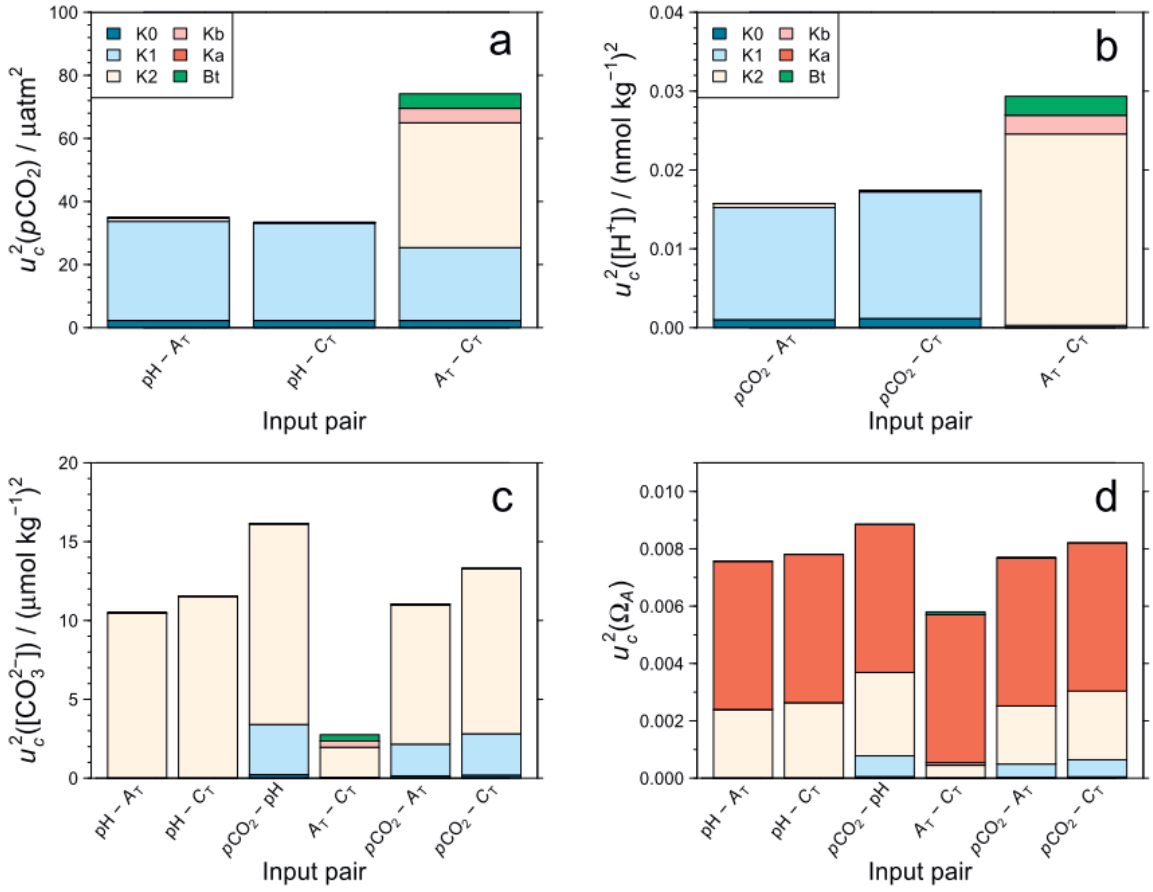

Fig. 1.5. Contributions of uncertainties in thermodynamic equilibria (denoted by colors in upper left corner, where K_a is the solubility product constant for aragonite) to standard squared uncertainty (u^2_c) of calculated (a) pCO_2, (b) $[H^+]$ (representing pH), (c) $[CO_3^{2-}]$, and (d) Ω_A for several combinations of CO_2 system input parameters. (Figure is reproduced from Orr et al. (2018). Reproduced with permission.)

1.4 Ionic strength determinations

1.4.1 Overview

Ionic strength (I), required in descriptions of chemical equilibria, is defined as the sum of charge-weighted ion concentrations present in solution (Lewis and Randall, 1921):

$$I = \tfrac{1}{2} \sum_i m_i z_i^2 \quad (1.7)$$

where m_i and z_i are ion concentrations (mol kg^{-1}) and charges.

Ionic strength is a particularly important contributor to uncertainty in interpretations of chemical equilibria at low ionic strength (i.e., rivers and lakes). The ionic strengths of natural waters are commonly assessed via conductivity measurements, which quantify the ability of solutions to conduct electricity. These measurements typically involve the use of a conductivity probe or other conductometric instrument such as a salinometer. Alternatively, measurement of solution compositions via inductively coupled plasma−mass spectrometry (ICP-MS) can be made, though this technique is extremely time consuming and is therefore not reasonable for most studies.

1.4.2 Uncertainties in conductivity measurements

Conductometric measurements are based on measurements of a solutions' electrical conductivity (κ), which is then converted to an estimate of I. A significant limitation is that dozens of empirical equations have been developed to make this conversion using numerous artificial solutions with varying ions present (McCleskey et al., 2012). Furthermore, because there is a difference between an ion's contribution to ionic strength versus its contribution to conductivity, systematic offsets between the two characterizations can develop. There is no way to a priori estimate these systematic offsets without precise measurements of the concentration of each ion in solution (i.e., via ICP-MS). Importantly, accurate estimates of I are required in models of chemical

equilibria (including K_2), estimates of pH, Ω, etc., but the accuracy of I estimates from conductometric measurements are not well known. There is surprisingly little literature highlighting this problem; the work in Ch. 4 attempts to mitigate such uncertainties and provide a better means of directly measuring ionic strength.

1.5 Overview of dissertation

The primary objective of this dissertation is the utilization of spectrophotometric analytical techniques to improve our understanding of chemical equilibria in natural waters from river to sea. The dissertation is outlined as follows:

Chapter 2, published in *Geochimica et. Cosmochimica Acta*, describes a novel spectrophotometric method developed to determine the bicarbonate dissociation constant, K_2, in seawater for a range of $15 \leq t \leq 35$ °C and $20 \leq S_P \leq 40$. The experimental measurements used for the new K_2 parameterization are far more precise than the measurements reported in previous works. Based on comparisons between measured and calculated CO_2 system parameters, this new K_2 parameterization improves internal consistency relative to other available K_2 equations.

Chapter 3, in preparation for journal submission, describes determinations of K_2 at low temperatures (i.e., $3 \leq t \leq 15$ °C), applicable to polar surface waters and the deep ocean. These analyses required modifications to my Ch. 2 methods in order to maintain high quality spectrophotometric pH measurements at low temperatures. The combination of results from Ch. 2 and 3 provides a new K_2 parameterization for a wide range of open ocean conditions. Ch. 3 also presents the results of NOAA's 2021 West Coast Ocean Acidification (WCOA) Cruise. Internal

consistency assessments highlight that (a) pH should be directly measured (rather than calculated from A_T and C_T), and (b) pH measured at 25 °C can be used to reliably characterize equilibrium parameters (e.g., pH, fCO_2, and Ω) under in situ conditions.

Chapter 4, published in *Analytica Chimica Acta*, describes the development of a novel titration-based conductometric/spectrophotometric method to measure ionic strength of natural fresh waters. This method mitigates systematic errors in traditional ionic strength measurements by (a) improving conductometric ionic strength calibrations and (b) utilizing novel spectrophotometric procedures for measurement of ionic strength.

Chapter 5 summarizes/highlights the findings from this dissertation and describes future directions of study.

1.6 References

Bates, N.R., Astor, Y.M., Church, M.J., Currie, K., Dore, J.E., Gonzalez-Davila, M., Lorenzoni, L., Muller-Karger, F., Olafsson, J., and Santana-Casiano, J.M. (2014) A time-series view of changing surface ocean chemistry due to ocean uptake of anthropogenic CO_2 and ocean acidification. *Oceanography* **27**, 126−141. doi:10.5670/oceanog.2014.16

Byrne, R.H. (2014) Measuring ocean acidification: New technology for a new era of ocean chemistry. *Environ. Sci. Technol*. **48**, 5352−5360. doi:10.1021/es405819p

Cai, W.-J. and Wang, Y. (1998) The chemistry, fluxes, and sources of carbon dioxide in the estuarine waters of the Satilla and Altamaha Rivers, Georgia. *Limnol. Oceanogr*. **43**, 657−668. doi:10.4319/lo.1998.43.4.0657

Caldeira, K. and Wickett, M.E. (2003) Anthropogenic carbon and ocean pH. *Nature* **425**, 365. doi:10.1038/425365a

Carter, B.R., Feely, R.A., Williams, N.L., Dickson, A.G., Fong, M.B., and Takeshita, Y. (2018) Updated methods for global locally interpolated estimation of alkalinity, pH, and nitrate. *Limnol. Oceanogr. Methods* **16**, 119−131. https://doi.org/10.1002/lom3.10232

Clayton, T.D. and Byrne, R.H. (1993) Spectrophotometric seawater pH measurements: Total hydrogen ion concentration scale calibration of m-cresol purple and at-sea results. *Deep Sea Res. Part I. Oceanogr. Res. Papers* **40**, 2115−2129. https://doi.org/10.1016/0967-0637(93)90048-8

Cuyler, E.E. and Byrne, R.H. (2018) Spectrophotometric calibration procedures to enable calibration-free measurements of seawater calcium carbonate saturation states. *Anal. Chim. Acta*. **1020**, 95−103. https://doi.org/10.1016/j.aca.2018.02.071

Dickson, A. and Millero, F.J. (1987) A comparison of the equilibrium constants for the dissociation of carbonic acid in seawater media. *Deep Sea Res. Part A. Oceanogr. Res. Papers* **34**, 1733−1743. https://doi.org/10.1016/0198-0149(87)90021-5

Dickson, A.G., Sabine, C.L., and Christian, J.R. (2007) *Guide to best practices for ocean CO_2 measurements*. PICES Special Publication 3, 191 pp.

Dlugokencky, E. and Tans, P. (2021) Trends in atmospheric carbon dioxide: Global. NOAA/GML. gml.noaa.gov/ccgg/trends/

Edmond, J.M. and Gieskes, J.M.T.M. (1970) On the calculation of the degree of saturation of sea water with respect to calcium carbonate under in situ conditions. *Geochim. Cosmochim. Acta* **34**, 1261−1291. https://doi.org/10.1016/0016-7037(70)90041-4

Feely, R.A., Doney, S.C., and Cooley, S.R. (2009) Ocean acidification: Present conditions and future changes in a high-CO_2 world. *Oceanography* **22**, 36−47. https://doi.org/10.5670/oceanog.2009.95

Feely, R.A., Sabine, C.L., Byrne, R.H., Millero, F.J., Dickson, A.G., Wanninkhof, R., Murata, A., Miller, L.A., and Greeley, D. (2012) Decadal changes in the aragonite and calcite saturation state of the Pacific Ocean. *Glob. Biogeochem. Cycles* **26**, 1−15. https://doi.org/10.1029/2011GB004157

Feely, R.A., Sabine, C.L., Hernandez-Ayon, J.M., Ianson, D., and Hales, B. (2008) Evidence for upwelling of corrosive "acidified" water onto the continental shelf. *Science* **320**, 1490−1492. doi:10.1126/science.1155676

Fong, M.B. and Dickson, A.G. (2019) Insights from GO-SHIP hydrography data into the thermodynamic consistency of CO_2 system measurements in seawater. *Mar. Chem*. **211**, 52−63. https://doi.org/10.1016/j.marchem.2019.03.006

Friedlingstein, P., Jones, M.W., O'Sullivan, M., Andrew, R.M., Bakker, D.C.E., Hauck, J., Le Quéré, C., Peters, G.P., Peters, W., Pongratz, J., Sitch, S., Canadell, J.G., Ciais, P., Jackson, R.B., Alin, S.R., Anthoni, P., Bates, N.R., Becker, M., Bellouin, N., Bopp, L., Chau, T.T.T., Chevallier, F., Chini, L.P., Cronin, M., Currie, K.I., Decharme, B., Djeutchouang, L.M., Dou, X., Evans, W., Feely, R.A., Feng, L., Gasser, T., Gilfillan, D., Gkritzalis, T., Grassi, G., Gregor, L., Gruber, N., Gürses, Ö., Harris, I., Houghton, R.A., Hurtt, G.C., Iida, Y., Ilyina, T., Luijkx, I.T., Jain, A., Jones, S.D., Kato, E., Kennedy, D., Klein Goldewijk, K., Knauer, J., Korsbakken, J.I., Körtzinger, A., Landschützer, P., Lauvset, S.K., Lefèvre, N., Lienert, S., Liu, J., Marland, G., McGuire, P.C., Melton, J.R., Munro, D.R., Nabel, J.E.M.S., Nakaoka, S.I., Niwa, Y., Ono, T., Pierrot, D., Poulter, B., Rehder, G., Resplandy, L., Robertson, E., Rödenbeck, C., Rosan, T.M., Schwinger, J., Schwingshackl, C., Séférian, R., Sutton, A.J., Sweeney, C., Tanhua, T., Tans, P.P., Tian, H., Tilbrook, B., Tubiello, F., van der Werf, G.R., Vuichard, N., Wada, C., Wanninkhof, R., Watson, A.J., Willis, D., Wiltshire, A.J., Yuan, W., Yue, C., Yue, X., Zaehle, S., and Zeng, J. (2022) Global carbon budget 2021. *Earth Syst. Sci. Data* **14**, 1917−2005. doi:10.5194/essd-14-1917-2022

Goyet, C. and Poisson, A. (1989) New determination of carbonic acid dissociation constants in seawater as a function of temperature and salinity. *Deep Sea Res. Part A. Oceanogr. Res. Papers* **36**, 1635−1654. http://dx.doi.org/10.1016/0198-0149(89)90064-2

Gruber, N., Clement, D., Carter, B.R., Feely, R.A., van Heuven, S., Hoppema, M., Ishii, M., Key, R.M., Kozyr, A., Lauvset, S.K., Lo Monaco, C., Mathis, J.T., Murata, A., Olsen, A., Perez, F.F., Sabine, C.L., Tanhua, T., and Wanninkhof, R. (2019) The oceanic sink for anthropogenic CO_2 from 1994 to 2007. *Science* **363**, 1193−1199. doi:10.1126/science.aau5153

Hansson, I. (1973) The determination of the dissociation constants of carbonic acid in synthetic sea water in the salinity range of 20–40‰ and temperature range of 5–30 °C. *Acta. Chem. Scand*. **27**, 931−944. doi:10.3891/acta.chem.scand.27-0931

Harned, H.S. and Davis, R. (1943) The ionization constant of carbonic acid in water and the solubility of carbon dioxide in water and aqueous salt solutions from 0 to 50 °. *J Am. Chem. Soc*. **65**, 2030−2037. doi:10.1021/ja01250a059

IPCC, 2021: Climate Change 2021: The physical science basis. Contribution of Working Group I to the Sixth Assessment Report of the Intergovernmental Panel on Climate Change [Masson-Delmotte, V., Zhai, P., Pirani, A., Connors, S.L., Péan, C., Berger, S., Caud, N., Chen, Y., Goldfarb, L., Gomis, M.I., Huang, M., Leitzell, K., Lonnoy, E., Matthews, J.B.R., Maycock, T.K., Waterfield, T., Yelekçi, O., Yu, R., and Zhou, B. (eds.)]. Cambridge University Press. In Press.

Jiang, L.-Q., Carter, B.R., Feely, R.A., Lauvset, S.K., and Olsen, A. (2019) Surface ocean pH and buffer capacity: Past, present and future. *Sci. Rep*. **9**, 18624. https://doi.org/10.1038/s41598-019-55039-4

Johnson, G., Lumpkin, R., Alin, S., Amaya, D., Baringer, M., Boyer, T., Brandt, P., Carter, B., Cetinić, I., Chambers, D., Cheng, L., Collins, A., Cosca, C., Domingues, R., Dong, S., Feely, R., Frajka-Williams, E., Franz, B., Gilson, J., and Zhang, H.-M. (2021) Global oceans. *Bull. Amer. Meteorol. Soc*. **102**, S143−S198. doi:10.1175/BAMS-D-21-0083.1

Keeling, C.D., Bacastow, R.B., Bainbridge, A.E., Ekdahl Jr, C.A., Guenther, P.R., Waterman, L.S., and Chin, J.F.S. (1976) Atmospheric carbon dioxide variations at Mauna Loa Observatory, Hawaii. *Tellus* **28**, 538−551. doi:10.3402/tellusa.v28i6.11322

Le Quéré, C., Andrew, R.M., Friedlingstein, P., Sitch, S., Hauck, J., Pongratz, J., Pickers, P.A., Korsbakken, J.I., Peters, G.P., Canadell, J.G., Arneth, A., Arora, V.K., Barbero, L., Bastos, A., Bopp, L., Chevallier, F., Chini, L.P., Ciais, P., Doney, S.C., Gkritzalis, T., Goll, D.S., Harris, I., Haverd, V., Hoffman, F.M., Hoppema, M., Houghton, R.A., Hurtt, G., Ilyina, T., Jain, A.K., Johannessen, T., Jones, C.D., Kato, E., Keeling, R.F., Goldewijk, K.K., Landschützer, P., Lefèvre, N., Lienert, S., Liu, Z., Lombardozzi, D., Metzl, N., Munro, D.R., Nabel, J.E.M.S., Nakaoka, S.I., Neill, C., Olsen, A., Ono, T., Patra, P., Peregon, A., Peters, W., Peylin, P., Pfeil, B., Pierrot, D., Poulter, B., Rehder, G., Resplandy, L., Robertson, E., Rocher, M., Rödenbeck, C., Schuster, U., Schwinger, J., Séférian, R., Skjelvan, I., Steinhoff, T., Sutton, A., Tans, P.P., Tian, H., Tilbrook, B., Tubiello, F.N., van der Laan-Luijkx, I.T., van der Werf, G.R., Viovy, N., Walker, A.P., Wiltshire, A.J., Wright, R., Zaehle, S., and Zheng, B. (2018) Global carbon budget 2018. *Earth Syst. Sci. Data* **10**, 2141−2194. doi:10.5194/essd-10-2141-2018

Lee, K., Millero, F.J., Byrne, R.H., Feely, R.A., and Wanninkhof, R. (2000) The recommended dissociation constants for carbonic acid in seawater. *Geophys. Res. Lett.* **27**, 229−232. doi:10.1029/1999gl002345

Lewis, G.N. and Randall, M. (1921) The activity coefficient of strong electrolytes. *J. Am. Chem. Soc*. **43**, 1112−1154. https://doi.org/10.1021/ja01438a014

Lueker, T.J., Dickson, A.G., and Keeling, C.D. (2000) Ocean pCO_2 calculated from dissolved inorganic carbon, alkalinity, and equations for K_1 and K_2: Validation based on laboratory measurements of CO_2 in gas and seawater at equilibrium. *Mar. Chem.* **70**, 105−119. https://doi.org/10.1016/S0304-4203(00)00022-0

McCleskey, R.B., Nordstrom, D.K., and Ryan, J.N. (2012) Comparison of electrical conductivity calculation methods for natural waters. *Limnol. Oceanogr. Methods* **10**, 952−967. https://doi.org/10.4319/lom.2012.10.952

McElligott, S., Byrne, R., Lee, K., Wanninkhof, R., Millero, F., and Feely, R. (1998) Discrete water column measurements of CO_2 fugacity and pH_T in seawater: A comparison of direct measurements and thermodynamic calculations. *Mar. Chem.* **60**, 63−73. https://doi.org/10.1016/S0304-4203(97)00080-7

Mehrbach, C., Culberson, C., Hawley, J., and Pytkowicx, R. (1973) Measurement of the apparent dissociation constants of carbonic acid in seawater at atmospheric pressure. *Limnol. Oceanogr*. **18**, 897−907. https://doi.org/10.4319/lo.1973.18.6.0897

Millero, F.J. (2010) Carbonate constants for estuarine waters. *Mar. Freshw. Res*. **61**, 139−142. doi:10.1071/MF09254

Millero, F.J., Graham, T.B., Huang, F., Bustos-Serrano, H., and Pierrot, D. (2006) Dissociation constants of carbonic acid in seawater as a function of salinity and temperature. *Mar. Chem.* **100**, 80−94. doi:10.1016/j.marchem.2005.12.001

Millero, F.J., Pierrot, D., Lee, K., Wanninkhof, R., Feely, R., Sabine, C.L., Key, R.M., and Takahashi, T. (2002) Dissociation constants for carbonic acid determined from field measurements. *Deep Sea Res. Part I. Oceanogr. Res. Papers* **49**, 1705−1723. https://doi.org/10.1016/S0967-0637(02)00093-6

Mojica Prieto, F.J. and Millero, F.J. (2002) The values of $pK_1 + pK_2$ for the dissociation of carbonic acid in seawater. *Geochim. Cosmochim. Acta* **66**, 2529−2540. https://doi.org/10.1016/S0016-7037(02)00855-4

Mook, W.G. and Koene, B.K.S. (1975) Chemistry of dissolved inorganic carbon in estuarine and coastal brackish waters. *Estuar. Coast. Mar. Sci*. **3**, 325−336. https://doi.org/10.1016/0302-3524(75)90032-8

Orr, J.C., Epitalon, J.-M., Dickson, A.G., and Gattuso, J.-P. (2018) Routine uncertainty propagation for the marine carbon dioxide system. *Mar. Chem.* **207**, 84−107. https://doi.org/10.1016/j.marchem.2018.10.006

Orr, J.C., Epitalon, J.-M., and Gattuso, J.-P. (2015) Comparison of ten packages that compute ocean carbonate chemistry. *Biogeosciences* **12**, 1483−1510. https://doi.org/10.5194/bg-12-1483-2015

Orr, J.C., Fabry, V.J., Aumont, O., Bopp, L., Doney, S.C., Feely, R.A., Gnanadesikan, A., Gruber, N., Ishida, A., Joos, F., Key, R.M., Lindsay, K., Maier-Reimer, E., Matear, R., Monfray, P., Mouchet, A., Najjar, R.G., Plattner, G.K., Rodgers, K.B., Sabine, C.L., Sarmiento, J.L., Schlitzer, R., Slater, R.D., Totterdell, I.J., Weirig, M.F., Yamanaka, Y., and Yool, A. (2005) Anthropogenic ocean acidification over the twenty-first century and its impact on calcifying organisms. *Nature* **437**, 681−686. doi:10.1038/nature04095

Papadimitriou, S., Loucaides, S., Rérolle, V.M.C., Kennedy, P., Achterberg, E.P., Dickson, A.G., Mowlem, M., and Kennedy, H. (2018) The stoichiometric dissociation constants of carbonic acid in seawater brines from 298 to 267 K. *Geochim. Cosmochim. Acta* **220**, 55−70. https://doi.org/10.1016/j.gca.2017.09.037

Patsavas, M.C., Byrne, R.H., Wanninkhof, R., Feely, R.A., and Cai, W.-J. (2015) Internal consistency of marine carbonate system measurements and assessments of aragonite saturation state: Insights from two US coastal cruises. *Mar. Chem*. **176**, 9−20. https://doi.org/10.1016/j.marchem.2015.06.022

Penman, D.E., Hönisch, B., Zeebe, R.E., Thomas, E., and Zachos, J.C. (2014) Rapid and sustained surface ocean acidification during the Paleocene-Eocene Thermal Maximum. *Paleoceanography* **29**, 357−369. doi:10.1002/2014PA002621

Pierrot, D., Lewis, E., and Wallace, D. (2006) CO2SYS DOS Program developed for CO_2 system calculations. *ORNL/CDIAC-105*. Carbon Dioxide Inf. Anal. Cent., Oak Ridge Natl. Lab., US Dept. of Energy, Oak Ridge, TN.

Roy, R.N., Roy, L.N., Vogel, K.M., Porter-Moore, C., Pearson, T., Good, C.E., Millero, F.J., and Campbell, D.M. (1993) The dissociation constants of carbonic acid in seawater at salinities 5 to 45 and temperatures 0 to 45 °C. *Mar. Chem*. **44**, 249−267. http://dx.doi.org/10.1016/0304-4203(93)90207-5

Schlunegger, S., Rodgers, K.B., Sarmiento, J.L., Frölicher, T.L., Dunne, J.P., Ishii, M., and Slater, R. (2019) Emergence of anthropogenic signals in the ocean carbon cycle. *Nat. Clim. Change* **9**, 719−725. doi:10.1038/s41558-019-0553-2

Schockman, K.M. and Byrne, R.H. (2021) Spectrophotometric determination of the bicarbonate dissociation constant in seawater. *Geochim. Cosmochim. Acta* **300**, 231−245. https://doi.org/10.1016/j.gca.2021.02.008

Sulpis, O., Lauvset, S.K., and Hagens, M. (2020) Current estimates of K_1* and K_2* appear inconsistent with measured CO_2 system parameters in cold oceanic regions. *Ocean Sci*. **16**, 847−862. doi:10.5194/os-16-847-2020

Van Heuven, S., Pierrot, D., Rae, J., Lewis, E., and Wallace, D. (2011) MATLAB program developed for CO_2 system calculations. *ORNL/CDIAC-105b.* Carbon Dioxide Inf. Anal. Cent., Oak Ridge Natl. Lab., US Dept. of Energy, Oak Ridge, TN.

Wanninkhof, R., Lewis, E., Feely, R.A., and Millero, F.J. (1999) The optimal carbonate dissociation constants for determining surface water pCO_2 from alkalinity and total inorganic carbon. *Mar. Chem.* **65**, 291−301. https://doi.org/10.1016/S0304-4203(99)00021-3

Waters, J., Millero, F.J., and Woosley, R. (2014) Corrigendum to "The free proton concentration scale for seawater pH", [MARCHE: 149 (2013) 8−22]. *Mar. Chem*. **165**, 66−67. https://doi.org/10.1016/j.marchem.2014.07.004

Waters, J.F. and Millero, F.J. (2013) The free proton concentration scale for seawater pH. *Mar. Chem*. **149**, 8−22. https://doi.org/10.1016/j.marchem.2012.11.003

Williams, N.L., Juranek, L.W., Feely, R.A., Johnson, K.S., Sarmiento, J.L., Talley, L.D., Dickson, A.G., Gray, A.R., Wanninkhof, R., Russell, J.L., Riser, S.C., and Takeshita, Y. (2017) Calculating surface ocean pCO_2 from biogeochemical Argo floats equipped with pH: An uncertainty analysis. *Glob. Biogeochem. Cycles* **31**, 591−604. doi:10.1002/2016GB005541

Woosley, R.J. (2021) Evaluation of the temperature dependence of dissociation constants for the marine carbon system using pH and certified reference materials. *Mar. Chem.* **229**, 103914. https://doi.org/10.1016/j.marchem.2020.103914

Woosley, R.J., Millero, F.J., and Takahashi, T. (2017) Internal consistency of the inorganic carbon system in the Arctic Ocean. *Limnol. Oceanogr. Methods* **15**, 887−896. doi:10.1002/lom3.10208

Wu, H.C., Dissard, D., Douville, E., Blamart, D., Bordier, L., Tribollet, A., Le Cornec, F., Pons-Branchu, E., Dapoigny, A., and Lazareth, C.E. (2018) Surface ocean pH variations since 1689 CE and recent ocean acidification in the tropical South Pacific. *Nat. Commun*. **9**, 2543. doi:10.1038/s41467-018-04922-1

CHAPTER TWO:

SPECTROPHOTOMETRIC DETERMINATION OF THE BICARBONATE DISSOCIATION CONSTANT IN SEAWATER

Note: This chapter has been reprinted (adapted) with permission from:

Schockman, K.M and Byrne, R.H. (2021) Spectrophotometric determination of the bicarbonate dissociation constant in seawater. *Geochim. Cosmochim. Acta*. **300**, 231−245.

Copyright 2021 Elsevier.

2.1 Abstract

The aqueous carbon dioxide (CO_2) system stoichiometric dissociation constants K_1 and K_2 express the relative concentrations of CO_2, HCO_3^- (bicarbonate), and CO_3^{2-} (carbonate) in terms of pH. These constants are critical in the study of seawater and the oceans because any mathematical expression that relates the four major CO_2 system parameters (pH, here expressed on the total hydrogen ion concentration scale, pH_T; total dissolved inorganic carbon, C_T; total alkalinity, A_T; and CO_2 fugacity, fCO_2) requires the use of K_1 and K_2. Uncertainties associated with current characterizations of pK_1 and pK_2 (where $pK = -\log K$), on the order of 0.01 and 0.02, limit the accuracy of marine CO_2 system calculations. This work reports the results of a spectrophotometric method to experimentally determine the product K_1K_2 over environmentally relevant ranges of temperature ($288.15 \leq T \leq 308.15$ K) and salinity ($19.6 \leq S_P \leq 41$) where S_P denotes the practical salinity scale. Using previously published parameterizations of K_1, values of pK_2 could then be calculated from the new K_1K_2 values. The resulting set of pK_2 values was fitted

as a function of S_P and T to obtain a new pK_2 parameterization (denoted as $_{SW}pK_2$) calculated with the K_1 of Waters and Millero (2013) as revised by Waters et al. (2014):

$$_{SW}pK_2 = 116.8067 - 3655.02\ T^{-1} - 16.45817 \ln T + 0.04523\ S_P - 0.615\ S_P^{0.5} - 0.0002799\ S_P^2 + 4.969\ (S_P/T)$$

The average root mean square deviation between the equation and the observed data is 0.003. Residuals of this pK_2 fitting function (i.e., measured pK_2 minus parameterized pK_2) are substantially smaller than the residuals obtained in previous works. Similarly, the total standard uncertainty in pK_2 is reduced from 0.015 (previous characterizations) to 0.010 (this work). Internal consistency assessments (comparisons of measured versus calculated values of A_T, C_T, pH_T, and fCO_2) were used to evaluate the computational utility of the new K_2 parameterization. Assessments from both laboratory and shipboard data indicate that the internal consistency of CO_2 system calculations is improved using the K_2 parameterization of this work. This new K_2 parameterization provides the most precise, and potentially the most accurate, bicarbonate dissociation constant characterization presently available for open ocean conditions.

2.2 Introduction

Throughout the industrial era (1750s to present), approximately 30% of anthropogenic carbon dioxide (CO_2) emissions has been absorbed by the world's oceans (Le Quéré et al., 2018; Gruber et al., 2019). The resulting increase of CO_2 in ocean seawater has changed its chemical composition by decreasing pH by approximately 0.1 over this time period and lowering carbonate ion concentration (Caldeira and Wickett, 2003; Bates et al., 2014; Byrne, 2014). Consistent with this extent of ocean acidification, decreases in the calcium carbonate ($CaCO_3$) saturation states of seawater ($\Omega_{calcite}$ and $\Omega_{aragonite}$) have begun to negatively affect calcifying organisms (Riebesell et

al., 2000; Feely et al., 2004; Doney et al., 2012; Wittmann and Pörtner, 2013). Changes in the CO_2 system have also led to regional variations in the buffer capacity of seawater (Carter et al., 2017; Woosley, 2018). Additionally, increased warming and changing ocean circulation have caused fluctuations in the oceanic uptake of atmospheric CO_2 over time, with the magnitude of CO_2 fluxes in or out of the ocean varying not only through time but also by oceanic region (Gruber et al., 2019).

The CO_2 system in seawater includes dissolved carbon dioxide ($CO_2^* = CO_{2\,(aq)} + H_2CO_3$), bicarbonate ($HCO_3^-$), and carbonate ($CO_3^{2-}$). Constituent equilibria that involve the exchange of H^+ ions are:

$$CO_2^* + H_2O \leftrightarrow HCO_3^- + H^+ \tag{2.1}$$

$$HCO_3^- \leftrightarrow CO_3^{2-} + H^+ \tag{2.2}$$

These equilibria constitute the ocean's principal pH buffering mechanism.

The seawater CO_2 system can be described using four measurable parameters: total alkalinity (A_T), total dissolved inorganic carbon (C_T), pH, and CO_2 fugacity (fCO_2). The first three are defined as follows:

$$A_T = [HCO_3^-]_T + 2[CO_3^{2-}]_T + [B(OH)_4^-]_T + [OH^-]_T - [H^+]_T + 2[PO_4^{3-}]_T + [HPO_4^{2-}]_T + \ldots \tag{2.3}$$

$$C_T = [CO_3^{2-}]_T + [HCO_3^-]_T + [CO_2^*] \tag{2.4}$$

$$pH_T = -\log [H^+]_T \tag{2.5}$$

The subscripted brackets ($[\ ]_T$) generally denote free plus ion-paired concentrations (where concentration is measured in mol kg-soln^{-1}), whereas $[H^+]_T$ denotes the sum of free hydrogen and bisulfate ions, pH_T denotes pH on the total hydrogen ion concentration scale, and the ellipses in eq. (2.3) and throughout indicate additional terms of generally smaller quantitative importance.

For eq. (2.3), these excluded species may add uncertainty in the accuracy of calculated carbonate alkalinity.

Measurement of any two of the four parameters allows for calculation of all other CO_2 system parameters via thermodynamic relationships. Essentially all descriptions of CO_2 system parameters at in situ conditions require thermodynamic models. For example, pH_T at in situ conditions can be calculated through an iterative approach from C_T and A_T:

$$A_T = C_T\left(\frac{2K_1K_2+K_1[H^+]_T}{K_1K_2+K_1[H^+]_T+[H^+]_T^{\,2}}\right)+B_T\left(\frac{K_B}{K_B+[H^+]_T}\right)+K_w[H^+]_T^{\,-1}-[H^+]_T+\ldots \quad (2.6)$$

where additional terms of minor importance are omitted for simplicity. B_T is the total boron concentration, K_B and K_W are equilibrium constants that describe the dissociation of boric acid and water, and K_1 and K_2 are stoichiometric equilibrium constants appropriate to the equilibria shown in eq. (2.1–2.2), defined as follows:

$$K_1 = \frac{[HCO_3^{\,-}]_T[H^+]_T}{[CO_2^{\,*}]} \quad (2.7)$$

$$K_2 = \frac{[CO_3^{\,2-}]_T[H^+]_T}{[HCO_3^{\,-}]_T} \quad (2.8)$$

where $[H^+]_T$ is expressed on the total hydrogen ion concentration scale. The use of eq. (2.6) to accurately derive in situ $[CO_3^{2-}]_T$ and other CO_2 system parameters (e.g., $\Omega_{calcite}$, $\Omega_{aragonite}$, fCO_2, or pH_T) requires an accurate account of the dependencies of relevant dissociation constants (K_1, K_2, K_B, and K_W) on salinity (S), temperature (t in °C or T in K), and pressure (P) (Fong and Dickson, 2019).

Over-determination of the system (i.e., where three or more CO_2 system parameters are measured for a single seawater sample) allows for comparisons of measured and calculated values of the same parameter and, as such, evaluations of its internal consistency. Current models that

relate A_T, C_T, pH_T, and fCO_2 are not internally consistent (e.g., A_T (measured) ≠ A_T (calculated) from C_T and pH_T) (Patsavas et al., 2015; Fong and Dickson, 2019). Furthermore, the differences between calculated and measured parameters are larger than what would be expected based on previously reported measurement accuracies and precisions (Mojica Prieto and Millero, 2002; Millero et al., 2006). Accurate characterizations of the dissociation constants K_1 and K_2 are arguably the most critically important elements for obtaining internal consistency and, thereby, accurate predictions of in situ parameters.

Throughout the past several decades, extensive effort has been devoted to experimentally determine stoichiometric carbonic acid dissociation constants over ranges of S and T (Hansson, 1973; Mehrbach et al., 1973; Goyet and Poisson, 1989; Roy et al., 1993; Millero et al., 2002; Mojica Prieto and Millero, 2002; Millero et al., 2006; Papadimitriou et al., 2018). Still, the K_1 and K_2 parameterizations obtained in these studies produced calculated values of CO_2 system parameters that do not agree within the estimated parameter uncertainties (Dickson and Millero, 1987; Lee et al., 2000). Uncertainties for pK_1 and pK_2 (where $pK = -\log K$) have been recently estimated as 0.0075 and 0.015, respectively (Orr et al., 2018). Based on internal consistency checks, several publications have concluded that the K_1 and K_2 values of Mehrbach et al. (1973), as refit by Dickson and Millero (1987) on the seawater pH scale (SWS) and refit by Lueker et al. (2000) on the total hydrogen ion concentration pH scale (pH_T), provide the most internally consistent characterizations to date (Lee et al., 1996; Wanninkhof et al., 1999; Lee et al., 2000; Lueker et al., 2000; Patsavas et al., 2015). Notably, however, the study of Sulpis et al. (2020) found that the parameterizations of Lueker et al. (2000) overestimate K_1 and K_2 at low temperatures, and an overall lack of agreement between sets of constants led Naviaux et al. (2019) to recommend that new values of K_1 and K_2 be evaluated. Waters and Millero (2013), as revised by Waters et al.

(2014), used a Pitzer model to refit data from Mehrbach et al. (1973), Mojica Prieto and Millero (2002), and Millero et al. (2006) to provide an updated set of K_1 and K_2 parameterizations, but a thorough assessment of internal consistency with these parameterizations has not been carried out.

Most previous characterizations of K_1 and K_2 have relied on acid titrations and, consequently, are dependent on accurate assessments of several additional chemical parameters. These parameters include the boron/salinity ratio (B_T/S) (which currently has a relative uncertainty on the order of 2–3% (Orr et al., 2018; Fong and Dickson, 2019)), as well as K_B, K_W, and the concentrations and dissociation characteristics of all minor acid/base pairs in solution. Experimental determinations of the product K_1K_2, used by Mehrbach et al. (1973) and Mojica Prieto and Millero (2002), do not require acid titrations and furthermore are largely independent of several chemical parameter characteristics (B_T/S, K_B, K_W, minor acid/base pairs). This method is dependent on measured pH (as described below in Section 2.5) and, notably, has previously involved the use of either potentiometric methods or spectrophotometric measurements with unpurified pH indicators (Mehrbach et al., 1973; Mojica Prieto and Millero, 2002) — methods that can now be improved upon. Spectrophotometric pH measurements have a precision of approximately ±0.001 pH units or better (Yao and Byrne, 2001) and do not require periodic calibrations. The enhanced simplicity of spectrophotometric methods, compared to potentiometric methods, removes many systematic errors and is thereby conducive to improved accuracy.

In the present work, spectrophotometric procedures for measuring pH_T with a purified pH indicator are used to experimentally determine K_2 following the general procedures of Mehrbach et al. (1973). Use of the same procedures for measuring pH_T in field studies and for characterizing pK_2 (as in this work) enables improved CO_2 system assessments throughout the world's oceanic, estuarine, and riverine environments.

2.3 Theory

The fundamental CO_2 system relationship that expresses A_T in terms of C_T and $[H^+]_T$ is shown in eq. (2.6). Addition of a carbonate/bicarbonate salt to a mixture of seawater and added indicator dye at constant pH without diluting the solution is then appropriately described by:

$$A_T + A_T' = (C_T + C_T')\left(\frac{2K_1K_2 + K_1[H^+]_T}{K_1K_2 + K_1[H^+]_T + [H^+]_T^2}\right) + \Psi \quad (2.9)$$

where A_T' and C_T' are the A_T and C_T added via the salt. The term Ψ gives the non-carbonate alkalinity terms:

$$\Psi = B_T\left(\frac{K_B}{K_B + [H^+]_T}\right) + K_w[H^+]_T^{-1} - [H^+]_T + \cdots \quad (2.10)$$

where the ellipsis denotes terms of less importance (phosphate, silicate, indicator dye, etc.). When addition of the salt leads to negligible change in $[H^+]_T$ without significant modification of the solution, the non-carbonate alkalinity terms (eq. (2.10)) remain constant as well.

The difference between eqs. (2.6) and (2.9) before and after a salt addition at constant $[H^+]_T$ is given by:

$$A_T' = C_T'\left(\frac{2K_1K_2 + K_1[H^+]_T}{K_1K_2 + K_1[H^+]_T + [H^+]_T^2}\right) \quad (2.11)$$

The C_T'/A_T' ratio of added salt is termed as Φ:

$$\Phi = \frac{C_T'}{A_T'} = \left(\frac{K_1K_2 + K_1[H^+]_T + [H^+]_T^2}{2K_1K_2 + K_1[H^+]_T}\right) \quad (2.12)$$

This term can be experimentally determined via laboratory procedures (Mehrbach et al., 1973).

Eq. (2.12) can be rearranged (Mehrbach et al., 1973) to provide a relationship in which the product of K_1 and K_2 is expressed in terms of Φ and pH:

$$K_1K_2 = \frac{10^{-2pH} + (1 - \Phi)K_1 10^{-pH}}{2\Phi - 1} \quad (2.13)$$

This equation provides the basis for the experimental measurements in this study. A salt with an experimentally defined value of Φ is added to seawater to determine pH values at which pH remains constant within the precision of the measurement. Eq. (2.13) is used to determine K_2 from spectrophotometric measurements of pH and Φ in conjunction with independent experimental determinations of K_1.

A pure bicarbonate salt contributes equally to added C_T' and A_T', whereby $\Phi = 1$ ($A_T/C_T = 1$ in both the initial and the final solution). In this case, eq. (2.13) reduces to the following expression:

$$pH^0_{(\Phi=1)} = \tfrac{1}{2} (pK_1 + pK_2) \quad (2.14)$$

where pH^0 denotes a pH at which no pH change occurs with the addition of a specified salt (i.e., a salt with a specified Φ value). In eq. (2.14), $pH^0_{(\Phi=1)}$ is the arithmetic average of pK_1 and pK_2, and this value, like all pK values, depends on S, T, and P (Mehrbach et al., 1973). At $pH^0_{(\Phi=1)}$, approximately 95% of the C_T in seawater exists as HCO_3^-, and the minor forms, CO_2^* and CO_3^{2-}, have identical concentrations. Hence, the addition of pure sodium bicarbonate salt ($NaHCO_3$) to a solution at $pH^0_{(\Phi=1)}$ will not change the pH of the solution (Mehrbach et al., 1973).

2.4 Materials

2.4.1 Chemicals and reagents

Natural seawater was periodically collected offshore in the Gulf of Mexico and stored in sealed flint glass carboy containers to prevent evaporation. Chemicals used in the experiments included $NaHCO_3$ (Alfa Aesar Puratronic©, 99.998% metal basis, Lots 25312B, T03F021, and T18F042), $KHCO_3$ (Honeywell, ≥99.95% trace metals basis, 99.7–100.5% dry basis, Lot MKBT3696V), and pure CO_2 gas (Air Products, anaerobe grade). Adjustments to seawater pH

were made using 1 N HCl (Fisher Chemical, CAS 7647-01-0) or 1 N NaOH (Fisher Chemical, CAS 1310-73-2). The sulfonephthalein indicator, meta-cresol purple (mCP) (10 mM in 0.7 M NaCl), purified at the University of South Florida, was used for the spectrophotometric pH measurements (Liu et al., 2011).

2.4.2 Equipment

All pH measurements were carried out spectrophotometrically using a diode array spectrophotometer (Agilent 8453) with the UV lamp turned off. Sample absorbances were measured in two-port 10 cm cylindrical optical glass spectrophotometric cells that were periodically cleaned with HCl to prevent buildup of residue. Acid and base additions were made using Research grade PhysioCare concept pipettes (10 µL or 2.5 µL) obtained from Eppendorf Research. mCP was added with a 2 mL Gilmont micrometer buret (GS-1200). Salinity measurements were performed conductometrically with a Guildline Portasal salinometer (Model 8410) on the practical salinity scale (S_P).

A recirculating water bath (Fisher Scientific Isotemp 3013) connected to a water-jacketed cell holder inside the spectrophotometer was used to control the temperature of the spectrophotometric cells during measurements. An additional recirculating water bath (Lauda Model E100) connected to a custom-made cell warmer was used to pre-equilibrate samples in the spectrophotometric cells before measurements in the spectrophotometer. A digital handheld thermometer (Ertco-Eutechnics Model 4400) was used to measure the temperature of the cell contents (±0.025 °C) for all experiments. This handheld thermometer was calibrated against a quartz thermometer (Hewlett Packard Model 2804 A) throughout the duration of the experiments (approximately two years).

2.5 Methods

2.5.1 Purification of solids

Following the guidelines of Kolthoff and Stenger (1964), $NaHCO_3$ and $KHCO_3$ solids were purified by bubbling a slurry of each salt (approximately 0.5–1 g) in Milli-Q water (18.2 MΩ) under an atmosphere of pure CO_2 gas for several hours at room temperature. The purified solid was dried under an atmosphere of pure CO_2 gas prior to use on the same day, producing one batch of the solid. Each batch of purified solid was individually produced from the original salt Lots (provided in Section 2.4.1).

2.5.2 Spectrophotometric determinations of pH changes

The procedure for measuring pH^0 values was developed and modified from the original methods of Mehrbach et al. (1973); the major difference was our use of spectrophotometric pH measurements rather than potentiometric pH methods. The spectrophotometric measurements were made following the guidelines of Clayton and Byrne (1993) and Dickson et al. (2007). Baseline absorbance measurements were first obtained at 578 and 434 nm (absorbance maxima of the basic and acidic forms of mCP) as well as at 730 nm (a non-absorbing wavelength of mCP). After the addition of purified mCP indicator stock solution (10 μL) to the spectrophotometric cell, the cell was returned to the spectrophotometer and allowed to equilibrate for at least 30 seconds before absorbance measurements were taken again at the same three wavelengths. After small baseline corrections were made using the non-absorbing wavelength (Byrne, 1987; Clayton and Byrne, 1993; Liu et al., 2011), the ratios of absorbances at 578 and 434 nm were used to calculate seawater pH on the total scale via the mCP parameterization of Müller and Rehder (2018). The use of this mCP-based pH parameterization (rather than that of Liu et al. (2011)) facilitates future

extension of the pK_2 parameterization/characterization to salinities as low as 0. It should be noted, however, that the pH^0 results obtained in our work can be used to produce pK_2 parameterizations using alternative characterizations of the physical/chemical behavior of mCP. Additionally, no dye perturbation corrections were used in this work because, for the experiments detailed in Section 2.5.3, it was necessary to determine the pH of the pH-adjusted seawater (using mCP) at which $NaHCO_3$ addition caused no pH change rather than characterizing the pH of the original indicator-free seawater.

The salinities of the original seawater batches (i.e., seawater periodically collected offshore) were adjusted (by evaporation or addition of Milli-Q water) to yield nine batches with salinities within the range of $19.6 \leq S_P \leq 41$. These "modified" seawater batches were prepared throughout the duration of experiments (approximately two years) immediately prior to use. Each morning, seawater from a specified "modified" seawater batch was siphoned into spectrophotometric cells (approximately 8–15 cells each day) and then pre-equilibrated for at least 30 minutes in the custom-made cell warmer to achieve a final temperature within the range of $15 \leq t \leq 35$ °C. After a preliminary pH measurement (the process of which is described in the paragraph above), the pH of each sample was iteratively adjusted with small additions of HCl or NaOH as guided by repeated spectrophotometric measurements of pH (using the same initial background absorbance values), to achieve a pH near the expected equilibrium pH^0 appropriate to the sample's S_P and T. At this point, five replicate pH measurements were made, and the average was termed $pH_{initial}$ (i.e., the pH prior to addition of $NaHCO_3$). (Because Na^+ and Cl^- are major constituents of seawater, the additions of acid and base do not significantly alter the composition of seawater, and potential impurities such as bicarbonate or carbonate in the NaOH are inconsequential because they were already present at significantly higher natural levels in the

seawater samples.) Purified $NaHCO_3$ solid (approximately 0.075 g) was then added to the sample and the pH was measured again (five replicate samples), with the average providing pH_{final}. Only a small percentage of the added solid actually dissolved, and the remaining portion was allowed to quickly fall to the bottom of the spectrophotometric cell below the light path of the instrument. The temperature of the cell contents was then measured with the digital thermometer. Comparison of $pH_{initial}$ and pH_{final} established whether the sample pH increased, decreased, or did not change upon addition of $NaHCO_3$. The entire process for one sample typically took less than 30 minutes.

This procedure was then repeated using the remaining spectrophotometric cells in the cell-warmer by adjusting the $pH_{initial}$ value to be incrementally closer to the specific pH^0 value at which $NaHCO_3$ addition causes no pH change (i.e., the pH at which $pH_{final} = pH_{initial}$). The entire daily process (i.e., one set of spectrophotometric cells filled with a specific "modified" seawater batch and pH changes observed using one batch of purified $NaHCO_3$) was performed at least five times for each specified seawater (S_P, T) pair. This process resulted in approximately 1,400 $NaHCO_3$ additions for 26 pairs of S_P and T conditions between $19.6 \leq S_P \leq 41$ and $288.15 \leq T \leq 308.15$ K.

2.5.3 Calculation of pH^0

When $pH > pH^0$, addition of $NaHCO_3$ would be expected to lower the sample pH. When $pH < pH^0$, that addition would be expected to increase sample pH. Values of pH^0 could thus be calculated for each of the 26 (S_P, T) pairs by determining (a) the lowest $pH_{initial}$ for which the $NaHCO_3$ addition lowered the pH (this is the lowest pH value for which $pH_{initial} > pH^0$) and (b) the highest $pH_{initial}$ for which the $NaHCO_3$ addition increased the pH (this is the highest pH value for which $pH_{initial} < pH^0$). As such, this process identified pH values very slightly greater than pH^0 and very slightly smaller than pH^0. Measurements of $pH_{initial}$ were performed with five or more batches

of $NaHCO_3$ for each (S_P, T) pair until the difference between (a) and (b) was within 0.005 pH units (this process typically took around 30 samples). The average of these two $pH_{initial}$ values (which were not required to be from the same batch of $NaHCO_3$) is referred to as $pH^0_{i(avg)}$. A second pH^0 value was also calculated for each (S_P, T) pair by averaging the pH_{final} associated with observation (a) and the pH_{final} associated with observation (b). This pH_{final} average is referred to as $pH^0_{f(avg)}$. As a quality check, $pH^0_{i(avg)}$ and $pH^0_{f(avg)}$ were required to be within ±0.001; otherwise additional measurements (i.e., using an additional set of spectrophotometric cells filled with seawater and an additional batch of purified $NaHCO_3$) were carried out until this was achieved. Finally, the overall average of the four measurements was calculated and denoted as pH^0. Thus, the calculation of each pH^0 was based on two separate sets of pH measurements (one before and one after $NaHCO_3$ addition). This pH^0 value is, as noted previously, functionally dependent on S_P and T. The resulting 26 sets of $pH_{initial}$, pH_{final}, $pH^0_{i(avg)}$, and $pH^0_{f(avg)}$ values are provided in Table B.1.1 of Appendix B.1.

2.5.4 Assessment of $NaHCO_3$ purity (Φ)

$NaHCO_3$ (rather than the primary standard, potassium bicarbonate ($KHCO_3$)) was used in the pH^0 experiments because $NaHCO_3$ dries more rapidly than $KHCO_3$ under an atmosphere of $CO_{2(g)}$ and is therefore more convenient for daily use. Purity of the $NaHCO_3$ solid was assessed by comparison with $KHCO_3$, according to principles described in Kolthoff and Stenger (1964). Because $KHCO_3$ is a primary standard, the Φ value for this solid is, by definition, 1. Therefore, a comparison of pH^0 values obtained with $NaHCO_3$ and this primary standard will indicate any contamination of $NaHCO_3$ that needs to be accounted for. The method for assessing the purity of $NaHCO_3$ was modified from experiments described in Mehrbach et al. (1973), with these primary

differences: we used natural seawater (instead of 0.72 molal NaCl) and we obtained five replicates of the purity experiments to span the salinity range between $19.6 \leq S_P \leq 41$ (rather than a single experiment at one salinity). A key point for the determinations of $NaHCO_3$ purity is that the same medium is used for both the $NaHCO_3$- and $KHCO_3$-based determinations of pH^0, so that the influence of the medium is removed. We used natural seawater for both.

The experiments detailed in Sections 2.5.2 and 2.5.3 were repeated with identical batches of seawater at approximately 25 °C but with added purified $KHCO_3$ rather than $NaHCO_3$.The resulting values of $pH^0_{i(avg)}$ and $pH^0_{f(avg)}$ (required to be within ± 0.001 as specified in Section 2.5.3) were averaged to obtain five equilibrium pH values denoted as $pH^0_{(K)}$. These five equilibrium $pH^0_{(K)}$ values were then used to calculate five pK_2 values for the $KHCO_3$ experiments, denoted as $pK_{2(K)}$, using eq. (2.14). Details regarding these calculations are provided in Appendix B.2, and the data are provided in Table B.2.1.

Comparisons between the experimental determinations of pH^0 (obtained via $NaHCO_3$ additions as described in Section 2.5.3) and $pH^0_{(K)}$ (obtained via $KHCO_3$ additions) at each specified (S_P, T) pair were used to calculate Φ (details provided in Appendix B.2). Values of pH^0 were consistently larger than $pH^0_{(K)}$ (for a specified S_P, T condition), indicating the presence of Na_2CO_3 contaminant in the $NaHCO_3$ solid, whereupon Φ will be less than 1. Salinity was identical for the corresponding pH^0 and $pH^0_{(K)}$ measurements (because a single seawater batch was used for both). The temperatures of the samples differed by no more than 0.1 °C, and T was taken as the average of the two temperature measurements. Each value of Φ was calculated via eq. (2.12), using the equilibrium pH^0 values of this work, K_1 of Lueker et al. (2000), and $K_{2(K)}$ of this work. (Additional calculations of Φ using alternative K_1 parameterizations are provided in Appendix B.2.)

2.5.5 Calculation of K_2

Eq. (2.13) was used to calculate stoichiometric K_2 values for bicarbonate dissociation (Mehrbach et al., 1973) at each specific (S_P, T) condition. For the required input of pH to the equation, the experimentally determined values of pH^0 were used. For the required input of K_1, two different values were used, thus generating two independent values of output K_2: one based on the K_1 parameterization of Lueker et al. (2000) (with the output here termed ${}_{SL}K_2$) and one based on the K_1 parameterization of Waters and Millero (2013) as revised by Waters et al. (2014) (further referenced as Waters et al. (2013, 2014)) (with the output here termed ${}_{SW}K_2$). Calculating two independent sets of K_2 values was done to allow us to determine how the uncertainty in K_1 contributes to the calculation of K_2. This is discussed further in Section 2.6.2.

2.5.6 Deviations from K_1K_2 methods of previous works

The procedures used in the present study are in certain respects distinct from the procedures of Mehrbach et al. (1973) and of Mojica Prieto and Millero (2002). One difference is our use of purified $NaHCO_3$ in pH^0 experiments (as described in Section 2.5.1). In the experiments of Mehrbach et al. (1973), the $KHCO_3$ solid was purified in a similar manner as described in Section 2.5.1. However, as no mention was made of purification techniques for $NaHCO_3$, we infer that the sodium bicarbonate used in their work (Mehrbach et al., 1973) was not purified. The $NaHCO_3$ solid used by Mojica Prieto and Millero (2002) was likewise unpurified. To determine the purity of the $NaHCO_3$ solid, Mojica Prieto and Millero (2002) directly measured the C_T and A_T of a 0.7 M NaCl solution to which $NaHCO_3$ had been added. The background NaCl solution likely had non-zero A_T and C_T, and the $KHCO_3$ reference method of Mehrbach et al. (1973) was not utilized.

Another major deviation from the procedures of Mehrbach et al. (1973) and Mojica Prieto and Millero (2002) was our use of single $NaHCO_3$ additions to determine pH^0. Mehrbach et al. (1973) used multiple $NaHCO_3$ additions to alkalinity-free seawater to reach a potentiometrically measured steady-state pH. We opted not to use multiple additions because these additions alter the seawater composition, changing the sodium concentration and ionic strength and potentially titrating acid/base species. Furthermore, we chose to work with solution compositions as close as possible to natural seawater and therefore we did not drive off $CO_{2(g)}$ to create alkalinity-free waters beforehand. (Whether this methodological difference is consequential is difficult to assess.) Mehrbach et al. (1973) made additions of $NaHCO_3$ from both the acidic and basic sides of pH^0, whereas Mojica Prieto and Millero (2002) approached the final steady-state pH only from the acidic side. In our work, $pH_{initial}$ and pH_{final} values obtained before and after single $NaHCO_3$ additions were used to identify the equilibrium pH for a given (S_P, T) condition (as described in Section 2.5.3).

Mehrbach et al. (1973) and Mojica Prieto and Millero (2002) both determined steady-state pH by potentiometric measurements. The latter authors additionally measured the final steady-state pH values spectrophotometrically, but unpurified mCP was used because purified indicator was not available at the time. The present work used purified mCP and state-of-the-art spectrophotometric techniques.

2.5.7 CO_2 system calculations

Internal consistency was assessed by comparing measured and calculated values of CO_2 system parameters (i.e., calculated using different sets of dissociation constants). Differences between measured and calculated values of X are referred to as residuals of X (e.g., A_T residuals

= A_T measured – A_T calculated). The CO_2 system calculations were made using the CO2SYS-MATLAB software, version 2.0 (Van Heuven et al., 2011). All pH calculations were carried out on the total hydrogen ion concentration scale unless otherwise specified. Values for K_{HSO4} from Dickson (1990) and B_T/S from Lee et al. (2010) were used. The CO_2 system dissociation constants for each calculation were explicitly specified using the following notation: constants of Lueker et al. (2000) are denoted as "$_LK$", and constants of Waters et al. (2013, 2014) are denoted as "$_WK$". The K_2 parameterization produced in this work is denoted as "$_{SW}K_2$". This K_2 parameterization will be discussed further in Section 2.6.1. CO2SYSv3 in MATLAB, developed by Sharp et al. (2020), includes the $_{SW}K_2$ parameterization of this work as an option for calculations (for details see Appendix B.3).

2.5.8 Data sets for internal consistency assessments

Internal consistency of the CO_2 system calculations was assessed by using the newly obtained K_2 parameterization to generate calculated parameters that were then compared to measured parameters in two high-quality data sets: (1) the original experimental data set of Lueker et al. (2000) and (2) a compilation of nine large oceanic data sets in which three or more CO_2 system parameters had been measured using state-of-the-art techniques.

The data from Lueker et al. (2000) consisted of paired measurements of fCO_2, A_T, and C_T made on the same seawater sample over a range of fCO_2. The fCO_2 measurements were largely obtained over the ranges of $34.966 \leq S_P \leq 36.643$ and $15 \leq t \leq 25$ °C (n = 51). Five additional measurements made at 5 °C were excluded from our analysis because this temperature is well below the range investigated in our work.

The field data were obtained from a suite of repeat hydrography cruises (n = 21,475). These data sets were chosen to represent a wide range of oceanographic conditions throughout the major ocean basins. The National Oceanographic Data Center expedition codes (EXPOCODES) for these cruises are as follows: 32WC20110812 (West Coast Ocean Acidification Cruise (WCOA) 2011) (Feely et al., 2016), 33AT20120419 (A20 2012) (Wanninkhof et al., 2013), 33RO20120721 (Gulf of Mexico and East Coast Carbon Cruise 2 (GOMECC-2) 2012) (Wanninkhof et al., 2016), 318M20130321 (P02 2013) (Swift et al., 2014), 320620140320 (P16S 2014) (Talley et al., 2016), 33RO20150410 and 33RO20150525 (P16N 2015) (Cross et al., 2017), 33RR20160208 (I08S 2016) (Macdonald et al., 2018), 33RR20160321 (I09N 2016) (Barbero et al., 2018), and 33RO20161119 (P18 2016) (Carter et al., 2018). Full profiles of A_T, C_T, pH, T, S, P, silicate, and soluble reactive phosphate were measured for all data sets. Data records with flags indicating poor quality were removed prior to analysis. In most cases, pH was measured spectrophotometrically onboard using purified mCP, on the total hydrogen ion concentration scale, at temperatures of approximately 25 °C. Exceptions were P18 2016 (where pH was measured on the SWS scale) and P16S 2014 (where pH was measured at 20 °C). For all cruises, accuracies of the onboard A_T and C_T measurements were assessed using certified reference materials (CRMs) provided by the laboratory of Dr. Andrew Dickson at Scripps Institution of Oceanography. All of the cruise data can be found online at the website of the NOAA National Centers for Environmental Information (https://www.nodc.noaa.gov/ocads/oceans/RepeatSections/).

2.6 Results

2.6.1 Stoichiometric pK_2 parameterizations and residuals

The purity of the $NaHCO_3$ used in the K_2 determinations was determined as described in Section 2.5.4, using the experimental values of $pH^0_{i(avg)}$ and $pH^0_{f(avg)}$ in eq. (2.12). These values of Φ, as well as the average Φ for each set of calculations, are provided in Table B.2.2 of Appendix B.2. The purity of the $NaHCO_3$ used in this work is given by $\Phi = 0.9996 \pm 0.0003$. This value compares well to the value reported in Mehrbach et al. (1973), $\Phi = 0.9991 \pm 0.0002$.

Two sets of pK_2 values were determined as described in Section 2.5.5, using the experimentally derived pH^0 values and either the K_1 of Lueker et al. (2000) or the K_1 of Waters et al. (2013, 2014). The two sets of values, denoted as ${}_{SL}pK_2$ and ${}_{SW}pK_2$, are provided in Table 2.1. These two sets of pK_2 values agree remarkably well with one another. The largest difference between ${}_{SL}pK_2$ and ${}_{SW}pK_2$ values is 0.007, which is less than the uncertainty associated with the determinations of K_2.

Because the Waters K_1 results are appropriate over a wider range of salinity and temperature than Lueker et al. (2000), we elected to rely primarily on the K_1 description of Waters et al. (2013, 2014) for our parameterization of K_2. The S_P and T dependences of the resulting ${}_{SW}pK_2$ values are shown in Fig. 2.1 as a function of T^{-1}. The ${}_{SW}pK_2$ values given in Table 2.1 were parameterized using eq. (2.15):

$$pK_2 = e_1 + e_2 T^{-1} + e_3 \ln T + e_4 S_P + e_5 S_P^{0.5} + e_6 S_P^2 + e_7 (S_P/T) \qquad (2.15)$$

The e_n coefficients for this parameterization are given in Table 2.2. Eq. (2.15) is based on the original pK_2 parameterization of Lueker et al. (2000), with additional terms ($S_P^{0.5}$ and S_P/T) included based on an F-test to more appropriately represent the data. The root mean square error (RMSE) of ${}_{SW}pK_2$ is 0.0029.

Table 2.1.
Experimentally derived pH^0 values and associated standard deviations for a range of salinity and temperature conditions. The uncertainty of the listed temperatures is ±0.02 °C. The pH^0 values for each (S_P, T) pair were averaged from the two pH_{intial} and two pH_{final} values (provided in Table B.1.1). Also shown are the two sets of pK_2 values calculated using the K_1 parameterizations of Lueker et al. (2000) (denoted as ${}_{SL}pK_2$) and Waters et al. (2013, 2014) (denoted as ${}_{SW}pK_2$).

S_P	t (°C)	pH^0 (± stdev) (n = 4)	${}_{SL}pK_2$	${}_{SW}pK_2$
19.62	15.19	7.6605 ± 0.0024	9.2938	9.3000
19.62	20.03	7.6045 ± 0.0012	9.2289	9.2354
19.62	25.05	7.5443 ± 0.0015	9.1532	9.1596
19.62	29.93	7.4857 ± 0.0011	9.0754	9.0817
19.62	34.81	7.4297 ± 0.0008	8.9992	9.0053
24.70	15.24	7.6096 ± 0.0018	9.2257	9.2258
24.70	20.11	7.5477 ± 0.0014	9.1494	9.1502
24.70	25.07	7.4869 ± 0.0009	9.0718	9.0734
26.51	29.65	7.4145 ± 0.0009	8.9743	8.9754
26.51	34.65	7.3583 ± 0.0007	8.8987	8.9013
29.11	20.07	7.5154 ± 0.0007	9.1082	9.1048
29.11	24.99	7.4528 ± 0.0009	9.0266	9.0246
29.11	29.95	7.3932 ± 0.0015	8.9475	8.9471
31.70	15.35	7.5511 ± 0.0015	9.1456	9.1397
31.70	34.69	7.3125 ± 0.0013	8.8327	8.8336
35.50	15.43	7.5269 ± 0.0018	9.1126	9.1061
35.50	20.36	7.4627 ± 0.0010	9.0321	9.0266
36.33	25.10	7.3979 ± 0.0007	8.9472	8.9437
36.33	30.08	7.3374 ± 0.0011	8.8662	8.8653
36.33	35.02	7.2778 ± 0.0012	8.7831	8.7853
36.80	25.00	7.3992 ± 0.0010	8.9503	8.9470
40.98	15.05	7.5007 ± 0.0029	9.0717	9.0685
40.98	20.05	7.4319 ± 0.0009	8.9829	8.9808
40.98	25.09	7.3697 ± 0.0009	8.9032	8.9031
40.98	29.89	7.3101 ± 0.0009	8.8228	8.8255
40.98	34.88	7.2471 ± 0.0013	8.7332	8.7397

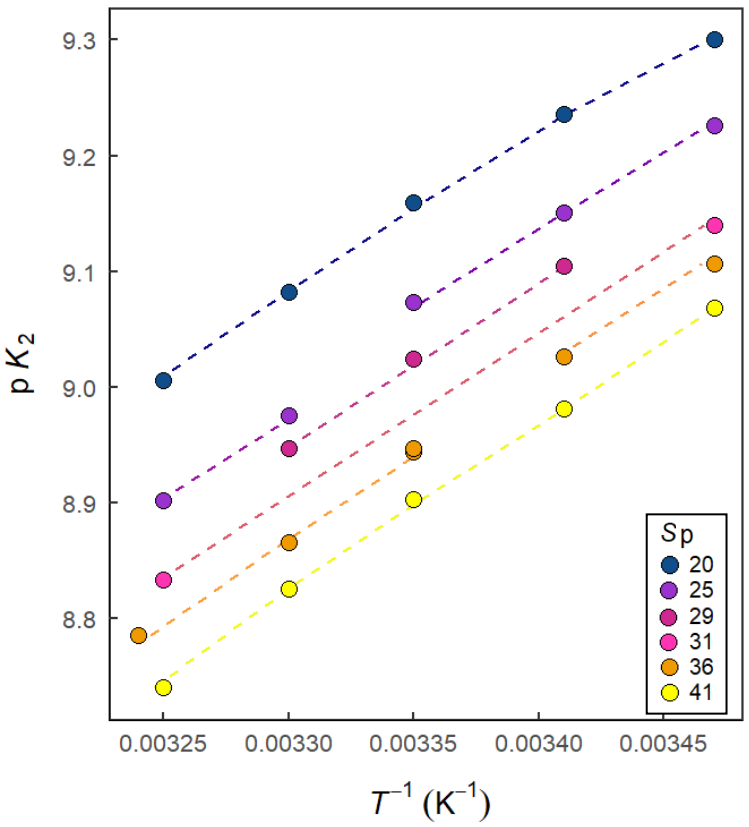

Fig. 2.1. Experimentally derived $_{SW}pK_2$ values as a function of inverse temperature (K^{-1}), with colors indicating approximate salinity. The dashed lines show the $_{SW}pK_2$ parameterization of eq. (2.15).

Table 2.2.
Coefficients for the $_{SW}pK_2$ parameterization of eq. (2.15) calculated using the K_1 of Waters et al. (2013, 2014). As a check, the value at S_P = 35 and T = 298.15 K is $_{SW}pK_2$ = 8.9608.

$pK_2 = e_1 + e_2\,T^{-1} + e_3 \ln T + e_4 S_P + e_5\,S_P^{0.5} + e_6\,S_P^{2} + e_7\,(S_P/T)$	
	$_{SW}pK_2$
e_1	116.8067
e_2	–3655.02
e_3	–16.45817
e_4	0.04523
e_5	–0.615
e_6	–0.0002799
e_7	4.969

Residuals for the $_{SW}pK_2$ parameterization (i.e., parameterized minus experimental values) are shown in Fig. 2.2. The standard deviation of the residuals is 0.0029, and all residuals are randomly distributed with respect to both S_P and T.

The set of $_{SL}pK_2$ values calculated using the K_1 of Lueker et al. (2000), also parameterized as described in this section (Section 2.6.1), is given in Appendix B.4 along with the corresponding e_n coefficients. Differences between the parameterizations of $_{SL}pK_2$ and $_{SW}pK_2$ and, as well, the closely linked pK_1 characterizations of Lueker et al. (2000) and Waters et al. (2013, 2014) are shown in Fig. 2.3 in terms of S_P and T.

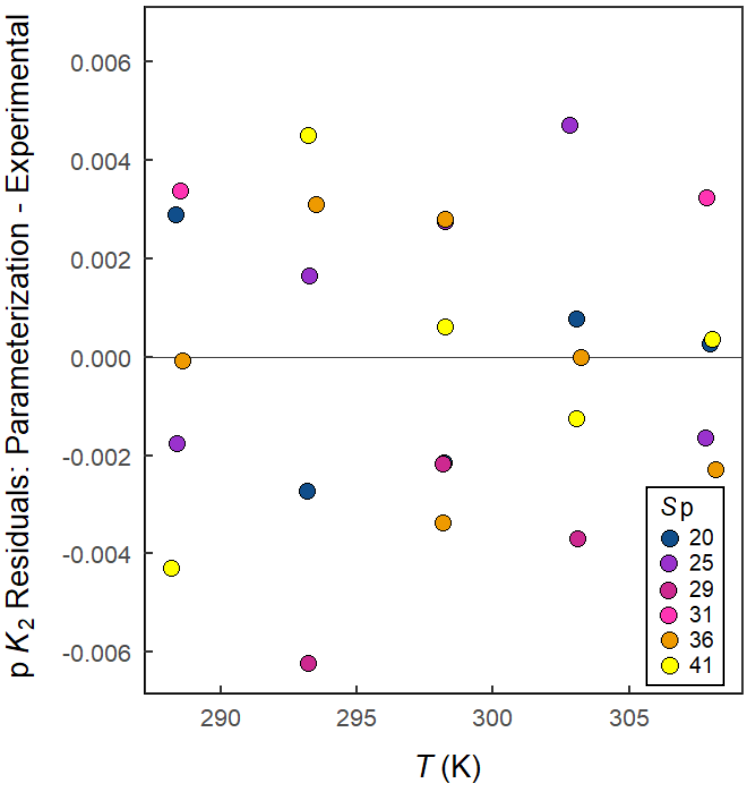

Fig. 2.2. $_{SW}pK_2$ residuals (i.e., parameterized pK_2 minus experimental pK_2) as a function of temperature (K), with colors indicating approximate salinity.

2.6.2 Estimating uncertainties

The pooled standard deviation in measurements of pH^0 was calculated to be 0.0013 (individual standard deviations are provided in Table 2.1). To further assess the uncertainty in our original measurements of pH^0 and associated $p(K_1K_2)$ values (calculated with the K_1 of Waters et al. (2013, 2014)) (provided in Table B.4.1 of Appendix B.4), both were fitted using eq. (2.15). The e_n coefficients are given in Table B.4.2 of Appendix B.4. The root mean square error for pH^0 is 0.0014 and for $p(K_1K_2)$ is 0.0028. Because our method requires the use of previous K_1 parameterizations, any estimated uncertainty in K_1 will influence the uncertainty in our K_2 parameterization. The uncertainty in pK_1 is 0.0075 according to Orr et al. (2018) which, as shown in Fig. 2.3b, is the approximate magnitude of the difference between our pK_2 parameterizations ($_{SL}pK_2$ and $_{SW}pK_2$). Notably, as shown in Fig. 2.3, systematic overestimates in a utilized K_1 parameterization will produce underestimates in the conjugate K_2 parameterization. Our estimates of K_2 are also influenced by the assumption that $KHCO_3$ is completely pure (i.e., $\Phi = 1$). Any systematic deviation from this assumption will, of course, lead to systematic errors in calculations of K_1K_2. It is not possible, at present, to quantify this potential source of error.

Estimates of uncertainty in pK_2 were assessed by a method similar to that of Orr et al. (2018). Based on the pK_2 parameterizations obtained (a) in this work ($_{SW}pK_2$), (b) by Lueker et al. (2000), and (c) by Waters et al. (2013, 2014), estimates of systematic uncertainty in pK_2 were assessed to be on the order of ±0.01. Random uncertainty in pK_2 was estimated based on the standard deviation of the pK_2 residuals. For this work, the estimated random uncertainty is 0.003, which is less than a third of the 0.01 uncertainty estimated by Orr et al. (2018) for the pK_2 parameterization of Lueker et al. (2000). The total standard uncertainty for pK_2 (based on the

combined random and systematic components of uncertainty) for this work is 0.010. The total standard uncertainty estimated by Orr et al. (2018) for previous parameterizations of pK_2 is 0.015.

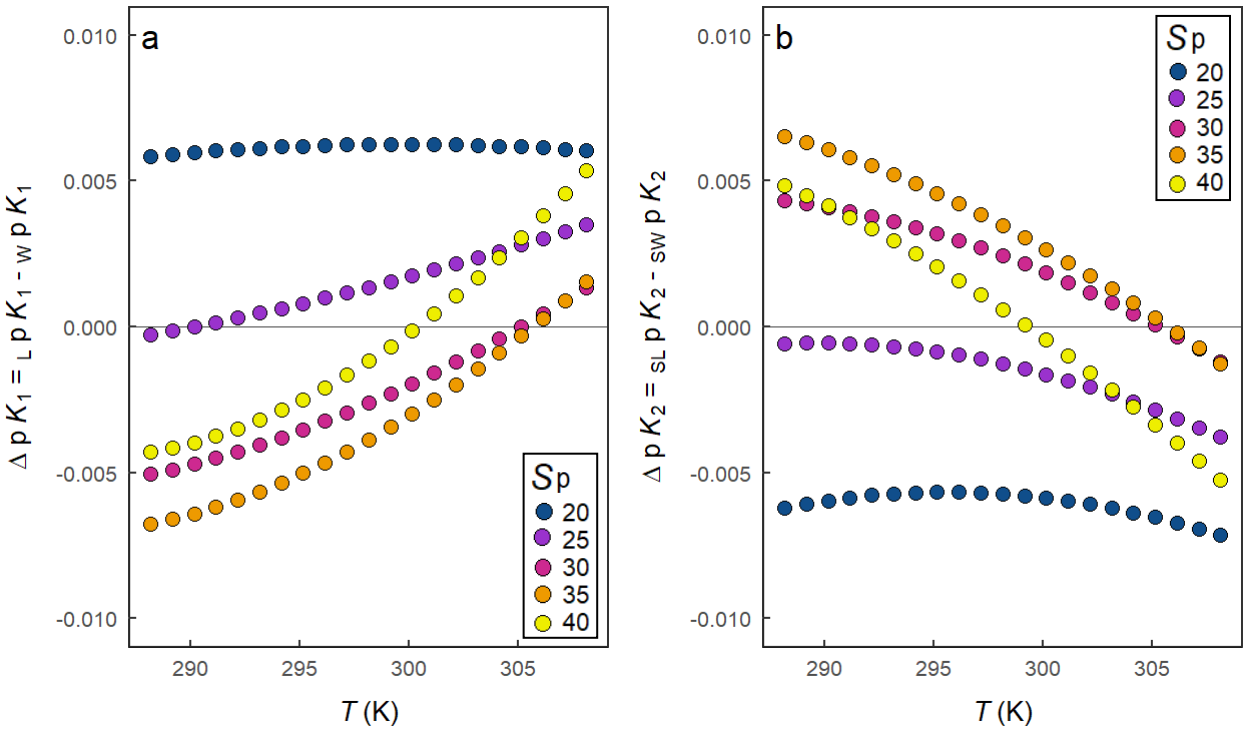

Fig. 2.3. Differences between pK parameterizations as a function of temperature (K), color-coded by salinity for (a): $\Delta pK_1 = pK_1$ of Lueker et al. (2000) minus pK_1 of Waters et al. (2013, 2014) and (b) $\Delta pK_2 = {}_{SL}pK_2$ minus ${}_{SW}pK_2$.

2.7 Discussion

2.7.1 Comparison with other pK_2 parameterizations

In Fig. 2.4, the pK_2 residuals for this work (i.e., ${}_{SW}pK_2$ – pK_2 experimental) are compared to the residuals of other recent parameterizations. The pK_2 residuals of this work (Fig. 2.4a) are more tightly and evenly distributed about zero than are the residuals of Lueker et al. (2000) and Millero et al. (2006) (Figs. 2.4b and 2.4c). This result affirms the improved pK_2 precision that can be obtained using the methods described in Section 2.5. Notably, Fig. 2.4b and 2.4c show that the residuals of Lueker et al. (2000) and Millero et al. (2006) are not randomly distributed with respect

to S_P and T. In an attempt to obtain improved residuals, we refit the original data from these two studies to parameterizations with fewer terms and additional terms, but the uneven distributions of residuals remained.

The ${}_{SW}pK_2$ parameterization obtained in this work was compared to the pK_2 parameterizations of Lueker et al. (2000) and Waters et al. (2013, 2014). Fig 2.5 shows differences in terms of $\Delta pK_2 = {}_{SW}pK_2$ (this work) – pK_2 (Lueker or Waters). For $25 \leq S_P \leq 41$, the best agreement between ${}_{SW}pK_2$ and the pK_2 of Lueker et al. (2000) or Waters et al. (2013, 2014) is generally seen within the temperature range of $20 \leq t \leq 30$ °C, where the range of ΔpK_2 is ≤0.02, with a slight negative offset. At higher and lower temperatures, the range of ΔpK_2 has a slightly larger negative offset. At the lowest salinity ($S_P = 20$), ΔpK_2 is typically positive over the entire range of temperatures, with the largest ΔpK_2 (0.022) being observed at $t = 26$ °C. Overall, although ${}_{SW}pK_2$ is based in part on the pK_1 of Waters et al. (2013, 2014), better agreement is observed with the pK_2 parameterization of Lueker et al. (2000) over the range of temperatures considered in this work.

Differences between ${}_{SL}pK_2$ and the pK_2 parameterizations of Lueker et al. (2000) and Waters et al. (2013, 2014) are similar to those described above for ${}_{SW}pK_2$. Agreement is best within the range $20 \leq t \leq 30$ °C with larger differences being observed at higher and lower temperatures (not shown). The agreement of ${}_{SL}K_2$ and ${}_{SW}K_2$ with both Lueker et al. (2000) and Waters et al. (2013, 2014) is significant because ${}_{SL}K_2$ and ${}_{SW}K_2$ are derived from different K_1 parameterizations. Because, as noted previously, the pK_1 parameterization of Waters et al. (2013, 2014) extends to much lower salinities than the pK_1 of Lueker et al. (2000), the Waters parameterization can be used in future K_1K_2 determinations to extend ${}_{SW}pK_2$ to a much wider range of salinity conditions.

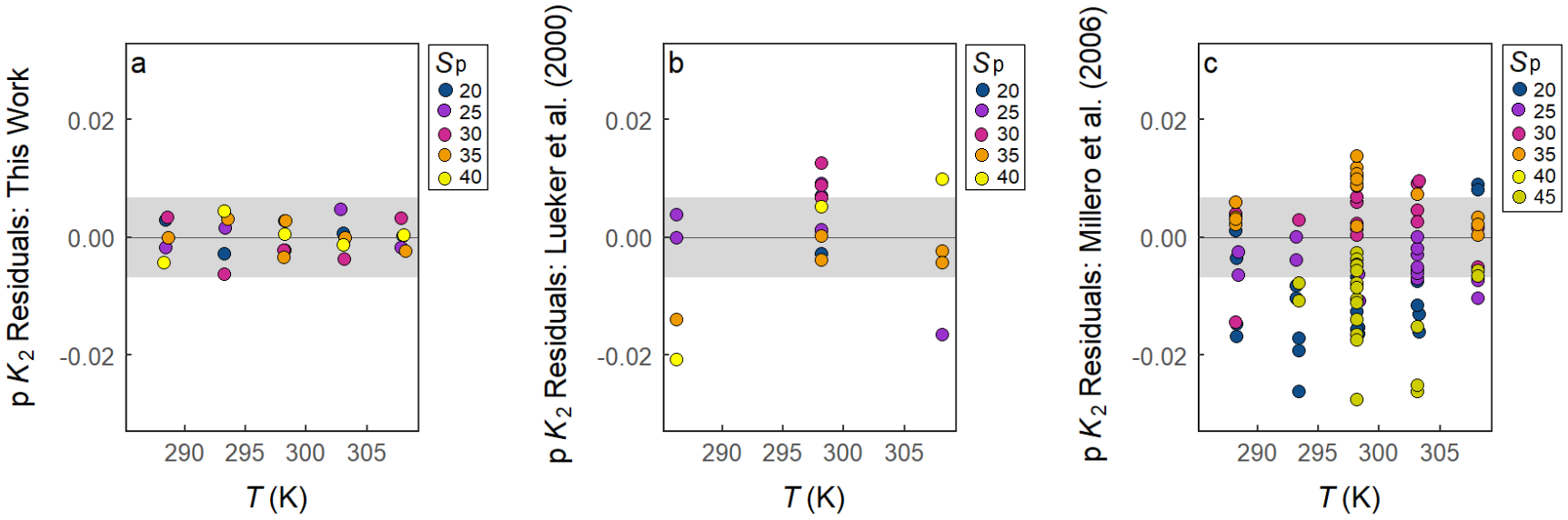

Fig. 2.4. pK_2 residuals (i.e., parameterized pK_2 minus experimental pK_2) as a function of temperature (within the range of $288.15 \leq T \leq 308.15$ K), color-coded by salinity for: (a) this work's $_{SW}$pK_2, (b) Lueker et al. (2000), and (c) Millero et al. (2006) (which provide the experimental basis for the Waters constants). For ease of comparison, the gray shaded region shows ± two standard deviations for the residuals of this work (±0.0068). Data were grouped by S_P in increments of five and therefore color indicates approximate salinity. Thus, for example, S_P of 30 denotes data obtained within the range of 30 ± 2.5.

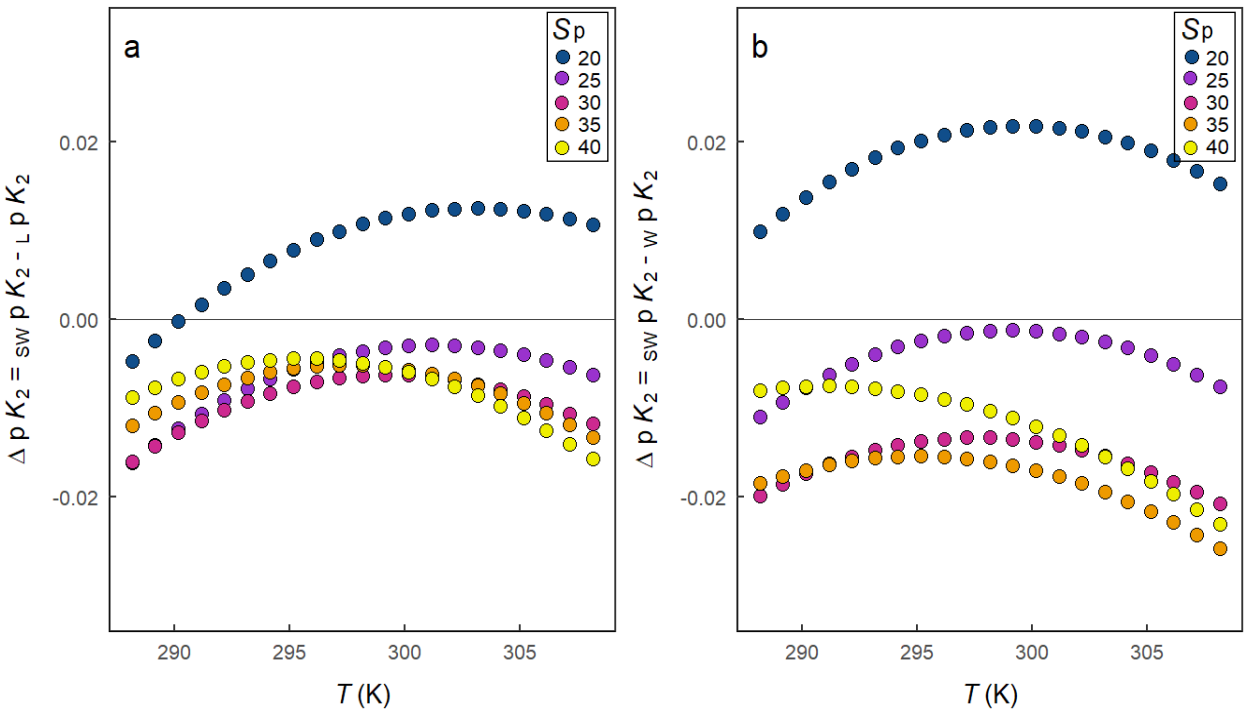

Fig. 2.5. Differences between the $_{SW}pK_2$ parameterization of this work and the pK_2 parameterizations of (a) Lueker et al. (2000) ($_{L}pK_2$) and (b) Waters et al. (2013, 2014) ($_{W}pK_2$) as a function of temperature (K), color-coded by salinity.

2.7.2 Assessments of internal consistency

2.7.2.1 Lueker et al. (2000) data set: fCO_2, A_T, and C_T

One assessment of internal consistency was conducted using the original experimental data of Lueker et al. (2000) (n = 47), in combination with the sets of dissociation constants introduced in Section 2.5.7: set A = $_{L}K_1$ and $_{L}K_2$ (the constants of Lueker et al. (2000)), set B = $_{W}K_1$ and $_{W}K_2$ (the constants of Waters et al. (2013, 2014)), and set C = $_{W}K_1$ and $_{SW}K_2$ of this work. Summary statistics of the resulting relative residuals of fCO_2 (i.e., (fCO_2 measured – fCO_2 calculated), expressed as a percentage of the calculated fCO_2 value) are listed in Table 2.3. (All residuals are provided in Table B.5.1 of Appendix B.5.)

For all sets of dissociation constants, the mean relative residuals for fCO_2 < 500 µatm (characterized as "low-fCO_2 conditions") are negative. For fCO_2 > 500 µatm (characterized as

"high-fCO_2 conditions"), the mean relative residuals calculated using set C are internally consistent within the uncertainty of measurements, while those calculated using sets A and B are both positive. For both low- and high-fCO_2 conditions, these two sets of mean relative residuals are not significantly different from one another at the 95% confidence level. In contrast, for both low- and high-fCO_2 conditions, the mean relative residuals of set C (i.e., ${}_{SW}pK_2$ of this work) are significantly different from those of sets A and B at the 95% confidence level. Overall, the mean relative fCO_2 residuals for all constants at low-fCO_2 conditions show that observations and predictions (calculated values) are not internally consistent within the uncertainty of measurements (i.e., the mean ± 95% confidence intervals do not include zero for any sets of constants). Thus, there are clear differences in the degree of internal consistency based on the choice of CO_2 system dissociation constants. Under high-fCO_2 conditions, only the parameterization of the set C constants provides internally consistent observations and predictions.

Table 2.3.
Mean relative fCO_2 residuals ((fCO_2 measured – fCO_2 calculated) / fCO_2 calculated) calculated using the different sets of K_1 and K_2 listed in the left column with the experimental fCO_2, A_T, and C_T data of Lueker et al. (2000) (excluding their data collected at 5 °C*). Uncertainty is given as the 95% confidence interval on the mean.

Constants	Mean relative fCO_2 residuals ± uncertainty (%)	
	fCO_2 < 500 µatm (n = 28)	fCO_2 > 500 µatm (n = 19)
Set A = Lueker ${}_{L}K_1$ and ${}_{L}K_2$	−1.27 ± 0.33	1.37 ± 0.93
Set B = Waters ${}_{W}K_1$ and ${}_{W}K_2$	−0.64 ± 0.36	1.97 ± 0.89
Set C = Waters ${}_{W}K_1$ and this work ${}_{SW}K_2$	–2.93 ± 0.35	0.01 ± 0.86

*Data also excludes four points that were excluded from Fig. 4b of Lueker et al. (2000).

Calculations of fCO_2 were also made using the B_T/S of Uppström (1974). In this case, compared to residuals calculated using the B_T/S of Lee et al. (2010), the mean residuals for low-fCO_2 conditions are increased by approximately 5 µatm while the mean residuals for high-fCO_2 conditions are increased by approximately 11 µatm for calculations with all three sets of K_1 and K_2 constants. Mean residuals calculated with the B_T/S of Uppström (1974) therefore prompt different interpretations with respect to which sets of dissociation constants provide the most internally consistent results. The mean residuals at low-fCO_2 become closer to zero (i.e., more internally consistent) for sets A and C, while the mean residuals at high-fCO_2 move farther from zero (i.e., less internally consistent) for all sets of constants. The choice of parameterization for B_T/S will clearly influence interpretations regarding which calculations are internally consistent.

2.7.2.2 Cruise data sets: A_T, C_T, and pH_T

A second assessment of internal consistency was conducted using the cruise data described in Section 2.5.8 (n = 21,475) in combination with the three sets of dissociation constants listed in Section 2.7.2.1. The measured parameters used were A_T, C_T, and pH_T (pH_{SWS} was used only for P18 2016). The mean residuals of A_T for all cruises (Fig. 2.6) are generally within the ±10 µmol kg^{-1} measurement uncertainty (95% confidence interval) of a single at-sea A_T measurement (McLaughlin et al., 2015). When the set A (Lueker) or set C (this work) characterizations are used, the mean residuals generally provide internally consistent results. When the set B (Waters) constants are used, however, the mean residuals for five of the nine cruises are offset from zero by more than one standard deviation, with an average mean A_T residual (nine cruises) of approximately 4 µmol kg^{-1} (Table B.5.2 of Appendix B.5). For the P16N 2015 cruise, only the mean A_T residuals calculated using ${}_{SW}pK_2$ (i.e., Set C) provide internally consistent results,

whereas the mean A_T residuals calculated with both Lueker et al. (2000) and Waters et al. (2013, 2014) are offset from zero by more than one standard deviation. The mean residuals of C_T (not shown) displayed similar patterns to the mean A_T residuals but with opposite sign, as would be expected. For pH assessments, when the set A (Lueker) or set C (this work) characterizations are used, the mean residuals generally provide internally consistent results, whereas mean residuals calculated with set B (Waters) are generally offset from zero by more than one standard deviation (Table B.5.3 of Appendix B.5). The K_{HSO4} of Waters et al. (2013, 2014) was also used in CO_2 system calculations and produced no meaningful changes in the internal consistency assessments described in this section (which uses the K_{HSO4} of Dickson (1990)).

Whereas this type of analysis (i.e., comparisons of mean residuals) provides a simple way to assess the degree of internal consistency across sets of dissociation constants (with all other parameter uncertainties being held constant), it is recognized that such comparisons provide only limited insight into the accuracy. As a note of caution, although the Lueker et al. (2000) K_1 and K_2 parameterizations appear to yield better internal consistency than the parameterizations of Waters et al. (2013, 2014), it must be noted that the A_T measurements in Fig. 2.6 likely include contributions from organic bases (Kim and Lee, 2009; Sharp and Byrne, 2020). If these contributions were appropriately accounted for, the calculated values of A_T would be increased, thus potentially reducing the mean offsets calculated here. If organic contributions were sufficiently large, the most positive residuals in Fig. 2.6 could become considerably smaller and the residuals now near zero could become negative. As such, with improved accounts of organic alkalinity distributions in the ocean, the internal consistency evaluation shown in Fig. 2.6 could be significantly revised.

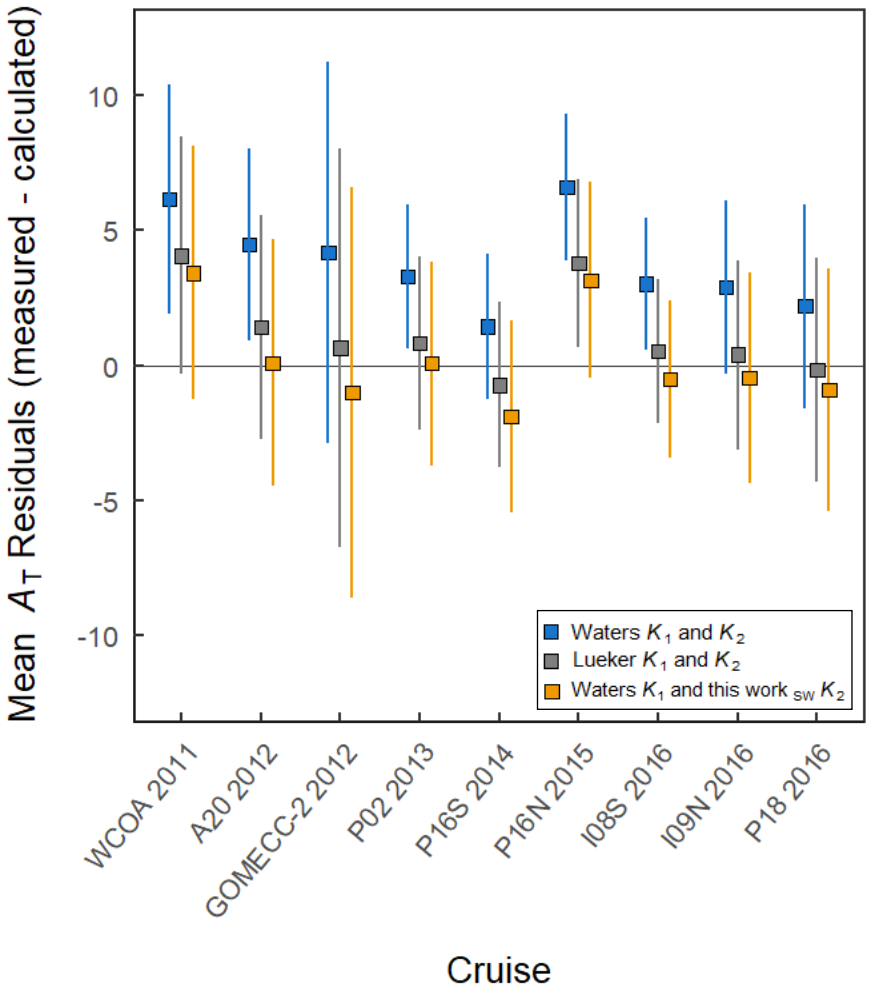

Fig. 2.6. Average residuals (measured – calculated) of A_T (µmol kg^{-1}) for the nine cruise data sets calculated using the three sets of dissociation constants (shown in colors). Standard deviations are shown by the colored bars.

2.8 Conclusions and implications

This study provides significant improvements in the characterization of K_2, the stoichiometric dissociation constant of bicarbonate. As shown in Fig. 2.4, the calculated residuals for $_{SW}pK_2$ are randomly distributed and are substantially smaller than those obtained in previous studies. This result indicates that our new method reduces the likelihood of systematic errors in pK_2 that vary with temperature and salinity. Furthermore, if future studies improve the characterization of K_1, the original experimental pH^0 data summarized in Table 2.1 (and

parameterized in Table B.4.2 of Appendix B.4) can be used to recalculate K_2. The $_{SW}pK_2$ parameterization developed in this work (using the K_1 parameterization of Waters et al. (2013, 2014)) agrees well with the pK_2 dissociation constant parameterizations of both Lueker et al. (2000) and Waters et al. (2013, 2014) within the ranges of $25 \leq S_P \leq 41$ and $20 \leq t \leq 30$ °C. Nevertheless, there are pronounced differences at low salinities and at higher and lower temperatures.

In previous determinations of CO_2 system dissociation constants, assessments of the quality of the experimental K_1 and K_2 results have typically been limited to direct comparisons with earlier K_1 and K_2 parameterizations. In this work, we evaluated our new pK_2 parameterization by making similar historical comparisons and, in addition, by conducting internal consistency assessments that relied on two independent and extensive data sets: (a) the fCO_2, A_T, and C_T data set of Lueker et al. (2000) and (b) the A_T, C_T, and pH data sets from nine ocean research cruises. Assessments based on the Lueker data set show that calculations made with the $_{SW}K_2$ parameterization of this work perform as well as or better than calculations carried out with the constants of Lueker et al. (2000) or Waters et al. (2013, 2014). Assessments based on the large oceanographic data sets show that A_T residuals calculated using $_{SW}K_2$ compared well with calculations that used the Lueker et al. (2000) dissociation constants. Based on these results we recommend, for the salinity and temperature ranges of $19.6 \leq S_P \leq 41$ and $15 \leq t \leq 35$ °C, the use of $_{SW}pK_2$ (eq. (2.15) and Table 2.2) paired with the pK_1 of Waters et al. (2013, 2014).

Internal consistency assessments constitute an important tool for comparing K_2 parameterizations, but the available data cover only a small range of environmentally relevant S and T. Most of the Lueker et al. (2000) laboratory data encompass a small range of temperature (approximately 15 to 25 °C), all at salinities near 36. The oceanographic (cruise) data cover a wider

range of salinities, but nearly all at 25 °C. Additional internal consistency comparisons should be obtained over wider ranges of S and T. It would be very useful, for example, if measurements of A_T and C_T could be combined with pH_T and high quality fCO_2 measurements obtained over a wide range of temperatures to better identify likely causes of calculated discrepancies. This extension is important because the internal consistency assessments in this work are largely made at a temperature (25 °C) where ${}_{SW}pK_2$ and the pK_2 parameterizations of Lueker et al. (2000) and Waters et al. (2013, 2014) most closely agree. At lower temperatures, where the pK_2 parameterizations show larger differences (see Fig. 2.5), less internal consistency would be expected. An expanded range of temperatures in evaluations of A_T, C_T, and pH_T internal consistency could also help to address discrepancies between in situ measurements and calculated in situ CO_2 system parameters, including calcium carbonate saturation states (Ω) (Naviaux et al., 2019).

Experimental determinations of K_1K_2 should be expanded to extend the K_2 parameterizations to estuarine conditions. Notably, the K_1 of Lueker et al. (2000) is valid only within the range $19 \leq S_P \leq 43$, but the K_1 of Waters et al. (2013, 2014) is appropriate for $0 \leq S_P \leq 45$. As noted in Section 2.7.1, the two pK_2 parameterizations obtained in the present work (one based on the pK_1 parameterization of Lueker et al. (2000) and the other based on that of Waters et al. (2013, 2014)) are in good agreement. Therefore, it is expected that future determinations of K_1K_2 for estuarine conditions, in conjunction with the K_1 of Waters et al. (2013, 2014), could be directly combined with the results of this work to obtain an accurate pK_2 parameterization that encompasses both estuarine and marine conditions.

The accuracy of pK determinations is most reliably assessed through comparisons of results obtained by independent investigators who, ideally, used dissimilar measurement procedures. Based on such criteria, it is difficult to quantitatively assess the absolute accuracy of the pK

characterizations obtained in the present study. As noted above, evaluations of internal consistency are useful but are narrow in scope. Assessments of accuracy are currently limited by uncertainties such as (unknown) organic base contributions to A_T and uncertainty in the B_T/S ratio. Nevertheless, it is possible to make useful statements about what does and does not contribute to systematic errors in determinations of pK and characterizations of the marine carbonate system.

Because the pK_2 parameterization obtained in our work was derived using the pK_1 parameterization of Waters et al. (2013, 2014), any errors inherent in this parameterization will be propagated to ${}_{SW}pK_2$. It should be noted that, via eq. (2.14), K_1 and K_2 are anti-correlated (i.e., overestimates of ${}_WK_1$ will produce underestimates of ${}_{SW}K_2$ and vice versa). The quantitative relationship between pK_1 and pK_2 given in eq. (2.14) can be used to explore the influence of pK_1 perturbations on internal consistency evaluations (e.g., Table 2.3 and Fig. 2.6).

The determinations of pH in this work are based on the mCP parameterization of Müller and Rehder (2018). Examination of eq. (2.14) shows that the accuracy of the log(K_1K_2) characterizations is intimately (directly) related to the accuracy of the pH characterizations. For example, if the pH parameterization of Müller and Rehder (2018) is in error by +0.01 then log(K_1K_2) will be in error by an identical offset. Nevertheless, as an important point, the combination of these directly correlated errors should provide an accurate depiction of $[CO_3^{2-}]_T$ / $[CO_2^*]$ ratios (i.e., $[CO_3^{2-}]_T$ / $[CO_2^*] = K_1K_2$ / $[H^+]_T^2$ with offsetting errors in K_1K_2 and $[H^+]_T^2$). Thus, whereas errors in spectrophotometric pH parameterizations will produce corresponding errors in log(K_1K_2), the accuracy of carbonate system characterizations will not be affected. In this sense, the accuracy of CO_2 system calculations is maintained even in the presence of some types of systematic errors. An important point here is that, due to correlation of errors in measured pH and parameterized pK, the pK results in this work should best be paired with the mCP (pH)

parameterization of Müller and Rehder (2018). Other pH parameterizations could be used, but only after the p*K* results in the present work are recalculated and made compatible with the alternative pH model (e.g., Liu et al., 2011).

2.9 Supplemental information

Supplementary data for this chapter can be found in Appendix B.

2.10 Acknowledgements

This work was supported by the Paul L. Getting Memorial Fellowship in Marine Science and the St. Petersburg Downtown Partnership Endowed Fellowship in Coastal Science (University of South Florida College of Marine Science), the U.S. Geological Survey, and the National Science Foundation (grant number OCE-1657894). We would like to sincerely thank Dr. Tonya Clayton for editorial assistance and guidance in improving the manuscript. We would also like to thank Dr. Alfonso Mucci, Dr. Andrew Dickson, and two anonymous reviewers whose constructive comments greatly improved the final work.

2.11 References

Barbero, L., Wanninkhof, R., Dickson, A.G., Carlson, C.A., Key, R.M., Becker, S., Swift, J.H., McNichol, A., and Rodriguez, C. (2018) Discrete profile measurements of dissolved inorganic carbon, total alkalinity, pH on total scale and other hydrographic and chemical data obtained during the R/V Roger Revelle Repeat Hydrography Cruise in the Indian Ocean: GO-SHIP Section I09N, (EXPOCODE 33RR20160321) from 2016-03-21 to 2016-04-28 (NCEI Accession 0178637). NOAA National Centers for Environmental Information. Dataset. https://doi.org/10.25921/f59c-dy18

Bates, N.R., Astor, Y.M., Church, M.J., Currie, K., Dore, J.E., Gonzalez-Davila, M., Lorenzoni, L., Muller-Karger, F., Olafsson, J., and Santana-Casiano, J.M. (2014) A time-series view of changing surface ocean chemistry due to ocean uptake of anthropogenic CO_2 and ocean acidification. *Oceanography* **27**, 126–141. doi:10.5670/oceanog.2014.16

Byrne, R.H. (1987) Standardization of standard buffers by visible spectrometry. *Anal. Chem.* **59**, 1479–1481. https://doi.org/10.1021/ac00137a025

Byrne, R.H. (2014) Measuring ocean acidification: New technology for a new era of ocean chemistry. *Environ. Sci. Technol.* **48**, 5352–5360. doi:10.1021/es405819p

Caldeira, K. and Wickett M.E. (2003) Anthropogenic carbon and ocean pH. *Nature* **425**, 365. doi:10.1038/425365a

Carter, B.R., Feely, R.A., Mecking, S., Cross, J.N., Macdonald, A.M., Siedlecki, S.A., Talley, L.D., Sabine, C.L., Millero, F.J., Swift, J.H., Dickson, A.G., and Rodgers, K.B. (2017) Two decades of Pacific anthropogenic carbon storage and ocean acidification along Global Ocean Ship-based Hydrographic Investigations Program sections P16 and P02. *Glob. Biogeochem. Cycles* **31**, 306–327. doi:10.1002/2016gb005485

Carter, B.R., Sonnerup, R.E., Millero, F.J., Woosley, R.J., Wanninkhof, R., Feely, R.A., Hansell, D.A., Bullister, J.L., Mordy, C., Baringer, M.O., Langdon, C., Key, R.M., McNichol, A., Doney, S.C., and Johnson, G.C. (2018) Carbon dioxide, hydrographic and chemical data collected from profile discrete samples during the NOAA Ship Ronald H. Brown cruise RB-16-06 along the GO-SHIP Repeat Hydrography Section P18 (EXPOCODE 33RO20161119) in the Pacific Ocean from 2016-11-19 to 2017-02-03 (NCEI Accession 0171546). NOAA National Centers for Environmental Information. Dataset. https://doi.org/10.7289/v5cv4g1w

Clayton, T.D. and Byrne, R.H. (1993) Spectrophotometric seawater pH measurements: Total hydrogen ion concentration scale calibration of m-cresol purple and at-sea results. *Deep Sea Res. Part I. Oceanogr. Res. Papers* **40**, 2115–2129. https://doi.org/10.1016/0967-0637(93)90048-8

Cross, J.N., Macdonald, A.M., Alin, S.R., Wanninkhof, R., Dickson, A.G., Carlson, C.A., Johnson, G.C., Baringer, M.O., Mordy, C., Langdon, C., Key, R.M., McNichol, A., Bullister, J.L., Jenkins, W.J., and Nelson, N. (2017) Dissolved inorganic carbon (DIC), total alkalinity, pH on total scale, dissolved organic carbon (DOC), chlorofluorocarbons (CFC-11, CFC-12), temperature, salinity and other hydrographic and chemical variables collected from discrete samples and profile observations during the R/V Ronald H. Brown cruise along the GO-SHIP Section P16N_2015, Legs 1 and 2 (EXPOCODEs 33RO20150410 and 33RO20150525) in the Pacific Ocean, from 2015-04-10 to 2015-06-27 (NCEI Accession 0163182). NOAA National Centers for Environmental Information. Dataset. https://doi.org/10.3334/cdiac/otg.go_ship_p16n_2015

Dickson, A.G. (1990) Standard potential of the reaction: $AgCl(s) + 12H_2(g) = Ag(s) + HCl(aq)$, and and the standard acidity constant of the ion HSO_4^- in synthetic sea water from 273.15 to 318.15 K. *J. Chem. Thermodyn.* **22**, 113–127. https://doi.org/10.1016/0021-9614(90)90074-Z

Dickson, A.G. (2010) The carbon dioxide system in seawater: Equilibrium chemistry and measurements. *Guide to Best Practices for Ocean Acidification Research and Data Reporting*, 17–40.

Dickson, A. and Millero, F.J. (1987) A comparison of the equilibrium constants for the dissociation of carbonic acid in seawater media. *Deep Sea Res. Part A. Oceanogr. Res. Papers* **34**, 1733–1743. https://doi.org/10.1016/0198-0149(87)90021-5

Dickson, A., Sabine, C.L., and Christian, J.R. (Eds) (2007) *Guide to best practices for ocean CO_2 measurements*. PICES Special Publication 3, 191 pp.

Doney, S.C., Ruckelshaus, M., Duffy, J.E., Barry, J.P., Chan, F., English, C.A., Galindo, H.M., Grebmeier, J.M., Hollowed, A.B., Knowlton, N., Polovina, J., Rabalais, N.N., Sydeman, W.J., and Talley, L.D. (2012) Climate change impacts on marine ecosystems. *Annu. Rev. Mar. Sci.* **4**, 11–37. doi:10.1146/annurev-marine-041911-111611

Feely, R.A., Alin, S.R., Hales, B., Johnson, G.C., Juranek, L.W., Byrne, R.H., Peterson, W.T., Goni, M., Liu, X., and Greeley, D. (2016) Dissolved inorganic carbon, pH, alkalinity, temperature, salinity and other variables collected from discrete sample and profile observations using Alkalinity titrator, CTD and other instruments from WECOMA in the Gulf of the Farallones National Marine Sanctuary, Monterey Bay National Marine Sanctuary and others from 2011-08-12 to 2011-08-30 (NCEI Accession 0157458). NOAA National Centers for Environmental Information. Dataset. https://accession.nodc.noaa.gov/0157458

Feely, R.A., Sabine, C.L., Lee, K., Berelson, W., Kleypas, J., Fabry, V.J., and Millero, F.J. (2004) Impact of anthropogenic CO_2 on the $CaCO_3$ system in the oceans. *Science* **305**, 362–366. doi:10.1126/science.1097329

Fong, M.B. and Dickson, A.G. (2019) Insights from GO-SHIP hydrography data into the thermodynamic consistency of CO_2 system measurements in seawater. *Mar. Chem.* **211**, 52–63. https://doi.org/10.1016/j.marchem.2019.03.006

Goyet, C. and Poisson, A. (1989) New determination of carbonic acid dissociation constants in seawater as a function of temperature and salinity. *Deep Sea Res. Part A. Oceanogr. Res. Papers* **36**, 1635–1654. http://dx.doi.org/10.1016/0198-0149(89)90064-2

Gruber, N., Clement, D., Carter, B.R., Feely, R.A., van Heuven, S., Hoppema, M., Ishii, M., Key, R.M., Kozyr, A., Lauvset, S.K., Lo Monaco, C., Mathis, J.T., Murata, A., Olsen, A., Perez, F.F., Sabine, C.L., Tanhua, T., and Wanninkhof, R. (2019) The oceanic sink for anthropogenic CO_2 from 1994 to 2007. *Science* **363**, 1193–1199. doi:10.1126/science.aau5153

Hansson, I. (1973) The determination of the dissociation constants of carbonic acid in synthetic sea water in the salinity range of 20–40‰ and temperature range of 5–30 °C. *Acta Chem. Scand.* **27**, 931–944. doi:10.3891/acta.chem.scand.27-0931

Kim, H.-C. and Lee, K. (2009) Significant contribution of dissolved organic matter to seawater alkalinity. *Geophys. Res. Lett*. **36**. doi:10.1029/2009GL040271

Kolthoff, I.M., Menzel, H., and Stenger, V.A. (1942) *Volumetric analysis*. New York, NY: Interscience.

Kolthoff, I.M. and Stenger, V.A. (1964) *Volumetric analysis. acid-base, precipitation, and complex-formation reactions Vol. 2,* New York, NY: Interscience.

Le Quéré, C., Andrew, R.M., Friedlingstein, P., Sitch, S., Hauck, J., Pongratz, J., Pickers, P.A., Korsbakken, J.I., Peters, G.P., Canadell, J.G., Arneth, A., Arora, V.K., Barbero, L., Bastos, A., Bopp, L., Chevallier, F., Chini, L.P., Ciais, P., Doney, S.C., Gkritzalis, T., Goll, D.S., Harris, I., Haverd, V., Hoffman, F.M., Hoppema, M., Houghton, R.A., Hurtt, G., Ilyina, T., Jain, A.K., Johannessen, T., Jones, C.D., Kato, E., Keeling, R.F., Goldewijk, K.K., Landschützer, P., Lefèvre, N., Lienert, S., Liu, Z., Lombardozzi, D., Metzl, N., Munro, D.R., Nabel, J.E.M.S., Nakaoka, S.I., Neill, C., Olsen, A., Ono, T., Patra, P., Peregon, A., Peters, W., Peylin, P., Pfeil, B., Pierrot, D., Poulter, B., Rehder, G., Resplandy, L., Robertson, E., Rocher, M., Rödenbeck, C., Schuster, U., Schwinger, J., Séférian, R., Skjelvan, I., Steinhoff, T., Sutton, A., Tans, P.P., Tian, H., Tilbrook, B., Tubiello, F.N., van der Laan-Luijkx, I.T., van der Werf, G.R., Viovy, N., Walker, A.P., Wiltshire, A.J., Wright, R., Zaehle, S., and Zheng, B. (2018) Global carbon budget 2018. *Earth Syst. Sci. Data* **10**, 2141–2194. doi:10.5194/essd-10-2141-2018

Lee, K., Kim, T.-W., Byrne, R.H., Millero, F.J., Feely, R.A., and Liu, Y.-M. (2010) The universal ratio of boron to chlorinity for the North Pacific and North Atlantic oceans. *Geochim. Cosmochim. Acta* **74**, 1801–1811. https://doi.org/10.1016/j.gca.2009.12.027

Lee, K., Millero, F.J., Byrne, R.H., Feely, R.A., and Wanninkhof, R. (2000) The recommended dissociation constants for carbonic acid in seawater. *Geophys. Res. Lett.* **27**, 229–232. doi:10.1029/1999gl002345

Lee, K., Millero, F.J., and Campbell, D.M. (1996) The reliability of the thermodynamic constants for the dissociation of carbonic acid in seawater. *Mar. Chem.* **55**, 233–245. http://dx.doi.org/10.1016/S0304-4203(96)00064-3

Liu, X., Patsavas, M.C., and Byrne, R.H. (2011) Purification and characterization of meta-cresol purple for spectrophotometric seawater pH measurements. *Environ. Sci. Technol.* **45**, 4862–4868. doi:10.1021/es200665d

Lueker, T.J., Dickson, A.G., and Keeling, C.D. (2000) Ocean pCO_2 calculated from dissolved inorganic carbon, alkalinity, and equations for K_1 and K_2: Validation based on laboratory measurements of CO_2 in gas and seawater at equilibrium. *Mar. Chem.* **70**, 105–119. https://doi.org/10.1016/S0304-4203(00)00022-0

Macdonald, A.M., Wanninkhof, R., Dickson, A.G., Carlson, C.A., Key, R.M., Becker, S., Swift, J.H., McNichol, A., Schlosser, P., and Fripiat, F. (2018) Discrete profile measurements of dissolved inorganic carbon, total alkalinity, pH and other hydrographic and chemical data obtained during the R/V Roger Revelle Repeat Hydrography and SOCCOM Cruise in the Indian Ocean and Southern Ocean: GO-SHIP Section I08S, (EXPOCODE 33RR20160208) from 2016-02-08 to 2016-03-16 (NCEI Accession 0171457). NOAA National Centers for Environmental Information. Dataset. https://doi.org/10.7289/v5hm56qr

McLaughlin, K., Weisberg, S.B., Dickson, A.G., Hofmann, G.E., Newton, J.A., Aseltine-Neilson, D., Barton, A., Cudd, S., Feely, R.A., Jefferds, I.W., Jewett, E.B., King, T., Langdon, C.J., McAfee, S., Pleschner-Steele, D., and Steele, B. (2015) Core principles of the California current acidification network: Linking chemistry, physics, and ecological effects. *Oceanography* **28**, 160−169. doi:174.105.34.230

Mehrbach, C., Culberson, C., Hawley, J., and Pytkowicx, R. (1973) Measurement of the apparent dissociation constants of carbonic acid in seawater at atmospheric pressure. *Limnol. Oceanogr.* **18**, 897–907. https://doi.org/10.4319/lo.1973.18.6.0897

Millero, F.J. (2010) Carbonate constants for estuarine waters. *Mar. Freshw. Res.* **61**, 139–142. doi:10.1071/MF09254

Millero, F.J., Graham, T.B., Huang, F., Bustos-Serrano, H., and Pierrot, D. (2006) Dissociation constants of carbonic acid in seawater as a function of salinity and temperature. *Mar. Chem.* **100**, 80–94. doi:10.1016/j.marchem.2005.12.001

Millero, F.J., Pierrot, D., Lee, K., Wanninkhof, R., Feely, R., Sabine, C.L., Key, R.M., and Takahashi, T. (2002) Dissociation constants for carbonic acid determined from field measurements. *Deep Sea Res. Part I. Oceanogr. Res. Papers* **49**, 1705–1723. https://doi.org/10.1016/S0967-0637(02)00093-6

Mojica Prieto, F.J. and Millero, F.J. (2002) The values of $pK_1 + pK_2$ for the dissociation of carbonic acid in seawater. *Geochim. Cosmochim. Acta* **66**, 2529–2540. https://doi.org/10.1016/S0016-7037(02)00855-4

Müller, J.D. and Rehder, G. (2018) Metrology of pH measurements in brackish waters—part 2: Experimental characterization of purified meta-Cresol Purple for spectrophotometric pH_T measurements. *Front. Mar. Sci.* **5**, 1–9. doi:10.3389/fmars.2018.00177

Naviaux, J.D., Subhas, A.V., Dong, S., Rollins, N.E., Liu, X., Byrne, R.H., Berelson, W.M., and Adkins, J.F. (2019) Calcite dissolution rates in seawater: Lab vs. in-situ measurements and inhibition by organic matter. *Mar. Chem.* **215**, 103684. https://doi.org/10.1016/j.marchem.2019.103684

Orr, J.C., Epitalon, J.-M., Dickson, A.G., and Gattuso, J.-P. (2018) Routine uncertainty propagation for the marine carbon dioxide system. *Mar. Chem.* **207**, 84–107. https://doi.org/10.1016/j.marchem.2018.10.006

Orr, J.C., Fabry, V.J., Aumont, O., Bopp, L., Doney, S.C., Feely, R.A., Gnanadesikan, A., Gruber, N., Ishida, A., Joos, F., Key, R.M., Lindsay, K., Maier-Reimer, E., Matear, R., Monfray, P., Mouchet, A., Najjar, R.G., Plattner, G.K., Rodgers, K.B., Sabine, C.L., Sarmiento, J.L., Schlitzer, R., Slater, R.D., Totterdell, I.J., Weirig, M.F., Yamanaka, Y., and Yool, A. (2005) Anthropogenic ocean acidification over the twenty-first century and its impact on calcifying organisms. *Nature* **437**, 681–686. doi:10.1038/nature04095

Papadimitriou, S., Loucaides, S., Rérolle, V.M.C., Kennedy, P., Achterberg, E.P., Dickson, A.G., Mowlem, M., and Kennedy, H. (2018) The stoichiometric dissociation constants of carbonic acid in seawater brines from 298 to 267 K. *Geochim. Cosmochim. Acta* **220**, 55–70. https://doi.org/10.1016/j.gca.2017.09.037

Patsavas, M.C., Byrne, R.H., Wanninkhof, R., Feely, R.A., and Cai, W.-J. (2015) Internal consistency of marine carbonate system measurements and assessments of aragonite saturation state: Insights from two US coastal cruises. *Mar. Chem.* **176**, 9–20. http://dx.doi.org/10.1016/j.marchem.2015.06.022

Riebesell, U., Zondervan, I., Rost, B., Tortell, P.D., Zeebe, R.E., and Morel, F.M. (2000) Reduced calcification of marine plankton in response to increased atmospheric CO_2. *Nature* **407**, 364–367. https://doi.org/10.1038/35030078

Roy, R.N., Roy, L.N., Vogel, K.M., Porter-Moore, C., Pearson, T., Good, C.E., Millero, F.J., and Campbell, D.M. (1993) The dissociation constants of carbonic acid in seawater at salinities 5 to 45 and temperatures 0 to 45 °C. *Mar. Chem.* **44**, 249–267. http://dx.doi.org/10.1016/0304-4203(93)90207-5

Sharp, J.D. and Byrne, R.H. (2020) Interpreting measurements of total alkalinity in marine and estuarine waters in the presence of proton-binding organic matter. *Deep Sea Res. Part I. Oceanogr. Res. Papers*, 103338. https://doi.org/10.1016/j.dsr.2020.103338

Sharp, J.D., Pierrot, D., Humphreys, M.P., Epitalon, J.-M., Orr, J.C., Lewis, E.R., and Wallace, D.W.R. (2020). CO2SYSv3 for MATLAB (Version v3.0.1). Zenodo. http://doi.org/10.5281/zenodo.3952803

Sulpis, O., Lauvset, S.K., and Hagens, M. (2020) Current estimates of K_1* and K_2* appear inconsistent with measured CO_2 system parameters in cold oceanic regions. *Ocean Sci*. **16**, 847−862. https://doi.org/10.5194/os-16-847-2020

Swift, J.H., Mecking, S., Feely, R.A., Dickson, A.G., Carlson, C.A., Jenkins, W.J., McNichol, A., Key, R.M., Ho, D.T., Sigman, D., Macdonald, A.M., Buesseler, K., and Martz, T.R. (2014) Dissolved inorganic carbon, pH, alkalinity, temperature, salinity and other variables collected from discrete sample and profile observations using CTD, bottle and other instruments from MELVILLE in the North Pacific Ocean and Philippine Sea from 2013-03-21 to 2013-05-01 (NCEI Accession 0117338). NOAA National Centers for Environmental Information. Dataset. https://doi.org/10.3334/cdiac/otg.goship_p02_318m20130321

Talley, L.D., Feely, R.A., Dickson, A.G., Swift, J.H., Carlson, C.A., Warner, M.J., McNichol, A., Key, R.M., and Schlosser, P. (2016) Dissolved inorganic carbon (DIC), total alkalinity, pH on total scale, dissolved organic carbon (DOC), chlorofluorocarbons, temperature, salinity and other hydrographic and chemical variables collected from discrete samples and profile observations during the R/V Nathaniel B. Palmer cruise GO-SHIP_P16S_2014 (EXPOCODE 320620140320) in the South Pacific Ocean from 2014-03-20 to 2014-05-05 (NCEI Accession 0157621). NOAA National Centers for Environmental Information. Dataset. https://doi.org/10.3334/cdiac/otg.go_ship_p16s_2014

Uppström, L.R. (1974) The boron/chlorinity ratio of deep-sea water from the Pacific Ocean. *Deep Sea Res. Oceanogr. Abstr.* **21**, 161–162. https://doi.org/10.1016/0011-7471(74)90074-6

Van Heuven, S., Pierrot, D., Rae, J., Lewis, E., and Wallace, D. (2011) MATLAB program developed for CO_2 system calculations. *ORNL/CDIAC-105b.* Carbon Dioxide Inf. Anal. Cent., Oak Ridge Natl. Lab., US Dept. of Energy, Oak Ridge, TN.

Wanninkhof, R., Feely, R.A., Dickson, A.G., Hansell, D.A., Key, R.M., Swift, J.H., Smethie, W.M., Jr., Fine, R.A., Jenkins, W.J., McNichol, A., McCartney, M.S., and Druffel, E.R.M. (2013) Partial pressure (or fugacity) of carbon dioxide, dissolved inorganic carbon, pH, alkalinity, temperature, salinity and other variables collected from discrete sample and profile observations using Alkalinity titrator, CTD and other instruments from ATLANTIS in the North Atlantic Ocean from 2012-04-19 to 2012-05-15 (NCEI Accession 0108160). NOAA National Centers for Environmental Information. Dataset. https://doi.org/10.3334/cdiac/otg.clivar_a20_2012

Wanninkhof, R., Lewis, E., Feely, R.A., and Millero, F.J. (1999) The optimal carbonate dissociation constants for determining surface water pCO_2 from alkalinity and total inorganic carbon. *Mar. Chem.* **65**, 291–301. https://doi.org/10.1016/S0304-4203(99)00021-3

Wanninkhof, R., Zhang, J.-Z., Baringer, M.O., Langdon, C., Cai, W.-J., Salisbury, J.E., and Byrne, R.H. (2016) Partial pressure (or fugacity) of carbon dioxide, dissolved inorganic carbon, pH, alkalinity, temperature, salinity and other variables collected from discrete sample and profile observations using CTD, bottle and other instruments from NOAA Ship RONALD H. BROWN in the Gray's Reef National Marine Sanctuary, Gulf of Mexico and North Atlantic Ocean from 2012-07-21 to 2012-08-13 (NCEI Accession 0157619). NOAA National Centers for Environmental Information. Dataset. https://doi.org/10.3334/cdiac/otg.coastal_gomecc2

Waters, J., Millero, F.J., and Woosley, R.J. (2014) Corrigendum to "The free proton concentration scale for seawater pH", [MARCHE: 149 (2013) 8–22]. *Mar. Chem.* **165**, 66–67. https://doi.org/10.1016/j.marchem.2014.07.004

Waters, J.F. and Millero, F.J. (2013) The free proton concentration scale for seawater pH. *Mar. Chem.* **149**, 8–22. https://doi.org/10.1016/j.marchem.2012.11.003

Wittmann, A.C. and Pörtner, H.-O. (2013) Sensitivities of extant animal taxa to ocean acidification. *Nat. Clim. Change* **3**, 995–1001. doi:10.1038/nclimate1982

Woosley, R.J. (2018) Complexity of marine CO_2 system highlighted by seasonal asymmetries. *Glob. Biogeochem. Cycles* **32**, 1434–1436. doi:10.1029/2018GB006081

Yao, W. and Byrne, R.H. (2001) Spectrophotometric determination of freshwater pH using bromocresol purple and phenol red. *Environ. Sci. Technol.* **35**, 1197–1201. https://doi.org/10.1021/es001573e

CHAPTER THREE:

LOW TEMPERATURE CHARACTERIZATION OF THE CO_2 SYSTEM IN SEAWATER: SPECTROPHOTOMETRIC DETERMINATION OF THE BICARBONATE DISSOCIATION CONSTANT ($20 \leq S_P \leq 40$, $3 \leq t \leq 35$ °C) AND EXAMINATION OF INTERNAL CONSISTENCY

Schockman, K.M., Byrne, R.H., Carter, B.R., and Feely, R.A.

3.1 Abstract

The temperature range of Earth's open-ocean waters is roughly 0−30 °C, yet our understanding of the carbon dioxide (CO_2) system in seawater is largely derived from analyses conducted within a narrow range of temperature (20 or 25 °C). In this work, we address two aspects of cool-water CO_2 system measurements and modeling: (1) we use a recently developed, highly precise spectrophotometric technique to determine the bicarbonate dissociation constant (K_2) in seawater at temperatures as low as 3 °C and (2) we use a large 2021 cruise dataset (uniquely over-determined, including pH measured at two temperatures) to investigate CO_2 system internal consistency at 12 °C, which is near the midpoint of open-ocean temperatures. The low-temperature K_2 determinations are based on spectrophotometric measurements of the pH at which additions of bicarbonate to seawater cause no change in pH (n = 20, RMSE = 0.0036). When combined with recently reported values similarly obtained for higher temperatures, the result is a parameterization of pK_2 (where pK = − log K) applicable for open-ocean conditions of temperature $3 \leq t \leq 35$ °C and salinity $20 \leq S_P \leq 40$. For $t > 17$ °C, this parameterization yields pK_2 results similar to those of

the mostly widely used analogous parameterization of Lueker et al. (2000) (i.e., within published uncertainties of pK_2), but at t < 17 °C it yields consistently smaller values. The reason for this difference is unknown. For the low-temperature assessment of CO_2 system internal consistency (comparing measured and calculated values of CO_2 system parameters), we used four quantities measured during NOAA's 2021 West Coast Ocean Acidification Cruise: total alkalinity (A_T), total dissolved inorganic carbon (C_T), pH measured at 25 °C, and pH measured at 12 °C (n = 265). The results indicate that pH measurements made at 25 °C can be reliably used to calculate other CO_2 system parameters at in situ conditions. Best in situ internal consistency is achieved when (a) derived parameters are calculated from pH paired with either A_T or C_T (rather than from A_T and C_T paired with each other) and (b) the previously published set of CO_2 system dissociation constants from Lueker et al. (2000) is used (rather than the constants of this work). These conclusions apply in the context of a CO_2 system model that excludes explicit consideration of the buffering contributions of organic acids and may therefore change as the effects of those contributions become better understood.

3.2 Introduction

As the effects of global climate change and ocean acidification continue to grow, accurate descriptions of the evolving chemical processes in seawater become ever more essential. One particularly important example includes the chemical reactions that accompany the oceanic uptake of anthropogenic carbon dioxide (CO_2). Understanding these reactions is critical for assessing the consequences of ocean acidification and the ocean's ability to ameliorate climate change. Exchange of hydrogen ions among inorganic carbon species buffers the pH of seawater and thus

exerts a strong influence on global carbon cycling (Feely et al., 2009, 2018; Gruber et al., 2019; Jiang et al., 2019; Friedlingstein et al., 2022).

The inorganic CO_2 system is composed of three species that exchange hydrogen ions: CO_2^* ($CO_{2(aq)} + H_2CO_3$), bicarbonate (HCO_3^-), and carbonate (CO_3^{2-}), where

$$CO_{2(g)} \leftrightarrow CO_2^* \tag{3.1}$$

$$CO_2^* + H_2O \leftrightarrow HCO_3^- + H^+ \tag{3.2}$$

$$HCO_3^- \leftrightarrow CO_3^{2-} + H^+ \tag{3.3}$$

The equilibrium constants relevant to eq. (3.2) and (3.3) can be expressed as:

$$K_1 = \frac{[HCO_3^-]_T[H^+]_T}{[CO_2^*]} \tag{3.4}$$

$$K_2 = \frac{[CO_3^{2-}]_T[H^+]_T}{[HCO_3^-]_T} \tag{3.5}$$

where $[\ ]_T$ denotes total substance contents (i.e., free ions plus ion pairs) expressed in mol kg-soln^{-1}. The CO_2 system dissociation constants K_1 and K_2 are dependent on salinity (S_P, practical salinity scale), temperature (T in K or t in °C), and hydrostatic pressure (P).

In practice, the CO_2 system is generally described in terms of four measurable parameters: total alkalinity (A_T), total dissolved inorganic carbon (C_T), pH, and CO_2 fugacity (fCO_2). These terms are defined by:

$$A_T = [HCO_3^-]_T + 2[CO_3^{2-}]_T + [B(OH)_4^-]_T + [OH^-]_T - [H^+]_T + 2[PO_4^{3-}]_T + [HPO_4^{2-}]_T + \ldots \tag{3.6}$$

$$C_T = [CO_3^{2-}]_T + [HCO_3^-]_T + [CO_2^*] \tag{3.7}$$

$$pH_T = -\log [H^+]_T \tag{3.8}$$

$$fCO_2 = [CO_2^*]/K_0 \quad (3.9)$$

where the ellipsis in eq. (3.6) denotes terms of quantitatively lesser significance, pH_T denotes pH on the total hydrogen ion concentration scale, and K_0 is the equilibrium constant describing CO_2 solubility. When two or more CO_2 system parameters are directly measured, all others can be calculated from those two measurements in conjunction with an equilibrium model and ancillary measurements of S_P, T, P, and certain nutrient concentrations (e.g., silicate, phosphate, and ammonium). Eqs. (3.6) and (3.7), for example, provide a means of using shipboard measurements (e.g., A_T and C_T) to estimate other equilibrium parameters (e.g., pH_T, fCO_2, and calcium carbonate saturation state (Ω)) at in situ conditions. When three or more CO_2 system parameters are directly measured, the system is overdetermined. In this case, measured and calculated values of a given parameter can be compared to help assess the internal consistency of the measurements and the model. ("Model" in this sense refers collectively to the equilibrium relationships expressed in eqs. (3.6)–(3.9) and others, the investigator's choices of equilibrium constants and the total-boron-to-salinity ratio (B_T/S), and an appropriate accounting of nutrient and organic acid alkalinity contributions.) In general, an internally consistent model provides calculated values of CO_2 system parameters that are not statistically different from measured values of the same parameter.

K_1 and K_2, as well as the dissociation constants of boric acid (K_B) and water (K_W), are essential components of the CO_2 system model, and thus CO_2 system calculations. Previous experimental determinations and evaluations of K_1 and K_2 include those of Lueker et al. (2000), Waters and Millero (2013) as revised by Waters et al. (2014), further denoted as Waters et al. (2013, 2014), Sulpis et al. (2020), and Schockman and Byrne (2021). Several studies (Lee et al., 2000; Patsavas et al., 2015; Woosley, 2021) have recommended use of the K_1 and K_2 characterizations of Lueker et al. (2000), largely based on internal consistency assessments at 20

or 25 °C. Community preferences for the Lueker et al. (2000) constants generally rely on the assumption that the good internal consistency observed at 20 or 25 °C is also applicable at lower temperatures, but this assumption has not yet been thoroughly verified. Neither the work of Sulpis et al. (2020), which is a re-determination of the K_1 and K_2 parameterization reported by Lueker et al. (2000) that utilizes additional cruise data, or the work of Schockman and Byrne (2021) has yet been extensively assessed with respect to internal consistency.

Schockman and Byrne (2021) developed a new high-precision spectrophotometric method to determine K_1K_2 over the temperature range $15 \leq t \leq 35$ °C. The present work uses the same methodology to expand that range to include the cooler temperatures commonly observed in open-ocean subsurface or high-latitude surface waters. Specifically, K_2 is determined from (a) the K_1 parameterization of Waters et al. (2013, 2014) in conjunction with (b) experimental determinations of the pH at which an addition of bicarbonate to a natural seawater solution of known salinity produces no change in pH (with this unchanging pH being denoted as pH^0). The K_2 values obtained in the present work were combined with the K_2 data of Schockman and Byrne (2021) to provide a single K_2 parameterization applicable for $20 \leq S_P \leq 40$ and $3 \leq t \leq 35$ °C.

As noted above, internal consistency assessments used to evaluate CO_2 system models have largely been limited to 20 or 25 °C. In this work, we used measured oceanic values of A_T and C_T (quantities that are not temperature-dependent) and pH_T (measured at both 25 and 12 °C) to evaluate the CO_2 system dissociation constant parameterizations of previous works (i.e., Lueker et al. (2000); Waters et al. (2013, 2014); and Sulpis et al. (2020)) and of this work, at a temperature closer to the midpoint of typical oceanic conditions (12 °C). We also quantitatively assessed (1) differences between measured pH and pH calculated from A_T and C_T, (2) the utility of measuring

pH at lower temperatures (i.e., t < 25 °C), and (3) the influence of uncertainties in K_1, K_2, B_T/S, and organic alkalinity on measured versus modeled A_T.

3.3 Materials

3.3.1 Chemicals and reagents

Chemicals used in the laboratory experiments to determine pH^0 were sodium bicarbonate ($NaHCO_3$) (Alfa Aesar Puratronic™, 99.998% metal basis, CAS 144-55-8; Lots T03F021, T18F042, and 25312B), HCl (1 N, Fisher Chemical, CAS 7647-01-0), NaOH (1 N, Fisher Chemical, CAS 1310-73-2), pure CO_2 gas (Air Products, anaerobic grade), and dry N_2 gas (Airgas, industrial grade, CGA-580). Seawater was collected offshore in the Gulf of Mexico prior to the start of experiments and stored in sealed glass carboys throughout the duration of the measurements (approximately seven months). Meta-cresol purple (mCP), a sulfonephthalein indicator, was purified at the University of South Florida according to Liu et al. (2011); this dye (10 mM in 0.7 M NaCl) was used for the laboratory experiments to determine pH^0 and for the at-sea measurements of pH_T.

3.3.2 Equipment

3.3.2.1 Laboratory pH^0 measurements to determine K_2

Samples were collected into two-port 10 cm cylindrical optical glass spectrophotometric cells, which had been regularly cleaned with HCl to prevent accumulation of solids on the glass interior surfaces. The filled sample cells were stored in a custom-made cell warmer connected to a recirculating water bath (Lauda Ecoline E 100) for thermal equilibration prior to measurements. A diode array spectrophotometer (Agilent 8453) with the UV lamp turned off was used for the

spectrophotometric pH measurements. A second recirculating water bath (Fisher Scientific Isotemp 3013) was connected to a custom-made insulated cell holder inside the spectrophotometer to maintain a consistent, specified temperature during measurements.

HCl/NaOH additions were made using pipettes (2.5 µL or 10 µL, Eppendorf Research). The mCP indicator was added to cells using a micrometer buret (2 mL, Gilmont GS-1200). Salinity (S_P) was measured conductometrically using a salinometer (Guildline Portasal Model 8410). Temperatures of the samples were measured using a handheld digital thermometer (±0.025 °C, Ertco-Eutechnics Model 4400) that had been calibrated against a quartz thermometer (Hewlett Packard Model 2804 A) prior to the start of the experiments.

Rubber tubing (Cole Parmer Pharmed BPT®) was used to flow N_2 gas across the outer walls of the spectrophotometric cells during experiments. For laboratory-based measurements at t < 9 °C, the work was conducted in a low-temperature environmental room (Harris Environmental Systems).

3.3.2.2 At-sea pH_T measurements

Shipboard cruise pH_T measurements were made using two diode array spectrophotometers (Agilent 8453), with the UV lamps turned off. For temperature equilibration before and during absorbance measurements, each spectrophotometer was connected to a custom-made cell warmer, with each being individually connected to its own recirculating water bath (one a Lauda Ecoline E 100 and the other a Lauda Ecoline RE 120) to maintain temperature at either 25 or 12 °C. Sample temperatures were measured using handheld digital thermometers (±0.025 °C for an Ertco-Eutechnics Model 4400 or ±0.05 °C for a VWR Traceable Data-Log 50) that had both been

calibrated against a quartz thermometer (Hewlett Packard Model 2804 A) prior to the start of the cruise.

3.4 Methods

3.4.1 Laboratory pH^0 measurements to determine K_2

This work follows the methods developed in Schockman and Byrne (2021) (i.e., Ch. 2), which are described here in abbreviated form. Experimental pH^0 values (i.e., the pH values at which an addition of bicarbonate to a natural seawater solution of known salinity produces no change in pH) were obtained via spectrophotometric measurements that allowed for the determination of K_2 (Mehrbach et al., 1973; Schockman and Byrne, 2021) via the following equation:

$$K_1K_2 = \frac{10^{-2pH^0} + (1-\Phi)K_1 10^{-pH^0}}{2\Phi - 1} \quad (3.10)$$

where K_1 (previously published) has been independently determined from potentiometric titrations (e.g., Waters et al. (2013, 2014)) and Φ is a small correction factor that accounts for the potential impurity of bicarbonate ($\Phi = 1$ if bicarbonate is completely pure, and $\Phi < 1$ if there is any carbonate contamination). Other impurities such as phosphate, silicate, and organic acids/bases do not participate in acid–base reactions during measurements at constant pH.

The experiments to determine pH^0 were performed for 20 pairs of (S_P, t) conditions between $20.4 \leq S_P \leq 44.6$ and $3.4 \leq t \leq 12.6$ °C. Nine batches of seawater of various salinities were made via evaporation (i.e., exposure to the atmosphere via an open-top container for several days until the target salinity was reached) or by dilution with Milli-Q water. Measurements at approximately 9 and 12 °C were performed in a normal laboratory environment, while measurements at approximately 3 and 6 °C were made in a temperature-controlled environmental

laboratory setting. Purification of $NaHCO_3$ was achieved by directing a stream of pure CO_2 gas on a slurry of the salt in the manner described by Schockman and Byrne (2021), such that additional assessments of $NaHCO_3$ purity beyond those of Schockman and Byrne (2021) were not required. All other experimental details are identical to those of Schockman and Byrne (2021).

3.4.2 At-sea pH_T measurements

NOAA's 2021 West Coast Ocean Acidification Cruise (WCOA2021) took place onboard the *R/V Ronald H. Brown* from June 23−July 26, 2021. (The National Centers for Environmental Information's expedition code for this cruise is not yet available. Once all data products are finalized, an EXPOCODE will be released, and all cruise data will be available online from NOAA's National Centers for Environmental Information (https://www.ncei.noaa.gov/access/ocean-carbon-data-system/oceans/Coastal/WCOA.html).) Vertical profiles (between approximately 0 to 4200 dbar) of A_T, C_T, and pH_T were measured at 133 stations, as were S_P, T, P, and concentrations of silicate, phosphate, ammonium, and other quantities. A_T was measured by potentiometric titration, and C_T was analyzed using coulometric titration (Dickson et al., 2007). The accuracies of the A_T and C_T measurements (±2 μmol kg^{-1}) were assessed using certified reference materials (CRMs) provided by Dr. Andrew Dickson's laboratory at the Scripps Institution of Oceanography. All pH_T measurements were made onboard spectrophotometrically, using purified mCP indicator. At all stations, pH_T was measured (n = 1663) at the traditional experimental temperature of 25 °C (here denoted as pH_{25}). For 29 of those stations, additional spectrophotometric pH_T measurements (n = 312) were made at a temperature of approximately 12 °C (denoted as pH_{12}). A temperature of 12 °C was the lowest measurement

temperature that could be reliably maintained onboard while still obtaining pH measurements in a reasonable time frame with the desired precision.

A detailed description of the spectrophotometric pH measurement procedure is given elsewhere (Liu et al., 2011; Schockman and Byrne, 2021). Ratios of absorbances at 578 and 434 nm, along with a small baseline correction (applied using the non-absorbing wavelength of 730 nm) (Byrne, 1987; Clayton and Byrne, 1993; Liu et al., 2011), were used to calculate pH_T with the mCP parameterization of Müller and Rehder (2018). To achieve thermal equilibration at 12 °C, the typical 25 °C measurement procedure was slightly modified. Samples collected in spectrophotometric cells directly from the CTD rosette were allowed to thermally equilibrate at low temperature in a custom-made cell warmer for at least 45 minutes (rather than the usual 30 minutes). Samples were then placed in the spectrophotometer's thermostatted cell holder for at least one minute (rather than the usual 30 seconds) before absorbances were recorded. As is standard practice, a small correction was applied to account for indicator pH changes caused by addition of indicator solution to the samples (Clayton and Byrne, 1993; Liu et al., 2011). Duplicates of pH_{25} samples (n = 207) had an average standard deviation of 0.0004, and duplicates of pH_{12} samples (n = 36) had an average standard deviation of 0.002. Our pH_{12} data can be found in Appendix C.1.

3.4.2.1 CO_2 system calculations

Internal consistency was assessed using the WCOA2021 at-sea data set, which included measurements of A_T, C_T, pH_{25}, and pH_{12}. Data with poor quality flags were removed from consideration, resulting in n = 265 samples with good-quality measurements for all four parameters. The CO_2 system calculations were made using CO2SYS (Pierrot et al., 2006; Van

Heuven et al., 2011) version 3.1.1 for MATLAB (Sharp et al., 2020), modified to include the K_1 of Waters et al. (2013, 2014) paired with the K_2 of this work as an available option. Calculations were performed on the total hydrogen ion concentration pH scale (pH_T) with the following parameters: K_1 and K_2 as specified, bisulfate dissociation constant (K_{HSO4}) of Dickson (1990), hydrogen fluoride dissociation constant (K_{HF}) of Perez and Fraga (1987), and B_T/S of Lee et al. (2010) (unless otherwise explicitly stated). Calculated values of a parameter X obtained using inputs of Y and Z are denoted throughout the manuscript as 'X(Y,Z)'. The difference between measured X and X(Y,Z) is a residual of X and is denoted as 'ΔX'.

3.5 Results and discussion

3.5.1 Spectrophotometric pK_2 determination for $20 \leq S_P \leq 40$ and $3 \leq t \leq 35$ °C

Experimentally determined average pH^0 values for 20 (S_P, t) pairings and their associated standard deviations are provided in Table 3.1. The individual values of $pH_{initial}$ and pH_{final} used to determine pH^0, as defined and described in Schockman and Byrne (2021), are provided in Appendix C.2. The pooled standard deviation of the pH^0 values given in Table 3.1 is 0.0021. The pK_2 values listed in Table 3.1 were determined using eq. (3.10) with inputs of the average pH^0 values from Table 3.1, a Φ value of 0.9996 (as reported in Schockman and Byrne (2021)), and the pK_1 parameterization of Waters et al. (2013, 2014). These calculated pK_2 values ($n = 20$, $3 \leq t \leq 13$ °C) were then combined with the pK_2 values from Schockman and Byrne (2021) ($n = 26$, $15 \leq t \leq 35$ °C)) to obtain one complete set of pK_2 values determined from the K_1K_2 spectrophotometric method over a range of temperatures and salinities appropriate to open-ocean seawater.

The combined pK_2 values ($n = 46$) were parameterized as:

$$pK_2 = e_1 + e_2 T^{-1} + e_3 \ln T + e_4 S_P + e_5 S_P^{0.5} + e_6 S_P^{2} + e_7 (S_P/T) + e_8 T^{0.5} \quad (3.11)$$

The e_n coefficient values are provided in Table 3.2. Based on an F-test, an additional term ($e_8 T^{0.5}$) was added to the original pK_2 parameterization of Schockman and Byrne (2021) to statistically improve the fit. The root mean square error (RMSE) of the pK_2 parameterization from this work is 0.0036. Residuals of pK_2 (i.e., experimental pK_2 values minus parameterized pK_2 values obtained using eq. (3.11)) are shown in Fig. 3.1. All residuals are randomly distributed in terms of S_P and T, with the standard deviation of all residuals (i.e., the random uncertainty in pK_2 (Orr et al., 2018)) being 0.0036.

Table 3.1.
Average experimental pH^0 values (± associated standard deviations (stdev)) and resulting pK_2 values for the specified (S_P, t) conditions. These pH^0 values and the pK_1 of Waters et al. (2013, 2014) were input into eq. (3.10) to determine the associated pK_2 values.

S_P	t (°C)	pH^0 (± stdev) (n = 4)	pK_2
20.35	3.44	7.8101 ± 0.0024	9.4692
20.35	6.50	7.7645 ± 0.0026	9.4159
20.35	9.77	7.7207 ± 0.0026	9.3665
20.35	12.20	7.6861 ± 0.0011	9.3244
24.45	3.63	7.7595 ± 0.0015	9.3923
24.45	6.02	7.7267 ± 0.0022	9.3560
25.78	9.48	7.6729 ± 0.0014	9.2952
25.78	12.32	7.6340 ± 0.0026	9.2490
31.24	3.61	7.7147 ± 0.0029	9.3321
31.24	6.09	7.6777 ± 0.0018	9.2883
31.08	9.74	7.6295 ± 0.0024	9.2336
31.08	12.40	7.5940 ± 0.0016	9.1921
35.09	3.43	7.6888 ± 0.0026	9.2930
35.09	6.09	7.6496 ± 0.0017	9.2469
35.36	9.32	7.6069 ± 0.0015	9.1998
35.36	12.34	7.5665 ± 0.0018	9.1524
40.97	3.56	7.6574 ± 0.0018	9.2531
40.97	6.16	7.6196 ± 0.0019	9.2086
44.61	9.66	7.5533 ± 0.0025	9.1282
44.61	12.59	7.5128 ± 0.0022	9.0791

Table 3.2.
Coefficients for the pK_2 parameterization of eq. (3.11): $pK_2 = e_1 + e_2 T^{-1} + e_3 \ln T + e_4 S_P + e_5 S_P^{0.5} + e_6 S_P^2 + e_7 (S_P/T) + e_8 T^{0.5}$. As a check value: at S_P = 35 and T = 298.15 K, pK_2 = 8.9608. This pK_2 parameterization is applicable for $3 \le t \le 35$ °C and $20 \le S_P \le 40$.

	pK_2
e_1	−2809.819
e_2	57877
e_3	607.4554
e_4	0.02596
e_5	−0.5037
e_6	−0.000174
e_7	5.766
e_8	−48.3447

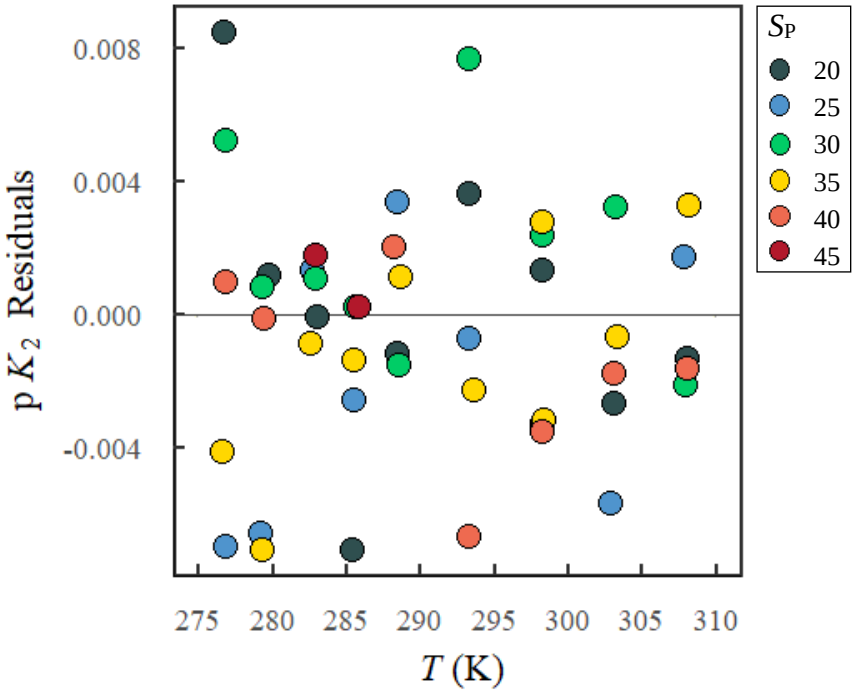

Fig. 3.1. Residuals of pK_2 (i.e., experimental pK_2 minus parameterized pK_2 (eq. (3.11))) as a function of temperature, with colors indicating approximate salinity. For T > 288.15 K, the experimentally derived pK_2 values are from Schockman and Byrne (2021); for T < 288.15 K, values are from this work.

The pK_2 residuals of Fig. 3.1 (RMSE = 0.0036) are comparable in magnitude to the residuals of Schockman and Byrne (2021) (RMSE = 0.0029) and are smaller than the residuals reported in the previous works of Lueker et al. (2000) (RMSE = 0.0092) and Millero et al. (2006) (which is the experimental basis of Waters et al. (2013, 2014)) (RMSE = 0.010). (For comparison, the residuals of Lueker et al. (2000) and Millero et al. (2006) are provided in Appendix C.3.) The smaller RMSE value for this work indicates that the spectrophotometric K_1K_2 method is more precise than the other methods previously employed at low temperatures. The improved precision of this spectrophotometric study should facilitate accurate extrapolation of our pK_2 model to temperatures somewhat above and below the experimental range of conditions. Furthermore, the parameterization of Lueker et al. (2000) is based on experimental measurements made at four temperatures (2, 13, 25, and 35 °C) for each discrete salinity, whereas the results from this work are based on experimental measurements at nine temperatures (3, 6, 9, 12, 15, 20, 25, 30, 35 °C) for each discrete salinity. The pK_2 parameterization of this work is therefore more comprehensive in terms of temperatures within the range $3 \leq t \leq 35$ °C.

The systematic uncertainty in pK_2 was determined to be ±0.015 based on the standard deviation of differences between this work and (a) Lueker et al. (2000) and (b) Waters et al. (2013, 2014). This approach is the recommended means of assessing systematic uncertainty as discussed in Orr et al. (2018). However, Schockman and Byrne (2021) noted that the experimental determinations of pK_2 from sources (a) and (b) were less precise than determinations obtained with the spectrophotometric technique described in Schockman and Byrne (2021) and, furthermore, that the residuals of the pK_2 parameterizations in those earlier works were not random with respect to temperature or salinity. Therefore, the overall estimated uncertainty of ±0.015 in pK_2 (summing

the random (±0.0036) and systematic (±0.015) components) is likely an overestimate. To our knowledge, no alternative method to estimate systematic uncertainty is presently available.

Our work uses the K_1 parameterization of Waters et al. (2013, 2014) to obtain our spectrophotometrically derived K_2 determination. (As noted in Section 3.4.1, the K_1 values of Waters et al. (2013, 2014) are combined with our experimentally determined K_1K_2 values to ultimately obtain K_2.) Therefore, any systematic errors in K_1 are propagated to our K_2 values. Orr et al. (2018) estimates the uncertainty in pK_1 to be ±0.0075, whereby an error of this magnitude would be directly reflected in our pK_2 values. However, importantly, this uncertainty is smaller than the ±0.015 estimated uncertainty in pK_2.

3.5.2 Direct comparison of pK_2 parameterizations

We first compared our pK_2 parameterization (eq. (3.11)) with that of Schockman and Byrne (2021) (their eq. (15)). Recall that those experimental data are included in the development of the parameterization reported in this work. Within the $15 \leq t \leq 35$ °C temperature range examined by Schockman and Byrne (2021), the maximum difference between their original pK_2 parameterization and ours is 0.002. This difference is less than the random uncertainty in pK_2 of 0.0036, which indicates that within the temperature range of $15 \leq t \leq 35$ °C, the pK_2 parameterization of Schockman and Byrne (2021) is not statistically different from the pK_2 parameterization of this work. Therefore, any CO_2 system calculations made using the pK_2 of Schockman and Byrne (2021) over this temperature range can be considered to be consistent with the parameterization described in the present work. This point is further illustrated by comparing the internal consistency assessments of Schockman and Byrne (2021) (calculating mean A_T, C_T, and pH residuals for nine oceanographic cruise data sets) with the same assessments calculated

using our new pK_2 parameterization (eq. (3.11)) (data tables provided in Appendix C.4). The results are nearly identical to one another.

Comparisons of our pK_2 values (eq. (3.11)) with those of other authors' works are shown in Fig. 3.2. The pK_2 parameterizations of this work and of Lueker et al. (2000) (Fig. 3.2a) are quite similar (i.e., within ±0.015, the reported uncertainty in pK_2) for all salinities $20 \leq S_P \leq 40$ at temperatures of approximately $17 \leq t \leq 35$ °C ($290.15 \leq T \leq 308.15$ K). In contrast, the pK_2 parameterizations of this work and of Waters et al. (2013, 2014) (Fig. 3.2b) are within ±0.015 only for $20 \leq S_P \leq 30$ and $S_P \geq 37$ at temperatures ranging from $5 \leq t \leq 35$ °C ($278.15 \leq T \leq 308.15$ K). For temperatures below approximately 10 °C ($T < 283.15$ K), the pK_2 parameterization of this work produces pK_2 values that are consistently smaller than those of Lueker et al. (2000) and Waters et al. (2013, 2014) at most salinities. The maximum difference between the pK_2 parameterization of this work and the pK_2 parameterizations of Lueker et al. (2000) or Waters et al. (2013, 2014) (−0.04) is observed at the lowest experimental temperature (3 °C, 276.15 K). Because the Sulpis et al. (2020) pK_2 parameterization is a re-fit of Lueker et al. (2000), the differences between our work and Sulpis et al. (2020) show similar patterns to Fig. 3.2a (not shown).

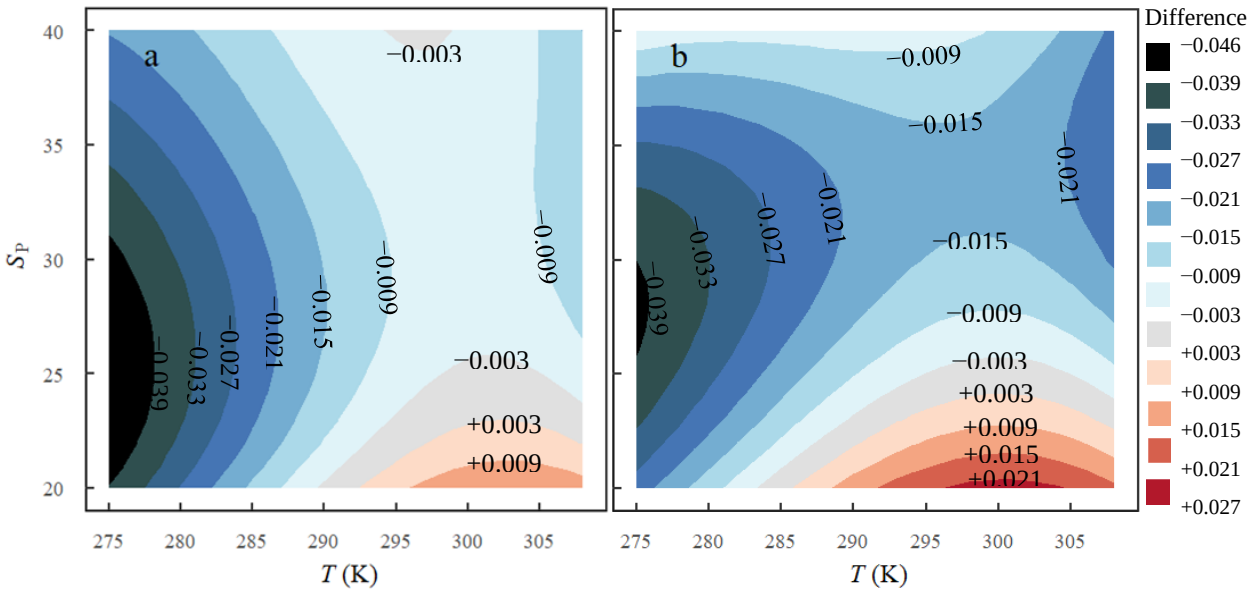

Fig. 3.2. Differences in pK_2 parameterizations shown as the pK_2 parameterization of this work (eq. (3.11)) minus the pK_2 parameterizations of (a) Lueker et al. (2000) and (b) Waters et al. (2013, 2014) as a function of S_P and T. The color contours indicate the magnitude of the difference.

3.5.3 Examination of internal consistency

Internal consistency assessments are commonly used (Lee et al., 2000; Patsavas et al., 2015; Schockman and Byrne, 2021; Woosley, 2021) as a basis for recommending a set of constants (parameterizations) for use within a given set of equilibrium equations (even though, to be clear, internal consistency is not a measure of accuracy). The general procedure is to calculate values of CO_2 system parameters using an over-determined dataset; the same calculations are performed using multiple dissociation constant parameterizations. Parameterizations that most consistently yield the smallest residuals are recommended for future use, though this process can be somewhat subjective. A given set of equations and parameterizations is said to yield internally consistent results if the mean residuals of the CO_2 system parameters (i.e., A_T, C_T, and pH) for a particular dataset are not statistically different from zero.

3.5.3.1 Mean residuals of A_T, C_T, pH_{25}, and pH_{12}

We performed internal consistency assessments using the CO_2 system model equations described in Section 3.2, the WCOA2021 cruise data described in Section 3.4.2, and four sets of dissociation constant parameterizations: K_1 and K_2 of Lueker et al. (2000); K_1 and K_2 of Waters et al. (2013, 2014); K_1 and K_2 of Sulpis et al. (2020); and K_1 of Waters et al. (2013, 2014) and K_2 of this work (eq. (3.11)) (this pairing is collectively referred to as "this work" when discussing CO_2 system calculations). Within this framework, we assessed the K_1 and K_2 parameterizations by calculating A_T, C_T, and pH_T with each parameterization and then comparing the calculated values to the measured cruise values. The resulting mean residuals (Table 3.3) show that CO_2 system calculations using the K_1 and K_2 parameterizations of all four works provide calculated values that are internally consistent with measured values at both 25 °C and 12 °C (i.e., mean residuals ± 2σ standard deviation were not statistically different from zero). The differences in mean residuals obtained using the four sets of dissociation constants (Table 3.3) are within ~4 μmol kg^{-1} for ΔA_T and ΔC_T and within ~0.01 for ΔpH.

Table 3.3.
Mean differences between measured and calculated CO_2 system parameters (i.e., residuals) resulting from the four sets of K_1 and K_2 parameterizations, as applied to the WCOA2021 data set (n = 265). Uncertainty is given as ±2σ standard deviation.

	Mean residuals (±2σ)			
	This work	Lueker et al. (2000)	Waters et al. (2013, 2014)	Sulpis et al. (2020)
$\Delta A_{T,25} = A_T - A_T(C_T,pH_{25})$	2.0 ± 6.6	2.7 ± 5.9	4.8 ± 5.6	3.5 ± 5.8
$\Delta A_{T,12} = A_T - A_T(C_T,pH_{12})$	−0.3 ± 8.3	2.3 ± 5.9	3.8 ± 5.9	3.9 ± 5.7
$\Delta C_{T,25} = C_T - C_T(A_T,pH_{25})$	−2.0 ± 6.5	−2.7 ± 5.8	−4.7 ± 5.6	−3.5 ± 5.8
$\Delta C_{T,12} = C_T - C_T(A_T,pH_{12})$	0.2 ± 8.0	−2.3 ± 5.9	−3.8 ± 5.9	−3.8 ± 5.7
$\Delta pH_{25} = pH_{25} - pH_{25}(A_T,C_T)$	−0.006 ± 0.018	−0.008 ± 0.017	−0.014 ± 0.017	−0.010 ± 0.017
$\Delta pH_{12} = pH_{12} - pH_{12}(A_T,C_T)$	0.000 ± 0.022	−0.007 ± 0.018	−0.012 ± 0.018	−0.012 ± 0.018

3.5.3.2 Patterns of A_T and C_T residuals

We plotted individual residual values for the purpose of examining potential patterns not immediately clear from mean residual analyses. Residuals of A_T at 25 °C are shown in Fig. 3.3 for calculations with the four sets of dissociation constants. Residuals of C_T at 25 °C are identical to the magnitude of A_T residuals and opposite in sign (not shown). All differences between individual calculated values of A_T (Fig. 3.3) or C_T (not shown) are within ±9 μmol kg^{-1}, which is within the reported A_T and C_T measurement uncertainty of ±10 μmol kg^{-1} (McLaughlin et al., 2015) (though the uncertainties in A_T and C_T from WCOA2021 are likely smaller than this value). Although all four sets of constants yield mean $\Delta A_{T,25}$ residuals that are not statistically different from zero (Table 3.3), Fig. 3.3 highlights that $\Delta A_{T,25}$ values calculated using the set of constants including the K_2 of our work are most symmetrically distributed about zero. Use of the other sets of constants yield somewhat larger positive offsets of varying magnitude (Fig. 3.3b-d). $\Delta A_{T,25}$ calculated using the Lueker et al. (2000) constants are systematically slightly positive (Fig. 3.3b), while $\Delta A_{T,25}$ calculated using the Waters et al. (2013, 2014) or Sulpis et al. (2020) constants (Fig. 3.3c and 3.3d) are systematically somewhat larger (more positive). In most cases, the more strongly positive $\Delta A_{T,25}$ values are associated with lower pH_T, with this pattern most pronounced when calculations are performed using the constants of this work.

Residuals of A_T at 12 °C are shown in Fig. 3.4 for calculations with the four sets of dissociation constants. Residuals of C_T at 12 °C are identical to the magnitude of A_T residuals and opposite in sign (not shown). Once again, all differences between individual calculated values of A_T (Fig. 4) or C_T (not shown) are within ±9 μmol kg^{-1}, which is within the reported A_T and C_T measurement uncertainty of ±10 μmol kg^{-1} (McLaughlin et al., 2015). As for $\Delta A_{T,25}$, while all four sets of constants yield mean $\Delta A_{T,12}$ residuals that are not statistically different from zero (Table

3.3), Fig. 3.4 highlights that the individual values of $\Delta A_{T,12}$ calculated using the set of constants of this work are the most symmetrically distributed about zero. Use of the other sets of constants yields positive offsets of varying magnitude. As seen with $\Delta A_{T,25}$ (Fig. 3.3), in most cases, more positive $\Delta A_{T,12}$ values are associated with lower measured pH_{12} values.

Comparisons between residuals in Fig. 3.3 and 3.4 show that, in all cases, $\Delta A_{T,25}$ residuals values are more positive than the corresponding $\Delta A_{T,12}$ residual values. This finding indicates that A_T calculated from pH_{12} and C_T is more internally consistent than A_T calculated from pH_{25} and C_T, though we cannot comment on accuracy at this time. Furthermore, the patterns of A_T residuals obtained using the dissociation constants of this work (Fig. 3.3a and 3.4a) are qualitatively different (i.e., a pronounced sloping pattern as a function of A_T) from those obtained using the dissociation constants of the three other works (Figs. 3.3b-d and 3.4b-d).

3.5.3.3 Patterns of pH residuals

The pH_{12} residuals can be examined in terms of either (1) $\Delta pH_{12} = pH_{12} - pH_{12}(A_T,C_T)$ or (2) $^{*}\Delta pH_{12} = pH_{12} - pH_{12}(pH_{25},C_T)$. (Calculations of pH_{12} using inputs of (pH_{25},C_T) and (pH_{25},A_T) provide closely identical results (not shown). For more details see Appendix C.5.) Both sets of residuals are shown in Fig. 3.5 for calculations made with the constants of this work (upper panels) and the constants of Lueker et al. (2000) (lower panels). The residuals calculated using the constants of Waters et al. (2013, 2014) and Sulpis et al. (2020) follow the same general patterns and are not shown. When pH is calculated from (A_T,C_T) (Figs. 3.5a and 3.5c), a previously reported (McElligott et al., 1998; Williams et al., 2017) pH-dependent offset is observed for calculations with all four sets of dissociation constants. The magnitude is similar in all cases.

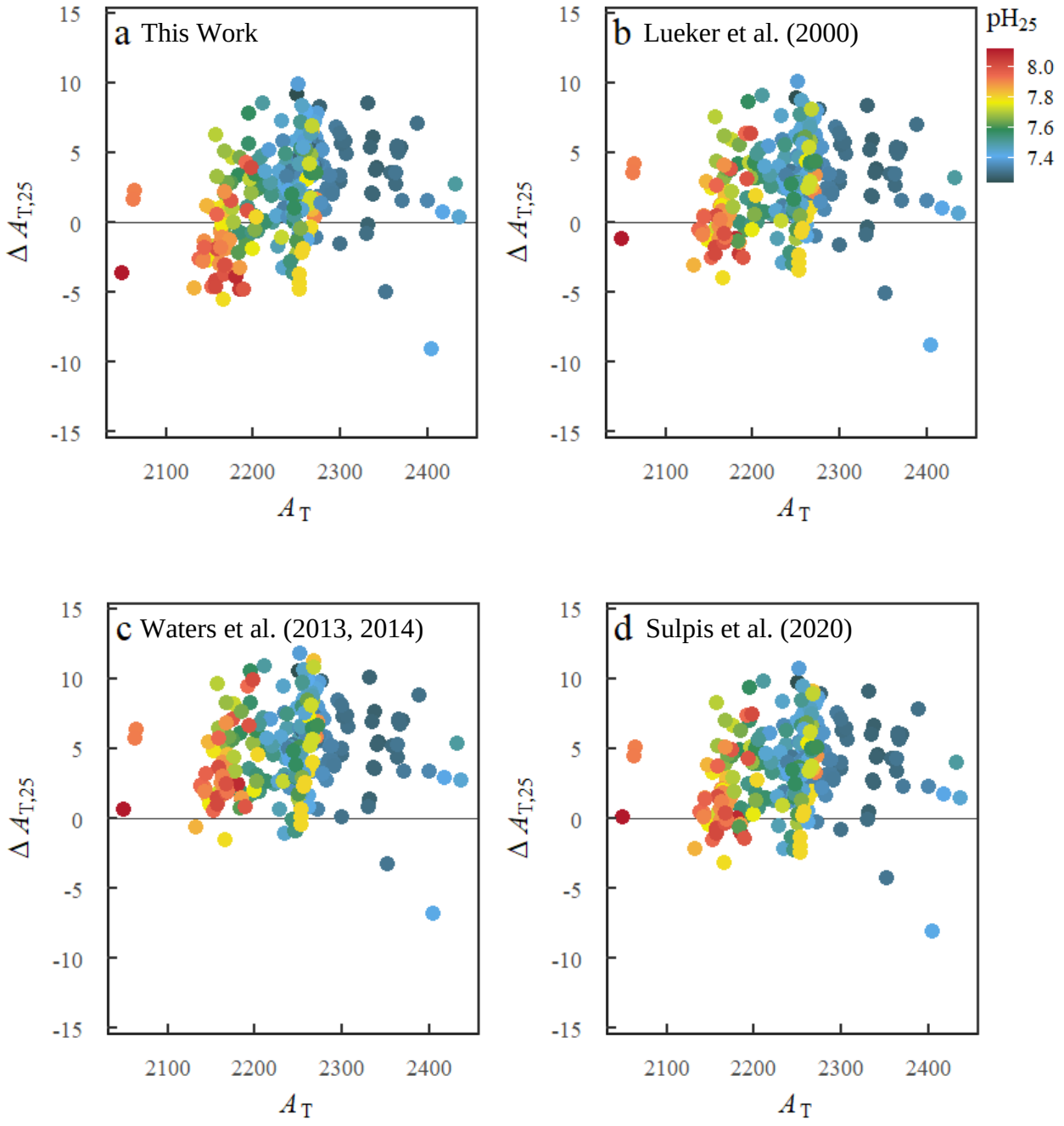

Fig. 3.3. Residuals of A_T at 25 °C ($\Delta A_{T,25} = A_T - A_T(C_T,pH_{25})$) obtained using the CO_2 system dissociation constants of (a) this work, (b) Lueker et al. (2000), (c) Waters et al. (2013, 2014), and (d) Sulpis et al. (2020), shown as a function of measured A_T. Dot colors indicate the measured pH_{25} value associated with each calculated $A_T(C_T,pH_{25})$.

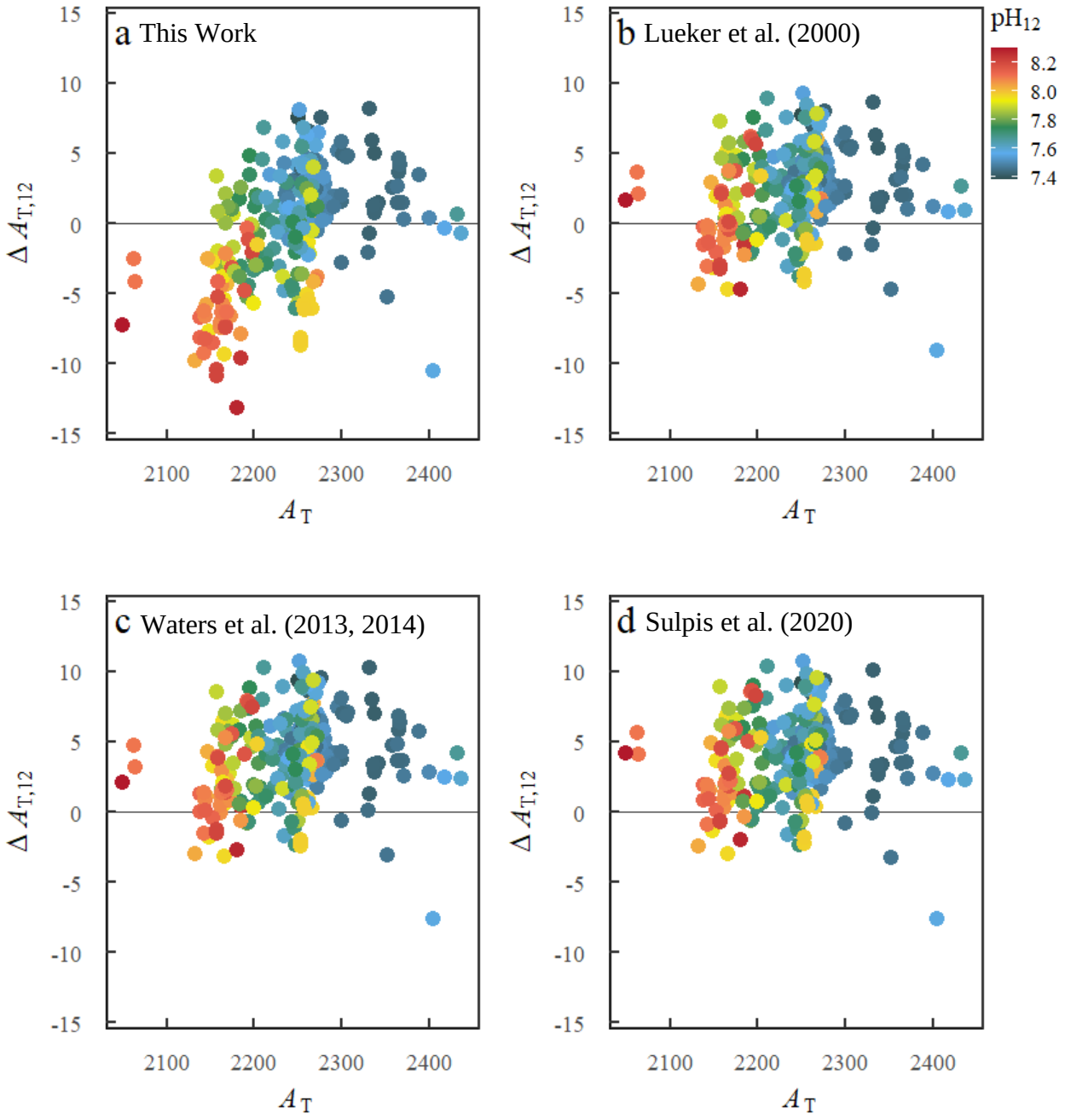

Fig. 3.4. Residuals of A_T at 12 °C ($\Delta A_{T,12} = A_T - A_T(C_T,pH_{12})$) obtained using the CO_2 system dissociation constants of (a) this work, (b) Lueker et al. (2000), (c) Waters et al. (2013, 2014), and (d) Sulpis et al. (2020), shown as a function of measured A_T. Dot colors indicate the measured pH_{12} associated with each calculated $A_T(C_T,pH_{12})$.

This pH-dependent offset can be substantially mitigated when pH_{12} is calculated as $pH_{12}(pH_{25},C_T)$ using the constants of this work (Fig. 3.5b) or even eliminated by using the constants of Lueker et al. (2000) (Fig. 3.5d). The ±0.015 $^{*}\Delta pH_{12}$ values shown Fig. 3.5b are within the ±0.02 measurement uncertainty reported by McLaughlin et al. (2015), and the Fig. 3.5d results show no trend as a function of pH. For comparison, pH_{25} was similarly calculated via inputs of (A_T,C_T) and (pH_{12},C_T), and the two resulting sets of residuals (i.e., ΔpH_{25} and $^{*}\Delta pH_{25}$) show similar patterns (see Appendix C.5).

We also tested whether agreement between measured and calculated pH_{12} might be improved by (a) applying the linear relationship between pH measured spectrophotometrically with purified indicator and calculated pH from Carter et al. (2018) or (b) using the Lui and Chen (2017) empirical model to convert measured pH to in situ estimates. Neither of these adjustments improved the internal consistency of our pH_{12} calculations. (For details see Appendix C.5.)

3.5.3.3.1 Sources of uncertainty in calculated pH

The systematic offsets in calculated $pH_{12}(A_T,C_T)$ compared to measured pH_{12} (Fig. 3.5a and 3.5c) could be explained by errors in the A_T and/or C_T values that are input to calculate pH. For example, organic alkalinity contributions are likely not appropriately accounted for in measurements of A_T (Byrne, 2014; Fong and Dickson, 2019; Sharp and Byrne, 2020). Previous studies have suggested, for example, that subtracting ~4 μmol kg^{-1} from measured titrimetric A_T values can help to correct for these unaccounted contributions (Patsavas et al., 2015; Fong and Dickson, 2019). Subtracting 4 μmol kg^{-1} from each WCOA2021 A_T measurement (i.e., mimicking the removal of organic alkalinity) does result in smaller calculated $pH_{12}(A_T,C_T)$ values, but yields only a modest reduction in the slope and y-intercept that describe the pH-dependent offset relative

to those shown in Fig. 3.5a and 3.5c. A uniform adjustment to account for organic alkalinity is likely too simplistic. Instead, the protonation characteristics of the organic species need to be appropriately characterized in order to accurately assess organic alkalinity contributions to A_T measurements (Byrne, 2014; Sharp and Byrne, 2020).

Values of $pH_{12}(A_T,C_T)$ are also influenced by the choice of B_T/S parameterization. For example, values of $pH(A_T,C_T)$ obtained using the B_T/S characterization of Uppström (1974) are consistently approximately 0.002 to 0.006 larger than those obtained using the B_T/S of Lee et al. (2010). Using either B_T/S characterization, the pH-dependent offset in $\Delta pH_{12}(A_T,C_T)$ remains. Furthermore, $pH_{12}(pH_{25},C_T)$ values calculated with use of either B_T/S parameterization are statistically indistinguishable.

Because calculated pH_T is quite sensitive to small changes in the C_T/A_T ratio, any imperfections in measured or modeled A_T or C_T are magnified when comparisons are made between measured and calculated pH. Overall, pairing C_T with pH (rather than with A_T) reduces uncertainty in calculations caused by (1) systematic errors and uncertainties in A_T and C_T measurements, (2) uncertainties in pH-dependent contributions of organic alkalinity, and (3) uncertainties arising from imperfect B_T/S parameterizations. As has been suggested by others (Patsavas et al., 2015; Woosley, 2021), pH should be routinely measured (not just calculated) in assessments of oceanic CO_2 system characteristics.

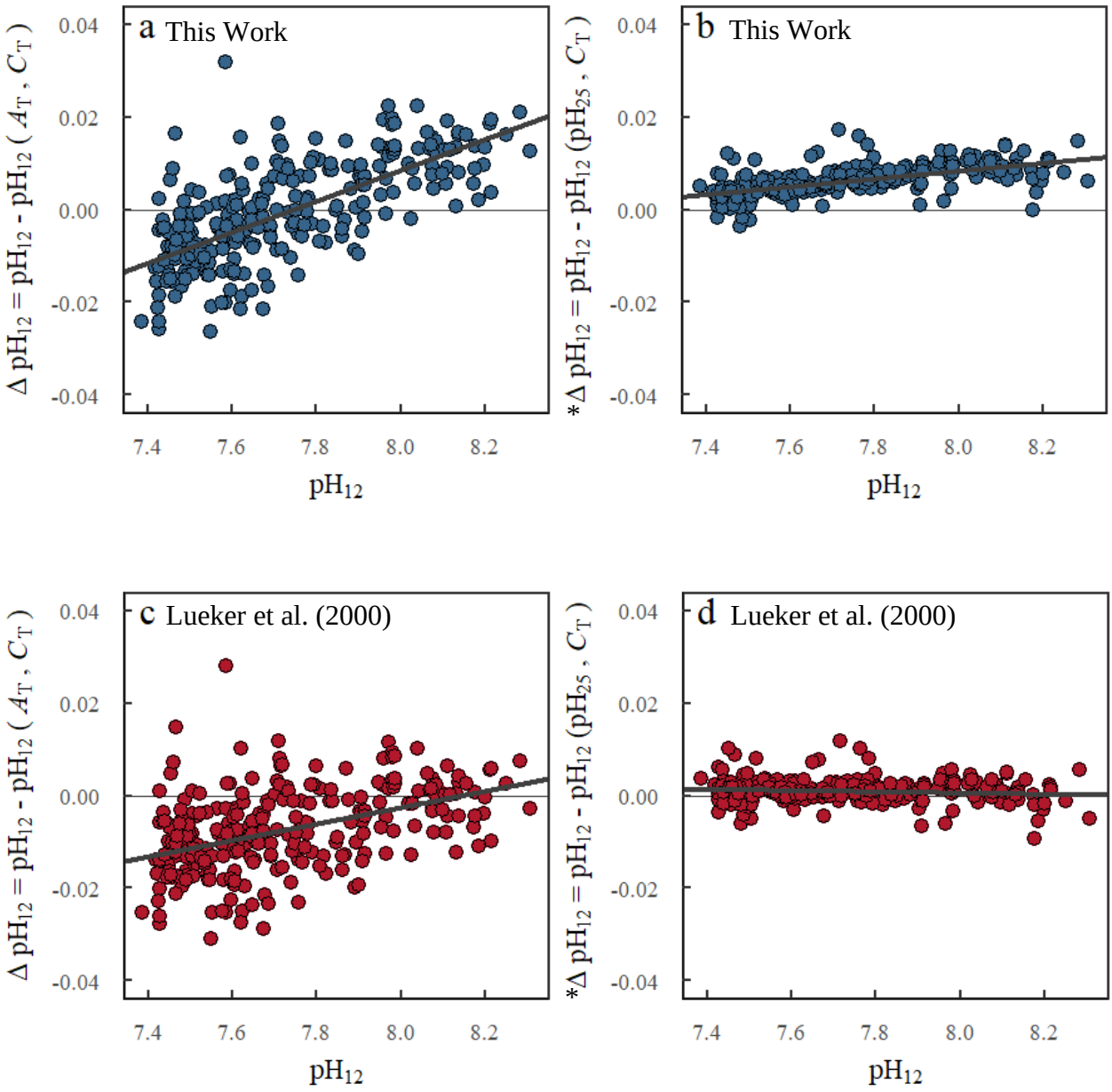

Fig. 3.5. Residuals of pH_{12}, shown as a function of measured pH_{12}: (1) $\Delta pH_{12} = pH_{12} - pH_{12}(A_T, C_T)$ in the left panels and (2) $^{*}\Delta pH_{12} = pH_{12} - pH_{12}(pH_{25}, C_T)$ in the right panels. The top panels (in blue) utilize the CO_2 system dissociation constants of this work, while the bottom panels (in red) utilize the constants of Lueker et al. (2000). The bold black lines show the linear regressions of the residuals.

3.5.3.4 Relationships between A_T residuals and pH residuals

Because alkalinities are conservative (i.e., not temperature dependent), $\Delta A_{T,25}$ produced using pH_{25} (Fig. 3.3) and $\Delta A_{T,12}$ produced using pH_{12} (Fig. 3.4) should ideally be identical. However, calculations using the four sets of constants provide residuals of $\Delta A_{T,25}$ and $\Delta A_{T,12}$ that are distinguishable from one another to varying degrees. Fig. 3.6 directly illustrates this point by showing plots of $\Delta A_{T,25}$ plotted against $\Delta A_{T,12}$ obtained with calculations using the constants of this work (Fig. 3.3a vs. 3.4a) and Lueker et al. (2000) (Fig. 3.3b vs. 3.4b). Using the constants from this work, there is an offset between A_T residuals generated at 25 °C and A_T residuals generated at 12 °C (Fig. 3.6a), with the former being generally larger. It is this relationship that leads to the observation that ${}^{*}\Delta pH_{12}$ residuals calculated with the constants of this work (Fig. 3.5b) exhibit a non-zero slope and intercept as a function of directly measured pH_{12}. In contrast, when using the constants of Lueker et al. (2000), A_T residuals generated at 25 °C and A_T residuals generated at 12 °C plot along the identity line (Fig. 3.6b), indicating that these A_T residuals are independent of temperature. It is this relationship that gives rise to the small magnitudes of ${}^{*}\Delta pH_{12}$ in Fig. 3.5d, indicating best agreement between calculated and measured pH_{12} results when using the constants of Lueker et al. (2000).

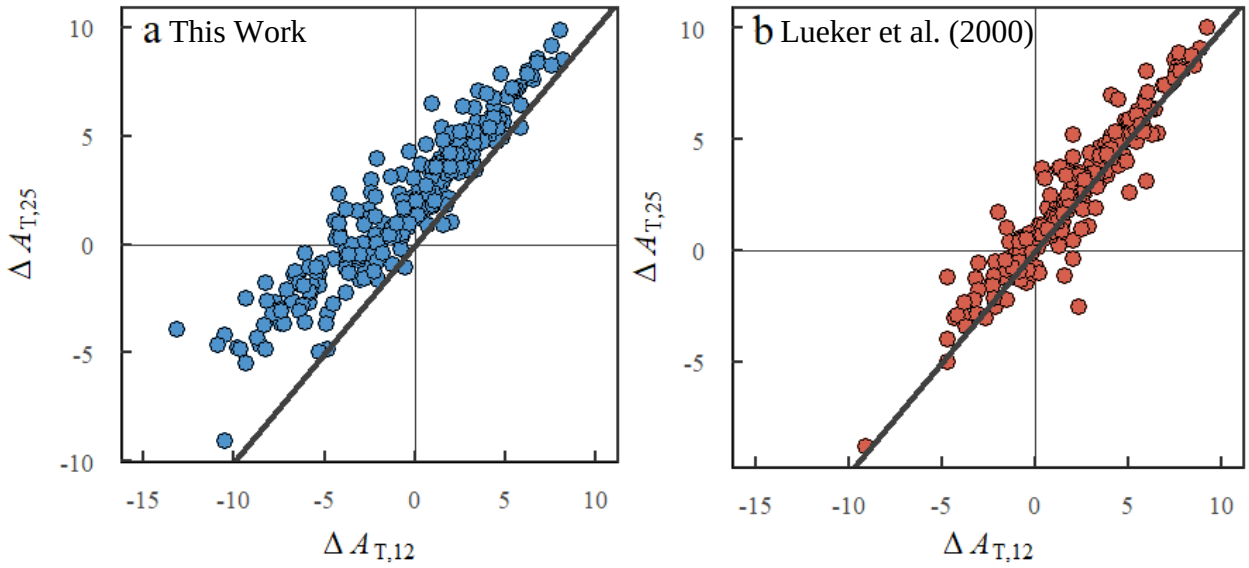

Fig. 3.6. Comparisons between $\Delta A_{T,25}$ (i.e., $A_T - A_T(C_T,pH_{25})$) versus $\Delta A_{T,12}$ (i.e., $A_T - A_T(C_T,pH_{12})$) for calculations performed using the CO_2 system dissociation constants of (a) this work and (b) Lueker et al. (2000). The bold black lines are identity lines (i.e., where $\Delta A_{T,25} = \Delta A_{T,12}$).

3.5.3.5 Calculations of in situ fCO_2 and aragonite saturation state (Ω_{ar})

To examine whether inputs of pH measured at temperatures close to in situ temperatures (rather than at standard experimental temperatures) might produce better in situ estimates of CO_2 system parameters (Woosley, 2021), we calculated in situ fCO_2 and Ω_{ar} from both pH_{12} and pH_{25} (Figs. 3.7 and 3.8). For purposes of comparison, we considered $fCO_2(A_T,C_T)$ and $\Omega_{ar}(A_T,C_T)$ to be the "true" in situ values.

For in situ fCO_2, inputs of pH_{12} (paired with C_T) and pH_{25} (paired with C_T) yielded residuals (Fig. 3.7a) that are of similar magnitude (±6%) to the stated uncertainties from McLaughlin et al. (2015) in calculated fCO_2: ±12% for $fCO_2(A_T,C_T)$ and ±6% for $fCO_2(pH,C_T)$. Notably, residuals calculated as ${}^{*}\Delta fCO_2 = fCO_2(pH_{25},C_T) - fCO_2(pH_{12},C_T)$ (Fig. 3.7b) are even smaller (±3%).

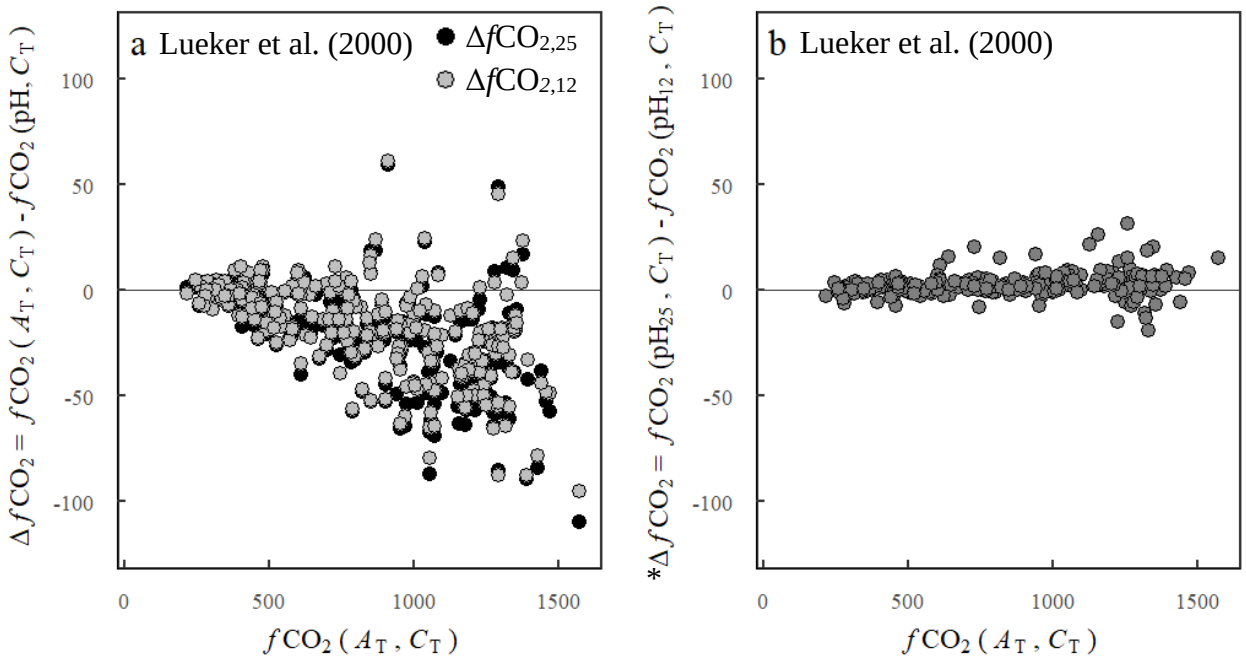

Fig. 3.7. Calculated residuals of fCO_2 for (a): $\Delta fCO_{2,25} = fCO_2(A_T,C_T) - fCO_2(pH_{25},C_T)$ in black and $\Delta fCO_{2,12} = fCO_2(A_T,C_T) - fCO_2(pH_{12},C_T)$ in gray and (b): ${}^{*}\Delta fCO_2 = fCO_2(pH_{25},C_T) - fCO_2(pH_{12},C_T)$. Calculations were performed using the CO_2 system dissociation constants of Lueker et al. (2000).

Similarly, for in situ Ω_{ar}, inputs of pH_{12} (paired with C_T) and pH_{25} (paired with C_T) yielded residuals (Fig. 3.8a) that are smaller (±7%) than the stated uncertainty from McLaughlin et al. (2015) in calculated saturation states: ±14% for $\Omega(A_T,C_T)$, ±8% for $\Omega(pH,C_T)$. Notably, residuals calculated as ${}^{*}\Delta\Omega_{ar} = \Omega_{ar}(pH_{25},C_T) - \Omega_{ar}(pH_{12},C_T)$ (Fig. 3.8b) are even smaller (±3%) and are similar in magnitude to the differences between $\Omega_{ar}(C_T,pCO_2)$ and $\Omega_{ar}(C_T,pH)$ reported by Patsavas et al. (2015).

We also ran similar calculations to examine the effect of using the four different sets of dissociation constants as input to the equilibrium model. The resulting four sets of calculated residuals for fCO_2 and for Ω_{ar} are statistically indistinguishable from one another (i.e., within the uncertainties of calculated fCO_2 and Ω_{ar}). Calculations of fCO_2 are most sensitive to uncertainties

in K_1, and calculations of Ω_{ar} are most sensitive to uncertainties in the solubility product of aragonite (K_A) (Orr et al., 2018).

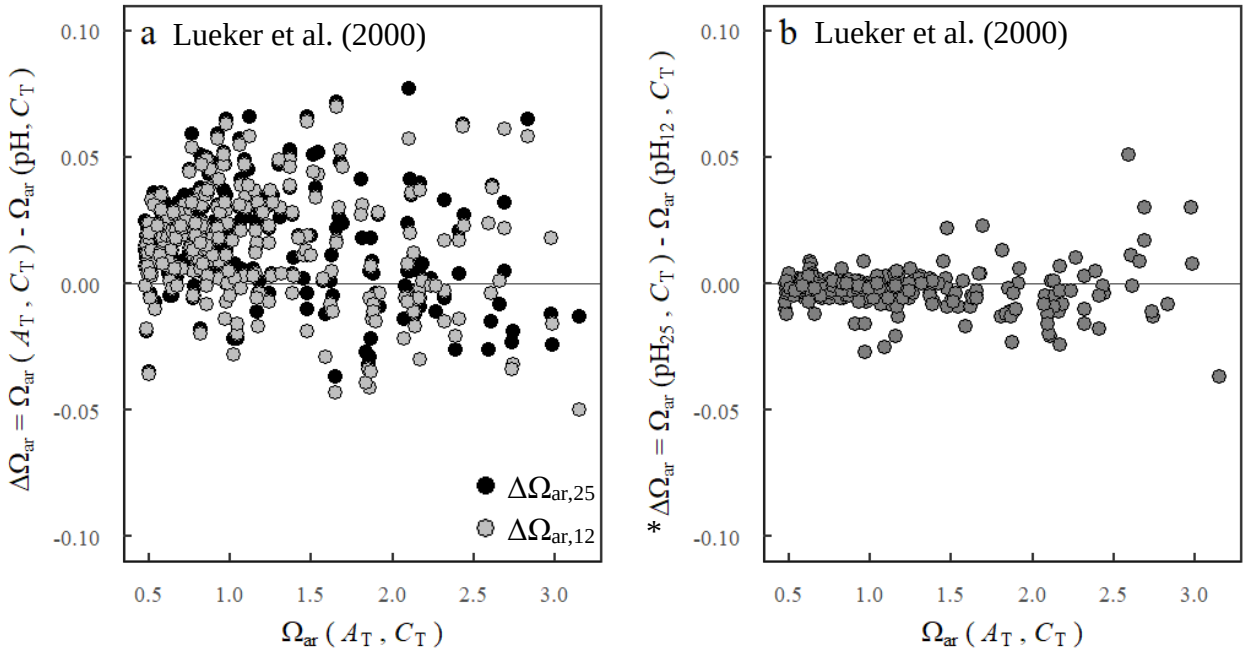

Fig. 3.8. Calculated residuals of Ω_{ar} for (a): $\Delta\Omega_{ar,25} = \Omega_{ar}(A_T,C_T) - \Omega_{ar}(pH_{25},C_T)$ in black or $\Delta\Omega_{ar,12} = \Omega_{ar}(A_T,C_T) - \Omega_{ar}(pH_{12},C_T)$ in grey and (b): ${}^*\Delta\Omega_{ar} = \Omega_{ar}(pH_{25},C_T) - \Omega_{ar}(pH_{12},C_T)$. Calculations were performed using the CO_2 system dissociation constants of Lueker et al. (2000).

The good agreement seen for in situ fCO_2 calculated from pH_{12} and from pH_{25} (Fig. 3.7b) and for Ω_{ar} calculated from pH_{12} and from pH_{25} (Fig. 3.8b) suggests that in situ estimates of fCO_2 and Ω_{ar} can, in at least some circumstances, be reliably estimated without the use of pH measurements obtained at in situ conditions. This conclusion is likely conditional on the extent to which pH buffering is influenced by organics that are not explicitly considered in the A_T equation shown in eq. (3.6). Furthermore, when in situ estimates of temperature-dependent CO_2 system parameters (e.g., pH and fCO_2) are desired, input measurements of pH paired with either A_T or C_T provide better internal consistency than do the input pair of A_T and C_T.

3.6 Conclusions

This work provides a pK_2 parameterization applicable for seawater under conditions of 3 $\leq t \leq$ 35 °C and 20 $\leq S_P \leq$ 40, based on spectrophotometrically determined values of K_1K_2. For 17 $\leq t \leq$ 35 °C, this new pK_2 parameterization is more similar to the parameterization of Lueker et al. (2000) than that of Waters et al. (2013, 2014). At lower temperatures, the pK_2 of this work is consistently smaller than the values of both of those earlier studies.

This work also reports results of analyses using an oceanographic set of A_T, C_T, pH_{25}, and pH_{12} data that assess the internal consistency of CO_2 system calculations at two temperatures, one at the traditional measurement temperature of pH (25 °C) and another closer to the midpoint (12 °C) of the oceanic temperature range. Mean residuals for A_T, C_T, pH_{25}, and pH_{12} (Table 3.3) are not statistically different from zero for calculations using all four sets of dissociation constants evaluated in this work. A_T residuals calculated using pH_{25} as an input parameter (Fig. 3.3) and those calculated using pH_{12} (Fig. 3.4) are quite similar, indicating that A_T calculations are not strongly dependent on the temperature at which pH measurements are made. (C_T residuals are essentially identical to A_T residuals and opposite in sign, so the same logic holds true for C_T calculations.) When pH is calculated from the input pair (A_T,C_T), the residuals of pH_{12} (i.e., ΔpH_{12}; Fig. 3.5a and 3.5c) and pH_{25} (i.e., ΔpH_{25}; not shown) both exhibit the commonly reported pattern of a pH-dependent pH offset for calculations using all four sets of dissociation constants analyzed in this work. In contrast, when pH_{12} is calculated using the input pair (pH_{25},C_T), the residuals of pH_{12} (i.e., $^*\Delta pH_{12}$) are substantially reduced using the constants of the present work (Fig. 3.5b) or are completely eliminated using the constants of Lueker et al. (2000) (Fig. 3.5d). This observation implies that pH_{12} can be reliably estimated by pairing pH_{25} with A_T or C_T for model input. We

additionally found that fCO_2 and Ω_{ar} values calculated at in situ conditions with either pH_{25} or pH_{12} are quite similar (Fig. 3.7b and Fig. 3.8b).

In totality, our findings indicate that pH should be directly measured and then paired with either A_T or C_T to obtain high-quality estimates of pH, fCO_2, and Ω_{ar} at in situ conditions. Furthermore, in situ estimates of CO_2 system parameters can be reliably estimated from measurement of pH at any temperature. As such, 25 °C is a satisfactory measurement temperature and there is presently no added value or harm from making pH measurements at other temperatures. Significantly, though, spectrophotometric pH measurements made at temperatures below the dew point can be problematic due to condensation on optical cells.

Based on our internal consistency assessments conducted using pH data obtained at 25 and 12 °C (Figs. 3.5d and 3.6), we recommend for CO_2 system calculations use of the K_1 and K_2 parameterizations of Lueker et al. (2000) and the B_T/S parameterization of Lee et al. (2010). The choices of K_{HSO4} and K_{HF} are insignificant. Calculated CO_2 system results obtained using the K_{HSO4} of Khoo et al. (1977) rather than Dickson (1990) or the K_{HF} of Dickson and Riley (1979) rather than Perez and Fraga (1987) are statistically indistinguishable. These recommendations are consistent with those that have been previously proposed by Woosley (2021).

The recommendations given here for optimal K_1 and K_2 parameterizations are based on our current ability to model the various components of the CO_2 system and our ability to evaluate the model through use of internal consistency assessments. One should remember that internally consistent data are not indicative of accuracy, and any improvements to the thermodynamic models or advances in the CO_2 system measurements may change these outcomes. Future models will likely include improved characterizations of the concentrations and characteristics of organic acid/base pairs, boron concentrations and boric acid buffering characteristics, and other factors.

Accordingly, the route to a truly rigorous model of the marine CO_2 system will include re-assessments of the parameterizations for K_1, K_2, K_B, B_T/S, and organic acid behavior that are likely to influence dissociation constant recommendations and preferences.

3.7 Supplemental information

Supplementary data for this chapter can be found in Appendix C.

3.8 Acknowledgements

This work was supported by the William and Elsie Knight Endowed Fellowship Fund for Marine Science (College of Marine Science at the University of South Florida), the National Science Foundation (Award #2042935), the Global Ocean Monitoring and Observing (GOMO) program of NOAA (National Oceanic and Atmospheric Administration) under the Global Carbon Data Management and Synthesis Project (Fund #100007298), and the NOAA Ocean Acidification Program. The PMEL and CICOES contributions to this manuscript are contribution numbers 5398 and 2022-1216, respectively. We would like to thank Dr. Sherwood Liu (University of South Florida) for his gracious help in the lab and Joe Donnelly (University of South Florida) for his assistance with the environmental room setup. We also are grateful for the crew of the *R/V Ronald H. Brown* and the scientists who participated in NOAA's 2021 West Coast Ocean Acidification Cruise. We especially thank Kalla Fleger and Macarena Martín-Mayor who assisted with the at-sea pH measurements featured in this work. This research was aided by discussions among participants of the Ocean Carbonate System Intercomparison Forum (OCSIF), which is supported by the Ocean Carbon and Biogeochemistry (OCB) Project Office based at the Woods Hole Oceanographic Institution. The OCB Project Office receives support from the National Science

Foundation (NSF OCE-1558412, NSF OCE-1850983) and the National Aeronautics and Space Administration (NASA NNX17AB17G).

3.9 References

Byrne, R.H. (1987) Standardization of standard buffers by visible spectrometry. *Anal. Chem.* **59**, 1479−1481. https://doi.org/10.1021/ac00137a025

Byrne, R.H. (2014) Measuring ocean acidification: New technology for a new era of ocean chemistry. *Environ. Sci. Technol.* **48**, 5352−5360. doi:10.1021/es405819p

Clayton, T.D. and Byrne, R.H. (1993) Spectrophotometric seawater pH measurements: Total hydrogen ion concentration scale calibration of m-cresol purple and at-sea results. *Deep Sea Res. Part I. Oceanogr. Res. Papers* **40**, 2115−2129. https://doi.org/10.1016/0967-0637(93)90048-8

Dickson, A.G. (1990) Standard potential of the reaction: $AgCl(s) + 12H_2(g) = Ag(s) + HCl(aq)$, and and the standard acidity constant of the ion HSO_4^- in synthetic sea water from 273.15 to 318.15 K. *J. Chem. Thermodyn.* **22**, 113−127. https://doi.org/10.1016/0021-9614(90)90074-Z

Dickson, A.G. and Riley, J.P. (1979) The estimation of acid dissociation constants in sea-water media from potentiometric titrations with strong base. II. The dissociation of phosphoric acid. *Mar. Chem.* **7**, 101−109. http://dx.doi.org/10.1016/0304-4203(79)90002-1

Dickson, A.G., Sabine, C.L., and Christian, J.R. (2007). *Guide to best practices for ocean CO_2 measurements*. PICES Special Publication 3, 191 pp.

Feely, R.A., Doney, S.C., and Cooley, S.R. (2009) Ocean acidification: Present conditions and future changes in a high-CO_2 world. *Oceanography* **22**, 36−47. https://doi.org/10.5670/oceanog.2009.95

Feely, R.A., Okazaki, R.R., Cai, W.J., Bednarsek, N., Alin, S.R., Byrne, R.H., and Fassbender, A. (2018) The combined effects of acidification and hypoxia on pH and aragonite saturation in the coastal waters of the California current ecosystem and the northern Gulf of Mexico. *Cont. Shelf Res.* **152**, 50−60. doi:10.1016/j.csr.2017.11.002

Fong, M.B. and Dickson, A.G. (2019) Insights from GO-SHIP hydrography data into the thermodynamic consistency of CO_2 system measurements in seawater. *Mar. Chem.* **211**, 52−63. https://doi.org/10.1016/j.marchem.2019.03.006

Friedlingstein, P., Jones, M.W., O'Sullivan, M., Andrew, R.M., Bakker, D.C.E., Hauck, J., Le Quéré, C., Peters, G.P., Peters, W., Pongratz, J., Sitch, S., Canadell, J.G., Ciais, P., Jackson, R.B., Alin, S.R., Anthoni, P., Bates, N.R., Becker, M., Bellouin, N., Bopp, L., Chau, T.T.T., Chevallier, F., Chini, L.P., Cronin, M., Currie, K.I., Decharme, B., Djeutchouang, L.M., Dou, X., Evans, W., Feely, R.A., Feng, L., Gasser, T., Gilfillan, D., Gkritzalis, T., Grassi, G., Gregor, L., Gruber, N., Gürses, Ö., Harris, I., Houghton, R.A., Hurtt, G.C., Iida, Y., Ilyina, T., Luijkx, I.T., Jain, A., Jones, S.D., Kato, E., Kennedy, D., Klein Goldewijk, K., Knauer, J., Korsbakken, J.I., Körtzinger, A., Landschützer, P., Lauvset, S.K., Lefèvre, N., Lienert, S., Liu, J., Marland, G., McGuire, P.C., Melton, J.R., Munro, D.R., Nabel, J.E.M.S., Nakaoka, S.I., Niwa, Y., Ono, T., Pierrot, D., Poulter, B., Rehder, G., Resplandy, L., Robertson, E., Rödenbeck, C., Rosan, T.M., Schwinger, J., Schwingshackl, C., Séférian, R., Sutton, A.J., Sweeney, C., Tanhua, T., Tans, P.P., Tian, H., Tilbrook, B., Tubiello, F., van der Werf, G.R., Vuichard, N., Wada, C., Wanninkhof, R., Watson, A.J., Willis, D., Wiltshire, A.J., Yuan, W., Yue, C., Yue, X., Zaehle, S., and Zeng, J. (2022) Global carbon budget 2021. *Earth Syst. Sci. Data* **14**, 1917−2005. doi:10.5194/essd-14-1917-2022

Gruber, N., Clement, D., Carter, B.R., Feely, R.A., van Heuven, S., Hoppema, M., Ishii, M., Key, R.M., Kozyr, A., Lauvset, S.K., Lo Monaco, C., Mathis, J.T., Murata, A., Olsen, A., Perez, F.F., Sabine, C.L., Tanhua, T., and Wanninkhof, R. (2019) The oceanic sink for anthropogenic CO_2 from 1994 to 2007. *Science* **363**, 1193−1199. doi:10.1126/science.aau5153

Jiang, L.-Q., Carter, B.R., Feely, R.A., Lauvset, S.K., and Olsen, A. (2019) Surface ocean pH and buffer capacity: Past, present and future. *Sci. Rep.* **9**, 18624. doi:10.1038/s41598-019-55039-4

Khoo, K.H., Ramette, R.W., Culberson, C.H., and Bates, R.G. (1977) Determination of hydrogen ion concentrations in seawater from 5 to 40 °C: Standard potentials at salinities from 20 to 45%. *Anal. Chem.* **49**, 29−34. doi:10.1021/ac50009a016

Lee, K., Kim, T.-W., Byrne, R.H., Millero, F.J., Feely, R.A., and Liu, Y.-M. (2010) The universal ratio of boron to chlorinity for the North Pacific and North Atlantic oceans. *Geochim. Cosmochim. Acta* **74**, 1801−1811. https://doi.org/10.1016/j.gca.2009.12.027

Lee, K., Millero, F., Byrne, R.H., Feely, R., and Wanninkhof, R. (2000) The recommended dissociation constants for carbonic acid in seawater. *Geophys. Res. Lett.* **27**, 229−232. doi:10.1029/1999gl002345

Lui, H.-K. and Chen, C.-T.A. (2017) Reconciliation of pH_{25} and pH_{insitu} acidification rates of the surface oceans: A simple conversion using only in situ temperature. *Limnol. Oceanogr. Methods* **15**, 328−335. https://doi.org/10.1002/lom3.10170

Liu, X., Patsavas, M.C., and Byrne, R.H. (2011) Purification and characterization of meta-cresol purple for spectrophotometric seawater pH measurements. *Environ. Sci. Technol.* **45**, 4862−4868. doi:10.1021/es200665d

Lueker, T.J., Dickson, A.G., and Keeling, C.D. (2000) Ocean pCO_2 calculated from dissolved inorganic carbon, alkalinity, and equations for K_1 and K_2: Validation based on laboratory measurements of CO_2 in gas and seawater at equilibrium. *Mar. Chem.* **70**, 105−119. https://doi.org/10.1016/S0304-4203(00)00022-0

Millero, F.J., Graham, T.B., Huang, F., Bustos-Serrano, H., and Pierrot, D. (2006) Dissociation constants of carbonic acid in seawater as a function of salinity and temperature. *Mar. Chem.* **100**, 80−94. https://doi.org/10.1016/j.marchem.2005.12.001

McElligott, S., Byrne, R., Lee, K., Wanninkhof, R., Millero, F., and Feely, R. (1998) Discrete water column measurements of CO_2 fugacity and pH_T in seawater: A comparison of direct measurements and thermodynamic calculations. *Mar. Chem.* **60**, 63−73. https://doi.org/10.1016/S0304-4203(97)00080-7

McLaughlin, K., Weisberg, S.B., Dickson, A.G., Hofmann, G.E., Newton, J.A., Aseltine-Neilson, D., Barton, A., Cudd, S., Feely, R.A., Jefferds, I.W., Jewett, E.B., King, T., Langdon, C.J., McAfee, S., Pleschner-Steele, D., and Steele, B. (2015) Core principles of the California current acidification network: Linking chemistry, physics, and ecological effects. *Oceanography* **28**, 160−169. doi:174.105.34.230

Mehrbach, C., Culberson, C., Hawley, J., and Pytkowicx, R. (1973) Measurement of the apparent dissociation constants of carbonic acid in seawater at atmospheric pressure *Limnol. Oceanogr.* **18**, 897−907. https://doi.org/10.4319/lo.1973.18.6.0897

Orr, J.C., Epitalon, J.-M., Dickson, A.G., and Gattuso, J.-P. (2018) Routine uncertainty propagation for the marine carbon dioxide system. *Mar. Chem.* **207**, 84−107. https://doi.org/10.1016/j.marchem.2018.10.006

Patsavas, M.C., Byrne, R.H., Wanninkhof, R., Feely, R.A., and Cai, W.-J. (2015) Internal consistency of marine carbonate system measurements and assessments of aragonite saturation state: Insights from two US coastal cruises. *Mar. Chem.* **176**, 9−20. http://dx.doi.org/10.1016/j.marchem.2015.06.022

Perez, F.F. and Fraga, F. (1987) Association constant of fluoride and hydrogen ions in seawater. *Mar. Chem.* **21**, 161−168. https://doi.org/10.1016/0304-4203(87)90036-3

Pierrot, D., Lewis, E., and Wallace, D. (2006) CO2SYS DOS Program developed for CO_2 system calculations. *ORNL/CDIAC-105.* Carbon Dioxide Inf. Anal. Cent., Oak Ridge Natl. Lab., US Dept. of Energy, Oak Ridge, TN.

Schockman, K.M. and Byrne, R.H. (2021) Spectrophotometric determination of the bicarbonate dissociation constant in seawater. *Geochim. Cosmochim. Acta* **300**, 231−245. https://doi.org/10.1016/j.gca.2021.02.008

Sharp, J.D. and Byrne, R.H. (2020) Interpreting measurements of total alkalinity in marine and estuarine waters in the presence of proton-binding organic matter. *Deep Sea Res. Part I Oceanogr. Res. Papers* **165**, 103338. https://doi.org/10.1016/j.dsr.2020.103338

Sharp, J.D., Pierrot, D., Humphreys, M.P., Epitalon, J.-M., Orr, J.C., Lewis, E.R., and Wallace, D.W.R. (2020). CO2SYSv3 for MATLAB (Version v3.1.1). Zenodo. http://doi.org/10.5281/zenodo.3952803

Sulpis, O., Lauvset, S.K., and Hagens, M. (2020) Current estimates of K_1* and K_2* appear inconsistent with measured CO_2 system parameters in cold oceanic regions. *Ocean Sci.* **16**, 847−862. doi:10.5194/os-16-847-2020

Uppström, L.R. (1974) The boron/chlorinity ratio of deep-sea water from the Pacific Ocean. *Deep Sea Res. Oceanogr. Abstr.* **21**, 161−162. https://doi.org/10.1016/0011-7471(74)90074-6

Van Heuven, S., Pierrot, D., Rae, J., Lewis, E., and Wallace, D. (2011) MATLAB program developed for CO_2 system calculations. *ORNL/CDIAC-105b.* Carbon Dioxide Inf. Anal. Cent., Oak Ridge Natl. Lab., US Dept. of Energy, Oak Ridge, TN.

Waters, J.F. and Millero, F.J. (2013) The free proton concentration scale for seawater pH. *Mar. Chem.* **149**, 8−22. https://doi.org/10.1016/j.marchem.2012.11.003

Waters, J., Millero, F., and Woosley, R. (2014) Corrigendum to "The free proton concentration scale for seawater pH", [MARCHE: 149 (2013) 8−22]. *Mar. Chem.* **165**, 66−67. https://doi.org/10.1016/j.marchem.2014.07.004

Williams, N.L., Juranek, L.W., Feely, R.A., Johnson, K.S., Sarmiento, J.L., Talley, L.D., Dickson, A.G., Gray, A.R., Wanninkhof, R., Russell, J.L., Riser, S.C., and Takeshita, Y. (2017) Calculating surface ocean pCO_2 from biogeochemical Argo floats equipped with pH: An uncertainty analysis. *Glob. Biogeochem. Cycles* **31**, 591−604. doi:10.1002/2016GB005541

Woosley, R.J. (2021) Evaluation of the temperature dependence of dissociation constants for the marine carbon system using pH and certified reference materials. *Mar. Chem.* **229**, 103914. https://doi.org/10.1016/j.marchem.2020.103914

CHAPTER FOUR:

A HYBRID CONDUCTOMETRIC/SPECTROPHOTOMETRIC METHOD FOR DETERMINING IONIC STRENGTH OF DILUTE AQUEOUS SOLUTIONS

Note: This chapter has been reprinted (adapted) with permission from:

Schockman, K.M. and Byrne, R.H. (2022) A hybrid conductometric/spectrophotometric method for determining ionic strength of dilute aqueous solutions. *Anal. Chim. Acta* **1220**, 340008.

Copyright 2022 Elsevier.

4.1 Abstract

This work describes a novel conductometric/spectrophotometric method to determine the ionic strength (I) of dilute aqueous solutions (e.g., natural waters from rivers and lakes). Because $I \leq 0.01$ mol kg^{-1} in such waters, precision as well as accuracy is of paramount importance. In current practice the ionic strength of natural waters is determined almost exclusively with conductometric measurements. We used solutions of artificial freshwater to assess the performance of two commonly used types of conductometric instruments and found that a conductivity probe systematically overestimated I while a salinometer systematically underestimated I. We therefore recommend here an empirical correction that can be easily implemented to improve the accuracy of both types of conductivity measurements. Additional improvement in measurements of I can be achieved by using that high-quality conductometric measurement as input to a hybrid conductometric/spectrophotometric procedure that makes use of robust quantitative characterizations of the influence of ionic strength on the dissociation characteristics of phosphate pH buffers and sulfonephthalein pH indicators. This approach

mitigates systematic conductometric errors associated with solution composition, thus yielding measurements of ionic strength with substantially improved accuracy and precision. The method was validated by testing on a broad suite of artificial freshwaters (n = 64) with compositions that include the major ions present in dilute natural waters (Na^+, K^+, Mg^{2+}, Ca^{2+}, Cl^-, HCO_3^-, and SO_4^{2-}). This new hybrid method is applicable to waters of $0 \leq I \leq 0.01$ mol kg^{-1} (i.e., electrical conductivity of up to 900 µS cm^{-1} at 25 °C), with an accuracy of ±0.0003 and a precision of ±0.0003.

4.2 Introduction

The characteristics of chemical equilibria in natural aqueous solutions are critically dependent on temperature, pressure, and ionic strength (I) (Stumm and Morgan, 1996; Millero and Pierrot, 1998; Powell et al., 2005; Dickson, 2010; Schockman and Byrne, 2021; Woosley, 2021), where I is defined in terms of the charge-weighted concentrations of ionic species in the solution:

$$I = \tfrac{1}{2} \sum_i m_i z_i^2 \quad (4.1)$$

where I is expressed in mol kg^{-1} and m_i and z_i are the concentrations and charges of each ion (Lewis and Randall, 1921; Debye and Hückel, 1923). Inductively coupled plasma–mass spectrometry (ICP-MS) or ion chromatography can be used to accurately assess solution compositions, from which I can be obtained via eq. (4.1). For many applications, however, such measurements may be unacceptably laborious.

Measurements of specific conductance (i.e., electrical conductivity of 1 cm^3 of solution at 25 °C ($\kappa_{25°C}$) (U.S. Geological Survey, 2019)) are therefore more typically used to deduce I (e.g., using a conductivity probe or a salinometer). This method works well for open-ocean seawater, where the relative concentrations of major ions in seawater are closely consistent. For natural

freshwaters (e.g., river and lake waters), however, ionic compositions are diverse, varying with location, time of year, and so on (Livingstone, 1963; Mackenzie and Garrels, 1966). Because individual ions contribute differently to ionic strength versus the overall conductivity of a solution, there can be a quantitatively significant difference between ionic strength modeled from comprehensive measurements of solution ion composition (eq. (4.1)) versus ionic strength modeled from measurements of conductivity. For natural solutions of low ionic strength, then, conductivity measurements can create uncertainties in ionic strength assessments, and these uncertainties can propagate into many applications – for example, chemical modeling of river and lake waters.

In the present work, we seek to mitigate some of these uncertainties by providing (a) an empirical linear-fit method to improve conductometric determinations of the ionic strength of dilute aqueous solutions and (b) a hybrid conductometric/spectrophotometric method that further improves such measurements. This method is appropriate for waters of $0 \leq I \leq 0.01$ mol kg^{-1} (roughly equivalent to $0 \leq \kappa_{25°C} \leq 900$ µS cm^{-1}).

4.3 Theory

Monohydrogen and dihydrogen phosphate, HPO_4^{2-} and $H_2PO_4^-$, contribute to the buffering of natural solutions at circumneutral pH through the hydrogen ion exchange equilibrium shown in eq. (4.2):

$$H^+ + HPO_4^{2-} \leftrightarrow H_2PO_4^- \tag{4.2}$$

The equilibrium constant for this reaction, K_2, is given as:

$$K_2 = \frac{[H_2PO_4^-]}{[H^+][HPO_4^{2-}]} \tag{4.3}$$

In theory, then, with knowledge of $[H_2PO_4^-]/[HPO_4^{2-}]$ and solution pH (where pH = $-\log [H^+]$), eq. (4.3) can be solved for K_2.

Critically selected K_2 data were found by Powell et al. (2005) to be well described as a function of ionic strength:

$$\log K_2 + 2.044\, I^{0.5}/(1+1.160\, I^{0.5}) = 7.200 + 0.061\, I \quad (4.4)$$

at 25 °C for simple NaCl solutions over $0 \leq I \leq 6$ mol kg^{-1}. Thus, the value of K_2 obtained from eq. (4.3) can be used in eq. (4.4) to solve for the ionic strength of an unknown freshwater solution.

In practice, a known $[H_2PO_4^-]/[HPO_4^{2-}]$ concentration ratio can be obtained from titration with solutions of phosphate salts. The works of Mehrbach et al. (1973), Byrne and Kester (1974), and Schockman and Byrne (2021) have previously shown that weak-acid dissociation constants such as K_2 (eq. (4.3)) can be determined through the addition of salts that contain the relevant acid/base pairs (e.g., sodium borate decahydrate and sodium bicarbonate) in known stoichiometric ratios. In the present work, it is shown that KH_2PO_4 and Na_2HPO_4 can be added to dilute solutions in a manner that produces no net change in pH. At that point, added $[H_2PO_4^-]/[HPO_4^{2-}]$, which is known gravimetrically and is equal to $[H_2PO_4^-]/[HPO_4^{2-}]$ of the original sample solution, can be used in eq. (4.3).

Solution pH can be obtained spectrophotometrically (Robert-Baldo et al., 1985; Byrne and Breland, 1989; Clayton and Byrne, 1993; Liu et al., 2011; Douglas and Byrne, 2017; Müller and Rehder, 2018). Because the algorithms for calculating solution pH from absorbance measurements are themselves characterized in terms of salinity (S) and therefore, implicitly, ionic strength, we rearrange eq. (4.3) as follows:

$$\frac{[H_2PO_4^-]}{[HPO_4^{2-}]} = K_2\,[H^+] \quad (4.5)$$

By taking the log of both sides and rearranging the terms, eq. (4.5) becomes:

$$\log K_2 = \log ([H_2PO_4^-]/[HPO_4^{2-}]) + pH \quad (4.6)$$

In eq. (4.6), the only unknown is ionic strength (implicit in the terms K_2 and pH). Therefore, in theory, iterative estimates of ionic strength can be made until the relationship in eq. (4.6) is satisfied and I is thus known as well.

4.4 Materials and methods

4.4.1 Chemicals and reagents

All solutions were prepared in Milli-Q water (Millipore, 18.2 MΩ). The salts used to create artificial freshwater solutions were $NaHCO_3$ (Alfa Aesar Puratronic©, CAS 144-55-8, Lot R04G040), NaCl (MP Biomedicals, CAS 7647-14-5, Lot M1620), KCl (Thermo Fisher Scientific, CAS 7447-40-7, Lot U15F039), $CaCl_2{\cdot}2H_2O$ (EMSURE, CAS 10035-04-8, Lot A1396782919), $MgCl_2{\cdot}6H_2O$ (Fisher Chemical, CAS 7791-18-6, Lot 195243), Na_2SO_4 (Alfa Aesar, CAS 7757-82-6, Lot M28G020), and $MgSO_4{\cdot}7H_2O$ (J.T. Baker Chemical, CAS 10034-99-8, Lot 620173). The $NaHCO_3$, NaCl, and KCl were stored as salts. The hygroscopic salts $CaCl_2$, $MgCl_2$, Na_2SO_4, and $MgSO_4$ were composed into stock solutions for storage, with their concentrations determined through ICP-MS analysis (Element XR™, Thermo Fisher Scientific). The salts used to create the phosphate titrant solutions were KH_2PO_4 (Fisher Chemical, CAS 7778-77-0, Lot 200158) and Na_2HPO_4 (Fisher Chemical, CAS 7558-79-4, Lot 192899). Adjustments to solution pH were made using 1 N HCl (Fisher Chemical, CAS 7647-01-0) and/or 1 N NaOH (Fisher Chemical, CAS 1310-73-2). Spectrophotometric measurements of pH on the total hydrogen ion concentration scale (pH_T) were obtained using the sulfonephthalein indicator meta-cresol purple (mCP) (10 mM in Milli-Q water; $R \approx 0.4$, where R is the ratio of absorbances at 578 and 434 nm, as defined in Liu

et al. (2011)). The mCP powder was purified as described in Liu et al. (2011). A potassium chloride conductivity standard (2765 µS cm^{-1} at 25 °C, RICCA Chemical, Lot 1102279) and IAPSO standard seawater (salinity 9.993, OSIL Environmental Instruments and Systems, Batch 10L20) were used for conductivity calibrations.

4.4.2 Equipment

Stoppered glass volumetric flasks were used to store the analytical solutions: 100 mL for KH_2PO_4 and Na_2HPO_4, 500 mL for artificial freshwater solutions, and 2 L for hygroscopic salt solutions. Pipettes (2.5 µL, Eppendorf Research Plus) were used to add HCl and NaOH to sample solutions, and micrometer burets (2 mL, Gilmont GS-1200) were used to add mCP and the titrating solutions KH_2PO_4 and Na_2HPO_4. A Thermolyne Type 1500 furnace was used to heat salts (KH_2PO_4, Na_2HPO_4, and KCl) to remove impurities (as detailed in Appendices D.1 and D.2). A high-precision balance (±10^{-5} g, Mettler Toledo XP205) was used to weigh salts and quantify additions of the KH_2PO_4 and Na_2HPO_4 titrants. A larger-capacity balance (±0.1 g, Mettler Toledo PB5001) was used to weigh Milli-Q additions. A YSI Pro 30 conductivity probe was used to obtain measurements of specific conductance (µS cm^{-1} at 25 °C), and a Guildline 8400B Autosal conductive salinometer was used to obtain measurements of salinity. According to the manufacturers' user manuals, ideal operating ranges are $0 \leq I \leq 3$ mol kg^{-1} for the conductivity probe (YSI, 2011) and $0.005 \leq S \leq 42$ (i.e., $0.0001 \leq I \leq 0.87$ mol kg^{-1}) for the salinometer (Guildline Instruments, 2004), with reported accuracies of ±0.0001 mol kg^{-1} in I for both instruments (Guildline Instruments, 2004; YSI, 2011).

The spectrophotometric pH measurements were conducted using a diode-array spectrophotometer (Agilent 8453) with the UV lamp off. Absorbance measurements were made

using two-port 10 cm cylindrical optical glass spectrophotometric cells of ~30 mL volume. Temperature was controlled to approximately 25 °C via a recirculating water bath (Lauda RC6) connected to both a custom-built cell warmer (to pre-equilibrate samples prior to measurements) and a water-jacketed cell holder within the spectrophotometer (to stabilize temperature during measurements). Sample temperatures were measured using a handheld digital thermometer (±0.025 °C, Ertco-Eutechnics Model 4400) that had been calibrated against a quartz thermometer (Hewlett Packard Model 2804 A).

4.4.3 Experimental methods

4.4.3.1 Preparation of sample solutions and titrants

A suite of artificial low-*I* solutions was formulated by adding the salts $NaHCO_3$, NaCl, KCl, $CaCl_2$, $MgCl_2$, Na_2SO_4, and $MgSO_4$ in various combinations to deionized water to generally mimic seven different types of natural freshwater (Berner and Berner, 1987; Markich and Brown, 1998; Pillsbury, 2004). Each artificial-solution type contained a specific suite of salts (Table 4.1), and within each type, multiple batches were formulated with different absolute concentrations to encompass a range of ionic strengths, $0 \leq I \leq 0.01$ mol kg^{-1} (n = 64 unique solutions). All seven types contained $NaHCO_3$ because HCO_3^- is the most prevalent ion in natural freshwaters. Solution type A is the simplest type, with only NaCl added as a second salt. Types B−E contain various combinations of ions, formulated to assess whether the method is biased by the presence or absence of certain ions. Type F represents mean world river water and type G represents mean North American river water, both as specified in Pillsbury (2004). Solution concentrations and the details of solution preparation are provided in Appendix D.1.

Table 4.1.
General compositions of the seven artificial freshwater solution types, A through G, expressed in terms of the ratio of each salt's concentration relative to the concentration of $NaHCO_3$. For each solution type, *n* batches were formulated, all with approximately the same relative ion concentrations but different absolute concentrations ($0 \leq I \leq 0.01$ mol kg^{-1}). Specific formulations are provided in Appendix D.1.

	A	**B**	**C**	**D**	**E**	**F**	**G**
$NaHCO_3$	1	1	1	1	1	1	1
NaCl	1.1						
KCl			0.06	0.05	0.07	0.05	0.06
$CaCl_2$		0.07	0.07		0.07	0.19	0.07
$MgCl_2$					0.08		
Na_2SO_4			0.05				
$MgSO_4$		0.07		0.07		0.09	0.07
n	4	11	11	11	11	3	13

For solutions composed with the major ions of the salts listed in Table 4.1, ionic strength is given as:

$$I = \tfrac{1}{2}([Na^+] + [K^+] + 4[Ca^{2+}] + 4[Mg^{2+}] + [HCO_3^-] + [Cl^-] + 4[SO_4^{2-}]) \quad (4.7)$$

For the dilute solutions utilized in this work, ion pairing is insignificant ((Millero and Schreiber, 1982); see Appendix D.1 for details) and eq. (4.7) can be equivalently written as:

$$I = [NaHCO_3] + [NaCl] + [KCl] + 3[CaCl_2] + 3[MgCl_2] + 3[Na_2SO_4] + 4[MgSO_4] \quad (4.8)$$

For each batch of artificial freshwater solution, eq. (4.8) was used to determine the true ionic strength (i.e., I_{true} based on gravimetric compositional analysis; uncertainty = $\pm 10^{-5}$ mol kg^{-1}).

The two titrant solutions, KH_2PO_4 and Na_2HPO_4, were prepared by adding purified salts to Milli-Q water. The KH_2PO_4 titrant concentration was 0.009 mol kg^{-1}, and the Na_2HPO_4 titrant concentration was 0.02 mol kg^{-1}. Gilmont burets (one for each titrant) were filled with fresh titrant each day prior to measurements. Each batch of titrant solution was used for approximately two weeks, though our work has shown them to be stable for approximately five months. Details of salt purification, titrant storage, and stability are provided in Appendix D.2.

4.4.3.2 Conductivity calibrations and measurements

The YSI conductivity probe was calibrated approximately every two weeks with the potassium chloride conductivity standard solution ($I \approx 0.04$ mol kg^{-1}), following the single-point calibration method recommended in the manufacturer's user manual (YSI, 2011). To determine the probe-derived ionic strength (I_{probe}) of a sample solution, the probe was submerged in ~200 mL of solution at room temperature and a pseudo-linear approach (Marion and Babcock, 1976) was used to convert the reported specific conductance to I_{probe}:

$$I_{probe} = 10^{\left(\frac{\log(\kappa_{25°C}/6.67\cdot10^{4})}{0.991}\right)} \tag{4.9}$$

where I_{probe} is in units of mol kg^{-1}. Estimates of I_{probe} can be converted to S_{probe} (if needed) with this well-established relationship between ionic strength (mol kg^{-1}) and salinity (Dickson et al., 2007):

$$I = 19.924\ S/(1000 - 1.005\ S) \tag{4.10}$$

The Autosal conductive salinometer was calibrated daily with IAPSO standard seawater ($I \approx 0.2$ mol kg^{-1}), following the single-point calibration method recommended in the manufacturer's user manual (Guildline Instruments, 2004). To determine the salinometer-derived ionic strength (I_{sal}) of a sample solution, conductive salinity (S_{sal}) was measured using ~150 mL of solution and then converted to I_{sal} via eq. (4.10).

4.4.3.3 Spectrophotometric titration procedure

Spectrophotometric cells (each of known mass) were filled with sample solution (Table 4.1), and the initial mass of solution was recorded. Each cell was then thermally pre-equilibrated to 25 °C for at least 30 minutes prior to measuring absorbances. Baseline absorbances were measured at 434 and 578 nm (wavelengths of maximum absorbance for the acidic and basic forms

of mCP) and at 730 nm (a non-absorbing wavelength). The ratio of absorbances at 578 and 434 nm, with a small correction (Clayton and Byrne, 1993; Liu et al., 2011) for any baseline changes indicated by the non-absorbing wavelength, is denoted as *R*. These baseline absorbance measurements account for any color (i.e., absorbances) of the natural sample solution (e.g., the yellow color that may accompany high concentrations of dissolved organic matter (DOM)). Consequently, the background color of a sample will not influence the results. After the measurement of background absorbances, the indicator mCP (10 µL) was added to the spectrophotometric cell, and five replicate sets of absorbance measurements were obtained. Iterative additions of HCl and/or NaOH were then made as guided by repeated absorbance measurements until $0.36 \leq R \leq 0.41$. Another five sets of replicate absorbance measurements were obtained and averaged to give an initial *R* value (R_i) for the titration.

An aliquot of 50 µL of KH_2PO_4 titrant was then dispensed from a buret of known mass (i.e., the mass of the buret plus its initial contents) to the spectrophotometric cell to lower the pH, and *R* was remeasured. If this new (lower) *R* was still within 0.03 of R_i, an additional 10 µL of KH_2PO_4 was added. This check-and-add procedure was repeated until $R_i - R \geq 0.03$. (The maximum amount of KH_2PO_4 required in our titrations was 110 µL.) Next, Na_2HPO_4 titrant was incrementally added to the spectrophotometric cell, again from a buret of known mass (i.e., the mass of the buret plus its initial contents) to increase the sample solution pH back to its original pH — i.e., until the measured *R* was within ±0.003 of R_i. In general, this step involved adding an initial 90 µL of Na_2HPO_4 followed by a few subsequent additions of ≥4 µL. (The maximum amount of Na_2HPO_4 required in our titrations was 250 µL.) Finally, five replicate absorbance measurements were averaged to obtain the final *R* of the titration (R_f) and solution temperature

was measured. An average R for the titration was calculated as $R_{avg} = (R_i + R_f)/2$, and both burets were reweighed to determine the mass of dispensed titrant for each.

This procedure was replicated three times for each of the 64 sample batches.

4.4.3.4 Calculation of sample ionic strength

In theory, as explained in Section 4.3, the ionic strength of a freshwater sample solution can be determined by iteratively solving eq. (4.6), given knowledge of only $[H_2PO_4^-]/[HPO_4^{2-}]$ and R. In practice, we found that best results were obtained by using a hybrid conductometric/spectrophotometric approach, with an initial conductive measurement of sample salinity (i.e., S_{probe} or S_{sal}) used to obtain an initial estimate of pH_T. From this value of S and the known values of $[H_2PO_4^-]/[HPO_4^{2-}]$ and R, values of K_2 and then I can be reliably calculated (denoted as I_{hybrid}).

The ratio $[H_2PO_4^-]/[HPO_4^{2-}]$ is obtained from the final concentrations of added KH_2PO_4 and Na_2HPO_4, which are calculated via gravimetrically based dilution factors. Importantly, because the titration procedure is based on additions of KH_2PO_4 (to lower pH) and Na_2HPO_4 (to raise pH back to the original pH of the sample), the concentration ratio ($[H_2PO_4^-]/[HPO_4^{2-}]$) of the added phosphate is identical to the ratio of $[H_2PO_4^-]/[HPO_4^{2-}]$ in the original solution. Therefore, phosphate present in the original solution does not influence the titration results. At the end of the titration, the total mass of sample solution is the initial mass of solution plus the known additions of mCP, HCl, NaOH, and the KH_2PO_4 and Na_2HPO_4 titrants. In practice, an estimate of 30 g can be used for the initial mass of sample solution added to a 10 cm spectrophotometric cell because the I calculations are only very weakly influenced by this quantity. (For example, a 30 g mass estimate, relative to a direct sample mass measurement, changes the calculated ionic strength by

only about 0.0001 mol kg^{-1}, which is less than the uncertainty of the measurements.) The small masses of added mCP, HCl, and NaOH are negligible. Thus, the total mass is estimated as 30 g plus the mass of added KH_2PO_4 titrant plus the mass of added Na_2HPO_4 titrant. To determine the mass contributions of the titrant additions, the titrant burets were weighed before and after each series of additions, as noted in Section 4.4.3.3. Accurate accounting of the phosphate titrant additions (±0.0001 g) is critical for appropriately estimating $[H_2PO_4^-]/[HPO_4^{2-}]$ and ultimately I_{hybrid}.

Sample pH is calculated using the parameterization of Douglas and Byrne (2017):

$$pH_T = p(K_1e_2) + \log\left(\frac{R - e_1}{1 - R\frac{e_3}{e_2}}\right) \tag{4.11}$$

where definitions and values of the salinity- and temperature-dependent variables $p(K_1e_2)$, e_1, and e_3/e_2 may be found in their eq. (2) and their Table 2. For salinity, either S_{probe} or S_{sal} is used. Temperature is as measured at the end of the titration. The R to be used in eq. (4.11) is R_{avg}.

Log K_2 can then be calculated using the known $[H_2PO_4^-]/[HPO_4^{2-}]$ concentration ratio and the estimated pH_T (eq. (4.11)) as inputs to eq. (4.6). Finally, K_2 can be used in eq. (4.4) to calculate the ionic strength of the experimental solution, $I_{expSoln}$. (For eq. (4.4), the intercept value given by Powell et al. (2005) is 7.200 ± 0.008. We elected to use an intercept of 7.195 because this value resulted in smaller differences between I_{hybrid} and I_{true}. Results obtained using the Powell et al. (2005) intercept of 7.200 are provided for comparison in Appendix D.3.)

Strictly speaking, the ionic strength of the original sample solution is equal to $I_{expSoln}$ minus the ionic strength contributions of any added solutions (i.e., mCP, HCl, NaOH, KH_2PO_4, and Na_2HPO_4). In practice, however, the I contributions of added mCP, HCl, and NaOH are negligible. These additions influence ionic strength by $\leq 10^{-6}$ mol kg^{-1}, which is much less than the uncertainty

of the measurements. Therefore, the ionic strength of the original sample solution is calculated as $I_{expSoln}$ minus the ionic strength contributions of the added KH_2PO_4 and Na_2HPO_4 titrants: $I_{hybrid} = I_{expSoln} - I_{KH_2PO_4} - I_{Na_2HPO_4}$.

A full derivation of the ionic strength contributions and an example calculation of I_{hybrid} are provided in Appendix D.3.

4.5 Results and discussion

4.5.1 Conductometric determinations of ionic strength

4.5.1.1 Conductometric *I* measurements based on single-point calibrations

Comparisons between the true ionic strengths of the artificial freshwater solutions and determinations made with the conductivity probe calibrated as recommended in the manufacturer's user manual are shown in Fig. 4.1a. The probe does well at estimating I_{true} values very close to 0 mol kg^{-1} but increasingly overestimates ionic strength as I_{true} increases. At I_{true} = 0.01 mol kg^{-1}, this overestimate is as large as ~27%, and the data trend suggests that deviations will likely continue to increase with further increases of I_{true}. Tabulated probe data are provided in Appendix D.4.

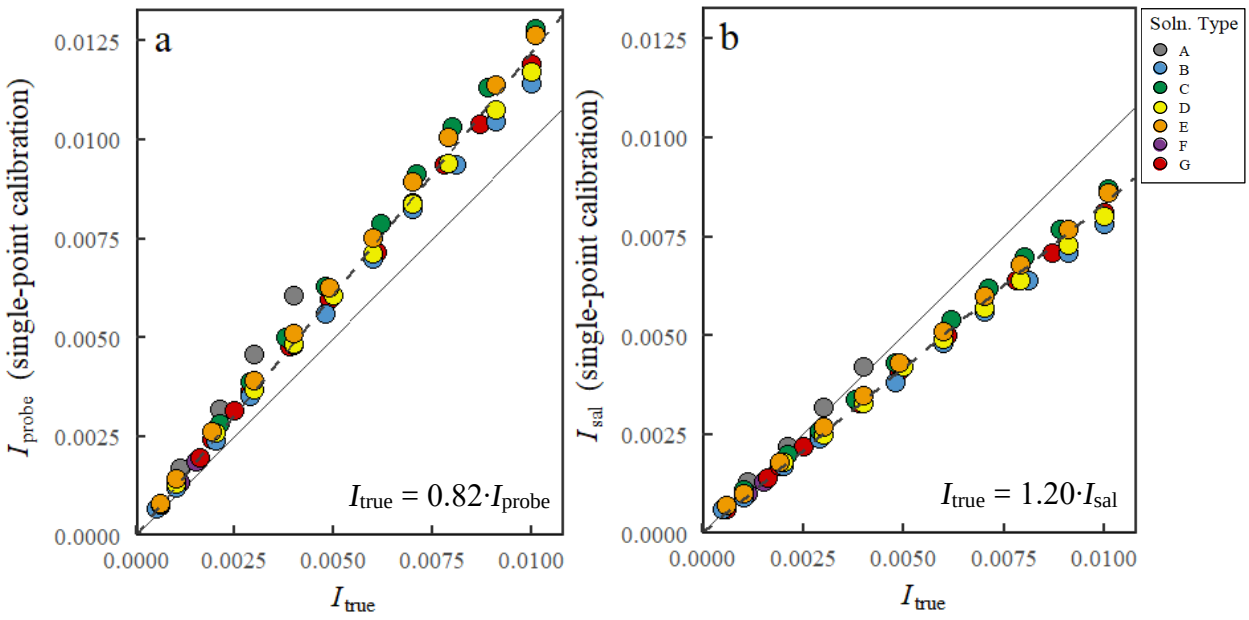

Fig. 4.1. Comparisons between true ionic strength (I_{true}, determined via gravimetric compositional analysis) and ionic strength measured via (a) conductivity probe and (b) salinometer, both calibrated according to manufacturers' recommendations. The solid diagonal line shows the identity line (i.e., the line where conductivity I would be equal to I_{true}), and the dotted diagonal line shows the linear fit of the data points. Line equations are shown in the bottom right corner of each panel. Estimates of I are expressed in mol kg^{-1}. Solution types are described in Table 4.1.

Comparisons between true ionic strengths and ionic strengths measured with the conductive salinometer calibrated as recommended in the manufacturer's user manual are shown in Fig. 4.1b. The salinometer does well at estimating ionic strength at very low I_{true} but increasingly underestimates ionic strength as I_{true} increases. At I_{true} = 0.01 mol kg^{-1}, the salinometer underestimates ionic strength by as much as ~22%, and the data trend suggests that deviations will likely become increasingly large for I_{true} > 0.01 mol kg^{-1}. Tabulated salinometer data are provided in Appendix D.4.

The residuals for the Fig. 4.1 conductivity data are shown in Figs. 4.2a and 4.2b. This presentation shows that (a) the residuals, which are within ±0.0007 mol kg^{-1} (1σ standard deviation) of I_{true}, are not randomly distributed about zero and (b) the patterns of residuals differ

not only between the two different conductivity instruments but also across the different solution types. For example, for solution type A ($NaHCO_3$ + NaCl), the probe significantly overestimates I_{true} while the salinometer yields accurate estimates. For the more complex solution types, the residuals tend to fall into two groups: those that include the 2^+:2^- salt $MgSO_4$ (i.e., solution types B, D, F, and G) and those that do not include a 2^+:2^- salt (i.e., types C and E). These patterns suggest that the observed systematic errors are caused by differences in the relative contributions of each ion to ionic strength and conductivity.

Estimates of methodological precision are not reported in the probe or salinometer manuals (Guildline Instruments, 2004; YSI, 2011).

4.5.1.2 Empirical correction of conductometric *I* data

Given the sensitivity of the conductometric instruments to solution composition and concentration, we fit the Fig. 4.1 data to obtain a correction factor that could be applied to the original conductometric data (essentially a multipoint recalibration):

$$I_{true} = 0.82\ (\pm 0.01) \cdot I_{probe} \tag{4.12}$$

$$I_{true} = 1.20\ (\pm 0.01) \cdot I_{sal} \tag{4.13}$$

R^2 values for both regressions are ≥0.997.

We then multiplied each original conductivity *I* measurement by the appropriate instrument-specific factor to obtain corrected *I* values: I_{probeC} and I_{salC} (Figs. 4.2c and 4.2d). These simple empirical corrections improved the estimates of ionic strength to within ±0.0003 mol kg^{-1} (1σ) of I_{true} — more than a factor of 2 improvement from measurements obtained using the single-point calibrations alone (±0.0007 mol kg^{-1}). The residuals are, however, still non-random.

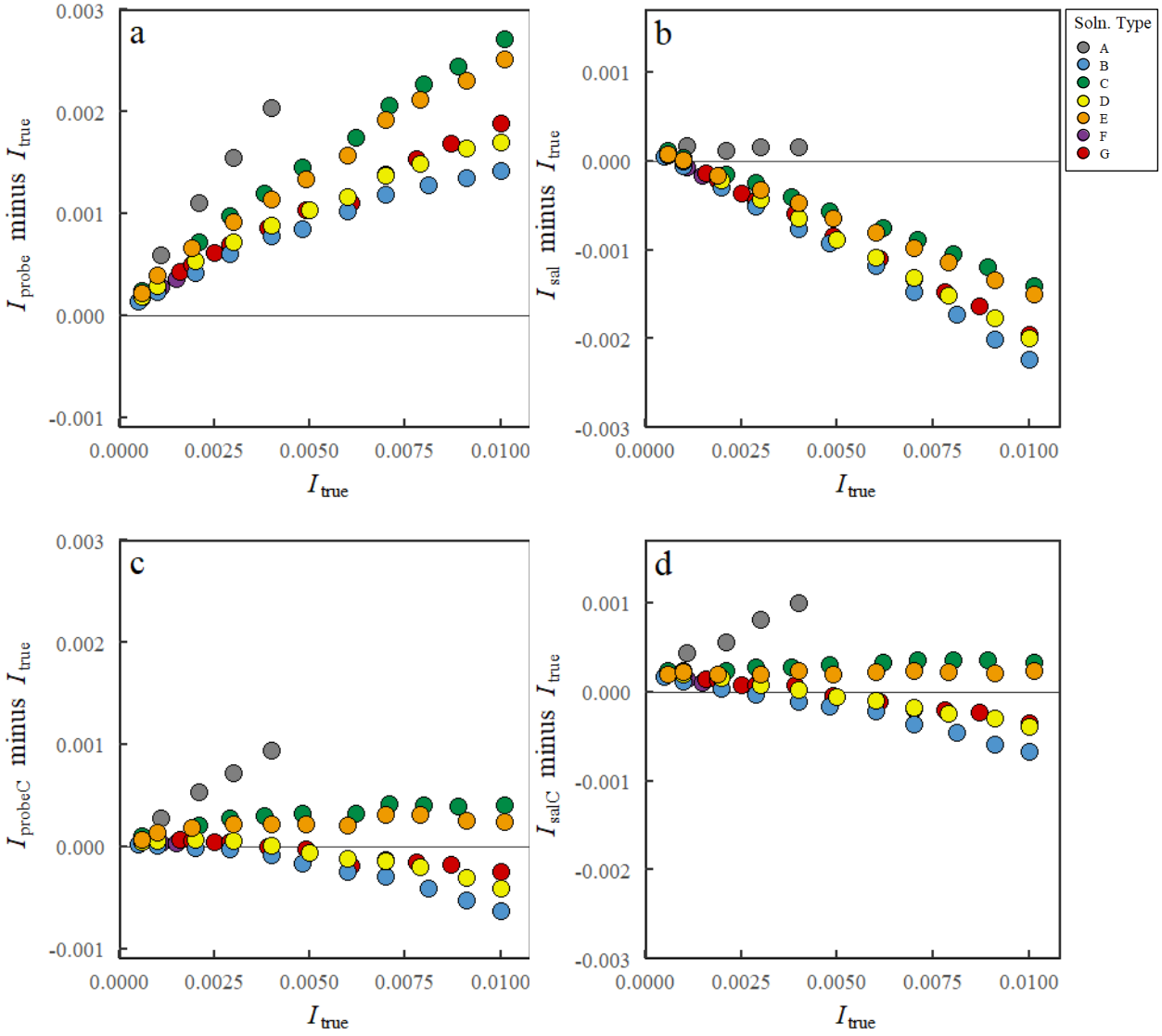

Fig. 4.2. Residuals for conductometric determinations of ionic strength based on (panels a and b) single-point calibrations and (panels c and d) single-point calibrations with empirical multipoint correction. The left panels show probe results, and the right panels show salinometer results. Estimates of I are expressed in mol kg^{-1}. Solution types are described in Table 4.1.

One implication of Figs. 4.2c and 4.2d is that significant improvement in conductometric determinations of I can be achieved through empirical correction even if the spectrophotometric part of the hybrid method is not used. Investigators with the same model of YSI probe or Autosal salinometer that we used can likely apply the corrective factors of eq. (4.12) or eq. (4.13) directly

to their single-point–calibrated values of I_{probe} or I_{sal}. Investigators with other models may need to perform their own linear fits to determine corrective factors appropriate for their instruments. In practice, fewer data points than we used here would be adequate (for details, see Section 4.5.3). Further work is required to determine the frequency with which such corrective regressions would need to be performed.

4.5.2 Hybrid conductometric/spectrophotometric determinations of ionic strength

Comparisons of I_{true} and I determined by the hybrid conductometric/spectrophotometric technique (I_{hybrid}) are shown in Figs. 4.3a and 4.3b. These I_{hybrid} values, which incorporate an initial S estimate from either the empirically corrected probe measurements (to yield $I_{hybrid(probeC)}$) or the empirically corrected salinometer measurements (to yield $I_{hybrid(salC)}$), consistently agree well with I_{true} and exhibit no systematic offset with increasing I_{true}. The residuals of I_{hybrid} (Figs. 4.3c and 4.3d) are randomly distributed about zero with a standard deviation of ±0.0003 mol kg^{-1} (1σ) for both $I_{hybrid(probeC)}$ and $I_{hybrid(salC)}$. No grouping of residuals according to solution type is observed.

Based on triplicate measurements of I_{hybrid} for each of the 64 solutions, the precision of the conductometric/spectrophotometric method is estimated as ±0.0003 mol kg^{-1} (1σ). Individual data values are tabulated in Appendix D.4.

The hybrid conductometric/spectrophotometric method for measuring the ionic strength of dilute natural and artificial solutions thus provides a convenient alternative to traditional conductometric measurements. This new method mitigates the significant systematic over/underestimates obtained with conductometric-only measurements, provides a quantitative estimate of methodological precision (±0.0003 mol kg^{-1}), and maintains an improved level of accuracy relative to conventional conductometric measurements (±0.0003 mol kg^{-1} for the

empirically corrected conductometric-only measurements and for the hybrid-method measurements).

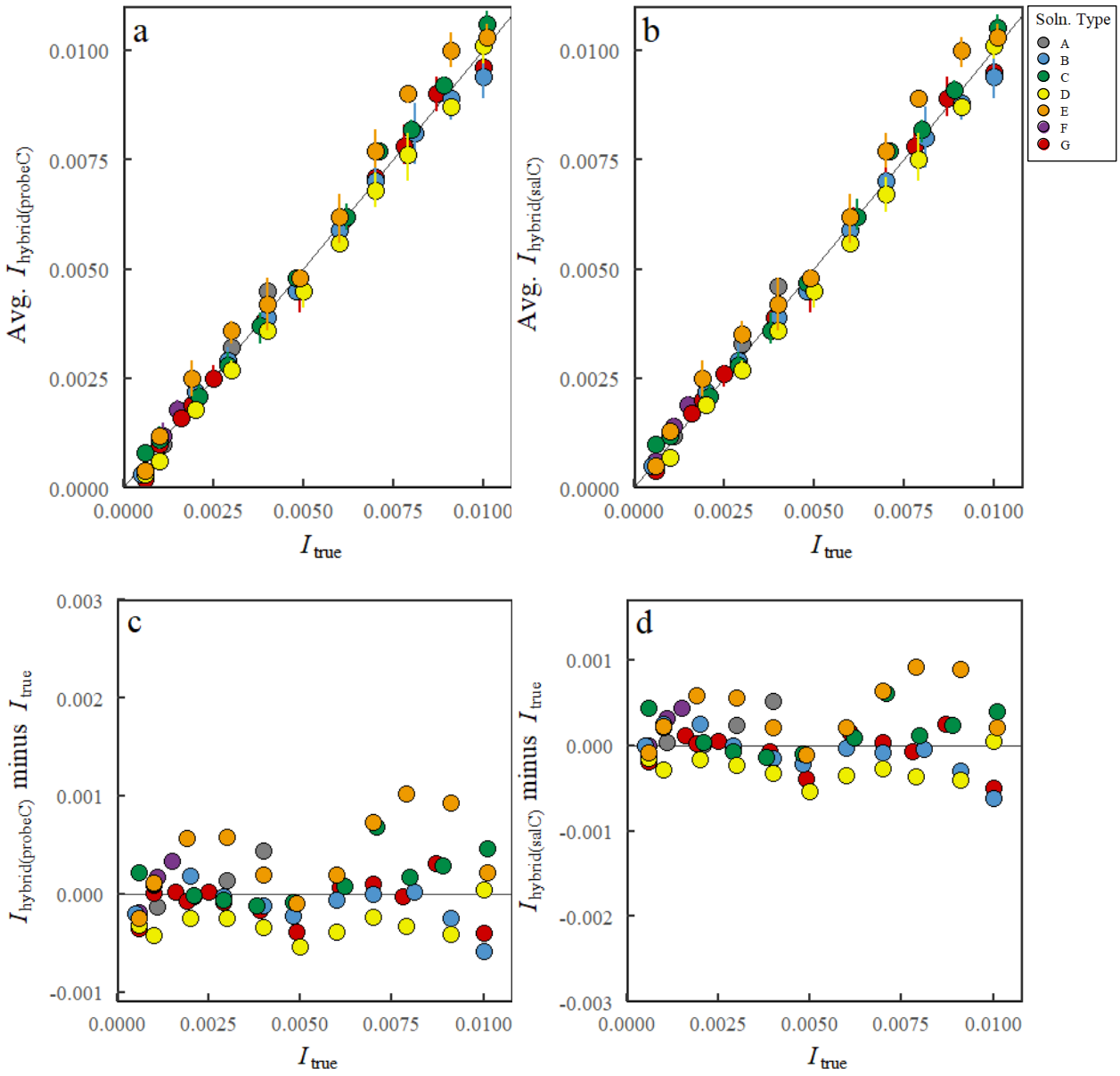

Fig. 4.3. Comparisons between I_{true} and ionic strengths obtained using the hybrid conductometric/spectrophotometric method, I_{hybrid}. Absolute values of I_{hybrid} (i.e., the average of n = 3 independent measurements for each dilution batch) and standard deviations are shown in panels a and b, and residuals are shown in panels c and d. For left-side panels, I_{probeC} was used to calculate pH_T; for right-side panels, I_{salC} was used. Estimates of I are expressed in mol kg^{-1}. Solution types are described in Table 4.1.

4.5.3 Recommended procedures

The hybrid conductometric/spectrophotometric method developed here for measuring ionic strength is intended for use in natural freshwaters ($0 \leq I \leq 0.01$ mol kg^{-1}, which corresponds to approximately $0 \leq \kappa_{25°C} \leq 900$ µS cm^{-1}) or similarly dilute artificial solutions. The overall recommended procedure is summarized in Fig. 4.4 and is outlined in detail in Appendix D.5.

Prior to sample analysis, the conductometric instrument (conductivity probe or conductive salinometer, depending on user preference) must be calibrated and an instrument-specific correction factor should be determined. The instrument is first calibrated according to manufacturers' instructions. To then determine the empirical correction factor (e.g., as in eqs. (4.12) and (4.13)), we recommend use of our solution type D. This solution type contains only three salts ($NaHCO_3$, KCl, and $MgSO_4$) and is thus convenient to formulate. In addition, our D-based conductivity measurements aligned well with those made in the more complex artificial solutions representing mean river water (i.e., solution types F and G) (Fig. 4.2). The ionic strengths of the two D-type solutions should be approximately 0.001 and 0.01 mol kg^{-1} to encompass the I range of natural freshwaters. Alternatively, two potassium chloride conductivity standards (for a conductivity probe) or two standard seawater samples (for a salinometer) could also be used to develop the empirical correction factor.

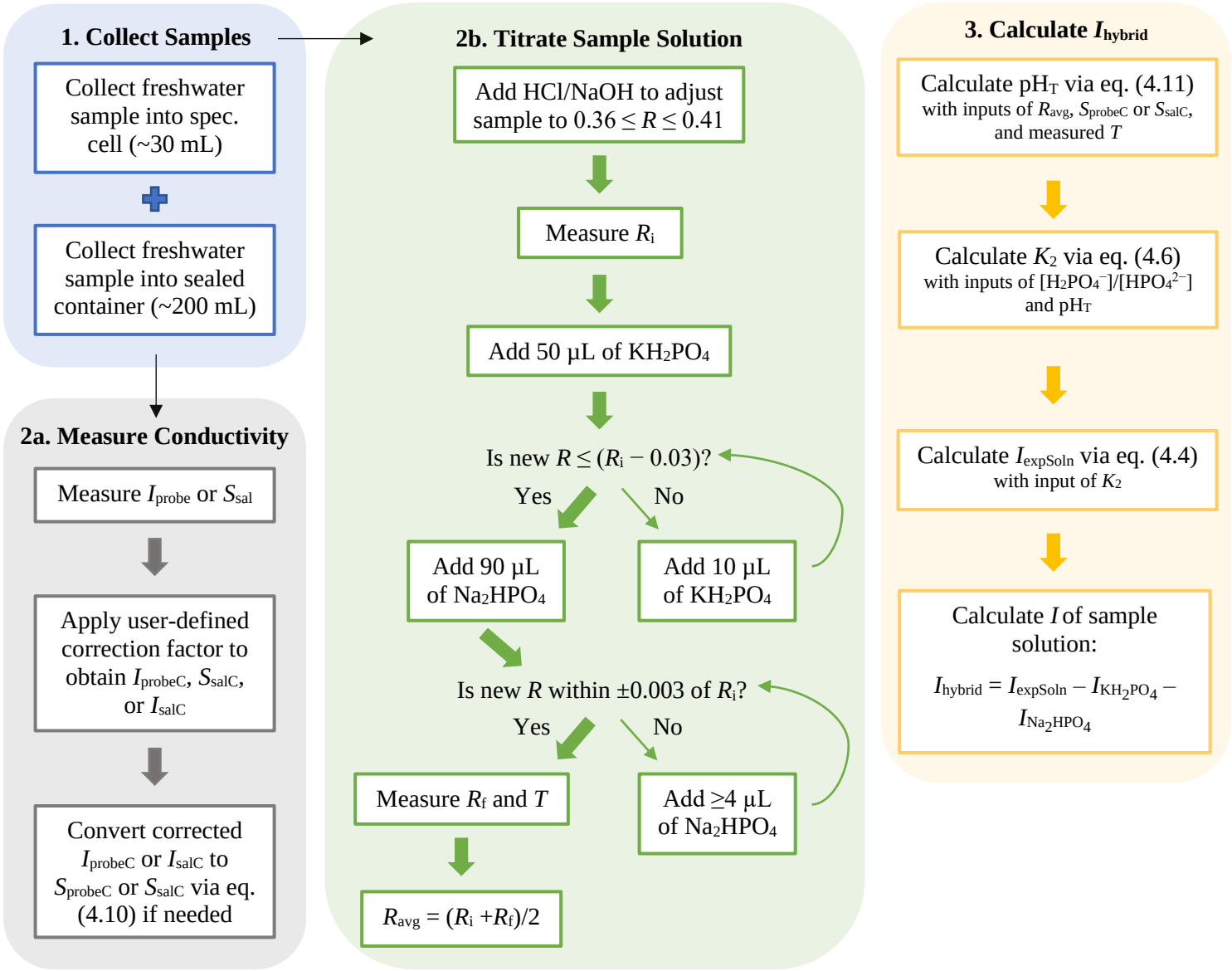

Fig. 4.4. Flow chart of hybrid conductometric/spectrophotometric procedure for measuring the ionic strength of dilute natural waters, $0 \leq I \leq 0.01$ mol kg^{-}.

Detailed instructions for preparing the calibrating solutions and determining a correction factor are provided in Appendix D.5. Generally, I_{probe} or S_{sal} is measured in both solutions, and then a linear fit is obtained to describe the measured I (or S) values as a function of I_{true} (or S_{true}). The corrective factor thus obtained should be applied to all conductometric determinations of sample I (or sample S). Conversions between I are S are obtained, as needed, using eq. (4.10). We generally calibrate conductivity probes every two weeks and salinometers daily. We recommend the correction factor be redetermined no less frequently than every two months for both instrument types, though our results suggest the correction factor may be relatively constant for a given instrument.

For users opting to use conductometric-only I determinations, the I_{probe} or S_{sal} of each sample is measured with the calibrated instrument and then the user-determined correction factor is applied (Fig. 4.4, step 2a). This simple correction will provide better results than can be obtained using only the typical single-point calibration. We found that the two-point correction procedure recommended here yielded correction factors of 0.86 and 1.28 (as compared to 0.82 and 1.20 for the full 64-point fit) and provided the same level of accuracy for I_{probeC} and I_{salC} (± 0.0003 mol kg^{-1}) as did the 64-point fit.

For users opting to use the hybrid method, a conductivity measurement (I_{probe} or S_{sal}) is obtained with the calibrated instrument and the user-determined correction factor is applied (Fig. 4.4, step 2a). Then, the spectrophotometric titration to determine $[H_2PO_4^-]/[HPO_4^{2-}]$ and R of the experimental solution is performed (Fig. 4.4, step 2b). Details of this step are provided in Section 4.4.3.3. With these data, the ionic strength of the sample solution, I_{hybrid}, can be calculated (Fig. 4.4, step 3). The details of this calculation are described in Section 4.4.3.4, with an example calculation and additional details provided in Appendices D.3 and D.5.

To determine the precision of the hybrid method, we measured *I* for three replicates of each of our 64 artificial freshwater solutions, which yielded a methodological precision of ±0.0003 mol kg^{-1}. Users of the method should also determine and report the analytical precision of their own analyses. For this purpose, a single set of replicates from each sample series or series of analyses will likely suffice.

4.6 Conclusions

Ionic strength is a critically important parameter for modeling chemical equilibria in low–ionic strength waters (Stumm and Morgan, 1996). Because the range of ionic strength in fresh waters is small ($0 \leq I \leq 0.01$ mol kg^{-1}), small differences in *I* are important but also challenging to quantify. This work reports, for the first time, the novel concept of determining ionic strength through observations of the dissociation characteristics of pH buffers and sulfonephthalein pH indicators. By drawing on the combined strengths of conductometric and spectrophotometric methods, this approach provides precise (±0.0003 mol kg^{-1}) and accurate (±0.0003 mol kg^{-1}) determinations of ionic strength and mitigates systematic discrepancies observed with purely conductometric techniques. This work also illustrates that conductometric measurements of ionic strength are substantially dependent on medium composition and that reported conductometric accuracies of ±0.0001 mol kg^{-1} (Guildline Instruments, 2004; YSI, 2011) may be overly optimistic. For users without spectrophotometric capabilities, even a simple empirical correction can improve the accuracy of their conductometric determinations of ionic strength to within ±0.0003 mol kg^{-1} of gravimetrically determined ionic strength.

Our hybrid approach should be implemented when accurate assessments of *I* are required, with each user assessing that need in the context of a given application of interest. For example,

we found the error in I obtained from conventional conductometric probe measurements to be 27% at I_{true} = 0.01 mol kg^{-1} (see Section 4.5.1.1). How significant is that level of error for your desired application? If you are using I to calculate some other desired parameter, how will that 27% error influence your calculated results? For example, consider the calculation of spectrophotometric pH_T (eq. (4.11)). A 27% error in I (as at I_{true} = 0.01 mol kg^{-1}) results in an error of approximately 0.02 in calculated pH_T. In contrast, the analogous 3% error in I of the hybrid method results in a pH_T error of 0.002 (10 times smaller than the error resulting from a conventional I_{probe} measurement and also within the ±0.002 reported accuracy of state-of-the-art spectrophotometric pH_T measurements (Clayton et al., 1995)). As another example, consider the calculation of aragonite saturation state (Ω_{ar}). A 27% error in I results in an error of approximately 0.13 in Ω_{ar}. This large an error is significant because such uncertainties under conditions near saturation (i.e., near Ω_{ar} = 1) can create ambiguities in interpretations of aragonite (or calcite) stability and dissolution rates (Naviaux et al., 2019). In contrast, the 3% error in I of the hybrid method results in an Ω_{ar} error of 0.02 (7 times smaller). For details of these examples, see Appendix D.6.

It is important to note that natural waters can contain substantial levels of DOM, which may contribute to a sample's ionic strength. For most studies and most samples, these DOM species will be uncharacterized, and it will be impossible to know whether a given sample's DOM is contributing equally to conductivity and ionic strength. If these contributions are not equal, the DOM may well increase the error in conductometric I measurements. The hybrid method, in contrast, directly measures ionic strength contributions from any source, regardless of whether that source is inorganic or organic. Thus, when charged components of DOM contribute to a sample's ionic strength, the hybrid method inherently accounts for this contribution. Therefore, when

samples contain substantial amounts of DOM, the hybrid method is recommended for determinations of *I*.

Future studies can use the concepts presented in this work to advance the development of ionic strength determinations based solely on spectrophotometric methods. In that case, eq. (4.6) would be solved for *I* without an initial conductometric estimate of ionic strength or salinity. As a part of that work, precise spectrophotometric methods would need to be used to redetermine the K_2 parameterization for phosphate in low–ionic strength waters (rather than the potentiometric methods and wide range of *I* that are the basis for the critical assessment of Powell et al. (2005)). These K_2 redeterminations combined with published mCP pH parameterizations (Liu et al., 2011; Douglas and Byrne, 2017; Müller and Rehder, 2018) would provide an internally consistent set of equations for calculating ionic strength based solely on spectrophotometric techniques. Importantly, measurement quality can also be improved through the use of automated (rather than manual) spectrophotometric titration procedures.

4.7 Supplemental information

Supplementary data for this chapter can be found in Appendix D.

4.8 Acknowledgements

This work was supported by the William and Elsie Knight Endowed Fellowship Fund for Marine Science (University of South Florida College of Marine Science) and the National Science Foundation (grant #1658321). We would like to thank Dr. Sherwood Liu (University of South Florida) for purifying our mCP indicator powder and sharing his overall laboratory expertise, as well as Ethan Goddard (University of South Florida) for providing ICP-MS measurements of our

salt solution concentrations. We would like to especially thank Dr. Tonya Clayton for her editorial assistance; her insightful comments and suggestions greatly improved the quality of this manuscript. We would also like to thank two anonymous reviewers whose comments substantially improved the final work.

4.9 References

Berner, E.K. and Berner, R.A. (1987) *The Global Water Cycle: Geochemistry and Environment*. Prentice-Hall. Englewood Cliffs, NJ.

Byrne, R.H. and Breland, J.A. (1989) High precision multiwavelength pH determinations in seawater using cresol red. *Deep Sea Res. Part A. Oceanogr. Res. Papers* **36**, 803–810. https://doi.org/10.1016/0198-0149(89)90152-0

Byrne, R. and Kester, D. (1974) Inorganic speciation of boron in seawater. *J. Mar. Res*. **32**, 119−127.

Clayton, T.D. and Byrne, R.H. (1993) Spectrophotometric seawater pH measurements: Total hydrogen ion concentration scale calibration of m-cresol purple and at-sea results. *Deep Sea Res. Part I. Oceanogr. Res. Papers* **40**, 2115–2129. https://doi.org/10.1016/0967-0637(93)90048-8

Clayton, T.D., Byrne, R.H., Breland, J.A., Feely, R.A., Millero, F.J., Campbell, D.M., Murphy, P.P., and Lamb, M.F. (1995) The role of pH measurements in modern oceanic CO_2-system characterizations: Precision and thermodynamic consistency. *Deep Sea Res. Part II: Top. Stud. Oceanogr*. **42**, 411−429. https://doi.org/10.1016/0967-0645(95)00028-O

Debye, P. and Hückel, E. (1923) Zur theorie der elektrolyte. I. Gefrierpunktserniedrigung und verwandte erscheinunge (The theory of electrolytes. I. Lowering of freezing point and related phenomena). *Phys. Zeitschr.* **24**, 185–206.

Dickson, A. (2010) Ch. 1: The carbon dioxide system in seawater: Equilibrium chemistry and measurements. Riebesell, U., Fabry, V.J., and Gattuso, J.-P. (Eds.). *Guide to Best Practices for Ocean Acidification Research and Data Reporting*, 17−40. European Union. Brussels, Belgium.

Dickson, A.G., Sabine, C.L., and Christian, J.R. (Eds.) (2007) *Guide to Best Practices for Ocean CO_2 Measurements*, Vol. 3. PICES Special Publication, 191 pp.

Douglas, N.K. and Byrne, R.H. (2017) Spectrophotometric pH measurements from river to sea: Calibration of mCP for $0 \leq S \leq 40$ and $278.15 \leq T \leq 308.15$ K. *Mar. Chem*. **197**, 64–69. https://doi.org/10.1016/j.marchem.2017.10.001

Guildline Instruments. (2004) Model 8400B Autosal laboratory salinometer, Technical manual. Smith Falls, ON, Canada: Author.

Lewis, G.N. and Randall, M. (1921) The activity coefficient of strong electrolytes. *J. Am. Chem. Soc.* **43**, 1112–1154. doi:10.1021/ja01438a014

Liu, X., Patsavas, M.C., and Byrne, R.H. (2011) Purification and characterization of meta-cresol purple for spectrophotometric seawater pH measurements. *Environ. Sci. Technol*. **45**, 4862–4868. doi:10.1021/es200665d

Livingstone, D.A. (1963) Chemical composition of rivers and lakes. Professional Paper, *USGS Numbered Series*, 440-G. doi:10.3133/pp440G

Mackenzie, F.T. and Garrels, R.M. (1966) Chemical mass balance between rivers and oceans. *Am. J. Sci.* **264**, 507. doi:10.2475/ajs.264.7.507

Marion, G.M. and Babcock, K.L. (1976) Predicting specific conductance and salt concentration in dilute aqueous solutions. *Soil Sci.* **122**, 181. doi:10.1097/00010694-197610000-00001

Markich, S. and Brown, P. (1998) Relative importance of natural and anthropogenic influences on the fresh surface water chemistry of the Hawkesbury-Nepean River, south-eastern Australia. *Sci. Total Environ.* **217**, 201–230. doi:10.1016/S0048-9697(98)00188-0

Mehrbach, C., Culberson, C., Hawley, J., and Pytkowicx, R. (1973) Measurement of the apparent dissociation constants of carbonic acid in seawater at atmospheric pressure *Limnol. Oceanogr.* **18**, 897−907. https://doi.org/10.4319/lo.1973.18.6.0897

Millero, F.J. and Pierrot, D. (1998) A chemical equilibrium model for natural waters. *Aquat. Geochem.* 4, 153−199. https://doi.org/10.1023/A:1009656023546

Millero, F.J. and Schreiber, D.R. (1982) Use of the ion pairing model to estimate activity coefficients of the ionic components of natural waters. *Am. J. Sci.* **282**, 1508−1540. doi:10.1023/a:1009656023546

Müller, J.D. and Rehder, G. (2018) Metrology of pH measurements in brackish waters—Part 2: Experimental characterization of purified meta-cresol purple for spectrophotometric pH_T measurements. *Front. Mar. Sci.* **5**, 1–9. doi:10.3389/fmars.2018.00177

Naviaux, J.D., Subhas, A.V., Dong, S., Rollins, N.E., Liu, X., Byrne, R.H., Berelson, W.M., and Adkins, J.F. (2019) Calcite dissolution rates in seawater: Lab vs. in-situ measurements and inhibition by organic matter. *Mar. Chem.* **215**, 103684. https://doi.org/10.1016/j.marchem.2019.103684

Pillsbury, L.A. (2004) Spatial and temporal chemical variations in the Hillsborough river system. University of South Florida, USF Graduate Theses and Dissertations.

Powell, K.J., Brown, P.L., Byrne, R.H., Gajda, T., Hefter, G., Sjöberg, S., and Wanner, H. (2005) Chemical speciation of environmentally significant heavy metals with inorganic ligands. Part 1: The Hg^{2+}– Cl^-, OH^-, CO_3^{2-}, SO_4^{2-}, and PO_4^{3-} aqueous systems (IUPAC Technical Report). *Pure Appl. Chem.* **77**, 739−800. https://doi.org/10.1351/pac200577040739

Robert-Baldo, G.L., Morris, M.J., and Byrne, R.H. (1985) Spectrophotometric determination of seawater pH using phenol red. *Anal. Chem*. **57**, 2564–2567. doi:10.1021/ac00290a030

Schockman, K.M. and Byrne, R.H. (2021) Spectrophotometric determination of the bicarbonate dissociation constant in seawater. *Geochim. Cosmochim. Acta* **300**, 231−245. https://doi.org/10.1016/j.gca.2021.02.008

Stumm, W. and Morgan, J.J. (1996) *Aquatic Chemistry*, Third ed. Wiley. New York, NY.

U.S. Geological Survey (2019) *Specific conductance: USGS Techniques and Methods*, Book 9, Ch. A6.3, 15 p. [Supersedes *USGS Techniques of Water-Resources Investigations*, Book 9, Ch. A6.3, v1.2.]

Woosley, R.J. (2021) Evaluation of the temperature dependence of dissociation constants for the marine carbon system using pH and certified reference materials. *Mar. Chem.* **229**, 103914. https://doi.org/10.1016/j.marchem.2020.103914

YSI. (2011) Professional 30 (Pro30) handheld conductivity meter, User manual. Yellow Springs, OH: Author.

CHAPTER FIVE:

IMPLICATIONS AND FUTURE DIRECTIONS

5.1 Dissertation summary

This dissertation describes how spectrophotometric techniques can be utilized to improve our understanding of chemical equilibria in natural waters. We provide important information in Ch. 2 and 3 regarding a new K_2 parameterization and highlight the role of K_2 in the CO_2 system model with respect to uncertainty and internal consistency. The data set in Ch. 3 is an important contribution to the oceanographic community to assess future refinements of the CO_2 system model. Ch. 4 highlights how traditional conductometric measurements, which are utilized by scientists in a wide range of research studies, are often performed with a "black-box" assumption of accuracy. This dissertation helps to both improve conductometric measurements of ionic strength and provides a novel hybrid method to characterize the ionic strength of natural waters more accurately.

5.2 Measurements of chemical equilibria

While my dissertation addresses improved characterization of the influence of salinity and temperature on bicarbonate dissociation behavior, and improvement in procedures for measuring the ionic strength of dilute solutions, there are several additional important problems relevant to CO_2 system modeling that require further extensive effort. Foremost, development and utilization of a method for spectrophotometric determination of K_1 should be given a high priority. Improved K_1 parameterizations could be used in conjunction with the K_1K_2 measurements in Ch. 2 and 3 to

provide a comprehensive characterization of marine CO_2 system equilibria based solely on spectrophotometric techniques. Future work should also focus on development of improved models of K_1 and K_2 behavior appropriate for estuarine (low salinity) conditions (Schockman and Byrne, 2021; Woosley, 2021). Another important cornerstone of CO_2 system calculations, the dissociation constant of boric acid, K_B, has an uncertainty similar to those that have been estimated for K_1 and K_2 (Orr et al., 2018). A spectrophotometric method quite similar to that described in Ch. 2 could be used to determine K_B spectrophotometrically. Such an investigation would be especially interesting from the standpoint of assessing the compatibility of (a) K_B parameterizations obtained in synthetic seawater with Harned cells (Dickson, 1990) and (b) K_B determinations in natural seawater using spectrophotometric indicators. Finally, another significant chemical equilibrium that should be studied over a wide range of salinity (i.e., ionic strength) is the dissociation of dihydrogen phosphate ($H_2PO_4^-$). As discussed in Ch. 4, careful spectrophotometric determinations of the dihydrogen phosphate dissociation constant could facilitate measurements of ionic strength based solely on spectrophotometric techniques (Schockman and Byrne, 2022).

5.3 CO_2 system internal consistency

An internally consistent model of the CO_2 system is required to accurately interpret biogeochemical observations, model global carbon cycling with appropriate assessments of uncertainty, and make accurate projections of future climate (Gruber et al., 2019; Jiang et al., 2019; Friedlingstein et al., 2022). Accordingly, improvements in measurement/model internal consistency are a high priority of the oceanographic community. As discussed throughout this dissertation, inconsistencies between measured and calculated parameters highlight limitations in

our understanding of the system. Such inconsistencies have thus far largely been ascribed to uncertainties and potential systematic errors in thermodynamic constants and/or in the parameter measurements themselves (Fong and Dickson, 2019; Álvarez et al., 2020; Takeshita et al., 2020). Future studies should aim to examine other aspects of the overall CO_2 system model uncertainties including the ratio of total boron to salinity (B_T/S) and contributions of organic buffers to the acid/base behavior of seawater. Characterizations of the behavior of organic acid/base pairs are particularly challenging because it appears these components of seawater are present at low but significant concentrations, and the properties of these seawater components appear to vary substantially, at least in coastal environments (Byrne, 2014; Sharp and Byrne, 2020).

As was emphasized in Ch. 3, more data are needed for assessments of internal consistency over a wider range of conditions. Data sets that include measured fCO_2 may be especially useful. At-sea measurements of fCO_2 can be quite challenging and have been limited relative to measurements of other CO_2 system parameters (Dinauer and Mucci, 2017). It would be valuable to include fCO_2 measurements on repeat hydrography cruises that already consistently include measurements of A_T, C_T, and pH. When possible, these types of paired measurements should be collected over a wide range of salinity conditions, rather than the narrow ranges typical of most open ocean studies. Assessments of CO_2 system internal consistency for estuarine and freshwater environments are notably lacking (Carstensen et al., 2018). Additionally, studies can expand on my work in Ch. 3 to include measurements of pH and fCO_2 over a wide range of temperature, providing useful insights about internal consistency and efficacy of available CO_2 system models outside the traditional measurement temperatures of 20−25 °C (Woosley, 2021). In the future, it will be critical for assessments to also incorporate a wider range of pH (i.e., lower pH as the ocean becomes less basic) and fCO_2 (i.e., higher pCO_2 as the ocean absorbs more anthropogenic carbon

emissions) to aid researchers in predictions of future climate. Additionally, assessments of internal consistency in organic-rich estuarine environments would be valuable; these assessments have thus far been limited by the inability to accurately measure organic alkalinity and our limited understanding of the physical/chemical characteristics of organic acids/bases present within the system.

5.4 Conclusions

This dissertation presents important research with respect to chemical equilibria of natural waters. It is anticipated that my new K_2 parameterization and CO_2 system dataset can be utilized to promote accurate assessments of the CO_2 system in seawater. My novel procedures for measurement of ionic strength can be easily implemented to obtain automated measurements. It is hoped that this dissertation highlights how analytical techniques, specifically spectrophotometric measurements, can be applied in unique ways to diverse problems. Overall, this dissertation demonstrates that precise and accurate characterizations of chemical equilibria are critical pieces to understanding the chemistry of natural waters.

5.5 References

Álvarez, M., Fajar, N.M., Carter, B.R., Guallart, E.F., Pérez, F.F., Woosley, R.J., and Murata, A. (2020) Global ocean spectrophotometric pH assessment: Consistent inconsistencies. *Environ. Sci. Technol.* **54**, 10977−10988. doi:10.1021/acs.est.9b06932

Byrne, R.H. (2014) Measuring ocean acidification: New technology for a new era of ocean chemistry. *Environ. Sci. Technol.* **48**, 5352−5360. doi:10.1021/es405819p

Carstensen, J., Chierici, M., Gustafsson, B.G., and Gustafsson, E. (2018) Long-term and seasonal trends in estuarine and coastal carbonate systems. *Glob. Biogeochem. Cycles* **32**, 497−513. doi:10.1002/2017GB005781

Dickson, A.G. (1990) Thermodynamics of the dissociation of boric acid in synthetic seawater from 273.15 to 318.15 K. *Deep Sea Res. Part A. Oceanogr. Res. Papers* **37**, 755−766. https://doi.org/10.1016/0198-0149(90)90004-F

Dinauer, A. and Mucci, A. (2017) Spatial variability in surface-water pCO_2 and gas exchange in the world's largest semi-enclosed estuarine system: St. Lawrence Estuary (Canada). *Biogeosciences* **14**, 3221−3237. https://doi.org/10.5194/bg-14-3221-2017

Fong, M.B. and Dickson, A.G. (2019) Insights from GO-SHIP hydrography data into the thermodynamic consistency of CO_2 system measurements in seawater. *Mar. Chem.* **211**, 52−63. https://doi.org/10.1016/j.marchem.2019.03.006

Friedlingstein, P., Jones, M.W., O'Sullivan, M., Andrew, R.M., Bakker, D.C.E., Hauck, J., Le Quéré, C., Peters, G.P., Peters, W., Pongratz, J., Sitch, S., Canadell, J.G., Ciais, P., Jackson, R.B., Alin, S.R., Anthoni, P., Bates, N.R., Becker, M., Bellouin, N., Bopp, L., Chau, T.T.T., Chevallier, F., Chini, L.P., Cronin, M., Currie, K.I., Decharme, B., Djeutchouang, L.M., Dou, X., Evans, W., Feely, R.A., Feng, L., Gasser, T., Gilfillan, D., Gkritzalis, T., Grassi, G., Gregor, L., Gruber, N., Gürses, Ö., Harris, I., Houghton, R.A., Hurtt, G.C., Iida, Y., Ilyina, T., Luijkx, I.T., Jain, A., Jones, S.D., Kato, E., Kennedy, D., Klein Goldewijk, K., Knauer, J., Korsbakken, J.I., Körtzinger, A., Landschützer, P., Lauvset, S.K., Lefèvre, N., Lienert, S., Liu, J., Marland, G., McGuire, P.C., Melton, J.R., Munro, D.R., Nabel, J.E.M.S., Nakaoka, S.I., Niwa, Y., Ono, T., Pierrot, D., Poulter, B., Rehder, G., Resplandy, L., Robertson, E., Rödenbeck, C., Rosan, T.M., Schwinger, J., Schwingshackl, C., Séférian, R., Sutton, A.J., Sweeney, C., Tanhua, T., Tans, P.P., Tian, H., Tilbrook, B., Tubiello, F., van der Werf, G.R., Vuichard, N., Wada, C., Wanninkhof, R., Watson, A.J., Willis, D., Wiltshire, A.J., Yuan, W., Yue, C., Yue, X., Zaehle, S., and Zeng, J. (2022) Global carbon budget 2021. *Earth Syst. Sci. Data* **14**, 1917−2005. doi:10.5194/essd-14-1917-2022

Gruber, N., Clement, D., Carter, B.R., Feely, R.A., van Heuven, S., Hoppema, M., Ishii, M., Key, R.M., Kozyr, A., Lauvset, S.K., Lo Monaco, C., Mathis, J.T., Murata, A., Olsen, A., Perez, F.F., Sabine, C.L., Tanhua, T., and Wanninkhof, R. (2019) The oceanic sink for anthropogenic CO_2 from 1994 to 2007. *Science* **363**, 1193−1199. doi:10.1126/science.aau5153

Jiang, L.-Q., Carter, B.R., Feely, R.A., Lauvset, S.K., and Olsen, A. (2019) Surface ocean pH and buffer capacity: Past, present and future. *Sci. Rep.* **9**, 18624. doi:10.1038/s41598-019-55039-4

Orr, J.C., Epitalon, J.-M., Dickson, A.G., and Gattuso, J.-P. (2018) Routine uncertainty propagation for the marine carbon dioxide system. *Mar. Chem.* **207**, 84−107. https://doi.org/10.1016/j.marchem.2018.10.006

Schockman, K.M. and Byrne, R.H. (2021) Spectrophotometric determination of the bicarbonate dissociation constant in seawater. *Geochim. Cosmochim. Acta* **300**, 231−245. https://doi.org/10.1016/j.gca.2021.02.008

Schockman, K.M. and Byrne, R.H. (2022) A hybrid conductometric/spectrophotometric method for determining ionic strength of dilute aqueous solutions. *Anal. Chim. Acta* **1220**, 340008. https://doi.org/10.1016/j.aca.2022.340008

Sharp, J.D. and Byrne, R.H. (2020) Interpreting measurements of total alkalinity in marine and estuarine waters in the presence of proton-binding organic matter. *Deep Sea Res. Part I Oceanogr. Res. Papers* **165**, 103338. https://doi.org/10.1016/j.dsr.2020.103338

Takeshita, Y., Johnson, K.S., Coletti, L.J., Jannasch, H.W., Walz, P.M., and Warren, J.K. (2020) Assessment of pH dependent errors in spectrophotometric pH measurements of seawater. *Mar. Chem.* **223**, 103801. https://doi.org/10.1016/j.marchem.2020.103801

Woosley, R.J. (2021) Evaluation of the temperature dependence of dissociation constants for the marine carbon system using pH and certified reference materials. *Mar. Chem.* **229**, 103914. https://doi.org/10.1016/j.marchem.2020.103914

APPENDIX A:

COPYRIGHT PERMISSIONS

Appendix A.1 Copyright permissions for Chapter One

Figs. 1.1 and **1.2:** These figures were published in *Earth Syst. Sci. Data*, 14, Friedlingstein, P., Jones, M.W., O'Sullivan, M., Andrew, R.M., Bakker, D.C.E., Hauck, J., Le Quéré, C., Peters, G.P., Peters, W., Pongratz, J., Sitch, S., Canadell, J.G., Ciais, P., Jackson, R.B., Alin, S.R., Anthoni, P., Bates, N.R., Becker, M., Bellouin, N., Bopp, L., Chau, T.T.T., Chevallier, F., Chini, L.P., Cronin, M., Currie, K.I., Decharme, B., Djeutchouang, L.M., Dou, X., Evans, W., Feely, R.A., Feng, L., Gasser, T., Gilfillan, D., Gkritzalis, T., Grassi, G., Gregor, L., Gruber, N., Gürses, Ö., Harris, I., Houghton, R.A., Hurtt, G.C., Iida, Y., Ilyina, T., Luijkx, I.T., Jain, A., Jones, S.D., Kato, E., Kennedy, D., Klein Goldewijk, K., Knauer, J., Korsbakken, J.I., Körtzinger, A., Landschützer, P., Lauvset, S.K., Lefèvre, N., Lienert, S., Liu, J., Marland, G., McGuire, P.C., Melton, J.R., Munro, D.R., Nabel, J.E.M.S., Nakaoka, S.I., Niwa, Y., Ono, T., Pierrot, D., Poulter, B., Rehder, G., Resplandy, L., Robertson, E., Rödenbeck, C., Rosan, T.M., Schwinger, J., Schwingshackl, C., Séférian, R., Sutton, A.J., Sweeney, C., Tanhua, T., Tans, P.P., Tian, H., Tilbrook, B., Tubiello, F., van der Werf, G.R., Vuichard, N., Wada, C., Wanninkhof, R., Watson, A.J., Willis, D., Wiltshire, A.J., Yuan, W., Yue, C., Yue, X., Zaehle, S., and Zeng, J., Global carbon budget 2021, 1917−2005, Creative Commons Attribution 4.0 License (2022).

Fig. 1.3: This figure was published in *Glob. Biogeochem. Cycles*, 31, Williams, N.L., Juranek, L.W., Feely, R.A., Johnson, K.S., Sarmiento, J.L., Talley, L.D., Dickson, A.G., Gray, A.R., Wanninkhof, R., Russell, J.L., Riser, S.C., and Takeshita, Y., Calculating surface ocean pCO_2 from biogeochemical Argo floats equipped with pH: An uncertainty analysis, 591−604, Not subject to U.S. Copyright (2017).

Fig. 1.4: This figure was published in *Mar. Chem.*, 176, Patsavas, M.C., Byrne, R.H., Wanninkhof, R., Feely, R.A., and Cai, W.-J., Internal consistency of marine carbonate system measurements and assessments of aragonite saturation state: Insights from two U.S. coastal cruises, 9−20, Copyright Elsevier (2015).

From: Permissions Helpdesk <permissionshelpdesk@elsevier.com>
Sent: Wednesday, September 21, 2022 9:05 AM
To: Katelyn Schockman
Subject: Re: Permission to include figure in dissertation [220920-027342]

Dear Katelyn Schockman,

We hereby grant you permission to reproduce the material detailed below in print and electronic format at no charge subject to the following conditions:

1. If any part of the material to be used (for example, figures) has appeared in our publication with credit or acknowledgement to another source, permission must also be sought from that source. If such permission is not obtained then that material may not be included in your publication/copies.

2. Suitable acknowledgement to the source must be made, either as a footnote or in a reference list at the end of your publication as follows:

"This article was published in Publication title, Vol number, Author(s), Title of article, Page Nos, Copyright Elsevier (or appropriate Society name) (Year)."

3. This permission is granted for non-exclusive world rights in all languages.

4. Reproduction of this material is granted for the purpose for which permission is hereby given, and includes use in any future editions.

Kind regards,

Kaveri Thakuria
Senior Copyrights Coordinator
ELSEVIER | HCM - Health Content Management

From: Katelyn Schockman
Date: Tuesday, September 20, 2022 03:02 PM GMT

I would like to include a part of figure 5 from Patsavas et al. (2015) http://dx.doi.org/10.1016/j.marchem.2015.06.022 in my dissertation. Appropriate credit is given and the figure is cited. Am I allowed to do so? Or what permissions do I need?

Fig. 1.5: This figure was published in *Mar. Chem.*, 207, Orr, J.C., Epitalon, J.-M., Dickson, A.G., and Gattuso, J.-P., Routine uncertainty propagation for the marine carbon dioxide system. *Mar. Chem.*, 84−107, Open Access under CC BY-NC-ND License (2018).

Table 1.2: This table was published in *Mar. Chem.*, 100, Millero, F.J., Graham, T.B., Huang, F., Bustos-Serrano, H., and Pierrot, D., Dissociation constants of carbonic acid in seawater as a function of salinity and temperature, 80−94, Copyright Elsevier (2006).

From: Permissions Helpdesk <permissionshelpdesk@elsevier.com>
Sent: Thursday, September 22, 2022 6:28 AM
To: Katelyn Schockman
Subject: Re: Permission to include table in dissertation [220922-001888]

Dear Katelyn Schockman,

Thank you for contacting us.

We hereby grant you permission to reprint the material below at no charge in your thesis subject to the following conditions:

1. If any part of the material to be used (for example, figures) has appeared in our publication with credit or acknowledgement to another source, permission must also be sought from that source. If such permission is not obtained then that material may not be included in your publication/copies.

2. Suitable acknowledgment to the source must be made, either as a footnote or in a reference list at the end of your publication, as follows:
"This article was published in Publication title, Vol number, Author(s), Title of article, Page Nos, Copyright Elsevier (or appropriate Society name) (Year)."

3. Your thesis may be submitted to your institution in either print or electronic form.

4. Reproduction of this material is confined to the purpose for which permission is hereby given

5. This permission is granted for non-exclusive world English rights only. For other languages please reapply separately for each one required. Permission excludes use in an electronic form other than submission. Should you have a

specific electronic project in mind please reapply for permission.

6. Should your thesis be published commercially, please reapply for permission.

This includes permission for the Library and Archives of Canada to supply single copies, on demand, of the complete thesis. Should your thesis be published commercially, please reapply for permission- Canada
This includes permission for UMI to supply single copies, on demand, of the complete thesis. Should your thesis be published commercially, please reapply for permission-ROW

7. Posting of the full article online is not permitted. You may post an abstract with a link to the Elsevier website www.elsevier.com, or to the article on ScienceDirect if it is available on that platform.

8. Article can used be in the University library if it is embedded in the thesis and not used commercially.

Kind regards,

Thomas Rexson Yesudoss
Copyrights Coordinator
ELSEVIER | HCM - Health Content Management

From: Katelyn Schockman
Date: Wednesday, September 21, 2022 04:51 PM GMT

Hello,

I would like to adapt Table 7 from Millero et al. (2006) https://doi.org/10.1016/j.marchem.2005.12.001 to include in my dissertation. Can I obtain permission for this?

Appendix A.2 Copyright permission for Chapter Two

From: Permissions Helpdesk <permissionshelpdesk@elsevier.com>
Sent: Thursday, December 16, 2021 5:29 AM
To: Katelyn Schockman
Subject: Re: Copyright for reprint in dissertation [211213-019799]

Dear Katelyn Schockman

Thank you for checking this with us.

As the author of the article, you are allowed to use it in your thesis with proper attribution and you do not need to obtain permission.

Please go ahead and use it and credit the original source.

Kind regards,

Roopa Lingayath
Senior Copyrights Coordinator
ELSEVIER | HCM - Health Content Management

Visit Elsevier Permissions

Appendix A.3 Copyright permission for Chapter Four

From: Permissions Helpdesk <permissionshelpdesk@elsevier.com>
Sent: Tuesday, June 14, 2022 12:41 PM
To: Katelyn Schockman
Subject: Re: Permission to include article in Dissertation [220613-023436]

Dear Katelyn Schockman,

Thank you for your query.

Please note that, as one of the authors of this article, you retain the right to reuse it in your thesis/dissertation. You do not require formal permission to do so. You are permitted to post this Elsevier article online if it is embedded within your thesis. You are also permitted to post your Author Accepted Manuscript online.

However posting of the final published article is prohibited.

*"As per our Sharing Policy, authors are permitted to post the Accepted version of their article on their institutional repository – as long as it is for **internal institutional use only.***

It can only be shared publicly on that site once the journal-specific embargo period has lapsed. For a list of embargo periods please see: Embargo List.

You are not permitted to post the Published Journal Article (PJA) on the repository."

Please feel free to contact me if you have any queries.

Kind regards,

Kaveri Thakuria
Senior Copyrights Coordinator
ELSEVIER | HCM - Health Content Management

Visit Elsevier Permissions

APPENDIX B:

SUPPLEMENTAL INFORMATION FOR CHAPTER TWO

Appendix B.1 Data table of pH measurements to determine pH^0 values

Table B.1.1.
Experimental measurements of $pH_{initial}$ and pH_{final} (i.e., before and after addition of $NaHCO_3$) — (a) is the lowest $pH_{initial}$ for which the $NaHCO_3$ addition lowered the pH, (b) is the highest $pH_{initial}$ for which the $NaHCO_3$ addition increased the pH, (c) is the corresponding pH_{final} to measurement (a), and (d) is the corresponding pH_{final} to measurement (b). These values were used to calculate values of $pH^0_{i(avg)}$ and $pH^0_{f(avg)}$ for a range of S_P and t. For details, see Section 2.5.3.

S_P	t (°C)	(a) $pH_{initial}$	(b) $pH_{initial}$	$pH^0_{i(avg)}$	(c) pH_{final}	(d) pH_{final}	$pH^0_{f(avg)}$
19.62	15.19	7.6618	7.6581	7.6600	7.6587	7.6632	7.6610
19.62	20.03	7.6052	7.6034	7.6043	7.6034	7.6058	7.6046
19.62	25.05	7.5448	7.5443	7.5446	7.5422	7.5457	7.5440
19.62	29.93	7.4862	7.4851	7.4857	7.4844	7.4869	7.4857
19.62	34.81	7.4299	7.4292	7.4296	7.4290	7.4308	7.4299
24.70	15.24	7.6119	7.6074	7.6097	7.6093	7.6098	7.6096
24.70	20.11	7.5490	7.5460	7.5475	7.5471	7.5488	7.5480
24.70	25.07	7.4874	7.4859	7.4867	7.4863	7.4879	7.4871
26.51	29.65	7.4156	7.4135	7.4146	7.4139	7.4148	7.4144
26.51	34.65	7.3589	7.3578	7.3584	7.3575	7.3589	7.3582
29.11	20.07	7.5156	7.5150	7.5153	7.5148	7.5163	7.5156
29.11	24.99	7.4533	7.4520	7.4527	7.4520	7.4538	7.4529
29.11	29.95	7.3934	7.3930	7.3932	7.3913	7.3950	7.3932
31.70	15.35	7.5524	7.5492	7.5508	7.5507	7.5521	7.5514
31.70	34.69	7.3129	7.3115	7.3122	7.3113	7.3141	7.3127
35.50	15.43	7.5291	7.5248	7.5270	7.5269	7.5268	7.5269
35.50	20.36	7.4640	7.4619	7.4630	7.4619	7.4631	7.4625
36.33	25.10	7.3980	7.3978	7.3979	7.3970	7.3987	7.3979
36.33	30.08	7.3383	7.3360	7.3372	7.3368	7.3383	7.3376
36.33	35.02	7.2781	7.2771	7.2776	7.2766	7.2793	7.2780
36.80	25.00	7.4003	7.3979	7.3991	7.3993	7.3992	7.3993
40.98	15.05	7.5012	7.4998	7.5005	7.4974	7.5044	7.5009
40.98	20.05	7.4321	7.4315	7.4318	7.4309	7.4331	7.4320
40.98	25.09	7.3706	7.3692	7.3699	7.3687	7.3701	7.3694
40.98	29.89	7.3112	7.3093	7.3103	7.3093	7.3105	7.3099
40.98	34.88	7.2484	7.2460	7.2472	7.2458	7.2480	7.2469

Appendix B.2 Additional information for $NaHCO_3$ purity calculations

B.2.1 Calculation of $pK_{2(K)}$

Additional details for the calculation of Φ from Section 2.5.4 using eq. (B.1) (denoted as eq. (2.12) in Ch. 2) are provided here. Eq. (B.1) is taken from eq. (3) in Mehrbach et al. (1973), where Φ is denoted as "A".

$$\Phi = \frac{C_T'}{A_T'} = \left(\frac{K_1K_2 + K_1[H^+]_T + [H^+]_T^2}{2K_1K_2 + K_1[H^+]_T} \right) \quad \text{(B.1)}$$

The terms K_1, K_2, and $[H^+]_T$ are dependent on S and T; therefore, calculation of Φ must be made at a specified S and T. For this work, Φ was calculated using five sets of (S_P, T) pairs. To calculate Φ, pH^0 values were measured (as described in Sections 2.5.3 and 2.5.4) by separately adding (a) purified $NaHCO_3$ and (b) purified $KHCO_3$, using identical batches of seawater to obtain pH^0 and $pH^0_{(K)}$ at identical S_P values. For experiments (a) and (b), the temperature was measured after solid addition, and the average of these two temperature measurements (approximately 25 °C) was taken as the T for the Φ calculations.

$KHCO_3$ is a primary standard and, by definition, is purely bicarbonate (Φ = 1), so the equilibrium pH is equidistant between pK_1 and pK_2. Using the measured $pH^0_{(K)}$ and pK_1 of Lueker et al. (2000), pK_2 from the $KHCO_3$ experiments (here denoted as $pK_{2(K)}$) can be calculated via:

$$pH^0_{(K)(\Phi=1)} = ½ (pK_1 + pK_{2(K)}) \quad \text{(B.2)}$$

whereby,

$$pK_{2(K)} = 2pH^0_{(K)(\Phi=1)} - pK_1 \quad \text{(B.3)}$$

B.2.2 Calculation of Φ

The term Φ can then be calculated via eq. (B.1), using the K_1 of Lueker et al. (2000), the $K_{2(K)}$ from eq. (B.3), and $[H^+]_T$ from pH^0 values obtained from $NaHCO_3$ experiments detailed in Sections 2.5.2 and 2.5.3 (provided in Table 2.1). This procedure is identical to the "A" calculation described in Mehrbach et al. (1973), except their work used K_1 from Hawley (1973). Here, Φ was calculated from eq. (B.1) at five discrete salinities, using $pH^0_{i(avg)}$ of $KHCO_3$ for one set of calculations and $pH^0_{f(avg)}$ of $KHCO_3$ for another set (see Table B.2.1). Each set of five Φ values was then averaged to obtain a final Φ value of 0.9996 calculated from $pH^0_{i(avg)}$ and calculated from $pH^0_{f(avg)}$ (values given in Table B.2.2). As a check, the K_1 parameterizations of Mojica Prieto and Millero (2002), Millero et al. (2006), Millero (2010), and Waters and Millero (2013) as revised by Waters et al. (2013, 2014) (i.e., Waters et al. (2013, 2014)) on the total pH scale were also used to calculate Φ. The resulting average Φ values were all identical to within ± 0.00001.

Table B.2.1.
Experimental measurements of $pH_{initial}$ and pH_{final} (i.e., before and after addition of $KHCO_3$) — (a) is the lowest $pH_{initial}$ for which the $KHCO_3$ addition lowered the pH, (b) is the highest $pH_{initial}$ for which the $KHCO_3$ addition increased the pH, (c) is the corresponding pH_{final} to measurement (a), and (d) is the corresponding pH_{final} to measurement (b). These values were used to calculate values of $pH^0_{i(avg)}$ and $pH^0_{f(avg)}$ for a range of S_P and t. For details, see Section 2.5.3. These average values were then used to calculate average $pH^0_{(K)}$ and $pK_{2(K)}$. For details, see Section 2.5.4.

S_P	t (°C)	(a) $pH_{initial}$	(b) $pH_{initial}$	$pH^0_{i(avg)}$	(c) pH_{final}	(d) pH_{final}	$pH^0_{f(avg)}$	$pH^0_{(K)}$	$pK_{2(K)}$
19.62	25.00	7.5380	7.5359	7.5370	7.5365	7.5380	7.5373	7.5371	9.1461
24.70	25.02	7.4859	7.4842	7.4851	7.4853	7.4863	7.4858	7.4854	9.0757
29.11	25.02	7.4471	7.4460	7.4466	7.4451	7.4471	7.4461	7.4463	9.0211
36.33	25.08	7.3977	7.3965	7.3971	7.3947	7.3976	7.3962	7.3966	8.9512
36.80	25.00	7.3976	7.3969	7.3973	7.3965	7.3974	7.3970	7.3971	8.9530

Table B.2.2.
Purity of $NaHCO_3$ solid assessed in terms of Φ at five discrete salinities. Each value of Φ was calculated using $pH^0_{i(avg)}$ and $pH^0_{f(avg)}$ provided in Table B.2.1. The bottom row shows average Φ and one standard deviation for both sets of calculations.

S_P	Φ from $pH^0_{i(avg)}$	Φ from $pH^0_{f(avg)}$
19.62	0.9992	0.9993
24.70	0.9999	0.9998
29.11	0.9993	0.9992
36.33	0.9998	0.9999
36.80	0.9998	0.9997
Average	0.9996 ± 0.0003	0.9996 ± 0.0003

Appendix B.3 CO2SYSv3-MATLAB routine

CO2SYSv3 in MATLAB, developed by Sharp et al. (2020), is available for download at doi: 10.5281/zenodo.3950562. In the CO2SYS routine, the user has the ability to specify the set of dissociation constants used for calculations. CO2SYSv3 includes Waters et al. (2013, 2014) K_1 on the total pH scale and this work $_{SW}K_2$ as option 17 for selecting K_1 and K_2 constants (discussed in Section 2.5.7). This option is provided on the total pH scale with $[H^+]_T$ expressed in mol kg-sw^{-1}. If you use this routine, please cite this original manuscript as well as Sharp et al. (2020).

Appendix B.4 Additional parameterizations for pH^0, $p(K_1K_2)$, and pK_2

Values of $p(K_1K_2)_{initial}$ and $p(K_1K_2)_{final}$ were calculated via eq. (2.13), where pH is either $pH_{initial}$ or pH_{final}, Φ = 0.9996 (as calculated in Appendix B.2), and K_1 is the parameterization of Waters et al. (2013, 2014). These two values, $p(K_1K_2)_{initial}$ and $p(K_1K_2)_{final}$, were averaged to give an overall $p(K_1K_2)$ value for each experimental (S_P, T) pair (provided in Table B.4.1).

The original pH^0 measurements (Table 2.1) and the associated calculated $p(K_1K_2)$ values were parameterized using the same equation as in Section 2.6.1 (eq. (2.15)) shown here as eq. (B.4):

$$\mathrm{pX} = e_1 + e_2 T^{-1} + e_3 \ln T + e_4 S_P + e_5 S_P^{0.5} + e_6 S_P^{2} + e_7 (S_P/T) \quad \text{(B.4)}$$

where pX represents either pH^0 or $p(K_1K_2)$. The e_n coefficients for these parameterizations are provided in Table B.4.2.

For the parameterization of pH^0, the standard deviation of the residuals is 0.0014 and the root mean square error (RMSE) is 0.0014. For the parameterization of $p(K_1K_2)$, the standard deviation of the residuals is 0.0029 and the RMSE is 0.0028.

We also provide a parameterization of our ${}_{SL}pK_2$ values using eq. (B.4) as described in Section 2.6.1. The coefficients for these parameterizations are provided in Table B.4.2. The standard deviation for ${}_{SL}pK_2$ is 0.0029 and the RMSE is 0.0028.

Table B.4.1.
Average values of $p(K_1K_2)$ calculated as described in Appendix B.4 above for each experimental (S_P, T) pair.

S_P	t (°C)	$p(K_1K_2)$
19.62	15.19	15.3127
19.62	20.03	15.2009
19.62	25.05	15.0807
19.62	29.93	14.9639
19.62	34.81	14.8523
24.70	15.24	15.2114
24.70	20.11	15.0879
24.70	25.07	14.9665
26.51	29.65	14.8220
26.51	34.65	14.7099
29.11	20.07	15.0235
29.11	24.99	14.8985
29.11	29.95	14.7796
31.70	15.35	15.0949
31.70	34.69	14.6186
35.50	15.43	15.0466
35.50	20.36	14.9185
36.33	25.10	14.7891
36.33	30.08	14.6683
36.33	35.02	14.5494
36.80	25.00	14.7917

Table B.4.1. (Continued).

40.98	15.05	14.9944
40.98	20.05	14.8571
40.98	25.09	14.7328
40.98	29.89	14.6139
40.98	34.88	14.4882

Table B.4.2.
Coefficients for the parameterizations of pH^0, $p(K_1K_2)$, and ${}_{SL}pK_2$. Values of $p(K_1K_2)$ were calculated using the K_1 of Waters et al. (2013, 2014) on the total pH scale. Calculations of ${}_{SL}pK_2$ were made using the K_1 of Lueker et al. (2000). As a check, the values at $S_P = 35$ and $T = 298.15$ K are $pH^0 = 7.4093$, $p(K_1K_2) = 14.8117$, and ${}_{SL}pK_2 = 8.9643$.

$pX = e_1+e_2T^{-1}+e_3 \ln T+e_4S_P+e_5S_P^{0.5}+e_6S_P^{2}+e_7(S_P/T)$			
	pH^0	$p(K_1K_2)$	${}_{SL}pK_2$
e_1	34.1985	67.3661	128.751
e_2	−302.29	−564.7	–4206.19
e_3	−4.31783	−8.4819	–18.18506
e_4	0.026455	0.05215	0.06343
e_5	−0.3887	−0.77195	–0.77021
e_6	−0.00017107	−0.0003395	–0.0004524
e_7	3.485	7.016	7.009

Appendix B.5 Data tables for internal consistency calculations

Table B.5.1.
Residuals of fCO_2 (i.e., (fCO_2 measured – fCO_2 calculated)), obtained using the three sets of dissociation constants: set A = ${}_LK_1$ and ${}_LK_2$ (the constants of Lueker et al. (2000)), set B = ${}_WK_1$ and ${}_WK_2$ (the constants of Waters et al. (2013, 2014)) and set C = ${}_WK_1$ and ${}_{SW}K_2$ of this work. For comparison, also shown are residuals obtained using set D = ${}_LK_1$ and ${}_{SL}K_2$ of this work (parameterization given in Appendix B.4). The experimental fCO_2, A_T, and C_T data are from Lueker et al. (2000). Summary statistics are given in Table 2.3.

Measured fCO_2	Residuals of fCO_2			
	Lueker K_1 and K_2	Waters K_1 and K_2	Waters K_1 and this work ${}_{SW}K_2$	Lueker K_1 and this work ${}_{SL}K_2$
217.9	−5.73	−3.89	−9.09	−6.32
248.1	−6.78	−4.68	−10.61	−7.44
251.3	−4.94	−2.82	−8.79	−5.62
262.5	−2.47	−0.30	−6.81	−3.15
276.1	−4.09	−5.45	−12.49	−5.75
279.9	0.13	2.42	−4.44	−0.59

Table B.5.1. (Continued).

314.0	−7.23	−4.55	−11.98	−8.09
321.4	−7.35	−4.64	−12.25	−8.20
339.4	−1.67	1.16	−6.75	−2.57
339.9	−4.33	−1.47	−9.45	−5.23
340.3	−8.00	−5.11	−13.18	−8.92
340.4	−5.02	−2.15	−10.16	−5.93
342.9	−1.80	1.05	−6.93	−2.70
343.2	−3.01	−0.15	−8.17	−3.91
343.8	-4.63	−5.00	−12.83	−5.42
343.8	−2.65	−3.02	−10.81	−3.44
344.7	−2.74	−3.11	−10.92	−3.53
357.2	−5.18	−2.20	−10.55	−6.12
361.8	1.30	4.24	−4.53	0.38
363.7	−4.10	−1.11	−10.04	−5.04
364.1	−8.93	−5.90	−14.95	−9.88
365.2	−7.44	−4.33	−12.91	−8.44
388.8	−6.43	−3.14	−12.22	−7.49
391.7	−8.90	−5.57	−14.76	−9.97
420.6	−4.18	−0.66	−10.38	−5.31
424.9	1.09	4.60	−5.09	−0.04
425.5	2.08	5.58	−4.10	0.95
467.5	−5.89	−8.09	−19.39	−8.58
569.7	16.81	21.19	8.17	15.44
572.1	5.04	9.65	−3.03	3.56
574.6	−0.47	4.13	−8.69	−1.91
607.0	13.96	18.63	4.78	12.51
609.7	2.77	7.65	−5.87	1.24
609.8	1.63	6.52	−7.02	0.09
767.1	32.70	38.31	21.68	30.96
981.1	31.25	38.39	18.85	28.96
1349.6	−48.96	−39.84	−65.13	−51.80
1354.1	−20.29	−11.24	−36.29	−23.11
1370.5	5.89	14.99	−10.05	3.03
1371.4	17.11	26.15	1.24	14.28
1372.0	33.60	42.58	17.84	30.79
1375.5	21.50	30.62	5.74	18.59
1382.6	53.69	52.71	31.26	51.51
1385.2	41.47	40.48	18.93	39.27
1385.8	47.34	46.36	24.84	45.15
1738.5	−22.34	−12.09	−40.44	−25.54
1739.2	19.12	29.27	1.20	15.96

Table B.5.2.
Average A_T residuals (measured – calculated) for nine hydrographic cruises, obtained using the three sets of dissociation constants: set A = ${}_LK_1$ and ${}_LK_2$ (the constants of Lueker et al. (2000)), set B = ${}_WK_1$ and ${}_WK_2$ (the constants of Waters et al. (2013, 2014)) and set C = ${}_WK_1$ and ${}_{SW}K_2$ of this work. For comparison, also shown are residuals obtained using set D = ${}_LK_1$ and ${}_{SL}K_2$ of this work (parameterization given in Appendix B.4).

Cruise	Average A_T residuals ± 1 stdev. (μmol kg^{-1})			
	Lueker K_1 and K_2	Waters K_1 and K_2	Waters K_1 and this work ${}_{SW}K_2$	Lueker K_1 and this work ${}_{SL}K_2$
WCOA 2011 (n = 1009)	4.0 ± 4.4	6.1 ± 4.2	3.4 ± 4.7	3.6 ± 4.5
A20 2012 (n = 1451)	1.4 ± 4.1	4.5 ± 3.6	0.1 ± 4.6	0.9 ± 4.3
GOMECC-2 2012 (n = 720)	0.6 ± 7.4	4.2 ± 7.0	–1.0 ± 7.6	0.0 ± 7.4
P02 2013 (n = 3398)	0.8 ± 3.2	3.3 ± 2.7	0.1 ± 3.8	0.4 ± 3.3
P16S 2014 (n = 2715)	–0.7 ± 3.1	1.4 ± 2.7	–1.9 ± 3.6	–1.1 ± 3.1
P16N 2015 (n = 3214)	3.8 ± 3.1	6.6 ± 2.7	3.1 ± 3.6	3.4 ± 3.2
I08S 2016 (n = 1757)	0.5 ± 2.7	3.0 ± 2.4	–0.5 ± 2.9	0.0 ± 2.7
I09N 2016 (n = 2564)	0.4 ± 3.5	2.9 ± 3.2	–0.5 ± 3.9	0.0 ± 3.6
P18 2016 (n = 4647)	–0.2 ± 4.1	2.2 ± 3.8	–0.9 ± 4.5	–0.5 ± 4.2

Table B.5.3.
Average pH residuals (measured – calculated) for nine hydrographic cruises, obtained using the three sets of dissociation constants: set A = ${}_{L}K_1$ and ${}_{L}K_2$ (the constants of Lueker et al. (2000)), set B = ${}_{W}K_1$ and ${}_{W}K_2$ (the constants of Waters et al. (2013, 2014)) and set C = ${}_{W}K_1$ and ${}_{SW}K_2$ of this work. For comparison, also shown are residuals obtained using set D = ${}_{L}K_1$ and ${}_{SL}K_2$ of this work (parameterization given in Appendix B.4). Measurements and calculations were made on the total hydrogen ion concentration pH scale (pH_T) for all cruises except for P18 2016 which is on the seawater pH scale (pH_{SWS}) (as explained in Section 2.5.8).

Cruise	Average pH residuals ± 1 stdev.			
	Lueker K_1 and K_2	Waters K_1 and K_2	Waters K_1 and this work ${}_{SW}K_2$	Lueker K_1 and this work ${}_{SL}K_2$
WCOA 2011 (n = 1009)	–0.012 ± 0.012	–0.017 ± 0.012	–0.010 ± 0.013	–0.011 ± 0.013
A20 2012 (n = 1451)	–0.004 ± 0.008	–0.011 ± 0.008	–0.002 ± 0.009	–0.003 ± 0.008
GOMECC-2 2012 (n = 720)	–0.002 ± 0.014	–0.009 ± 0.014	0.001 ± 0.014	–0.001 ± 0.014
P02 2013 (n = 3398)	–0.003 ± 0.008	–0.009 ± 0.007	–0.002 ± 0.009	–0.002 ± 0.008
P16S 2014 (n = 2715)	0.001 ± 0.006	–0.004 ± 0.006	0.004 ± 0.007	0.002 ± 0.006
P16N 2015 (n = 3214)	–0.011 ± 0.009	–0.016 ± 0.008	–0.009 ± 0.009	–0.010 ± 0.009
I08S 2016 (n = 1757)	–0.002 ± 0.006	–0.008 ± 0.006	0.001 ± 0.007	0.000 ± 0.006
I09N 2016 (n = 2564)	–0.002 ± 0.008	–0.008 ± 0.008	0.000 ± 0.008	–0.001 ± 0.008
P18 2016 (n = 4647)	–0.001 ± 0.010	–0.006 ± 0.010	0.001 ± 0.011	0.000 ± 0.010

Appendix B.6 References for Appendix B

Barbero, L., Wanninkhof, R., Dickson, A.G., Carlson, C.A., Key, R.M., Becker, S., Swift, J.H., McNichol, A., and Rodriguez, C. (2018) Discrete profile measurements of dissolved inorganic carbon, total alkalinity, pH on total scale and other hydrographic and chemical data obtained during the R/V Roger Revelle Repeat Hydrography Cruise in the Indian Ocean: GO-SHIP Section I09N, (EXPOCODE 33RR20160321) from 2016-03-21 to 2016-04-28 (NCEI Accession 0178637). NOAA National Centers for Environmental Information. Dataset. https://doi.org/10.25921/f59c-dy18

Carter, B.R., Sonnerup, R.E., Millero, F.J., Woosley, R.J., Wanninkhof, R., Feely, R.A., Hansell, D.A., Bullister, J.L., Mordy, C., Baringer, M.O., Langdon, C., Key, R.M., McNichol, A., Doney, S.C., and Johnson, G.C. (2018) Carbon dioxide, hydrographic and chemical data collected from profile discrete samples during the NOAA Ship Ronald H. Brown cruise RB-16-06 along the GO-SHIP Repeat Hydrography Section P18 (EXPOCODE 33RO20161119) in the Pacific Ocean from 2016-11-19 to 2017-02-03 (NCEI Accession 0171546). NOAA National Centers for Environmental Information. Dataset. https://doi.org/10.7289/v5cv4g1w

Cross, J.N., Macdonald, A.M., Alin, S.R., Wanninkhof, R., Dickson, A.G., Carlson, C.A., Johnson, G.C., Baringer, M.O., Mordy, C., Langdon, C., Key, R.M., McNichol, A., Bullister, J.L., Jenkins, W.J., and Nelson, N. (2017) Dissolved inorganic carbon (DIC), total alkalinity, pH on total scale, dissolved organic carbon (DOC), chlorofluorocarbons (CFC-11, CFC-12), temperature, salinity and other hydrographic and chemical variables collected from discrete samples and profile observations during the R/V Ronald H. Brown cruise along the GO-SHIP Section P16N_2015, Legs 1 and 2 (EXPOCODEs 33RO20150410 and 33RO20150525) in the Pacific Ocean, from 2015-04-10 to 2015-06-27 (NCEI Accession 0163182). NOAA National Centers for Environmental Information. Dataset. https://doi.org/10.3334/cdiac/otg.go_ship_p16n_2015

Feely, R.A., Alin, S.R., Hales, B., Johnson, G.C., Juranek, L.W., Byrne, R.H., Peterson, W.T., Goni, M., Liu, X., and Greeley, D. (2016) Dissolved inorganic carbon, pH, alkalinity, temperature, salinity and other variables collected from discrete sample and profile observations using Alkalinity titrator, CTD and other instruments from WECOMA in the Gulf of the Farallones National Marine Sanctuary, Monterey Bay National Marine Sanctuary and others from 2011-08-12 to 2011-08-30 (NCEI Accession 0157458). NOAA National Centers for Environmental Information. Dataset. https://accession.nodc.noaa.gov/0157458

Hawley, J.E. (1973) Bicarbonate and carbonate association with sodium, magnesium, and calcium at 25 °C and 0.72 ionic strength. PhD Thesis, Oregon State University.

Lewis, E., and Wallace, D.W.R. (1998) Program developed for CO_2 system calculations. *ORNL/CDIAC-105.* Carbon Dioxide Inf. Anal. Cent., Oak Ridge Natl. Lab., U.S. Dept. of Energy, Oak Ridge, TN.

Lueker, T.J., Dickson, A.G., and Keeling, C.D. (2000) Ocean pCO_2 calculated from dissolved inorganic carbon, alkalinity, and equations for K_1 and K_2: Validation based on laboratory measurements of CO_2 in gas and seawater at equilibrium. *Mar. Chem.* **70**, 105–119. https://doi.org/10.1016/S0304-4203(00)00022-0

Macdonald, A.M., Wanninkhof, R., Dickson, A.G., Carlson, C.A., Key, R.M., Becker, S., Swift, J.H., McNichol, A., Schlosser, P., and Fripiat, F. (2018) Discrete profile measurements of dissolved inorganic carbon, total alkalinity, pH and other hydrographic and chemical data obtained during the R/V Roger Revelle Repeat Hydrography and SOCCOM Cruise in the Indian Ocean and Southern Ocean: GO-SHIP Section I08S, (EXPOCODE 33RR20160208) from 2016-02-08 to 2016-03-16 (NCEI Accession 0171457). NOAA National Centers for Environmental Information. Dataset. https://doi.org/10.7289/v5hm56qr

Mehrbach, C., Culberson, C., Hawley, J., and Pytkowicx, R. (1973) Measurement of the apparent dissociation constants of carbonic acid in seawater at atmospheric pressure *Limnol. Oceanogr*. **18**, 897–907. https://doi.org/10.4319/lo.1973.18.6.0897

Millero, F.J. (2010) Carbonate constants for estuarine waters. *Mar. Freshw. Res.* **61**, 139–142. doi:10.1071/MF09254

Millero, F.J., Graham, T.B., Huang, F., Bustos-Serrano, H., and Pierrot, D. (2006) Dissociation constants of carbonic acid in seawater as a function of salinity and temperature. *Mar. Chem.* **100**, 80–94. doi:10.1016/j.marchem.2005.12.001

Mojica Prieto, F.J. and Millero, F.J. (2002) The values of $pK_1 + pK_2$ for the dissociation of carbonic acid in seawater. *Geochim. Cosmochim. Acta* **66**, 2529–2540. https://doi.org/10.1016/S0016-7037(02)00855-4

Sharp, J.D., Pierrot, D., Humphreys, M.P., Epitalon, J.-M., Orr, J.C., Lewis, E.R., and Wallace, D.W.R. (2020). CO2SYSv3 for MATLAB (Version v3.0.1). Zenodo. http://doi.org/10.5281/zenodo.3952803

Swift, J.H., Mecking, S., Feely, R.A., Dickson, A.G., Carlson, C.A., Jenkins, W.J., McNichol, A., Key, R.M., Ho, D.T., Sigman, D., Macdonald, A.M., Buesseler, K., and Martz, T.R. (2014) Dissolved inorganic carbon, pH, alkalinity, temperature, salinity and other variables collected from discrete sample and profile observations using CTD, bottle and other instruments from MELVILLE in the North Pacific Ocean and Philippine Sea from 2013-03-21 to 2013-05-01 (NCEI Accession 0117338). NOAA National Centers for Environmental Information. Dataset. https://doi.org/10.3334/cdiac/otg.goship_p02_318m20130321

Talley, L.D., Feely, R.A., Dickson, A.G., Swift, J.H., Carlson, C.A., Warner, M.J., McNichol, A., Key, R.M., and Schlosser, P. (2016) Dissolved inorganic carbon (DIC), total alkalinity, pH on total scale, dissolved organic carbon (DOC), chlorofluorocarbons, temperature, salinity and other hydrographic and chemical variables collected from discrete samples and profile observations during the R/V Nathaniel B. Palmer cruise GO-SHIP_P16S_2014 (EXPOCODE 320620140320) in the South Pacific Ocean from 2014-03-20 to 2014-05-05 (NCEI Accession 0157621). NOAA National Centers for Environmental Information. Dataset. https://doi.org/10.3334/cdiac/otg.go_ship_p16s_2014

Wanninkhof, R., Feely, R.A., Dickson, A.G., Hansell, D.A., Key, R.M., Swift, J.H., Smethie, W.M. Jr., Fine, R.A., Jenkins, W.J., McNichol, A., McCartney, M.S., and Druffel, E.R.M. (2013) Partial pressure (or fugacity) of carbon dioxide, dissolved inorganic carbon, pH, alkalinity, temperature, salinity and other variables collected from discrete sample and profile observations using Alkalinity titrator, CTD and other instruments from ATLANTIS in the North Atlantic Ocean from 2012-04-19 to 2012-05-15 (NCEI Accession 0108160). NOAA National Centers for Environmental Information. Dataset. https://doi.org/10.3334/cdiac/otg.clivar_a20_2012

Wanninkhof, R., Zhang, J.-Z., Baringer, M.O., Langdon, C., Cai, W.-J., Salisbury, J.E., and Byrne, R.H. (2016) Partial pressure (or fugacity) of carbon dioxide, dissolved inorganic carbon, pH, alkalinity, temperature, salinity and other variables collected from discrete sample and profile observations using CTD, bottle and other instruments from NOAA Ship RONALD H. BROWN in the Gray's Reef National Marine Sanctuary, Gulf of Mexico and North Atlantic Ocean from 2012-07-21 to 2012-08-13 (NCEI Accession 0157619). NOAA National Centers for Environmental Information. Dataset. https://doi.org/10.3334/cdiac/otg.coastal_gomecc2

Waters, J., Millero, F. and Woosley, R. (2014) Corrigendum to "The free proton concentration scale for seawater pH", [MARCHE: 149 (2013) 8–22]. *Mar. Chem.* **165**, 66–67. https://doi.org/10.1016/j.marchem.2014.07.004

Waters, J.F. and Millero, F.J. (2013) The free proton concentration scale for seawater pH. *Mar. Chem.* **149**, 8–22. https://doi.org/10.1016/j.marchem.2012.11.003

Van Heuven, S., Pierrot, D., Rae, J., Lewis, E., and Wallace, D. (2011) MATLAB program developed for CO_2 system calculations. *ORNL/CDIAC-105b.* Carbon Dioxide Inf. Anal. Cent., Oak Ridge Natl. Lab., US Dept. of Energy, Oak Ridge, TN.

APPENDIX C:

SUPPLEMENTAL INFORMATION FOR CHAPTER THREE

Appendix C.1 Low temperature pH_{12} measurements

Table C.1.1.
Measurements of pH_{12} along with the respective measurement temperature and associated QC flag (2 denotes good measurement, 6 denotes average of two duplicate good measurements) made on NOAA's 2021 West Coast Ocean Acidification Cruise (WCOA2021). The ID Code is a unique value based on the station, cast, and bottle number of each sample (10000*station number + 100*cast number + bottle number).

ID Code	Measured t (°C)	pH_{12}	QC Flag
10101	12.55	7.4671	2
10103	12.40	7.4498	6
10104	12.62	7.4261	2
10106	12.59	7.5825	2
10107	12.60	7.6647	2
10108	12.57	7.6740	2
10109	12.43	7.7636	2
10111	12.52	7.9033	2
10112	12.60	7.9067	2
10113	12.64	7.9643	6
20101	12.50	7.4354	2
20103	12.67	7.4280	6
20104	12.55	7.4565	2
20105	12.68	7.4805	2
20108	12.55	7.6075	2
20109	12.57	7.6419	2
20112	12.60	7.6817	2
20114	12.64	7.7839	2
20116	12.55	7.7999	2
20120	12.50	7.9139	6
30101	12.62	7.5180	2
30103	12.61	7.5933	6
30105	12.61	7.6473	2
30108	12.59	7.7152	2
30109	12.63	7.7295	2

Table C.1.1. (Continued).

30110	12.60	7.8072	2
30111	12.67	7.8327	2
30114	12.66	8.0413	6
40101	12.64	7.9580	2
40103	12.65	8.0383	6
40104	12.70	8.1098	2
40106	12.64	8.1087	2
50101	12.68	7.5387	2
50103	12.49	7.6033	6
50104	12.63	7.6334	2
50105	12.58	7.7556	2
50107	12.59	7.7567	2
50108	12.63	7.8455	2
50109	12.59	7.8601	2
50110	12.60	7.9075	2
50111	12.71	7.9637	2
50112	12.63	8.1091	2
50114	12.48	8.1385	6
50115	12.74	8.1323	2
60101	12.60	7.6144	2
60103	12.49	7.6220	6
60104	12.64	7.6780	2
60105	12.65	7.7894	2
60107	12.62	7.8177	2
60108	12.53	7.8665	2
60109	12.67	7.8920	2
60112	12.52	8.0339	2
60113	12.64	8.0875	6
60114	12.69	8.0960	2
360101	12.87	7.6055	2
360103	12.84	7.5632	6
360105	12.77	7.4384	2
360106	12.80	7.4224	2
360107	12.88	7.4446	2
360108	12.80	7.4800	2
360109	12.83	7.5404	2
360110	12.90	7.6013	2
360111	12.82	7.6468	2
360112	12.86	7.6909	2
360113	12.81	7.7808	2
360114	12.79	7.9132	2
360115	12.85	7.9565	2
360116	12.91	7.9715	2

Table C.1.1. (Continued).

360117	12.87	8.0174	2
360118	12.87	8.0695	2
360119	12.85	8.0739	6
360120	12.85	8.0747	2
360121	12.83	8.0768	2
370104	12.72	7.4461	6
370105	12.71	7.4289	2
370106	12.78	7.4524	2
370109	12.80	7.4989	2
370110	12.67	7.5794	2
370111	12.70	7.6079	2
370112	12.73	7.6522	2
370114	12.65	7.7341	2
370115	12.80	7.8828	2
370117	12.92	7.9498	2
370118	12.82	8.0835	2
370121	12.92	8.1370	2
370122	12.85	8.1366	2
380103	12.67	7.4484	2
380104	12.78	7.4275	2
380107	12.71	7.4799	2
380108	12.61	7.5037	2
380109	12.71	7.5421	2
380111	12.73	7.5851	2
380112	12.66	7.5915	2
380114	12.72	7.6536	2
380118	12.80	7.7418	2
380119	12.73	8.0842	2
380121	12.93	8.2105	2
390101	12.88	7.4858	2
390104	12.88	7.4901	6
390106	12.99	7.5048	2
390107	12.98	7.4696	2
390108	12.88	7.4961	2
390109	12.93	7.5517	2
390112	12.90	7.7008	2
390113	12.87	7.7229	2
390114	12.69	7.7054	2
390115	12.77	7.7129	2
390117	12.61	8.0733	2
390118	12.67	8.1960	2
390119	12.58	8.2149	2
400101	12.79	7.4278	2

Table C.1.1. (Continued).

400103	12.77	7.4236	6
400104	12.83	7.5162	2
400106	12.80	7.5904	2
400109	12.90	7.5448	2
400111	13.00	7.8489	2
400113	13.04	8.1713	2
400114	12.93	8.1754	2
410101	12.99	7.4195	2
410103	12.78	7.5029	6
410106	12.84	7.5088	2
410109	12.89	7.7346	2
410111	12.72	8.2498	2
410112	12.90	8.2829	2
420101	12.71	7.3870	2
420104	13.00	7.8928	2
420107	12.87	8.0780	2
430103	12.68	8.3056	2
440101	13.02	7.4287	2
440104	12.95	7.4388	6
440105	12.99	7.4653	2
440106	12.79	7.4801	2
440107	12.97	7.7059	2
440112	12.98	8.0633	2
530101	12.54	7.5046	2
530103	12.57	7.4502	6
530104	12.54	7.4367	2
530105	12.52	7.4551	2
530107	12.58	7.5052	2
530108	12.53	7.5529	2
530109	12.63	7.5942	2
530111	12.72	7.6417	2
530113	12.60	7.7075	2
530114	12.68	7.7658	2
530116	12.52	7.8767	6
530118	12.65	8.1036	2
530121	12.60	8.1535	2
540101	12.44	7.4472	2
540103	12.45	7.4385	6
540104	12.53	7.4653	2
540105	12.55	7.4794	2
540106	12.39	7.5046	2
540107	12.48	7.5163	2
540108	12.45	7.5658	2

Table C.1.1. (Continued).

540109	12.42	7.5847	2
540112	12.42	7.6037	2
540113	12.48	7.6056	2
540115	12.54	7.7927	2
540117	12.61	8.1159	2
540120	12.38	8.1982	2
550101	12.52	7.4909	2
550104	12.67	7.5067	6
550105	12.48	7.5504	2
550106	12.49	7.6616	2
550109	12.44	7.6909	2
550110	12.51	7.7387	6
550111	12.62	7.8225	2
550112	12.55	8.1308	2
550113	12.27	8.1762	2
560101	12.55	7.4916	2
560104	12.45	7.4885	6
560105	12.51	7.4881	2
560106	12.45	7.5391	2
560107	12.55	7.5047	2
560109	12.46	7.6100	2
560112	12.32	7.9472	6
560115	12.38	8.1837	2
560116	12.32	8.2133	2
570101	12.44	7.4564	2
570103	12.28	7.4974	6
570104	12.24	7.5045	2
570105	12.27	7.5070	2
570107	12.32	7.4922	2
570108	12.29	7.6153	2
570109	12.42	7.6726	2
570110	12.38	7.8375	2
570111	12.41	7.9830	2
580103	12.34	7.4804	6
580104	12.36	7.5229	2
580106	12.32	7.5675	2
580107	12.37	7.6199	2
590101	12.51	7.5257	2
590103	12.56	7.5356	2
590105	12.57	7.5745	2
590108	12.51	7.6276	2
590111	12.54	7.9055	2
790101	12.88	7.4766	2

Table C.1.1. (Continued).

790103	12.90	7.4662	6
790105	12.76	7.4681	2
790106	12.86	7.4962	2
790107	12.71	7.5332	2
790108	12.79	7.5798	2
790109	12.92	7.5964	2
790110	12.93	7.6126	2
790111	12.90	7.6484	2
790113	12.86	7.6710	2
790114	12.98	7.7116	2
790115	12.91	7.7451	2
790116	12.94	7.7755	6
790117	12.91	7.8699	2
790118	12.99	7.9722	2
790119	13.03	8.0757	2
790120	12.90	8.0971	2
800101	12.72	7.5959	2
800103	12.84	7.6060	6
800105	12.85	7.6435	2
800107	12.74	7.7088	2
800109	12.85	7.7770	2
800111	12.81	7.9539	2
800113	12.78	7.9825	2
800114	12.63	8.0230	2
810101	12.93	7.5469	2
810103	12.74	7.5639	6
810105	12.78	7.5892	2
810107	12.81	7.5956	2
810109	12.83	7.8598	2
810111	12.84	7.9805	2
810113	12.88	8.0277	2
820101	12.85	7.6289	2
820103	12.76	7.6510	6
820105	12.77	7.6923	2
820107	12.85	7.7493	2
820109	12.80	7.7707	2
830101	12.74	7.5751	2
830104	12.79	7.6209	6
830107	12.85	7.6871	2
830110	12.81	7.7177	2
830113	12.85	7.8071	2
840101	12.64	7.6070	2
840107	12.68	7.6476	2

Table C.1.1. (Continued).

840113	12.65	7.7513	2
840116	12.68	7.9000	2
840118	12.76	7.9094	2
840119	12.74	7.9137	2
840121	12.75	7.9116	2
850101	12.70	7.6747	2
850104	12.71	7.5860	2
850106	12.76	7.4657	2
850107	12.73	7.4532	2
850108	12.81	7.4593	2
850109	12.89	7.4741	2
850110	12.80	7.5212	2
850111	12.66	7.5867	2
850112	12.71	7.6116	2
850113	12.68	7.6240	2
850114	12.66	7.6859	2
850115	12.67	7.7194	2
850116	12.70	7.7518	2
850117	12.81	7.7853	2
850118	12.87	7.8331	2
850119	12.80	7.9794	2
850120	12.85	7.9795	2
850121	12.70	7.9845	2
850122	12.81	7.9847	2
850123	12.81	7.9854	2

Appendix C.2 Experimental determinations of pH^0

Table C.2.1.
Experimental measurements of $pH_{initial}$ and pH_{final} (i.e., before and after addition of $NaHCO_3$) as defined and described in Schockman and Byrne (2021) — (a) is the lowest $pH_{initial}$ where addition of $NaHCO_3$ lowered the pH, (b) is the highest $pH_{initial}$ where addition of $NaHCO_3$ increased the pH, (c) is the corresponding pH_{final} to measurement (a), and (d) is the corresponding pH_{final} to measurement (b). These values were used to calculate values of $pH^0_{i(avg)}$ and $pH^0_{f(avg)}$ for a range of S_P and t. For details, see Schockman and Byrne (2021).

S_P	t (°C)	(a) $pH_{initial}$	(b) $pH_{initial}$	$pH^0_{i(avg)}$	(c) pH_{final}	(d) pH_{final}	$pH^0_{f(avg)}$
20.35	3.44	7.8105	7.8087	7.8096	7.8078	7.8133	7.8106
20.35	6.50	7.7674	7.7630	7.7652	7.7617	7.7658	7.7638
20.35	9.77	7.7230	7.7196	7.7213	7.7176	7.7227	7.7202
20.35	12.20	7.6867	7.6860	7.6864	7.6846	7.6871	7.6859
24.45	3.63	7.7602	7.7591	7.7597	7.7576	7.7611	7.7594
24.45	6.02	7.7289	7.7252	7.7271	7.7244	7.7282	7.7263
25.78	9.48	7.6747	7.6714	7.6731	7.6725	7.6730	7.6728
25.78	12.32	7.6342	7.6328	7.6335	7.6315	7.6375	7.6345
31.24	3.61	7.7151	7.7132	7.7142	7.7118	7.7186	7.7152
31.24	6.09	7.6796	7.6765	7.6781	7.6757	7.6788	7.6773
31.08	9.74	7.6295	7.6273	7.6284	7.6282	7.6328	7.6305
31.08	12.40	7.5957	7.5921	7.5939	7.5947	7.5934	7.5941
35.09	3.43	7.6910	7.6859	7.6885	7.6871	7.6910	7.6891
35.09	6.09	7.6497	7.6483	7.6490	7.6484	7.6519	7.6502
35.36	9.32	7.6085	7.6051	7.6068	7.6065	7.6075	7.6070
35.36	12.34	7.5665	7.5656	7.5661	7.5650	7.5690	7.5670
40.97	3.56	7.6596	7.6563	7.6580	7.6556	7.6579	7.6568
40.97	6.16	7.6215	7.6170	7.6193	7.6200	7.6199	7.6200
44.61	9.66	7.5547	7.5514	7.5531	7.5511	7.5561	7.5536
44.61	12.59	7.5158	7.5116	7.5137	7.5107	7.5132	7.5120

Appendix C.3 Residuals of pK_2 parameterizations

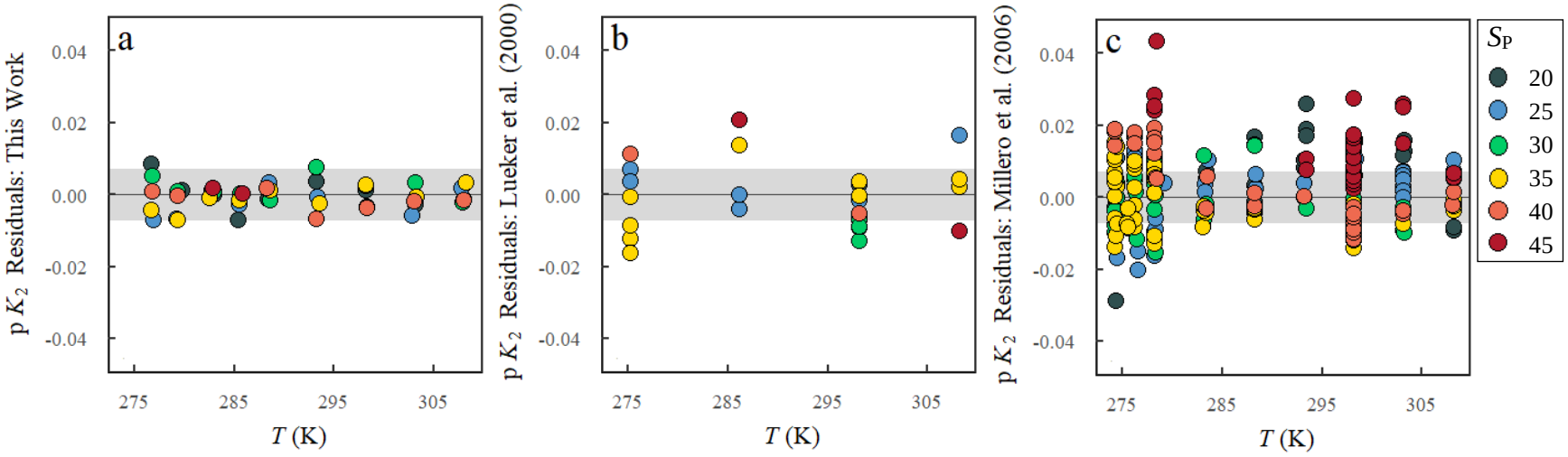

Fig. C.3.1. pK_2 residuals (i.e., experimental pK_2 minus parameterized pK_2) as a function of temperature (K), color-coded by approximate salinity for (a) this work, (b) Lueker et al. (2000), and (c) Millero et al. (2006). Grey shaded region depicts ±2σ standard deviation for the residuals of this work (±0.0072). Figure is similar to Fig. 4 of Schockman and Byrne (2021) with additions of residuals at lower temperatures (≤ 15 °C).

Appendix C.4 Internal consistency assessments from Schockman and Byrne (2021)

C.4.1 Cruise datasets

In Schockman and Byrne (2021), data from a suite of nine repeat hydrography cruises were used to assess the internal consistency of CO_2 system calculations. This was achieved by comparing measured and calculated values of A_T, C_T, and pH, where calculations were performed with several sets of K_1 and K_2 constants (i.e., K_1 of Waters et al. (2013, 2014) and K_2 of Schockman and Byrne (2021); K_1 and K_2 of Lueker et al. (2000); and K_1 and K_2 of Waters et al. (2013, 2014)). The same analyses are performed here using the K_1 of Waters et al. (2013, 2014) paired with the K_2 parameterization of this work (eq. (3.11)). Results highlight the similarity of calculations obtained using the K_2 of this work compared to using the K_2 of Schockman and Byrne (2021) at temperatures of $20 \leq t \leq 25$ °C (i.e., the temperature range of pH measurements from the nine selected cruises).

The National Centers for Environmental Information expedition codes (EXPOCODES) for the nine cruises are as follows: 32WC20110812 (West Coast Ocean Acidification Cruise (WCOA) 2011) (Feely et al., 2016), 33AT20120419 (A20 2012) (Wanninkhof et al., 2013), 33RO20120721 (Gulf of Mexico and East Coast Carbon Cruise 2 (GOMECC-2) 2012) (Wanninkhof et al., 2016), 318M20130321 (P02 2013) (Swift et al., 2014), 320620140320 (P16S 2014) (Talley et al., 2016), 33RO20150410 and 33RO20150525 (P16N 2015) (Cross et al., 2017), 33RR20160208 (I08S 2016) (Macdonald et al., 2018), 33RR20160321 (I09N 2016) (Barbero et al., 2018), and 33RO20161119 (P18 2016) (Carter et al., 2018). More details and ancillary information about the cruise datasets are provided in Schockman and Byrne (2021).

Table C.4.1.
Average residuals of A_T (measured A_T – $A_T(C_T,pH)$) ± standard deviations for a suite of oceanographic cruise datasets, where A_T was calculated using the dissociation constants of (a) this work, (b) Schockman and Byrne (2021), (c) Lueker et al. (2000), and (d) Waters et al. (2013, 2014). Uncertainties are given as ±1σ standard deviation to be consistent with the results of Schockman and Byrne (2021). (See Section C.4.1 and Schockman and Byrne (2021) for more details.)

Cruise	Average A_T residuals ± 1 stdev. (μmol kg^{-1})			
	This Work	Schockman and Byrne (2021)	Lueker et al. (2000)	Waters et al. (2013, 2014)
WCOA 2011 (n = 1009)	3.4 ± 4.7	3.4 ± 4.7	4.0 ± 4.4	6.2 ± 4.2
A20 2012 (n = 1451)	0.1 ± 4.5	0.1 ± 4.6	1.4 ± 4.1	4.6 ± 3.5
GOMECC-2 2012 (n = 720)	–1.0 ± 7.5	–1.0 ± 7.6	0.7 ± 7.4	4.4 ± 7.0
P02 2013 (n = 3398)	0.0 ± 3.8	0.1 ± 3.8	0.8 ± 3.2	3.4 ± 2.7
P16S 2014 (n = 2715)	–2.2 ± 3.6	–1.9 ± 3.6	–0.7 ± 3.1	1.7 ± 2.6
P16N 2015 (n = 3214)	3.1 ± 3.6	3.1 ± 3.6	3.8 ± 3.1	6.2 ± 2.6
I08S 2016 (n = 1757)	–0.5 ± 2.9	–0.5 ± 2.9	0.5 ± 2.7	3.1 ± 2.4
I09N 2016 (n = 2564)	–0.5 ± 3.9	–0.5 ± 3.9	0.4 ± 3.5	3.0 ± 3.2
P18 2016 (n = 4647)	–1.1 ± 4.5	–1.1 ± 4.5	–0.3 ± 4.2	2.2 ± 3.8

Table C.4.2.
Average residuals of pH (measured pH – pH(A_T,C_T)) ± standard deviations for a suite of oceanographic cruise datasets, where pH was calculated using the dissociation constants of (a) this work, (b) Schockman and Byrne (2021), (c) Lueker et al. (2000), and (d) Waters et al. (2013, 2014). Uncertainties are given as ±1σ standard deviation to be consistent with the results of Schockman and Byrne (2021). (See Section C.4.1 and Schockman and Byrne (2021) for more details.)

Cruise	Average pH residuals ± 1 stdev.			
	This Work	Schockman and Byrne (2021)	Lueker et al. (2000)	Waters et al. (2013, 2014)
WCOA 2011 (*n* = 1009)	–0.010 ± 0.013	–0.010 ± 0.013	–0.012 ± 0.012	–0.017 ± 0.012
A20 2012 (*n* = 1451)	–0.002 ± 0.009	–0.002 ± 0.009	–0.004 ± 0.008	–0.011 ± 0.008
GOMECC-2 2012 (*n* = 720)	0.000 ± 0.014	0.001 ± 0.014	–0.002 ± 0.014	–0.009 ± 0.014
P02 2013 (*n* = 3398)	–0.002 ± 0.009	–0.002 ± 0.009	–0.003 ± 0.008	–0.009 ± 0.007
P16S 2014 (*n* = 2715)	0.004 ± 0.007	0.004 ± 0.007	0.001 ± 0.006	–0.005 ± 0.006
P16N 2015 (*n* = 3214)	–0.009 ± 0.009	–0.009 ± 0.009	–0.011 ± 0.009	–0.017 ± 0.008
I08S 2016 (*n* = 1757)	0.001 ± 0.007	0.001 ± 0.007	–0.002 ± 0.006	–0.008 ± 0.006
I09N 2016 (*n* = 2564)	0.000 ± 0.008	0.000 ± 0.008	–0.002 ± 0.008	–0.008 ± 0.008
P18 2016 (*n* = 4647)	0.002 ± 0.011	0.002 ± 0.011	0.000 ± 0.010	–0.006 ± 0.010

Appendix C.5 Internal consistency assessments using WCOA2021 dataset

C.5.1 pH_{25} residuals

Similar to residuals of pH_{12} (discussed in Section 3.5.3.3.1), residuals of pH_{25} were examined in terms of (1) $\Delta pH_{25} = pH_{25} - pH_{25}(A_T,C_T)$ or (2) ${}^{*}\Delta pH_{25} = pH_{25} - pH_{25}(pH_{12},C_T)$. The two sets of residuals are shown in Fig. C.5.1 for calculations utilizing the constants of this work or Lueker et al. (2000). pH_{25} residuals show the same types of patterns and magnitudes of differences observed in the pH_{12} residuals (Fig. 3.5), though the slope of ${}^{*}\Delta pH_{25}$ is opposite in sign of ${}^{*}\Delta pH_{12}$.

C.5.2 Empirical algorithms to correct pH

In cases where only measurements of A_T and C_T are available, algorithms to adjust calculated $pH(A_T,C_T)$ data have been previously investigated as a means to improve the quality of pH calculations (Williams et al., 2017; Carter et al., 2018). Residuals between measured pH_{12} and calculated values of $pH_{12}(A_T,C_T)$, corrected by the Carter et al. (2018) adjustment (denoted as $pH_{12,Carter}(A_T,C_T)$), are shown in Fig. C.5.2. The sloping pH-offset is reduced using the constants of this work (Fig. C.5.2a), while the sloping pH-offset has become negative when utilizing the constants of Lueker et al. (2000) (Fig. C.5.2b). Overall, the residuals are similar in magnitude to non-corrected values (Fig. 3.5a and 3.5c) (i.e., not within the measurement uncertainty of ±0.015).

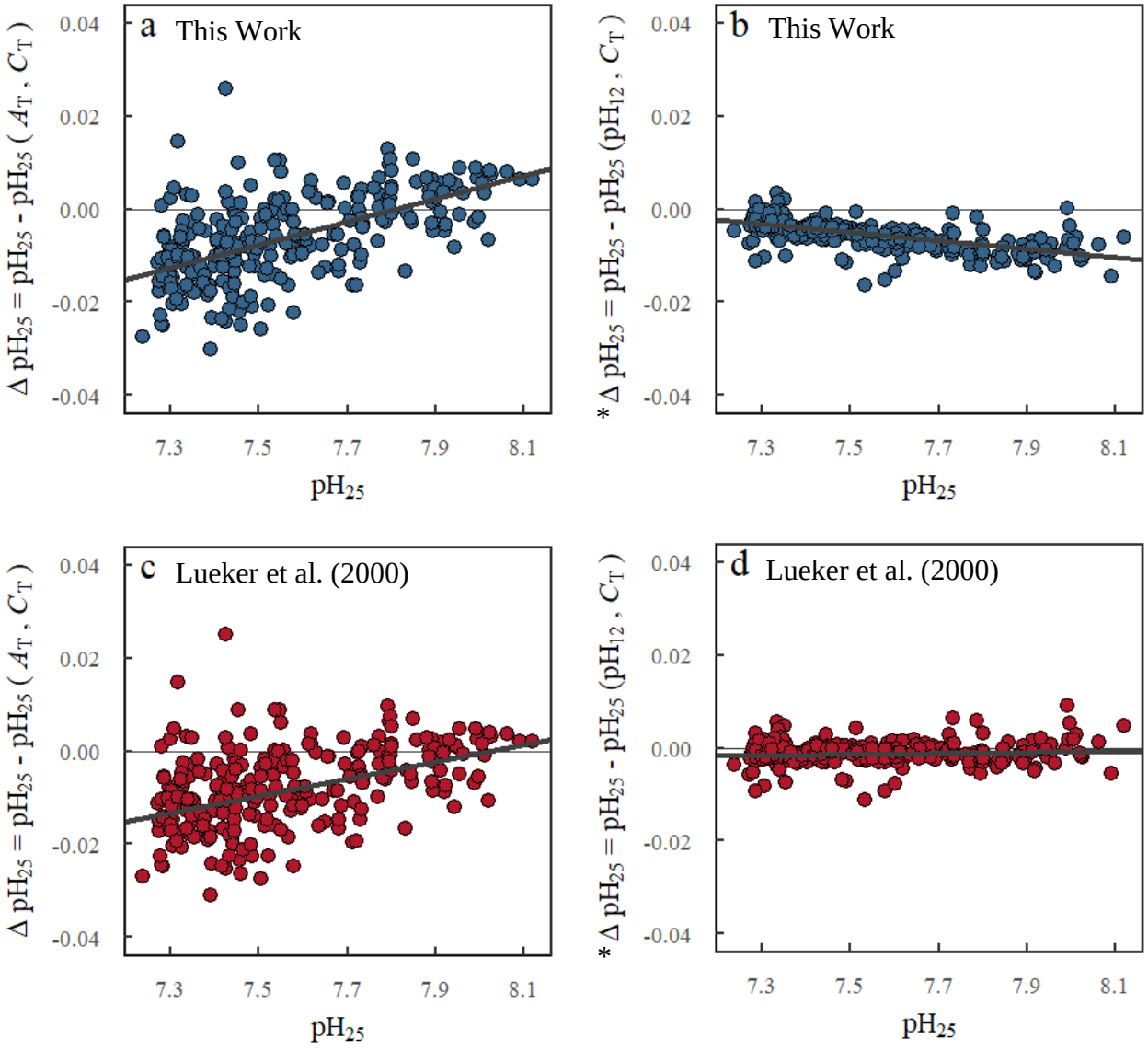

Fig. C.5.1. Residuals of pH_{25}, shown as a function of measured pH_{25}: (1) $\Delta pH_{25} = pH_{25} - pH_{25}(A_T, C_T)$ in the left panels and (2) $^{*}\Delta pH_{25} = pH_{25} - pH_{25}(pH_{12}, C_T)$ in the right panels. The top panels (in blue) utilize the CO_2 system dissociation constants of this work, while the bottom panels (in red) utilize the constants of Lueker et al. (2000). The bold black lines show the linear regressions of the residuals.

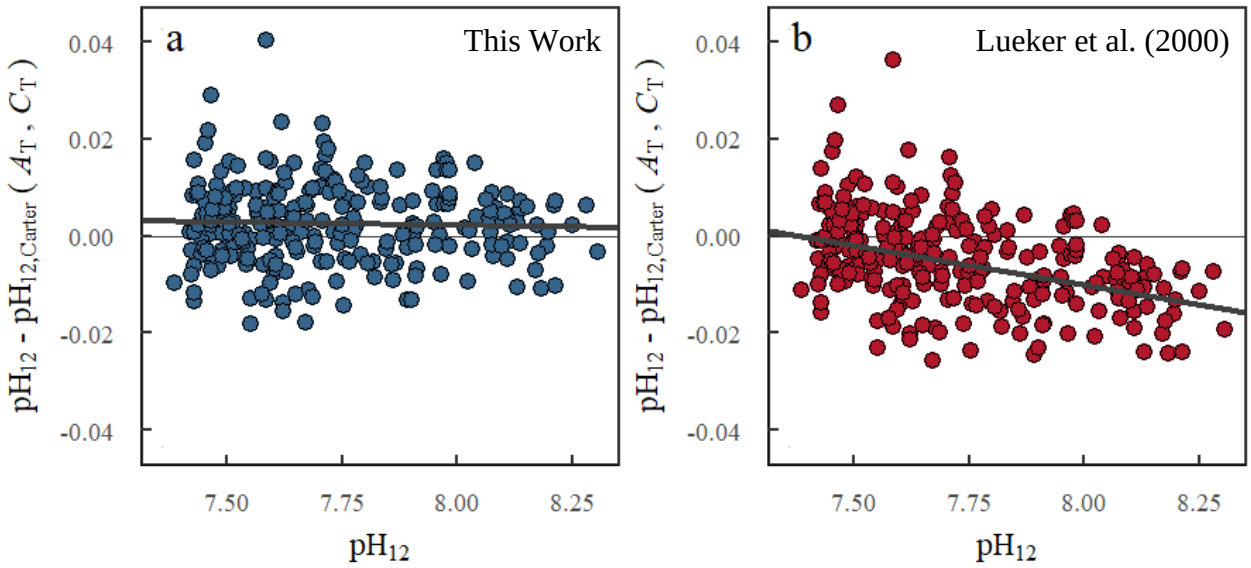

Fig. C.5.2. Residuals of pH_{12} (i.e., $pH_{12} - pH_{12,Carter}(A_T,C_T)$) shown as a function of measured pH_{12} for calculations utilizing the CO_2 system dissociation constants of (a) this work or (b) Lueker et al. (2000). The bold black lines show the linear regressions of the residuals.

Alternatively, Lui and Chen (2017) developed a temperature correcting algorithm to adjust pH without the use of another CO_2 system parameter (i.e., directly converting pH_{25} to pH_{12}). This algorithm, implemented using our pH_{25} data, resulted in calculated pH_{12} values (denoted as $pH_{12,Liu}$) that differed from measured pH_{12} by up to ±0.04 (Fig. C.5.3), which is much larger than the magnitudes of residuals when pH_{12} is calculated using either (A_T,C_T) or (pH_{25},C_T) (Fig. 3.5). Accordingly, this temperature-correcting algorithm should be implemented with caution and should only be used when no alternatives are available (i.e., no other CO_2 system parameters are measured).

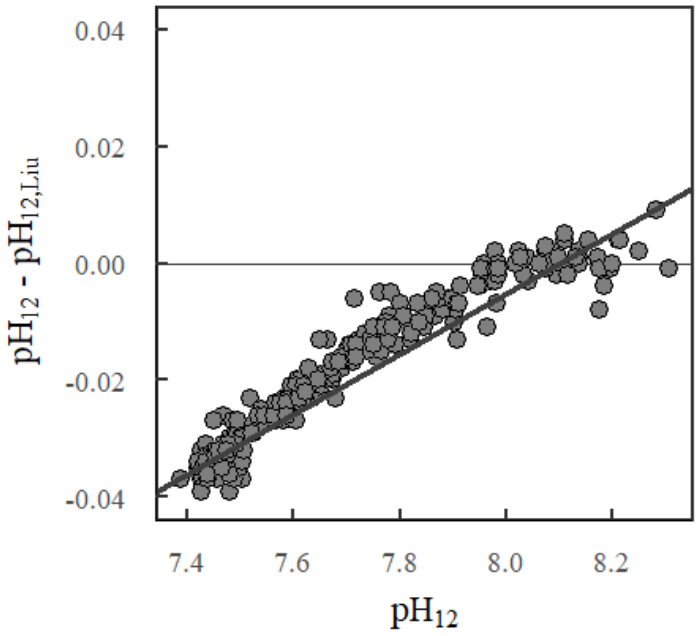

Fig. C.5.3. Differences between measured pH_{12} and pH_{12} estimated by applying the Liu and Chen (2017) temperature correction to measured pH_{25} (denoted as $pH_{12,Liu}$), shown as a function of measured pH_{12}. The bold black line shows the linear regression of the residuals.

C.5.3 Conceptualizing calculations using A_T

Calculations of $pH_{12}(pH_{25}, C_T)$ can alternatively be conceptualized as pH_{12} calculated using C_T and "corrected" A_T values, provided all other components of the carbonate system calculations are assumed to be accurate. Using CO2SYS, pH_{25} and C_T can be used to calculate A_T values (A_T'). Put another way, A_T' values are measured A_T values minus the A_T residuals (ΔA_T) shown in Fig. 3.3 and 3.4. These A_T' values, which are generally smaller than A_T (i.e., a corrected A_T), can then be combined with C_T to estimate pH at an alternative output temperature. Use of A_T', combined with C_T, produces much smaller pH residuals (Fig. 3.5b and 3.5d) than those calculated using directly measured A_T (Fig. 3.5a and 3.5c).

Appendix C.6 References for Appendix C

Barbero, L., Wanninkhof, R., Dickson, A.G., Carlson, C.A., Key, R.M., Becker, S., Swift, J.H., McNichol, A., and Rodriguez, C. (2018) Discrete profile measurements of dissolved inorganic carbon, total alkalinity, pH on total scale and other hydrographic and chemical data obtained during the R/V Roger Revelle Repeat Hydrography Cruise in the Indian Ocean: GO-SHIP Section I09N, (EXPOCODE 33RR20160321) from 2016-03-21 to 2016-04-28 (NCEI Accession 0178637). NOAA National Centers for Environmental Information. Dataset. https://doi.org/10.25921/f59c-dy18

Carter, B.R., Feely, R.A., Williams, N.L., Dickson, A.G., Fong, M.B., and Takeshita, Y. (2018) Updated methods for global locally interpolated estimation of alkalinity, pH, and nitrate. *Limnol. Oceanogr. Methods* **16**, 119−131. https://doi.org/10.1002/lom3.10232

Carter, B.R., Sonnerup, R.E., Millero, F.J., Woosley, R.J., Wanninkhof, R., Feely, R.A., Hansell, D.A., Bullister, J.L., Mordy, C., Baringer, M.O., Langdon, C., Key, R.M., McNichol, A., Doney, S.C., and Johnson, G.C. (2018) Carbon dioxide, hydrographic and chemical data collected from profile discrete samples during the NOAA Ship Ronald H. Brown cruise RB-16-06 along the GO-SHIP Repeat Hydrography Section P18 (EXPOCODE 33RO20161119) in the Pacific Ocean from 2016-11-19 to 2017-02-03 (NCEI Accession 0171546). NOAA National Centers for Environmental Information. Dataset. https://doi.org/10.7289/v5cv4g1w

Cross, J.N., Macdonald, A.M., Alin, S.R., Wanninkhof, R., Dickson, A.G., Carlson, C.A., Johnson, G.C., Baringer, M.O., Mordy, C., Langdon, C., Key, R.M., McNichol, A., Bullister, J.L., Jenkins, W.J., and Nelson, N. (2017) Dissolved inorganic carbon (DIC), total alkalinity, pH on total scale, dissolved organic carbon (DOC), chlorofluorocarbons (CFC-11, CFC-12), temperature, salinity and other hydrographic and chemical variables collected from discrete samples and profile observations during the R/V Ronald H. Brown cruise along the GO-SHIP Section P16N_2015, Legs 1 and 2 (EXPOCODEs 33RO20150410 and 33RO20150525) in the Pacific Ocean, from 2015-04-10 to 2015-06-27 (NCEI Accession 0163182). NOAA National Centers for Environmental Information. Dataset. https://doi.org/10.3334/cdiac/otg.go_ship_p16n_2015

Feely, R.A., Alin, S.R., Hales, B., Johnson, G.C., Juranek, L.W., Byrne, R.H., Peterson, W.T., Goni, M., Liu, X., and Greeley, D. (2016) Dissolved inorganic carbon, pH, alkalinity, temperature, salinity and other variables collected from discrete sample and profile observations using Alkalinity titrator, CTD and other instruments from WECOMA in the Gulf of the Farallones National Marine Sanctuary, Monterey Bay National Marine Sanctuary and others from 2011-08-12 to 2011-08-30 (NCEI Accession 0157458). NOAA National Centers for Environmental Information. Dataset. https://doi.org/10.7289/v5jq0xz1

Lui, H.-K. and Chen, C.-T.A. (2017) Reconciliation of pH_{25} and pH_{insitu} acidification rates of the surface oceans: A simple conversion using only in situ temperature. *Limnol. Oceanogr. Methods* **15**, 328−335. https://doi.org/10.1002/lom3.10170

Lueker, T.J., Dickson, A.G., and Keeling, C.D. (2000) Ocean pCO_2 calculated from dissolved inorganic carbon, alkalinity, and equations for K_1 and K_2: Validation based on laboratory measurements of CO_2 in gas and seawater at equilibrium. *Mar. Chem.* **70**, 105−119. https://doi.org/10.1016/S0304-4203(00)00022-0

Macdonald, A.M., Wanninkhof, R., Dickson, A.G., Carlson, C.A., Key, R.M., Becker, S., Swift, J.H., McNichol, A., Schlosser, P., and Fripiat, F. (2018) Discrete profile measurements of dissolved inorganic carbon, total alkalinity, pH and other hydrographic and chemical data obtained during the R/V Roger Revelle Repeat Hydrography and SOCCOM Cruise in the Indian Ocean and Southern Ocean: GO-SHIP Section I08S, (EXPOCODE 33RR20160208) from 2016-02-08 to 2016-03-16 (NCEI Accession 0171457). NOAA National Centers for Environmental Information. Dataset. https://doi.org/10.7289/v5hm56qr

Millero, F.J., Graham, T.B., Huang, F., Bustos-Serrano, H., and Pierrot, D. (2006) Dissociation constants of carbonic acid in seawater as a function of salinity and temperature. *Mar. Chem.* **100**, 80−94. https://doi.org/10.1016/j.marchem.2005.12.001

Schockman, K.M. and Byrne, R.H. (2021) Spectrophotometric determination of the bicarbonate dissociation constant in seawater. *Geochim. Cosmochim. Acta* **300**, 231−245. https://doi.org/10.1016/j.gca.2021.02.008

Swift, J.H., Mecking, S., Feely, R.A., Dickson, A.G., Carlson, C.A., Jenkins, W.J., McNichol, A., Key, R.M., Ho, D.T., Sigman, D., Macdonald, A.M., Buesseler, K., and Martz, T.R. (2014) Dissolved inorganic carbon, pH, alkalinity, temperature, salinity and other variables collected from discrete sample and profile observations using CTD, bottle and other instruments from MELVILLE in the North Pacific Ocean and Philippine Sea from 2013-03-21 to 2013-05-01 (NCEI Accession 0117338). NOAA National Centers for Environmental Information. Dataset. https://doi.org/10.3334/cdiac/otg.goship_p02_318m20130321

Talley, L.D., Feely, R.A., Dickson, A.G., Swift, J.H., Carlson, C.A., Warner, M.J., McNichol, A., Key, R.M., and Schlosser, P. (2016) Dissolved inorganic carbon (DIC), total alkalinity, pH on total scale, dissolved organic carbon (DOC), chlorofluorocarbons, temperature, salinity and other hydrographic and chemical variables collected from discrete samples and profile observations during the R/V Nathaniel B. Palmer cruise GO-SHIP_P16S_2014 (EXPOCODE 320620140320) in the South Pacific Ocean from 2014-03-20 to 2014-05-05 (NCEI Accession 0157621). NOAA National Centers for Environmental Information. Dataset. https://doi.org/10.3334/cdiac/otg.go_ship_p16s_2014

Wanninkhof, R., Feely, R.A., Dickson, A.G., Hansell, D.A., Key, R.M., Swift, J.H., Smethie, W.M. Jr., Fine, R.A., Jenkins, W.J., McNichol, A., McCartney, M.S., and Druffel, E.R.M. (2013) Partial pressure (or fugacity) of carbon dioxide, dissolved inorganic carbon, pH, alkalinity, temperature, salinity and other variables collected from discrete sample and profile observations using Alkalinity titrator, CTD and other instruments from ATLANTIS in the North Atlantic Ocean from 2012-04-19 to 2012-05-15 (NCEI Accession 0108160). NOAA National Centers for Environmental Information. Dataset. https://doi.org/10.3334/cdiac/otg.clivar_a20_2012

Wanninkhof, R., Zhang, J.-Z., Baringer, M.O., Langdon, C., Cai, W.-J., Salisbury, J.E., and Byrne, R.H. (2016) Partial pressure (or fugacity) of carbon dioxide, dissolved inorganic carbon, pH, alkalinity, temperature, salinity and other variables collected from discrete sample and profile observations using CTD, bottle and other instruments from NOAA Ship RONALD H. BROWN in the Gray's Reef National Marine Sanctuary, Gulf of Mexico and North Atlantic Ocean from 2012-07-21 to 2012-08-13 (NCEI Accession 0157619). NOAA National Centers for Environmental Information. Dataset. https://doi.org/10.3334/cdiac/otg.coastal_gomecc2

Waters, J., Millero, F., and Woosley, R. (2014) Corrigendum to “The free proton concentration scale for seawater pH", [MARCHE: 149 (2013) 8−22]. *Mar. Chem.* **165**, 66−67. https://doi.org/10.1016/j.marchem.2014.07.004

Waters, J.F. and Millero, F.J. (2013) The free proton concentration scale for seawater pH. *Mar. Chem.* **149**, 8−22. https://doi.org/10.1016/j.marchem.2012.11.003

Williams, N.L., Juranek, L.W., Feely, R.A., Johnson, K.S., Sarmiento, J.L., Talley, L.D., Dickson, A.G., Gray, A.R., Wanninkhof, R., Russell, J.L., Riser, S.C., and Takeshita, Y. (2017) Calculating surface ocean pCO_2 from biogeochemical Argo floats equipped with pH: An uncertainty analysis. *Global Biogeochem. Cycles* **31**, 591−604. doi:10.1002/2016GB005541

APPENDIX D:

SUPPLEMENTAL INFORMATION FOR CHAPTER FOUR

Appendix D.1 Artificial freshwater solutions

D.1.1 Solution preparation

As discussed in Section 4.4.3.1, artificial freshwater solutions were prepared by adding combinations of $NaHCO_3$, NaCl, KCl, $CaCl_2$, $MgCl_2$, Na_2SO_4, and $MgSO_4$ for a total of seven solution types (denoted as A−G). Concentrations of the salts in each solution are provided in Table D.1.1. $NaHCO_3$ and NaCl salts were directly added to solutions. KCl salt was heated at 500−600 °C for three hours to remove any hydration, and subsequently stored in a desiccator throughout the duration of experiments (Kolthoff and Stenger, 1964). $CaCl_2$, $MgCl_2$, Na_2SO_4, and $MgSO_4$ salts were made into solutions in Milli-Q water as these salts are hygroscopic, and solution concentrations were measured via ICP-MS.

Table D.1.1.
Concentrations (mmol kg^{-1}) of salts in each artificial freshwater solution. I_{true} (mol kg^{-1}) was determined via gravimetric compositional analysis (see Section 4.4.3.1 for more details).

Soln.	I_{true}	$NaHCO_3$	NaCl	KCl	$CaCl_2$	$MgCl_2$	Na_2SO_4	$MgSO_4$
A1	0.0011	0.581	0.537	0	0	0	0	0
A2	0.0021	0.990	1.097	0	0	0	0	0
A3	0.0030	1.436	1.606	0	0	0	0	0
A4	0.0040	1.923	2.120	0	0	0	0	0
B1	0.0005	0.382	0	0	0.019	0	0	0.026
B2	0.0010	0.641	0	0	0.047	0	0	0.052
B3	0.0020	1.299	0	0	0.094	0	0	0.096
B4	0.0029	1.947	0	0	0.140	0	0	0.139
B5	0.0040	2.734	0	0	0.186	0	0	0.181

Table D.1.1. (Continued).

B6	0.0048	3.173	0	0	0.230	0	0	0.223
B7	0.0060	4.102	0	0	0.279	0	0	0.259
B8	0.0070	4.630	0	0	0.355	0	0	0.338
B9	0.0081	5.201	0	0	0.429	0	0	0.398
B10	0.0091	5.749	0	0	0.493	0	0	0.468
B11	0.0100	6.275	0	0	0.552	0	0	0.514
C1	0.0006	0.340	0	0.073	0.028	0	0.021	0
C2	0.0010	0.707	0	0.081	0.046	0	0.035	0
C3	0.0021	1.533	0	0.124	0.084	0	0.063	0
C4	0.0029	1.997	0	0.182	0.140	0	0.098	0
C5	0.0038	2.703	0	0.174	0.188	0	0.116	0
C6	0.0048	3.421	0	0.196	0.231	0	0.176	0
C7	0.0062	4.455	0	0.226	0.279	0	0.211	0
C8	0.0071	5.050	0	0.260	0.328	0	0.257	0
C9	0.0080	5.741	0	0.269	0.382	0	0.296	0
C10	0.0089	6.348	0	0.277	0.426	0	0.328	0
C11	0.0101	7.152	0	0.328	0.495	0	0.379	0
D1	0.0006	0.407	0	0.055	0	0	0	0.035
D2	0.0010	0.720	0	0.066	0	0	0	0.053
D3	0.0020	1.534	0	0.127	0	0	0	0.097
D4	0.0030	2.265	0	0.130	0	0	0	0.142
D5	0.0040	3.065	0	0.142	0	0	0	0.191
D6	0.0050	3.925	0	0.169	0	0	0	0.237
D7	0.0060	4.657	0	0.196	0	0	0	0.278
D8	0.0070	5.420	0	0.220	0	0	0	0.341
D9	0.0079	6.064	0	0.252	0	0	0	0.396
D10	0.0091	6.969	0	0.297	0	0	0	0.462
D11	0.0100	7.635	0	0.299	0	0	0	0.522
E1	0.0006	0.378	0	0.043	0.028	0.031	0	0
E2	0.0010	0.639	0	0.093	0.047	0.053	0	0
E3	0.0019	1.316	0	0.107	0.083	0.092	0	0
E4	0.0030	1.938	0	0.152	0.140	0.155	0	0
E5	0.0040	2.597	0	0.182	0.190	0.209	0	0
E6	0.0049	3.252	0	0.187	0.233	0.257	0	0
E7	0.0060	4.098	0	0.205	0.279	0.271	0	0
E8	0.0070	4.745	0	0.265	0.325	0.344	0	0
E9	0.0079	5.364	0	0.270	0.365	0.402	0	0
E10	0.0091	6.150	0	0.290	0.417	0.462	0	0
E11	0.0101	6.867	0	0.338	0.461	0.514	0	0
F1	0.0006	0.418	0	0.020	0.037	0	0	0.017
F2	0.0011	0.504	0	0.026	0.110	0	0	0.051
F3	0.0015	0.628	0	0.036	0.169	0	0	0.079
G1	0.0006	0.366	0	0.035	0.019	0	0	0.026
G2	0.0010	0.607	0	0.051	0.047	0	0	0.052
G3	0.0016	0.987	0	0.096	0.065	0	0	0.069

Table D.1.1. (Continued).

G4	0.0019	1.201	0	0.077	0.095	0	0	0.096
G5	0.0025	1.623	0	0.106	0.113	0	0	0.113
G6	0.0029	1.827	0	0.130	0.142	0	0	0.141
G7	0.0039	2.471	0	0.155	0.189	0	0	0.184
G8	0.0049	3.138	0	0.177	0.234	0	0	0.226
G9	0.0061	3.936	0	0.208	0.279	0	0	0.269
G10	0.0070	4.574	0	0.199	0.327	0	0	0.316
G11	0.0078	5.074	0	0.253	0.368	0	0	0.352
G12	0.0087	5.742	0	0.286	0.396	0	0	0.371
G13	0.0100	6.561	0	0.328	0.464	0	0	0.433

D.1.2 Ion pairing

Calculation of I_{true} values via eq. (4.8) requires the assumption that ion pairing is insignificant for the dilute aqueous solutions in this work. To verify this, formation constants for ion pairs (K_f) were determined according to Millero and Schreiber (1982) at I = 0.01 mol kg^{-1} (shown in Table D.1.2). (As there is no formation constant data for $KHCO_3^0$ or any ion pairs with Cl^-, these ion pairs are not shown, and can be considered negligible.) With these formation constants, the concentrations of ion pairs can then be determined (also shown in Table D.1.2). We used total concentrations of each ion that represent typical freshwater concentrations (see footnote of Table D.1.2 for details) (Turner et al., 1981). We can then determine the free/total ratios in terms of the cation, which are also shown in Table D.1.2. Results show that, in each case, the free cation accounts for at least 99% of the total ion in solution. Overall, this analysis shows that ion pairing can indeed be assumed to be negligible at the low ionic strengths considered in this work.

Table D.1.2.
Data for ion pairing analysis described in Section D.1.2. Formation constants (K_f) were calculated using eq. (39) of Millero and Schreiber (1982) at I = 0.01 mol kg^{-1}. The concentrations of ion pairs were calculated using average total concentrations of each ion (denoted as [total ion], see footnote[*]) in conjunction with respective K_f values. Finally, the free/total ratio of the cation was determined as [ion pair]/[total ion].

Ion pair	K_f (mol kg^{-1})	[Ion pair] (μmol kg^{-1})	Free/total Ratio of Cation
$NaHCO_3^0$	0.531	0.176	0.999
$CaHCO_3^+$	6.675	2.719	0.992
$MgHCO_3^+$	5.994	1.224	0.993
$NaSO_4^-$	5.959	0.180	0.999
KSO_4^-	5.165	0.033	0.999
$CaSO_4^0$	86.675	3.220	0.990
$MgSO_4^0$	74.044	1.379	0.992

[*]Total ion concentrations (mol kg^{-1}): [Na^+] = $10^{-3.56}$, [K^+] = $10^{-4.23}$, [Ca^{2+}] = $10^{-3.47}$, [Mg^{2+}] = $10^{-3.77}$, [HCO_3^-] = $10^{-2.92}$, [SO_4^{2-}] = $10^{-3.96}$.

Appendix D.2 Titrant solutions

D.2.1 Titrant preparation

Titrant solutions of KH_2PO_4 and Na_2HPO_4 were prepared as discussed in Section 4.4.3.1. KH_2PO_4 and Na_2HPO_4 salts were purified by heating at 110−130 °C for two hours (Durst, 1975). Purified salts were added to Milli-Q to obtain titrant solutions. Solutions were stored in volumetric flasks; separate Gilmont burets (one for each titrant) were rinsed and re-filled daily with new titrant solution prior to measurements.

Titrants were made immediately after salts were heated. Titrant solutions in this work were used for approximately two weeks. A set of titrant solutions was also stored to assess the stability of the solutions over time. A solution of $NaHCO_3$ and NaCl (i.e., solution type A) at an I_{true} of ~0.004 mol kg^{-1} was made once a month. The hybrid conductometric/spectrophotometric method was then performed on the experimental solution (n = 2) using the stored KH_2PO_4 and Na_2HPO_4 titrants (for details of the hybrid method, see Sections 4.4.3.3 and 4.4.3.4) to determine I_{hybrid}. (S_{true}

was used in the calculation of pH_T as no conductivity measurements were made on these samples.) As shown in Fig. D.2.1, the titrants provided accurate estimates of I_{hybrid} (i.e., the titrants were stable) for approximately five months. We suggest new titrants be made after this time period for best results.

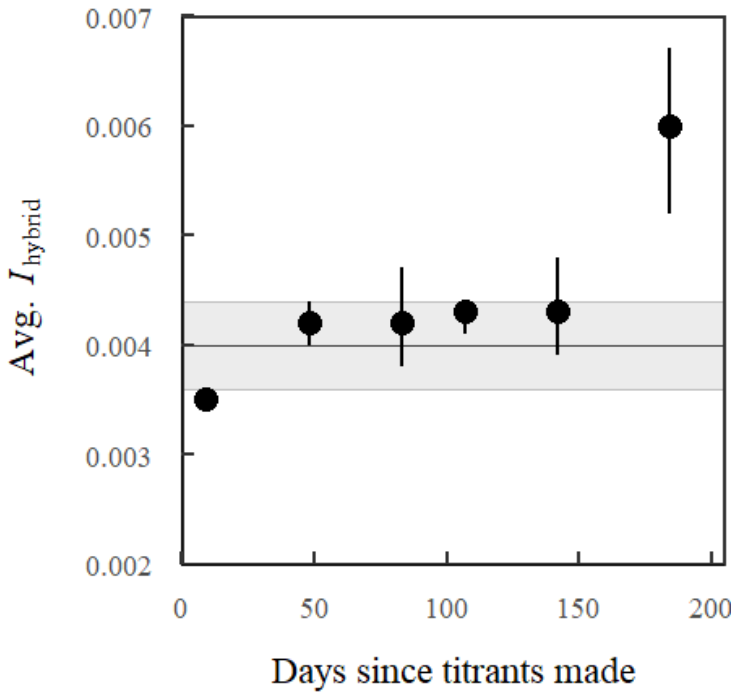

Fig. D.2.1. Average I_{hybrid} (n = 2) determined using stored KH_2PO_4 and Na_2HPO_4 titrants in terms of titrant age. I_{true} values of the solutions tested were 0.0040 ± 0.0001 mol kg^{-1}. Error bars indicate the standard deviation between duplicate measurements. The shaded grey region indicates the precision of the spectrophotometric titrant method (±0.0003 mol kg^{-1}).

Appendix D.3 Calculations for hybrid conductometric/spectrophotometric method

D.3.1 Ionic strength components

The ionic strength of KH_2PO_4 titrant is given as:

$$I_{KH_2PO_4} = ½ ([K^+] (1)^2 + [H_2PO_4^-] (1)^2) \quad (D.1)$$

Since $[K^+] = [H_2PO_4^-]$, which also equals the concentration of added KH_2PO_4, eq. (D.1) simplifies to $I_{KH_2PO_4} = [KH_2PO_4]$.

The ionic strength of Na_2HPO_4 titrant is given as:

$$I_{Na_2HPO_4} = ½ ([Na^+] (1)^2 + [HPO_4^{2-}] (2)^2) \quad \text{(D.2)}$$

Since $[Na^+] = 2[HPO_4^{2-}]$, and $[HPO_4^{2-}]$ equals the concentration of added Na_2HPO_4, eq. (D.2) simplifies to $I_{Na_2HPO_4} = 3[Na_2HPO_4]$.

The ionic strength contributions of added HCl, NaOH, and mCP indicator were found to be negligible.

The final ionic strength ($I_{expSoln}$) of an experimental solution, determined via the calculations outlined in Section 4.4.3.4, is equal to:

$$I_{expSoln} = I_{hybrid} + I_{KH_2PO_4} + I_{Na_2HPO_4} \quad \text{(D.3)}$$

where I_{hybrid} is the ionic strength of the experimental solution with no added components.

Rearranging terms of eq. (D.3), I_{hybid} can be calculated via:

$$I_{hybrid} = I_{expSoln} - [KH_2PO_4] - 3[Na_2HPO_4] \quad \text{(C.4)}$$

D.3.2 Example calculation of I_{hybrid}

As a check to users, a sample calculation of I_{hybrid} is provided here. Example input experimental values are provided in Table C.1.

Table D.3.1.
Example experimental values for the titration procedure outlined in Section 4.4.3.3.

Measured Term	Value
m_i	30.000 g
Added KH_2PO_4 (0.009 M)	0.095 g
Added Na_2HPO_4 (0.02 M)	0.205 g
R_{avg}	0.4000
T	298.15 K
S_{probeC} (or S_{salC})	0.500

With these example values, calculations are as follows. The final mass (m_t) is the sum of the initial sample mass (m_i, 30.000 g), KH_2PO_4 mass (0.095 g), and Na_2HPO_4 mass (0.205 g). The final concentrations of $[KH_2PO_4]_F$ and $[Na_2HPO_4]_F$ are calculated via gravimetric dilution. pH_T is calculated using the mCP pH parameterization of Douglas and Byrne (2017) with inputs of S_{probeC} (or S_{salC}), measured T, and R_{avg}. K_2 is then calculated via eq. (4.6) with inputs of pH_T and $[H_2PO_4^-]/[HPO_4^{2-}]$ from $[KH_2PO_4]_F$ and $[Na_2HPO_4]_F$. With this K_2, $I_{expSoln}$ is calculated via eq. (4.4). This I is the sum of the I of the original sample (I_{hybrid}) plus ionic strength inputs from added KH_2PO_4 and Na_2HPO_4 (eq. (D.3)). I_{hybrid} is determined by subtracting these added ionic strength inputs from $I_{expSoln}$ via eq. (D.4). Exact values for these computations can be found in Table D.3.2 to check user calculations.

Table D.3.2.
Example set of calculated values for terms required to determine I_{hybrid}. These calculations were made using the example inputs of measured values from Table D.3.1. Estimates of I are expressed in mol kg^{-1}.

Calculated Term	Value
m_t	30.300 g
$[KH_2PO_4]_F$	2.822×10^{-5} mol kg^{-1}
$[Na_2HPO_4]_F$	1.353×10^{-4} mol kg^{-1}
pH_T	7.6936
K_2	1.030×10^{7}
$I_{expSoln}$	0.00996
$I_{Na_2HPO_4}$	0.00041
$I_{KH_2PO_4}$	0.00003
I_{hybrid}	0.0095

D.3.3 K_2 intercept value for calculating I_{hybrid}

The K_2 intercept value in eq. (4.4) is 7.200 ± 0.008 (Powell et al., 2005). We determined that an intercept value of 7.195 provides the most accurate estimates of I_{hybrid} based on improved randomness of residuals (i.e., I_{hybrid} minus I_{true}) as shown in Fig. D.3.1. The largest difference between I_{hybrid} after adjusting the K_2 intercept from 7.200 to 7.195 was 0.0007, which is approximately 2σ of our observed measurement accuracy.

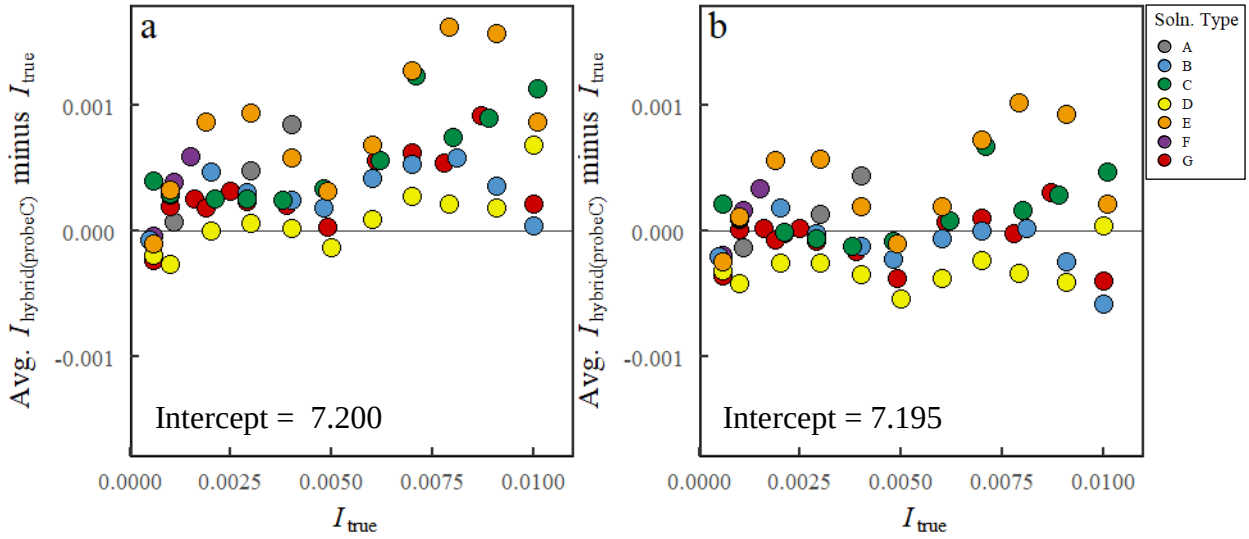

Fig D.3.1. Ionic strength residuals (i.e., avg. $I_{hybrid(probeC)}$ minus I_{true}) as a function of I_{true}. $I_{hybrid(probeC)}$ was calculated using a K_2 intercept of (a) 7.200 and (b) 7.195. Estimates of I are expressed in mol kg^{-1}. Colors indicate solution type (see Table 4.1).

Appendix D.4 Conductometric measurements and hybrid method results

Table D.4.1.
Conductometric measurements of ionic strength (mol kg^{-1}) for each of the artificial freshwater solutions using a conductivity probe (I_{probe}) and a salinometer (I_{sal}). I_{true} (mol kg^{-1}) was determined via gravimetric compositional analysis. Procedural details are provided in Section 4.4.3.2 and results are discussed in Section 4.5.1.1.

Soln.	I_{true}	I_{probe}	I_{sal}
A1	0.0011	0.0017	0.0013
A2	0.0021	0.0032	0.0022
A3	0.0030	0.0046	0.0032
A4	0.0040	0.0061	0.0042
B1	0.0005	0.0007	0.0006
B2	0.0010	0.0012	0.0009
B3	0.0020	0.0024	0.0017
B4	0.0029	0.0035	0.0024
B5	0.0040	0.0048	0.0033
B6	0.0048	0.0056	0.0038
B7	0.0060	0.0070	0.0048
B8	0.0070	0.0082	0.0056
B9	0.0081	0.0094	0.0064
B10	0.0091	0.0104	0.0071
B11	0.0100	0.0114	0.0078
C1	0.0006	0.0008	0.0007
C2	0.0010	0.0014	0.0011

Table D.4.1. (Continued).

C3	0.0021	0.0028	0.0020
C4	0.0029	0.0039	0.0026
C5	0.0038	0.0050	0.0034
C6	0.0048	0.0063	0.0043
C7	0.0062	0.0079	0.0054
C8	0.0071	0.0091	0.0062
C9	0.0080	0.0103	0.0070
C10	0.0089	0.0113	0.0077
C11	0.0101	0.0128	0.0087
D1	0.0006	0.0008	0.0007
D2	0.0010	0.0013	0.0010
D3	0.0020	0.0026	0.0018
D4	0.0030	0.0037	0.0025
D5	0.0040	0.0049	0.0033
D6	0.0050	0.0061	0.0042
D7	0.0060	0.0071	0.0049
D8	0.0070	0.0084	0.0057
D9	0.0079	0.0094	0.0064
D10	0.0091	0.0108	0.0073
D11	0.0100	0.0117	0.0080
E1	0.0006	0.0008	0.0007
E2	0.0010	0.0014	0.0010
E3	0.0019	0.0026	0.0018
E4	0.0030	0.0039	0.0027
E5	0.0040	0.0051	0.0035
E6	0.0049	0.0062	0.0043
E7	0.0060	0.0075	0.0051
E8	0.0070	0.0089	0.0060
E9	0.0079	0.0101	0.0068
E10	0.0091	0.0114	0.0077
E11	0.0101	0.0126	0.0086
F1	0.0006	0.0008	0.0007
F2	0.0011	0.0013	0.0010
F3	0.0015	0.0018	0.0013
G1	0.0006	0.0007	0.0006
G2	0.0010	0.0013	0.0010
G3	0.0016	0.0020	0.0014
G4	0.0019	0.0024	0.0017
G5	0.0025	0.0031	0.0022
G6	0.0029	0.0036	0.0025
G7	0.0039	0.0048	0.0033
G8	0.0049	0.0060	0.0041
G9	0.0061	0.0072	0.0050
G10	0.0070	0.0084	0.0057

Table D.4.1. (Continued).

G11	0.0078	0.0094	0.0064
G12	0.0087	0.0104	0.0071
G13	0.0100	0.0119	0.0081

Table D.4.2.
Empirically-corrected conductometric measurements of ionic strength (mol kg^{-1}) (as discussed in Section 4.5.1.2) for each of the artificial freshwater solutions using a conductivity probe (I_{probeC}) and salinometer (I_{salC}). I_{true} (mol kg^{-1}) was determined via gravimetric compositional analysis.

Soln.	I_{true}	I_{probeC}	I_{salC}
A1	0.0011	0.0014	0.0015
A2	0.0021	0.0026	0.0026
A3	0.0030	0.0038	0.0038
A4	0.0040	0.0050	0.0050
B1	0.0005	0.0006	0.0007
B2	0.0010	0.0010	0.0011
B3	0.0020	0.0020	0.0020
B4	0.0029	0.0029	0.0029
B5	0.0040	0.0039	0.0039
B6	0.0048	0.0046	0.0046
B7	0.0060	0.0057	0.0058
B8	0.0070	0.0068	0.0067
B9	0.0081	0.0077	0.0076
B10	0.0091	0.0086	0.0085
B11	0.0100	0.0094	0.0093
C1	0.0006	0.0007	0.0008
C2	0.0010	0.0012	0.0013
C3	0.0021	0.0023	0.0023
C4	0.0029	0.0032	0.0032
C5	0.0038	0.0041	0.0041
C6	0.0048	0.0052	0.0051
C7	0.0062	0.0065	0.0065
C8	0.0071	0.0075	0.0074
C9	0.0080	0.0085	0.0084
C10	0.0089	0.0093	0.0092
C11	0.0101	0.0105	0.0104
D1	0.0006	0.0006	0.0008
D2	0.0010	0.0011	0.0012
D3	0.0020	0.0021	0.0022
D4	0.0030	0.0030	0.0030
D5	0.0040	0.0040	0.0040
D6	0.0050	0.0050	0.0050
D7	0.0060	0.0058	0.0059
D8	0.0070	0.0069	0.0068

Table D.4.2. (Continued).

D9	0.0079	0.0077	0.0077
D10	0.0091	0.0088	0.0088
D11	0.0100	0.0096	0.0096
E1	0.0006	0.0007	0.0008
E2	0.0010	0.0012	0.0012
E3	0.0019	0.0021	0.0021
E4	0.0030	0.0032	0.0032
E5	0.0040	0.0042	0.0042
E6	0.0049	0.0051	0.0051
E7	0.0060	0.0062	0.0062
E8	0.0070	0.0073	0.0073
E9	0.0079	0.0082	0.0082
E10	0.0091	0.0093	0.0093
E11	0.0101	0.0104	0.0104
F1	0.0006	0.0007	0.0008
F2	0.0011	0.0011	0.0012
F3	0.0015	0.0015	0.0016
G1	0.0006	0.0006	0.0008
G2	0.0010	0.0010	0.0012
G3	0.0016	0.0016	0.0017
G4	0.0019	0.0020	0.0021
G5	0.0025	0.0026	0.0026
G6	0.0029	0.0030	0.0030
G7	0.0039	0.0039	0.0040
G8	0.0049	0.0049	0.0049
G9	0.0061	0.0059	0.0059
G10	0.0070	0.0069	0.0068
G11	0.0078	0.0077	0.0076
G12	0.0087	0.0085	0.0085
G13	0.0100	0.0098	0.0097

Table D.4.3.
Average ionic strength (n = 3) (mol kg^{-1}) determined for each of the artificial freshwater solutions using the hybrid conductometric/spectrophotometric method ($I_{\text{hybrid(probeC)}}$ and $I_{\text{hybrid(salC)}}$). I_{true} (mol kg^{-1}) was determined via gravimetric compositional analysis. Procedural details are provided in Section 4.4.3.4 and results are discussed in Section 4.5.2.

Soln.	I_{true}	$I_{\text{hybrid(probeC)}}$	$I_{\text{hybrid(salC)}}$
A1	0.0011	0.0010	0.0012
A2	0.0021	0.0021	0.0021
A3	0.0030	0.0032	0.0033
A4	0.0040	0.0045	0.0046
B1	0.0005	0.0003	0.0005
B2	0.0010	0.0011	0.0012

Table D.4.3. (Continued).

B3	0.0020	0.0022	0.0022
B4	0.0029	0.0029	0.0029
B5	0.0040	0.0039	0.0039
B6	0.0048	0.0045	0.0045
B7	0.0060	0.0059	0.0059
B8	0.0070	0.0070	0.0070
B9	0.0081	0.0081	0.0080
B10	0.0091	0.0089	0.0088
B11	0.0100	0.0094	0.0094
C1	0.0006	0.0008	0.0010
C2	0.0010	0.0011	0.0012
C3	0.0021	0.0021	0.0021
C4	0.0029	0.0028	0.0028
C5	0.0038	0.0037	0.0036
C6	0.0048	0.0048	0.0047
C7	0.0062	0.0062	0.0062
C8	0.0071	0.0077	0.0077
C9	0.0080	0.0082	0.0082
C10	0.0089	0.0092	0.0091
C11	0.0101	0.0106	0.0105
D1	0.0006	0.0003	0.0005
D2	0.0010	0.0006	0.0007
D3	0.0020	0.0018	0.0019
D4	0.0030	0.0027	0.0027
D5	0.0040	0.0036	0.0036
D6	0.0050	0.0045	0.0045
D7	0.0060	0.0056	0.0056
D8	0.0070	0.0068	0.0067
D9	0.0079	0.0076	0.0075
D10	0.0091	0.0087	0.0087
D11	0.0100	0.0101	0.0101
E1	0.0006	0.0004	0.0005
E2	0.0010	0.0012	0.0013
E3	0.0019	0.0025	0.0025
E4	0.0030	0.0036	0.0035
E5	0.0040	0.0042	0.0042
E6	0.0049	0.0048	0.0048
E7	0.0060	0.0062	0.0062
E8	0.0070	0.0077	0.0077
E9	0.0079	0.0090	0.0089
E10	0.0091	0.0100	0.0100
E11	0.0101	0.0103	0.0103
F1	0.0006	0.0004	0.0006
F2	0.0011	0.0012	0.0014
F3	0.0015	0.0018	0.0019

Table D.4.3. (Continued).

G1	0.0006	0.0002	0.0004
G2	0.0010	0.0010	0.0012
G3	0.0016	0.0016	0.0017
G4	0.0019	0.0019	0.0020
G5	0.0025	0.0025	0.0026
G6	0.0029	0.0029	0.0029
G7	0.0039	0.0038	0.0039
G8	0.0049	0.0045	0.0045
G9	0.0061	0.0061	0.0062
G10	0.0070	0.0071	0.0070
G11	0.0078	0.0078	0.0078
G12	0.0087	0.0090	0.0089
G13	0.0100	0.0096	0.0095

Appendix D.5 Details of recommended procedure to determine I_{hybrid}

D.5.1 Solution preparation for correction factor

We recommend an empirical correction factor for conductometric instruments (as discussed in Section 4.5.1.2) to improve the accuracy of results. We suggest that users create two artificial solutions based on our solution type D, which contains $NaHCO_3$, KCl, and $MgSO_4$ in a 1:0.05:0.07 ratio (see Table 4.1). The solutions' ionic strengths should be approximately 0.001 and 0.01 mol kg^{-1} to encompass the range of I appropriate to natural freshwaters. The $MgSO_4$ salt should be made into a solution of 0.1 M as the salt is hygroscopic – the concentration of this solution should be determined via ICP-MS or an appropriate alternative method. Exact amounts of salts/solutions required to create these two calibrating solutions are provided in Table D.5.1.

Table D.5.1.
Recipe for calibration solutions at $I = 0.001$ and $I = 0.01$ mol kg^{-1}. Solutions should be made in 1 L of Milli-Q water and stored in a sealed container.

	$I_{true} = 0.001$	$I_{true} = 0.01$
$NaHCO_3$ (salt)	0.0600 g	0.6400 g
KCl (salt)	0.0028 g	0.0300 g
$MgSO_4$ (0.1 M soln.)	0.50 mL	5.00 mL

D.5.2 Determining empirical correction factor

Measure I_{probe} or S_{sal} in each of these two calibration solutions. For probe measurements, obtain the linear fit that describes the measured I_{probe} values as a function of I_{true} (e.g., eq. (4.12)). For salinometer measurements, there are two options: (1) convert I_{true} to S_{true} using eq. (4.10) and obtain a linear fit that describes the measured S_{sal} values as a function of S_{true} or (2) convert S_{sal} to I_{sal} using eq. (4.10) and obtain a linear fit that describes the measured I_{sal} values as a function of I_{true} (e.g., eq. (4.13)). Both options are consistent with one another – the choice is simply dependent on the user's preference in obtaining conductivity measurements in terms of I or S.

If the user has opted to use two potassium chloride conductivity standards (for a conductivity probe) or two standard seawater samples (for a salinometer) to develop the empirical correction factor, the procedure is as follows. The two standards should encompass the range of I for solutions being measured (solutions from a manufacturer may need to be gravimetrically diluted as appropriate). One standard is first used to internally calibrate the instrument, and the other is then used to measure I_{probe} or S_{sal}. Then a linear fit can be obtained similarly as described above.

D.5.3 Hybrid conductometric/spectrophotometric determinations of I

For the hybrid conductometric/spectrophotometric determinations of *I*, a conductivity measurement is required (Fig. 4.4, step 2a). When using a conductivity probe, measure I_{probe} on the larger sample aliquot and apply the user-determined correction factor to obtain I_{probeC}. When using a salinometer, measure S_{sal} on the larger sample aliquot and apply the user-determined correction factor to obtain S_{salC} or I_{salC}.

The second part of the hybrid method is the spectrophotometric titration procedure detailed in Section 4.4.3.3 and outlined in Fig. 4.4, step 2b. After the titration procedure is complete, pH_T is calculated using the mCP parameterization of Douglas and Byrne (2017). Salinity is obtained from the empirically-corrected conductivity measurement described in the paragraph above. If the correction factor was determined as a function of *I* (i.e., I_{probeC} or I_{salC}), *I* values can then be converted to *S* (S_{probeC} or S_{salC}) via eq. (4.10). Alternatively, if a correction factor was determined as a function of *S* to obtain S_{salC}, no conversion is needed. Temperature is as measured at the end of the titration. The *R* to be used is R_{avg}. This pH_T value is input into eq. (4.6) to calculate K_2. This K_2 value is then substituted into eq. (4.4) to calculate $I_{expSoln}$. Finally, the *I* contributions of the added titrants are subtracted to obtain the ionic strength of the original sample (I_{hybrid}). An example calculation of I_{hybrid} is provided above in Section D.3.2.

Appendix D.6 Example uncertainty analysis

D.6.1 I uncertainty contribution to pH_T

As discussed in Section 4.6, we determined how an uncertainty in *I* is reflected in an error in pH_T when $I = 0.01$ mol kg^{-1}. We first converted *I* + uncertainty (3% for the hybrid method, 27% for conductometric method) to *S* via eq. (4.10). These estimates were used in conjunction with *R*

= 0.4 at 25 °C to determine pH_T (shown in Table D.6.1) using the mCP equation of Douglas and Byrne (2017).

Table D.6.1.
Estimates of pH_T when accounting for a 3% uncertainty in *I* for the hybrid method and a 27% uncertainty in *I* for the conductometric measurements. The true value of pH_T = 7.6933 when *I* = 0.01 mol kg^{-1} (at *R* = 0.4, 25 °C). The error in pH_T is the difference between this true pH_T value and pH_T determined with the 3% and 27% uncertainties in *I*.

I	pH_T	Error in pH_T
Hybrid: 0.0103 mol kg^{-1}	7.6909	0.0025
Conductometric: 0.0127 mol kg^{-1}	7.6729	0.0204

D.6.2 I uncertainty contribution to aragonite saturation state

As discussed in Section 4.6, we also determined how an uncertainty in *I* is reflected in an error in calculated aragonite saturation state (Ω_{ar}) when *I* = 0.01 mol kg^{-1}. We first converted *I* + uncertainty (3% for the hybrid method, 27% for conductometric method) to *S* via eq. (4.10). These estimates were used in conjunction with pH_T = 8.1 and total alkalinity (A_T) = 2435 µmol kg^{-1}, at 25 °C and 0 bar, to calculate Ω_{ar} (shown in Table D.6.2) via the CO_2 system calculation program CO2SYS (Van Heuven et al., 2011; Sharp et al., 2020).

Table D.6.2.
Estimates of Ω_{ar} when accounting for a 3% uncertainty in *I* for the hybrid method and a 27% uncertainty in *I* for the conductometric measurements. The true value of Ω_{ar} = 1.00 when *I* = 0.01 mol kg^{-1} (at pH_T = 8.1 and A_T = 2435 µmol kg^{-1}, at 25 °C and 0 bar). The error in Ω_{ar} is the difference between this true Ω_{ar} value and Ω_{ar} determined with the 3% and 27% uncertainties in *I*.

I	Ω_{ar}	Error in Ω_{ar}
Hybrid: 0.0103 mol kg^{-1}	1.02	0.02
Conductometric: 0.0127 mol kg^{-1}	1.13	0.13

Appendix D.7 References for Appendix D

Douglas, N.K. and Byrne, R.H. (2017) Spectrophotometric pH measurements from river to sea: Calibration of mCP for $0 \leq S \leq 40$ and $278.15 \leq T \leq 308.15$ K. *Mar. Chem.* **197**, 64−69. https://doi.org/10.1016/j.marchem.2017.10.001

Durst, R.A. (1975) Standard reference materials: Standardization of pH measurements. *NBS Special Publication* 260−53.

Kolthoff, I.M. and Stenger, V.A. (1964) *Volumetric analysis. Titration Methods: Acid-Base, Precipitation, and Complex-Formation Reactions*. Vol. 2. Interscience. New York, NY.

Millero, F.J. and Schreiber, D.R. (1982) Use of the ion pairing model to estimate activity coefficients of the ionic components of natural waters. *Am. J. Sci.* **282**, 1508−1540. doi:10.2475/ajs.282.9.1508

Powell, K.J., Brown, P.L., Byrne, R.H., Gajda, T., Hefter, G., Sjöberg, S., and Wanner, H. (2005) Chemical speciation of environmentally significant heavy metals with inorganic ligands. Part 1: The Hg^{2+}– Cl^-, OH^-, CO_3^{2-}, SO_4^{2-}, and PO_4^{3-} aqueous systems (IUPAC Technical Report). *Pure Appl. Chem.* **77**, 739−800. https://doi.org/10.1351/pac200577040739

Sharp, J.D., Pierrot, D., Humphreys, M.P., Epitalon, J.-M., Orr, J.C., Lewis, E.R., and Wallace, D.W.R. (2020) CO2SYSv3 for MATLAB (Version v3.1.1). Zenodo. http://doi.org/10.5281/zenodo.3952803

Turner, D.R., Whitfield, M., and Dickson, A.G. (1981) The equilibrium speciation of dissolved components in freshwater and seawater at 25 °C and 1 atm pressure. *Geochim. Cosmochim. Acta* **45**, 855−881. https://doi.org/10.1016/0016-7037(81)90115-0

Van Heuven, S., Pierrot, D., Rae, J., Lewis, E., and Wallace, D. (2011) MATLAB program developed for CO_2 system calculations. *ORNL/CDIAC-105b.* Carbon Dioxide Inf. Anal. Cent., Oak Ridge Natl. Lab., US Dept. of Energy, Oak Ridge, TN.